UNCLASSIFIED

ORNL-1613(Rev.(Del.))

REACTORS—POWER

UNITED STATES ATOMIC ENERGY COMMISSION

A CONCEPTUAL DESIGN OF A PRESSURIZED-WATER PACKAGE POWER REACTOR

By
A. L. Boch
W. R. Gall
G. F. Leichsenring
R. S. Livingston

June 6, 1955

Oak Ridge National Laboratory
Oak Ridge, Tennessee

Technical Information Service Extension, Oak Ridge, Tenn.

UNCLASSIFIED

II

Date Declassified: January 24, 1957.

Work performed under Contract No. W-7405-eng-26.

Printed in USA. Price $1.75. Available from the Office of Technical Services, Department of Commerce, Washington 25, D. C.

ABSTRACT

This conceptual design study describes a reactor and associated power plant that has been designed to produce 1000 kw of net electric power and 3535 kw of steam for heating purposes. The total thermal output of the reactor is 10,000 kw. The fuel plates consist of highly enriched UO_2 imbedded in a matrix of stainless steel and clad on all sides with stainless steel. The core is cooled and moderated with circulating light water, pressurized to 1200 psia. Saturated steam, produced in the heat exchanger at 200 psia, is used to drive a turbogenerator. Steam from the heat exchanger is also used, at a reduced pressure, for space heating.

The reactor is loaded with approximately 18 kg of U 235 and will supply 15 megawatt-years of energy before refueling is required. This corresponds to 2.5 years of operation at an average load factor of 60 percent. Burnout poison in the form of B_4C is incorporated to reduce the reactivity excursion and thus facilitate control.

The major objective has been to design a reactor which will require a minimum of development effort and yet be reliable and inexpensive. The estimated capital investment, exclusive of uranium, is $1,703,000. The estimated cost per kilowatt-hour for net electric and steam power at the bus, based on a 60-percent average load demand is 5.33 cents and 1.23 cents, respectively.

ACKNOWLEDGEMENTS

Many important contributions to this revised report were made by R. B. Briggs, W. H. Jordan, F. H. Neill, and R. C. Robertson, who assisted in the preparation of the original draft of the report, ORNL CF-53-10-106.

The nuclear calculations reported herein are the result of intensive work by A. M. Perry, with the assistance of R. L. Murray (North Carolina State College), Captain R. Bate (Corps of Engineers), and M. C. Edlund.

The Metallurgy Division personnel, J. E. Cunningham, R. J. Beaver, E. S. Bomar, Jr., and E. J. Boyle, contributed to the section on fuel element fabrication. The reactor simulator test results are due to the efforts of E. R. Mann and E. P. Green.

H. Bolwell and S. Oestricher (American Machine and Foundry Company) assisted in the preparation of the original draft. L. Scheib of the same company aided in the preparation of the corrosion section of the revised report. W. Pearce (Bendix Aviation Corporation) contributed the section on shielding.

Credit is due the Army Reactor Branch of the Corps of Engineers, under the direction of Colonel J. B. Lampert, for substantial assistance in establishing the proper basis for the design study and in obtaining much necessary information. Credit is also due the members of the ORNL Package Reactor Steering Committee, A. M. Weinberg, J. A. Swartout, W. R. Chambers, J. A. Lane, and R. A. Charpie, who provided a steady flow of sound advice and guidance.

The preparation of the final report was accomplished under the tireless and diligent editorial efforts of F. T. Howard. K. R. Goller (Corps of Engineers) assisted with the proofreading.

- The Authors

TABLE OF CONTENTS

Page

Page

LIST OF FIGURES

1.0 INTRODUCTION

The characteristics of a nuclear power system which distinguish it from a conventional power system fall into two general classes. First are those derived from the compactness of nuclear fuel; and second, those based on the long-range economy of nuclear fuel. Extensive studies have been made by a number of groups during the past several years, exploring the nuclear systems which might most adequately exploit this second feature. These studies have all been aimed at designs which could look forward to a comparison between nuclear fuel and conventional fuel on a strictly economic competitive basis. The compactness of nuclear fuel has not been seriously exploited, however, except perhaps in the case of the propulsion of military vehicles, the submarine and the aircraft being the two most conspicuous examples.

In the fall of 1952 a suggestion was made that another way to exploit the compactness of nuclear power units would be the development of a series of rather small nuclear power plants designated "package power plants" or "package reactors". The thinking was that these could be installed at remote or relatively inaccessible locations where strictly competitive fuel-cost economics is much less important than it is in heavily populated areas in the continental United States. It was further observed that the construction of one or a series of small compact reactors would contribute significantly to the practical experience in reactor design and construction. This experience which is essential to the founding of a substantial nuclear power industry might thus be obtained with only a very modest capital investment. It is also believed that small power plants of this type can be built rather inexpensively, particularly when compared with the power reactors which have

been built to date. If reactors can be built for a price not too far above a million dollars each, it then becomes much more feasible and desirable to construct a series of several different types. This then provides a means of advancing the general reactor knowledge without the committment of huge sums of money and large organizations of people devoted to high-speed "crash"-type development work.

It is not expected that the proposed reactor will generate power cheaply, based on modern conventional-fuel plant standards, but it is entirely possible that such a reactor can generate power at remote locations, where fuel supplies are very expensive, at lower gross cost than conventional plants. If this proves to be the case, then here is a firm basis for establishing a nuclear power industry entirely separate from the efforts to achieve long-range central-station competitive power.

This report describes the work done by a small group of engineers and physicists at the Oak Ridge National Laboratory on the design of a reactor to supply heat and electricity at an arctic military base. The electric power and heat generated are assumed to be 1000 kw and 3535 kw respectively. Although these values may not fit exactly the present needs of any arctic base, they were originally based on the average specifications for early-warning radar stations designated AC&W (Aircraft Control and Warning) stations.

The reactor described in this report is only one of a number of types being studied at this laboratory and elsewhere for this type of application. The particular reactor design chosen is a heterogeneous water-cooled and water-moderated stainless steel system which was selected primarily because of the advanced stage of engineering knowledge in this area and the small amount of development work which would be required. The fuel plates are similar to the

MTR and STR plates and consist of highly enriched UO_2 imbedded in a matrix of stainless steel and clad with stainless steel. The choice of stainless steel was governed by the objective of holding the costs of the reactor to a minimum. Although the critical mass is somewhat higher than for zirconium-clad fuel plates, the cost of fabrication of the stainless steel is very much less than for zirconium. The penalty for the larger critical mass is not serious in view of the various factors contributing to the gross cost of power in this system.

The principle objective of the design study reported herein was to establish a conceptual design for a complete system in sufficient detail to provide assurance of the feasibility of the reactor and to permit realistic cost estimates to be prepared. Standard components have been used wherever possible. Special components, such as the pressure vessel, heat exchangers, and control-rod mechanisms, have been designed to be well within the limits of present day technology. Much of the design has been done in conjunction with equipment manufacturers who have supplied courtesy bids on all the major components. It is clear that many factors have not been completely optimized in this conceptual design. This task should be undertaken when the detailed working plans for the reactor are prepared. The cost figures are based on the estimated cost of construction at Oak Ridge. The cost of construction at another site would need to be adjusted appropriately.

2.0 GENERAL CONSIDERATIONS

2.1 Site Conditions

A major factor which influences the design of the package reactor power plant, in addition to the basic power output requirement, is the location. The chief usefulness of the package reactor lies in the fact that it can be located in an extremely remote place where transportation is difficult and even impossible for extended periods of time.

A typical application for which a nuclear-powered plant would be ideally suited is an Aircraft Control and Warning (AC&W) Station. These installations are of necessity in remote locations where accessibility may be limited to air transportation and where the construction period may be as short as three months per year. If the reactor is to be used at these stations, such physical characteristics of the site as the weather conditions and the terrain must be investigated insofar as they will directly affect the design. The following site conditions are assumed or found to be applicable to the design of the plant:

The water supply is limited to amounts that can be hauled by trucks.

All structures must be constructed above grade, due to the existence of permafrost.

The ambient air temperature range is from -50°F to +75°F.

The maximum wind velocity is 50 miles per hour.

All equipment and materials for construction and operation must be transportable by air. Aggregates for concrete are available at the site.

Supplies for a 13-month period must be shipped in during the summer months and stored at the site.

2.2 Load Analysis

A typical Type-II AC&W station* is generally located at the base of a mountain with the radar towers and operating buildings at the top of the mountain. In certain cases the entire installation is located at the top. To minimize the cost of the electrical distribution lines and the heating and water distribution systems, the camps at Type-II stations are designed in two units. Each unit has a separate electric plant and heating plant rated at 500-kw electric generating capacity and 200-bhp heating capacity.

The data concerning the electric and heating systems used at a typical Type-II AC&W station is tabulated below:

Electrical System

Connected load, kw	1000
Average demand load, kw	600
Standby provided, kw	400
Peak demand load, kw	1000
Diesel driven generators (3 phase, 60 cps)	10
Rated capacity of each, kw	100
Voltage, volts	120/208
Transmission voltage, volts	4160
Station lighting, volts	120
Radar and associated equipment, volts	120/208

Heating System

Design temperature range, °F	-40 to +70
Design heating load, Btu/hr	11.2×10^6
EDR**	46,700
kw (including transmission losses)	3800
Cyclotherm steam generators	2
Capacity of each plant, boiler hp	200
Boilers, maximum working pressure, lb	150
Rated heating surface, sq ft	648
Rating, boiler hp	176
Steam, lb/hr	6900
Steam distribution, psig	45 to 50

* Study of the Possible Military Application of Nuclear Energy at Remote AC&W Stations, Mil. Plans Div., O.C.E., ORNL CF-53-7-135, July 23, 1953.

**EDR = Equivalent Direct Radiation, 1 EDR = 239.8 Btu/hr.

Low-pour diesel oil is used as the fuel for both the heating and electrical systems.

Graphical heating load data for the base at Thule, Greenland, indicates average values for any one month as follows:

Maximum heating load, kw	2650 (37,700 EDR)
Minimum heating load, kw	550 (7,820 EDR)

For any one day, the average values were:

Maximum heating load, kw	3800 (54,050 EDR)
Minimum heating load, kw	0

The average annual mean heating load is indicated as 1800 kw (25,600 EDR).

On the basis of the above data sources, the following design values were used for the reactor power plant.

Electrical

Peak demand, kw	1000
Peak demand of plant auxiliaries, kw	300
Installed capacity of generator, kw	1250
Average demand, kw	600
Average demand of auxiliaries, kw	275
Total average generator load, kw	875

Heating

Peak heating load	*
Average heating load, kw	1800 (25,600 EDR)
Minimum heating load, kw	0

*Since it was difficult to arrive at a value for the maximum heating load based on available data for arctic bases, this load was not fixed for design purposes. The reactor was designed for 10 Mw at full power output, the electric system designed for 1300 kw gross generation, and the remaining heat available for the peak heating system load computed to be approximately 3535 kw (12,070,000 Btu/hr, 50,300 EDR, 362 bhp). This value appears to be capable of supplying the heating requirements.

2.3 Plant Operation

The power cycle is composed of two main systems, the primary coolant and the secondary steam systems. Associated with these are the auxiliary systems for the primary coolant make-up, the pressurizer, the building heating, the condenser coolant, and for the boiler water make-up. A flow diagram of the entire reactor power cycle is shown in Fig. 1. The reactor vessel, primary coolant system, and secondary system are shown in a photograph of a model of the plant, Fig. 2.

Water circulating through the primary coolant system, Figs. 3-5, serves to transfer heat from the reactor core to the main heat exchanger where it is transferred to the secondary system. Steam generated in the heat exchanger drives the turbogenerator and also provides heat for building heating. The primary system consists of the following major items of equipment: the reactor pressure vessel, the pressurizer tank, two canned-rotor circulating pumps with their associated check valves, the demineralizer, a storage tank for make-up water, two filters, two make-up water pumps, and two seal pumps.

The secondary system, Figs. 6-9, consists of the following items: the turbogenerator with its associated condenser and condenser cooling system, the heating system condensate return unit, a steam-jet air ejector, two hot-well pumps, a deaerating feed-water heater and storage tank, two feed-water pumps, and the evaporator. The main heat exchanger is a component of both systems, the primary coolant passing through the tube side and steam being generated in the shell side.

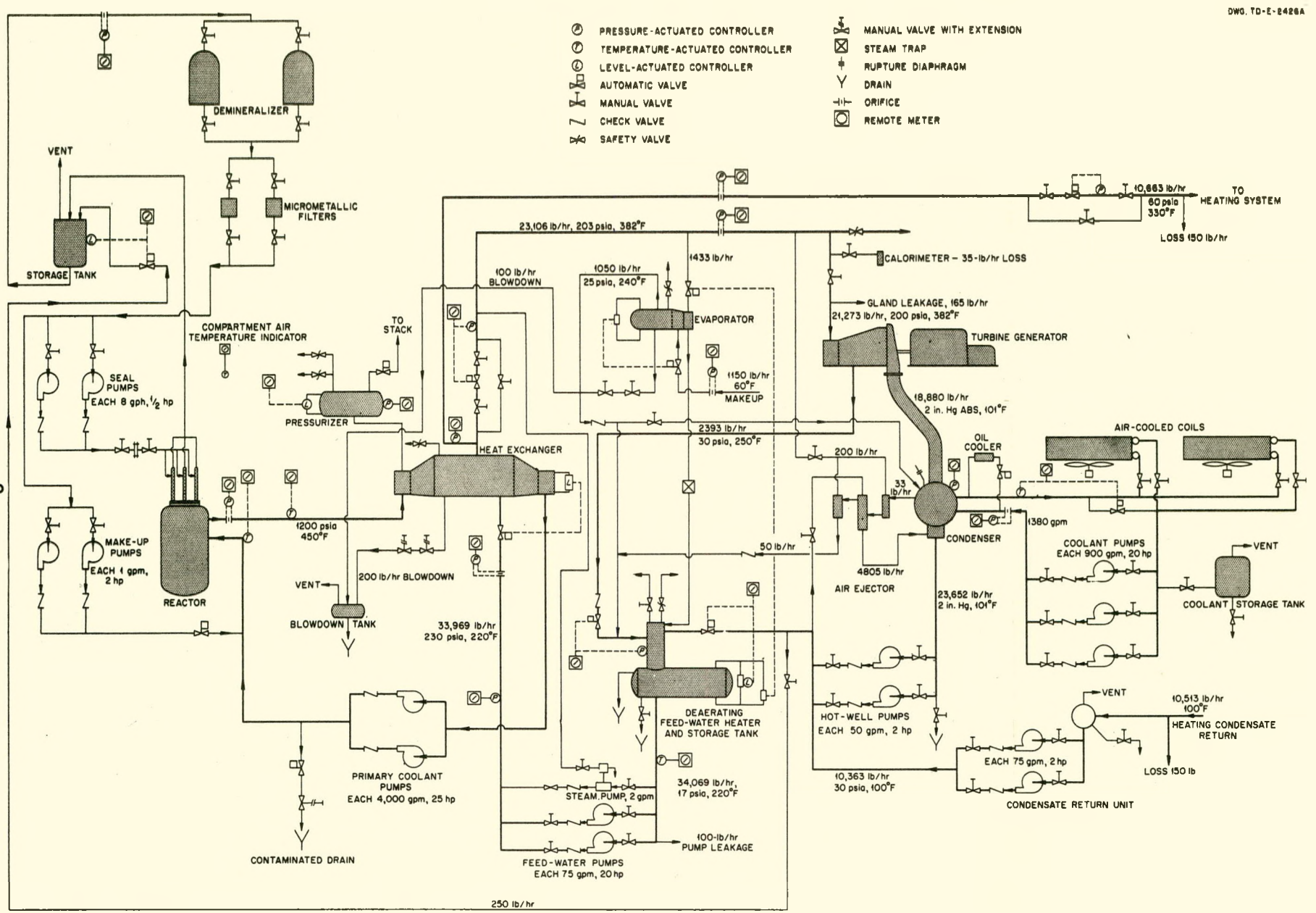

Fig. 1. Flow Diagram.

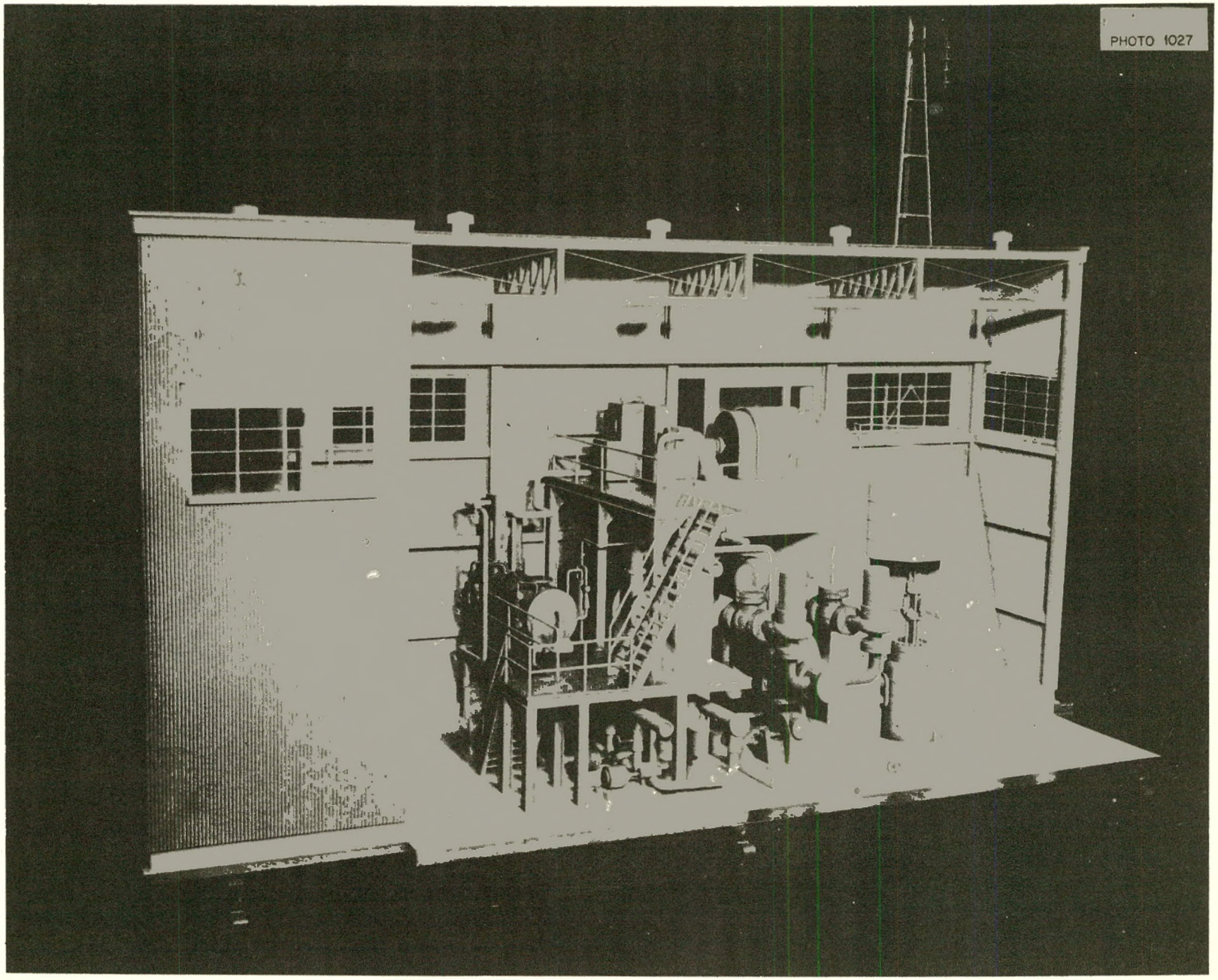

Fig. 2. Model of Package Power Plant.

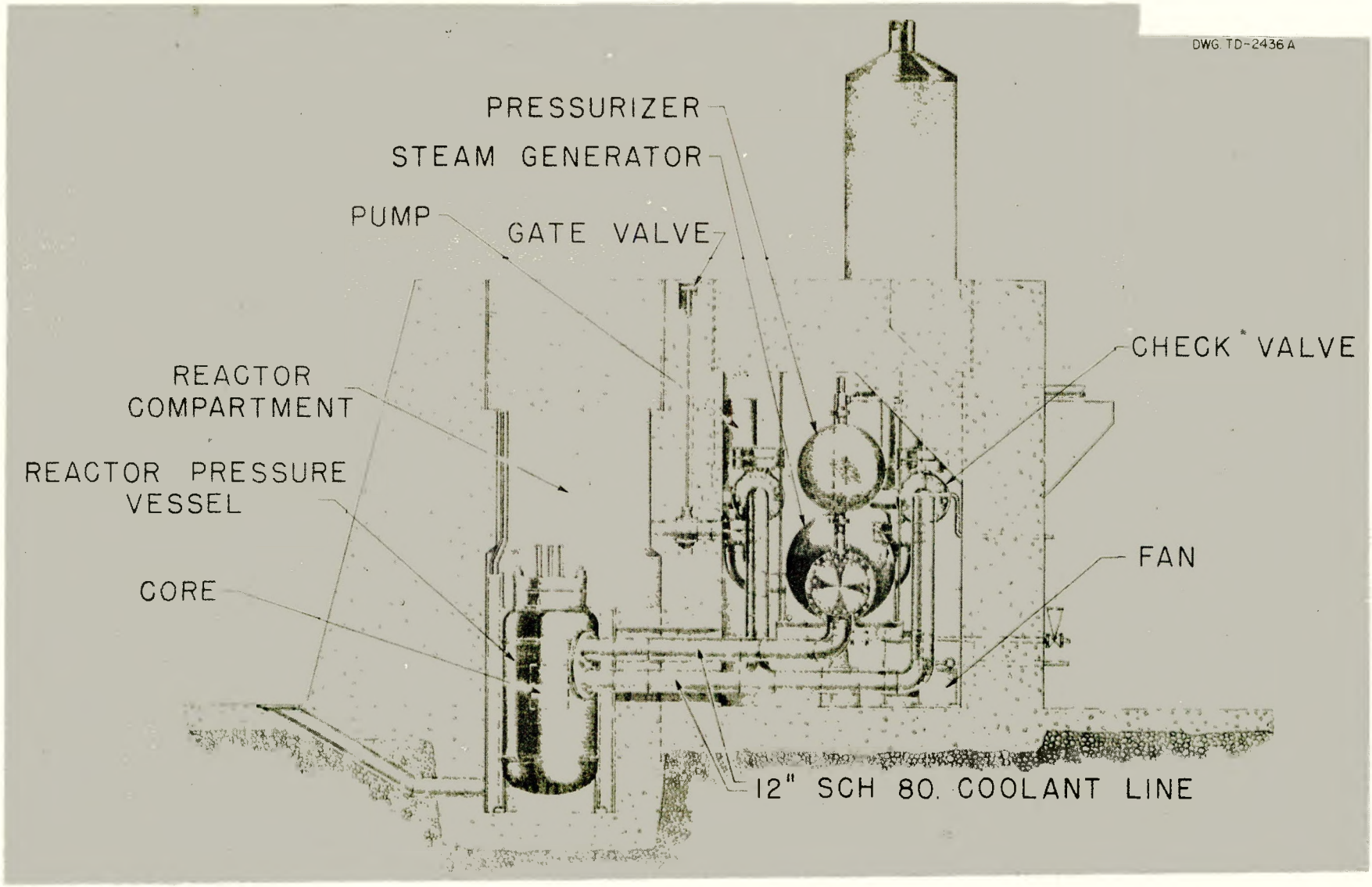

Fig. 3. Primary Coolant System, Equipment Layout, Vertical Section.

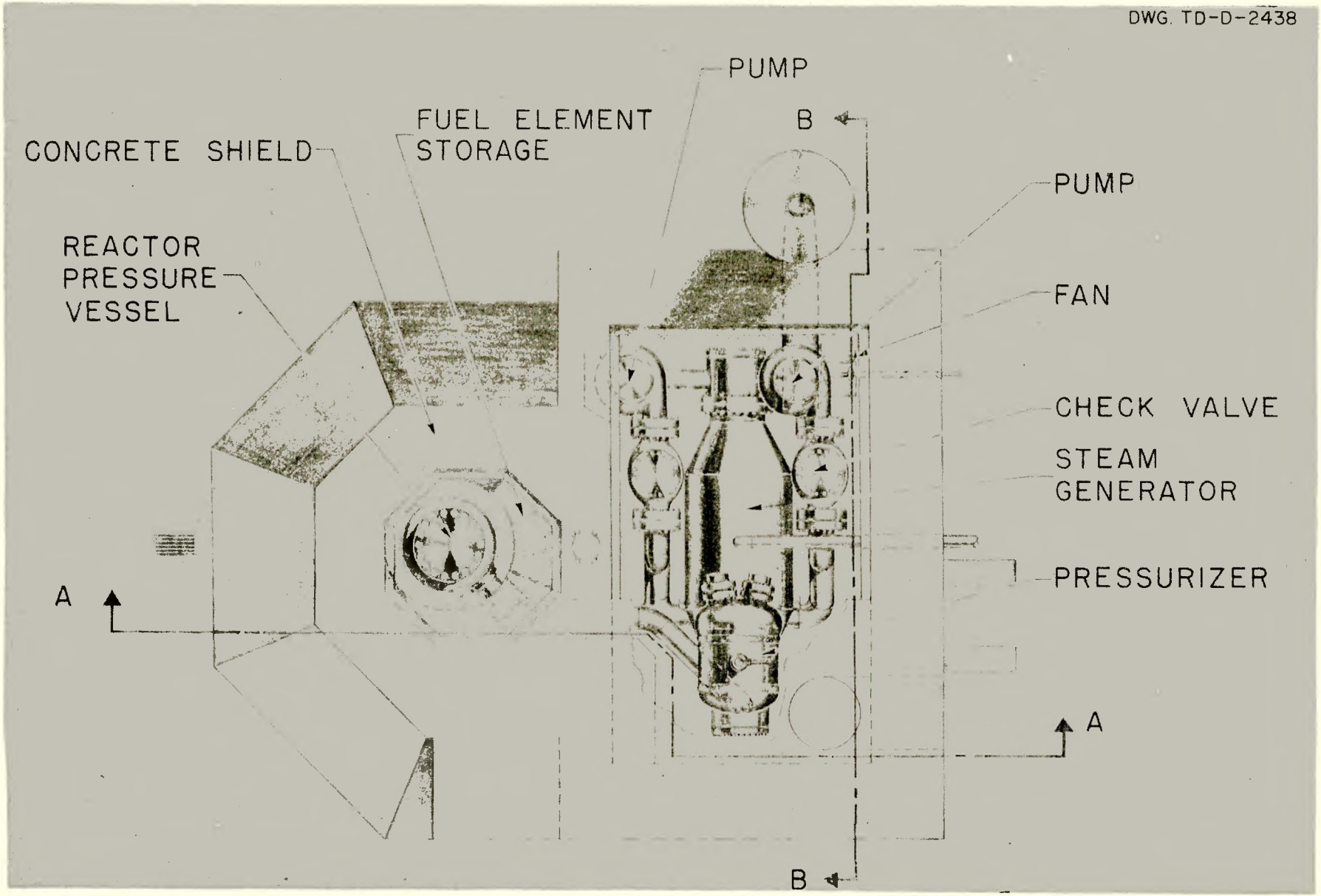

Fig. 4. Primary Coolant System, Equipment Layout, Plan View.

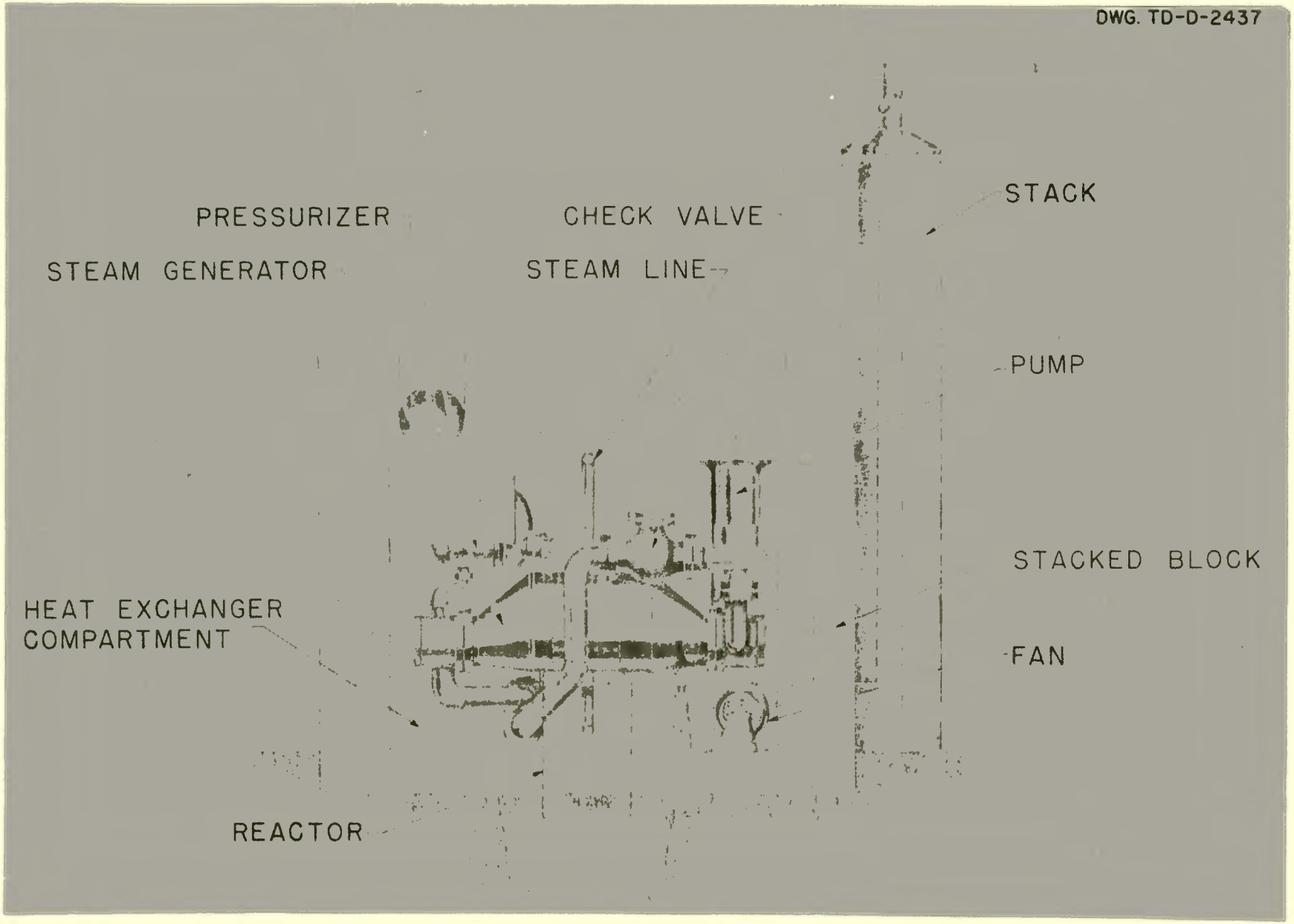

Fig. 5. Primary Coolant System, Heat Exchanger Compartment.

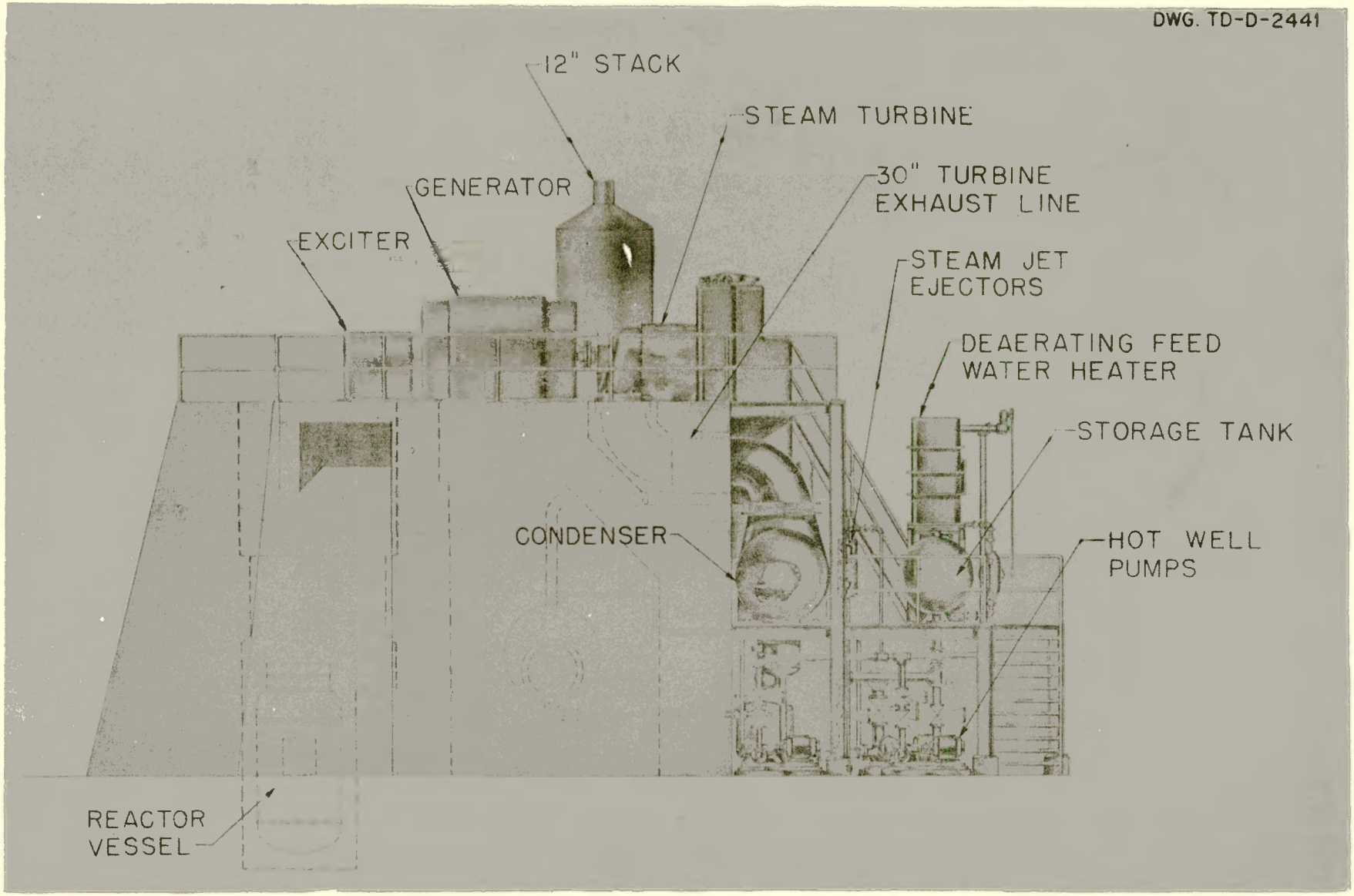

Fig. 6. Steam and Auxiliary Equipment, Side Elevation.

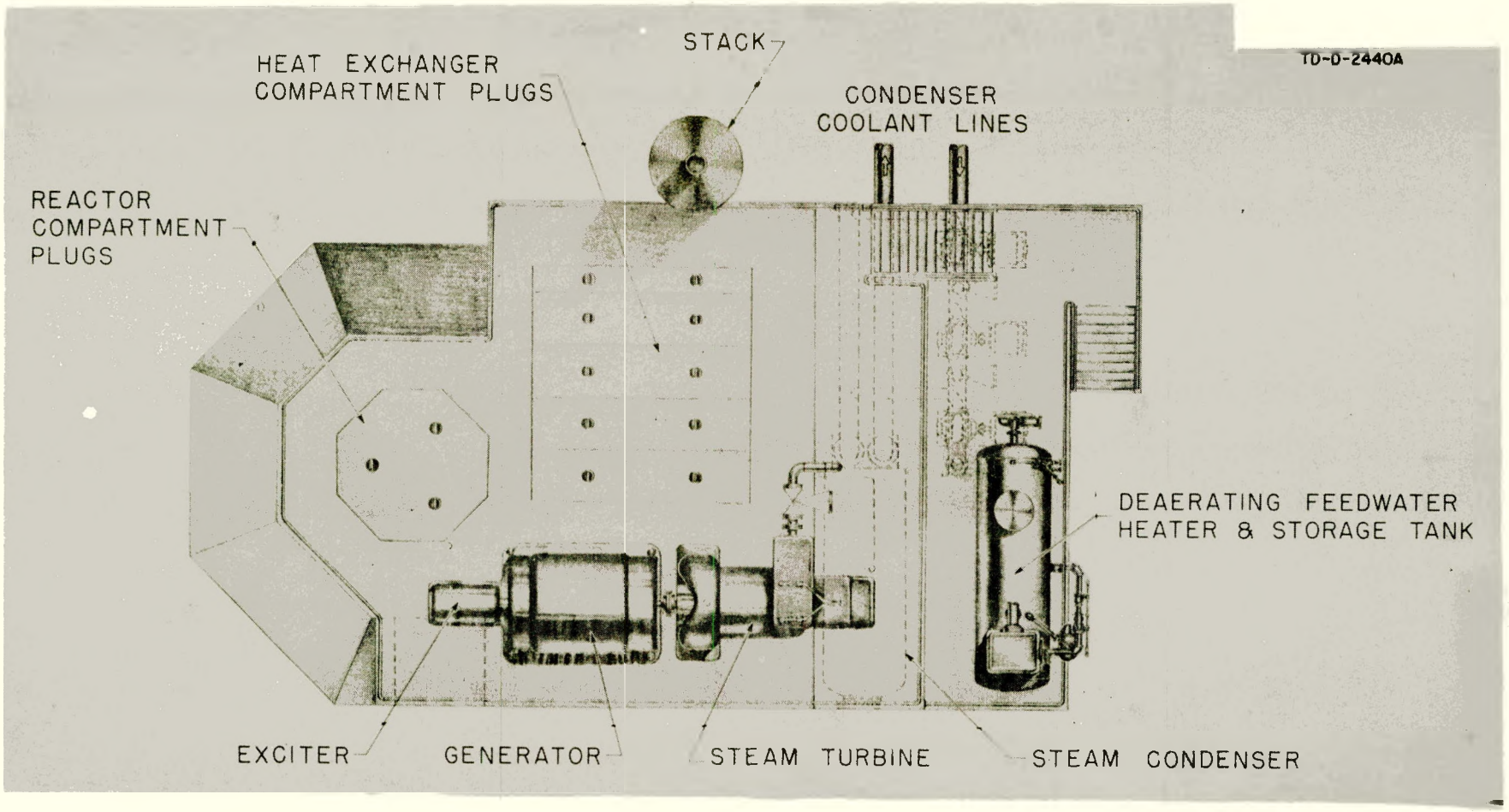

Fig. 7. Steam And Auxiliary Equipment Layout, Plan View.

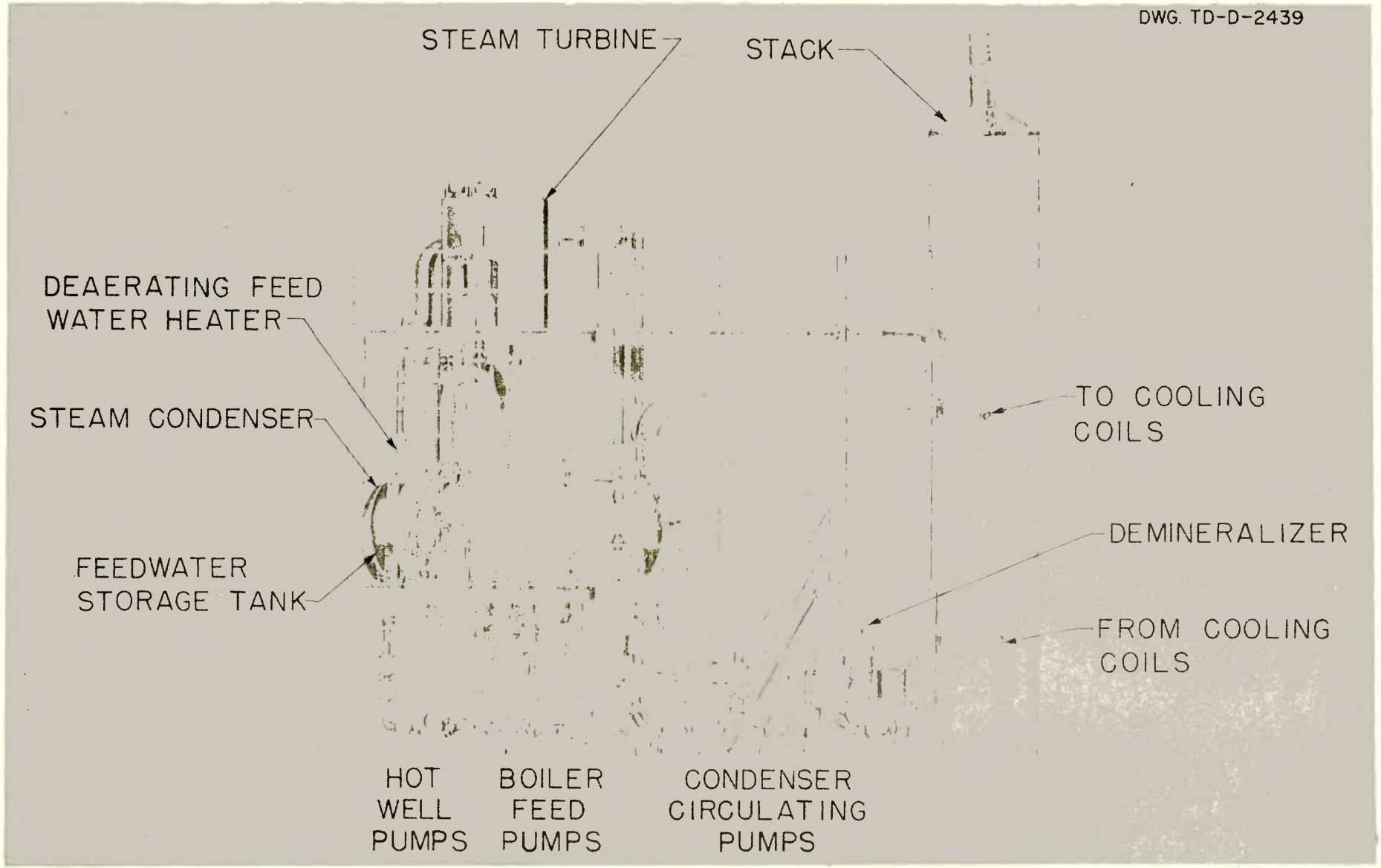

Fig. 8. Steam and Auxiliary Equipment, End Elevation.

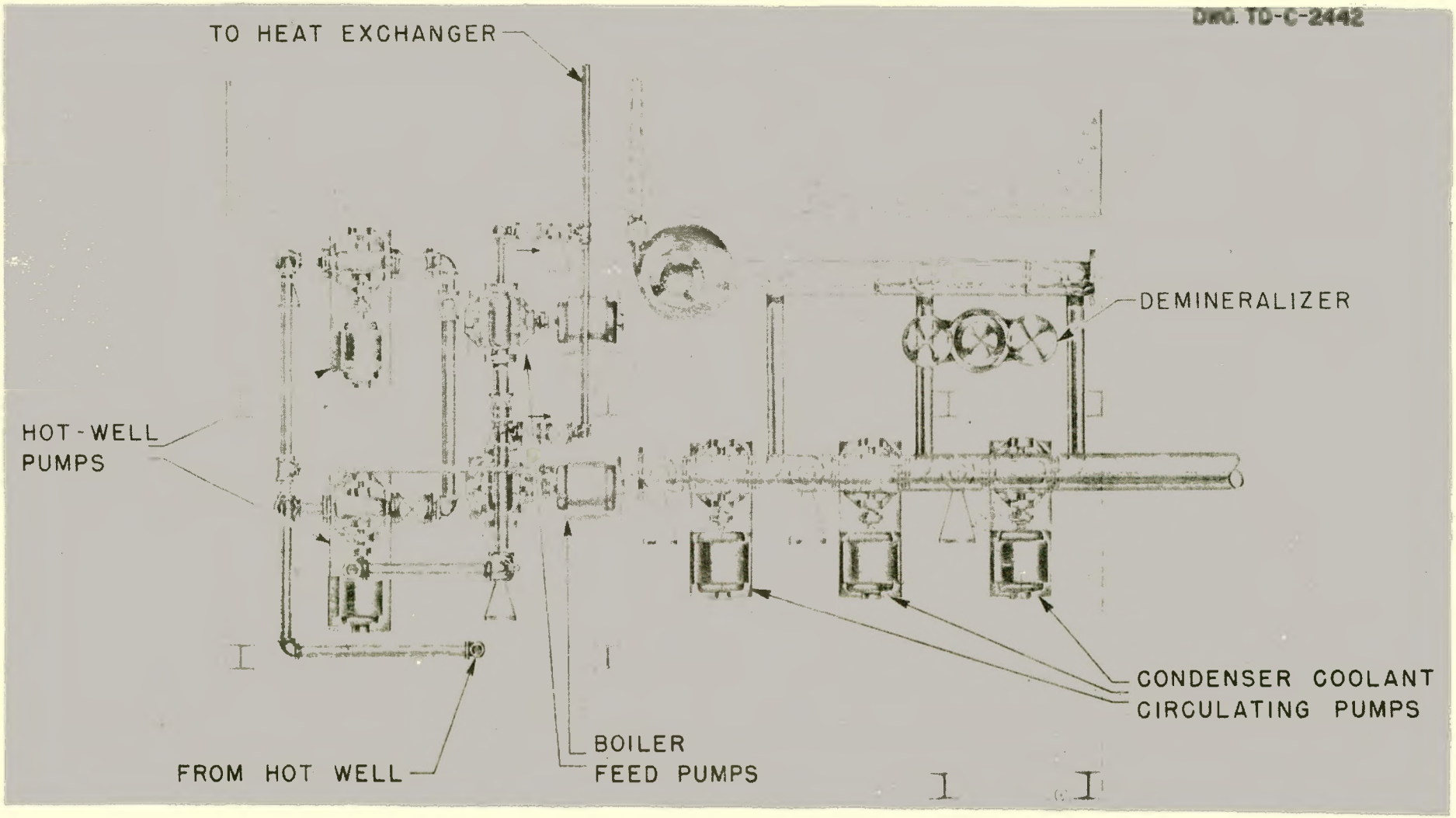

Fig. 9. Auxiliary Pump Layout.

Water for the primary system is obtained by periodically transferring a portion of the condensate from the steam cycle to a small make-up storage tank. A fixed amount of water is bled continuously from the primary coolant system and discarded in order to maintain a low concentration of corrosion products in the system. To replace this, an equal amount of water from the make-up storage tank is passed through the demineralizer unit and filters and then injected into the primary coolant cycle by the make-up pumps. The hot primary coolant leaves the reactor core at the rate of 4000 gpm at 450°F, passes through the tube side of the main heat exchanger where heat is transferred to the steam cycle, and is returned to the reactor by the primary coolant circulating pumps. An electrically heated pressurizer attached to the high point of the system maintains a pressure of 1200 psi and thus prevents boiling in the pressure vessel.

Raw water for make-up in the steam cycle is converted to steam in the evaporator; in the deaerator this steam is combined with and helps heat the feed water before it enters the heat exchanger. Steam generated in the main heat exchanger passes through the turbine and is condensed in the turbine condenser. The condensate is then returned to the deaerating feed-water heater by the hot-well pumps. Steam is also used to heat the evaporator, and in the steam-jet air ejector which maintains a vacuum in the turbine condenser.

Steam for the building heating load is taken directly from the heat exchanger, in parallel with the turbine load, and passes through a pressure-reducing valve to the building heating system. Condensate from this system is collected in a condensate return unit which consists of a storage tank and two pumps which force the condensate back into the secondary system. Air coolers are provided to remove heat from the main turbine condenser coolant.

2.4 Design Data

The following is a summary of design data on the pressurized-water reactor. More complete descriptions of the individual components listed here may be found in subsequent sections of the report, along with some of the design considerations involved.

2.4.1 Overall Plant Performance

Thermal power developed in reactor	kw Btu/hr	10,000 34.1×10^6
Electric power generated	kw	1300
Net electric power delivered	kw	1000
Power required for auxiliaries	kw	300
Steam heat load delivered	kw Btu/hr	3535 12×10^6
Overall thermal efficiency	%	45.4
Thermal efficiency of net electric power generation	%	15.5
Power density of reactor core	kw/liter	71.7
Core life before refueling	Mw-yr	15

2.4.2 Reactor Data

Core

Average diameter	in.	22.2
Height	in.	22.0
Volume of core	liters cu in.	139.5 8513
Uranium content of new core (93.5% U 235)	kg kg U 235	18.9 17.7
Critical mass after 15 Mw-yrs	kg U 235	10.2

Core (cont.)

Stainless steel content, excluding matrix	kg	110.06
Stainless steel content in matrix	kg	98.04
Poison content, natural boron	kg	0.172
B_4C content	kg	0.220
UO_2 content (1.136 kg/kg U)	kg	21.47
Water content,	liters	111.1
at 0.83 g/cm^3 (450°F)	kg	92.2
at 1.0 g/cm^3 (70° F)	kg	111.1
Metal-to-water ratio		0.256
Excess reactivity, new, cold, clean core	%	10
Maximum reactivity during operating period, hot	%	7
cold	%	16
Neutron flux, average, thermal, at end of 15 Mw-yr cycle	n/cm^2-sec	2.7×10^{13}
Reflector thickness (water)	in.	7

Fuel Plates

Type of plates: rectangular, flat, UO_2-ss-B_4C core, clad in 304L stainless steel.

Geometry of plates

		Overall
Thickness	in.	0.030
Width	in.	2.760
Length	in.	23.0
Spacing between plates	in.	0.134

Composition of fuel section of plates

UO_2	wt %	17.94
ss	wt %	81.88
B_4C	wt %	0.18

Fuel Plates (cont.)

Geometry of ss side plates		
Thickness	in.	0.050
Width	in.	2.912
Length	in.	23.0
Atom ratios in reactor core		
U 235	atoms	1
H_2O	molecules	68
Fe, Ni, Cr	atoms	48.4
B	atoms	0.212
Fuel plates per fuel assembly		18
Number of fuel assemblies		40
Fuel plates per control rod assembly		16
Number of control rod assemblies		5
Total number of fuel plates		800
Dimensions of fuel assembly (overall)		
Thickness	in.	2.912
Width	in.	2.800
Length	in.	35 1/4

Control Rods

Type: rectangular, to fit fuel space in lattice, upper section absorber material, lower section fuel sub-assembly.

Composition

Upper section: 16.3% B_4C by wt in Cu, 1/8" thick; clad with 304L ss, 1/32" thick; formed into square.

Lower section: previously described.

Geometry

Upper section: 2.750 x 2.750 x 29 in.

Lower section: 2.750 x 2.750 x 40 in.

Control Rods (cont.)

Number		
Shim rods		4
Regulating rods		1
Travel		
Shim rods	in.	22
Regulating rod	in.	22
Weight of rods	lb	60
Acceleration of rods after release	ft/sec^2	32.2
Maximum distance for rods to drop	in.	22

Thermal Data of Reactor at Full Power (10,000 kw)

Operating pressure in reactor	psia	1200
Coolant inlet temperature at reactor	°F	431.6
Coolant outlet temperature at reactor	°F	450
Properties of Coolant		
Density at 450°F	lb/ft^3	51.75
at 431.6°F	lb/ft^3	52.60
Change in density per °F	lb/ft^3	0.046
Viscosity at 445°F	lb/ft-hr	0.295
Thermal conductivity	$Btu/hr-ft^2-°F/ft$	0.39
Specific heat	Btu/°F-lb	1.115
Coolant flow through core	gpm	4000
	lb/hr	1.66×10^6
Number of flow passes through reactor		1
Flow area in core	ft^2	2.083
Velocity in core passages	fps	4.3
Design heat output	Btu/hr	34.1×10^6
Heat transfer area	ft^2	611.1
Average heat flux	$Btu/hr-ft^2$	55,900

Thermal Data (cont.)

Peak-to-average heat flux ratio used for design (assumed)*		4:1
Ratio of maximum to average heat flux in any one channel (cosine distribution)		1.31:1
Ratio of heat absorbed in hottest channel to average channel (4.0/1.31)		3.05:1
Maximum bulk water temperature, hottest channel	°F	487.6
Reynolds number in core		58,400
Film coefficient of heat transfer	Btu/hr-ft^2-°F	2,570
Maximum surface temperature	°F	554
Boiling temperature at 1200 psia	°F	567.2
Heat transfer coefficient of scale (assuming 0.010" scale at k = 1.0 Btu/hr-ft^2-°F/ft)	Btu/hr-ft^2-°F	1200
Maximum metal temperature		
with assumed scale	°F	742
with no scale	°F	565.7

Pressure Vessel, ASTM-A-212, clad with 304 ss)

Inside diameter	in.	48
Wall thickness	in.	2.25
Thickness of cladding, min	in.	0.125
Design stress	psi	17,000
Overall length of vessel	in.	110 1/4
Thickness of head	in.	7
Diameter of head	in.	40
Diameter of opening at top of vessel	in.	28

* Actual peak-to-average flux ratio not available at this time.

Pressure Vessel (cont.)

Inside diameter of thermal shield	in.	34 7/8
Thickness of thermal shield	in.	2
Length of thermal shield	in.	31 3/8
Insulation (Foamglas) thickness	in.	4

2.4.3 Primary Coolant System

Primary Coolant Pumps, centrifugal, canned rotor

Operating head of pump	ft	22.4
Operating temperature at suction	°F	431.6
Hydraulic horsepower at 4000 gpm, hot	hp	18.8
cold	hp	22.25
Number of pumps normally operated		1
Number of pumps installed		2

Steam Generator, single pass, horizontal shell and tube

Tube side fluid: primary coolant
Shell side fluid: boiling water

Materials
Tubes, tube sheets, and headers: 304 ss
Shell: ASTM-A-212

Design pressures		
Tube side	psi	1200
Shell side	psi	500
Design temperatures, full load		
Tube side	°F	431.6-450
Shell side	°F	450
Operating pressures		
Tube side	psia	1200
Shell side	psia	200-422
Full load heat transfer	Btu/hr	3.41×10^7
Heat transfer surface	ft^2	1190

Steam Generator (cont.)		
Number of tubes		505
Diameter of tubes, OD	in.	0.75
Tube wall thickness	in.	0.065
Effective length of tubes	ft	12
Velocity in tubes	fps	8.4
Reynolds number in tubes		275,400
Film coefficient in tubes	Btu/hr-ft^2-°F	3710
Scale coefficient inside tubes	Btu/hr-ft^2-°F	4000
Scale coefficient outside tubes	Btu/hr-ft^2-°F	2000
Conductivity of tube wall	Btu/hr-ft^2-°F/in.	130
Wall coefficient	Btu/hr-ft^2-°F	2000
Overall heat transfer coefficient	Btu/hr-ft^2-°F	482
Total head loss on tube side	ft of fluid	8.1
Full load steam flow	lb/hr	33,780
Feed water temperature	°F	220
Steam quality at exit	%	99.7
Steam pressure at full load	psia	200
Insulation (Foamglas) thickness	in.	4
Pressurizer, SA 212 carbon steel clad with 304 ss		1
Length	in.	56
Diameter, ID	in.	40
Wall thickness	in.	1 7/8
Heaters (two)	kw	50
Insulation (Foamglas) thickness	in.	4
Design pressure	psi	1200
Design temperature	°F	567
Pipe size, schedule 80	in.	6

Primary Coolant Piping, 304 ss

Pipe size, Schedule 80	in.	12
Diameter, OD	in.	12.75
Wall thickness	in.	0.687
Diameter, ID	in.	11.376
Maximum allowable internal pressure (ASA B31.1-1951)	psi	1500
Insulation (Foamglas) thickness	in.	4

2.4.4 Control-Rod Drive Mechanism

Total travel	in.	22
Rod speed, in either direction	fpm	1
Rod acceleration during scram	ft/sec^2	32
Fineness of position control	in.	0.02

Motor: Diehl SSZP 105-2212-1, servomotor, 200 watts 115 volts, 2 phase, 2 poles, 60 cycle, 1700 rpm, stall torque - 190 in.-oz

Clutch: Warner 500 size, 1-25052, 5-watt power rating.

Capacity at 3500 rpm	ft-lb	25
at 0 rpm	ft-lb	50
Time to release	millisec	30-75

Reduction gearing:

Worm, single thread	pitch	24
Worm wheel, 132 teeth	pitch	24
Spur gearing, 0.5" face width	pitch	16
Set #1	teeth	16, 48
Set #2	teeth	24, 48

Seal: spindle type rotary (Kuchler-Huhn Co.)

Leakage	lb/hr	10
Operating friction	in.-lb	3
Maximum break-away friction	in.-lb	12

Guide bushings, K-monel
Floating ring, Stellite-3
Shaft, 410 ss, chrome-plated

Rack and latch assembly		
Rack, 440C ss, 0.5" square	pitch	16
Pinion, 440C ss, 32 teeth, 0.375" face width	pitch	16
Speed	rpm	2.2
Rack back-up rollers		
Bracket, 304 ss		1
Rollers, Stellite-3		2
Roller pins, Stellite-12		2
Latch spring, Elgiloy		1
Indication: Helipot, AN type	turns	10

2.4.5 Water Purification System, single column, mixed bed

Capacity	gph	50
Effluent purity	ppm	1
Overall dimensions	in.	24 x 36 x 120
Approximate weight	lb	700
Chemical regenerants required per cycle (120 days)		
Cation	lb	17
Anion, caustic	lb	9

Primary Coolant Feed Pump, Triplex

Capacity	gpm	1
Discharge pressure	psia	1250
Motor size	hp	2
Number required for operation		1
Number to be installed		2

Control-Rod Seal Pumps

Capacity	gph	8
Discharge pressure	psia	1250
Motor size	hp	1/2
Number required for operation		1
Number to be installed		2

2.4.6 Shield, ordinary concrete

Density	g/cm^3	2.33
Tolerance dose for 56-hr week	mrep/hr	5.36
Thickness of concrete required around reactor vessel operating at 10 Mw:		
For 1/10 of tolerance dose rate	ft	9.5
For tolerance dose rate	ft	8.5
For ten times tolerance dose rate	ft	7.6
Thickness of concrete required around steam generator compartment when operating at 10 Mw:		
For tolerance	ft	3.8
Thickness of concrete required above reactor vessel operating at 10 Mw:		
For 1/10 tolerance	ft	7.9
For tolerance	ft	6.9
For ten times tolerance	ft	5.8
Dose rate one hour after shutdown at top of reactor well with plugs and lid removed and well flooded (14 ft of water over core)	mrep/hr	7.5
Total volume of concrete in shield	cu yd	500
Weight of shield	tons	957
Average foundation load at base of shield	lb/ft^2	2300
Design tolerances in multiples of 5.36 mr/hr		
Top of shield		1
Side toward control room		0.1
Side away from control room		10
End toward service area		1
End away from service area		10

Shield Ventilation

Heat to be removed from inside of shield	Btu/hr	500,000
Air temperature leaving shield	°F	150
Density of air	lb/ft^3	0.065
Heat removed by 1 cfm	Btu/hr	141
Total air flow required	cfm	3550

Shield Ventilation (cont.)

Diameter of discharge duct and stack, ID	in.	12
Height of stack	ft	100
Friction pressure drop	in. water	3
Fan size, diameter of wheel	in	26
Fan speed	rpm	998
Fan horsepower	hp	3
Weight of fan without drive motor	lb	540
Type of fan: New York Blower Co. Type 26 GI or equivalent, clockwise rotation, top horizontal discharge		

2.4.7 Steam System

Turbogenerator, straight, condensing, geared drive		1
Steam to throttle, saturated	psia	192
Exhaust pressure, abs	in. Hg	2
Rating, at 0.8 power factor	kw	1250
Voltage	volts	4160
Frequency	cps	60
Exciter - direct-connected		
Generator - open-air cooled		
Extraction nozzle, at 2500 lb/hr	psia	30
Steam to throttle, full load	lb/hr	~23,000
Turbine efficiency, full load	%	~65.5
Generator efficiency, full load	%	~94.1
Gear, bearings, and windage efficiency	%	~98.5
Automatic controls: frequency, voltage		

2.4.7 Steam System (cont.)

Safety devices: overspeed, low vacuum, vacuum breaker		
Exhaust quality, full load	%	~85.5
Condenser, horizontal, shell and tube, two-pass		1
Heat transfer	Btu/hr	20.5×10^6
Steam flow, max	lb/hr	~22,000
Hot well depression, max	°F	10
Coolant temperature, in, max	°F	95
Effective surface	ft^2	~1200
Velocity in tubes	fps	7.2
Quality of steam	%	85
Tubes (18 gage), diameter, OD	in.	3/4
Shell test pressure	psi	45
Coolant, summer: water winter: ethylene glycol solution		
Coolant circulation		
Water	gpm	1400
Ethylene glycol solution	gpm	1630
Ethylene glycol		
Specific gravity		1.08
Specific heat	Btu/lb-°F	0.70
Composition, ethylene glycol	wt %	60
water	wt %	40
Viscosity	millipoises	45
Air removal equipment Twin jet steam ejectors with intercooler.		
Liquid Coolers, horizontal, air-cooled		2
Heat transferred	Btu/hr	20.5×10^6
Liquid circulation rate, water	gpm	1400
ethylene glycol	gpm	1630
Face area, each	ft^2	360

Liquid Coolers (cont.)		
Air flow, each	cfm	240,000
Fan power, each	hp	40
Temperature, liquid in	°F	125
Mean daily maximum air temperature	°F	70
Dimensions, each	ft	23 x 19 x 13
Deaerating Feed-Water Heater, tray-type		1
Storage tank		
Capacity	gal	1000
Supply at full load	min	15
Outflow rate, max	lb/hr	35,000
Operating pressure	psia	18
Outflow temperature	°F	220
Performance, O_2/liter	cc	0.005
Controls: float, overflow, relief, low water alarm, pressure		
Evaporator, bent-tube, self de-scaling		1
Raw water inflow	lb/hr	1150
Evaporator blow-down	lb/hr	100
Steam supply pressure, saturated	psia	192
Heating-steam requirement	lb/hr	1435
Purity	ppm	5
Boiler Feed Pumps, two-stage centrifugal		2
Number running at full load		1
Speed	rpm	3500
Capacity, each	gpm	75
Head	ft	500
Water temperature	°F	220
Estimated efficiency	%	45
Rated power, each	hp	20

Hot-Well Pump, single-stage centrifugal		2
Number running at full load		1
Speed	rpm	1750
Capacity, each	gpm	50
Head	ft	75
Water temperature	°F	~91
Estimated efficiency	%	35
Rated power, each	hp	2
Coolant Circulating Pump, single-stage double-entry		3
Number running at full load		2
Fluid: water or 60% ethylene glycol		
Speed	rpm	1750
Capacity, each	gpm	900
Head	ft	75
Fluid temperature	°F	35-95
Estimated efficiency	%	85
Drive motor size, each	hp	20
Condensate Return Pump, single-stage centrifugal with float-control and alternator		2
Number running at full load, 1/3 of time		1
Receiver capacity	gal	100
Pump capacity, each	gpm	75
Water temperature	°F	100
Head	ft	75
Estimated efficiency	%	35
Drive motor size, each	hp	2

Reactor Shutdown Cooling Pump, steam-driven duplex		1
Size	in.	3 x 2 x 3
Speed	strokes/min	18
Capacity	gpm	2
Head	ft	500
Water temperature	°F	220

2.4.8 Power Plant Building

Overall dimensions, main part of building	ft	27 x 82 x 39
Dimensions of control room and storage wing	ft	18 x 42 x 30
Total floor area excluding area occupied by reactor shield	ft^2	~2441
Total volume of building	ft^3	~104,560
Bridge crane span	ft	25
Crane load capacity	tons	10

3.0 REACTOR COMPONENTS

In a thermal nuclear reactor the production of energy is accomplished by assembling the fissionable material in conjunction with a moderator and a reflector in such a manner as to produce a sustained chain reaction when the number of neutrons produced in the fission process just equals those lost by escape and by capture. The term "reactor" generally refers to the entire assembly while "core" is used for the active portion containing the fissionable material and moderator.

In the heterogeneous reactor considered in this report neutrons are reduced to thermal energies by a water moderator; the water also serves as the reflector and the heat transfer medium. Stainless steel-clad fuel plates containing highly enriched U 235 in the form of UO_2 are used in the core. The fuel plates

are supported by a framework attached to the cylindrical reactor vessel. The water flowing through the lattice arrangement of the fuel plates while the reactor is in operation serves as the moderator; the water in the space between the active core section and the reactor vessel wall acts as the reflector.

3.1 Reactor Core Assembly

The fuel assemblies, control rods, and their supporting structure make up the reactor core assembly; there are 40 fuel assemblies and five control rods. The arrangement of these units into a lattice with a supporting structure can best be seen by referring to Figs. 10-12. It can be seen that the end fittings of the fuel assemblies fit into the upper and lower grids of the core assembly. The spring section of the upper fitting allows each assembly

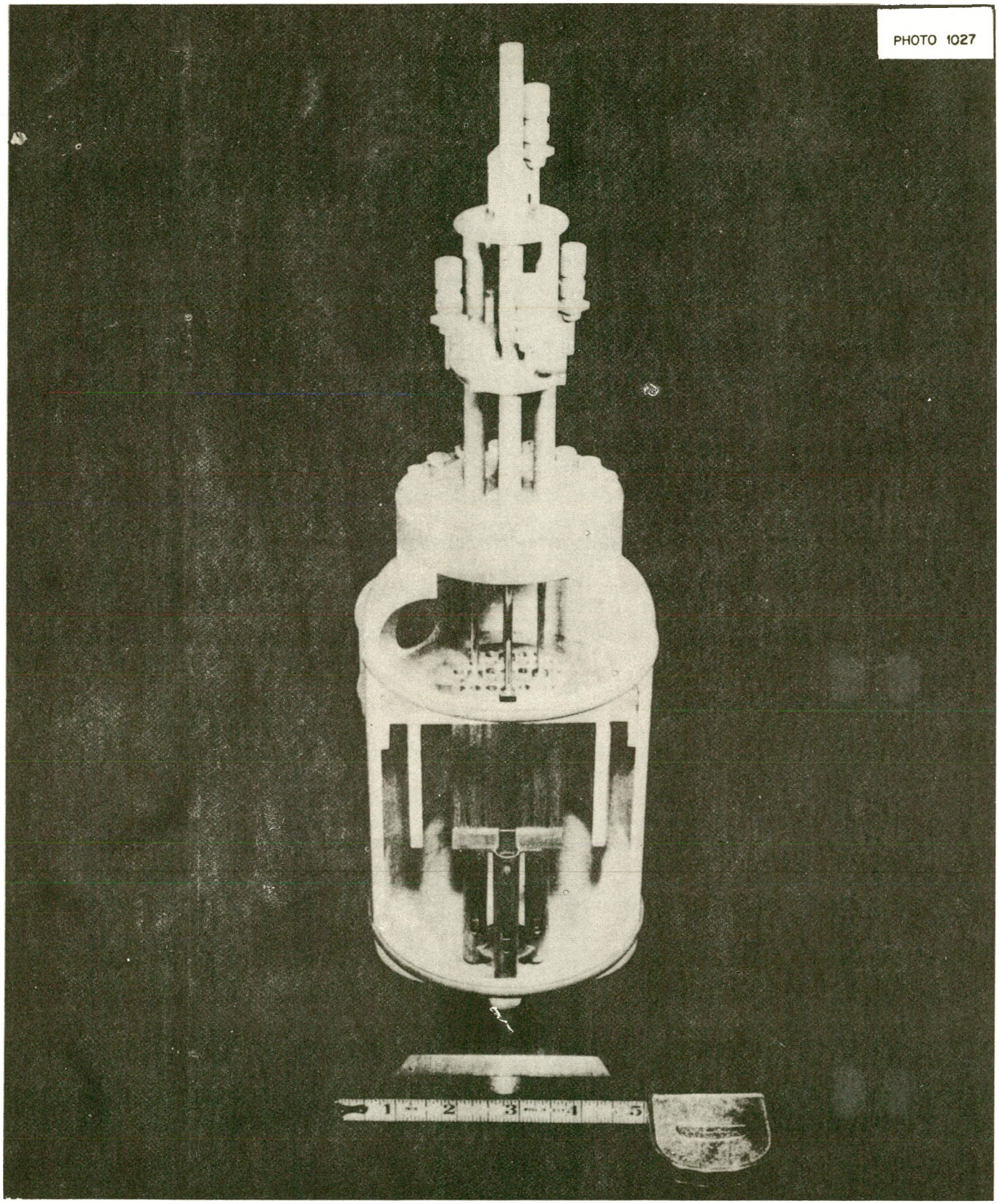

Fig 10 Model of Reactor Vessel and Core

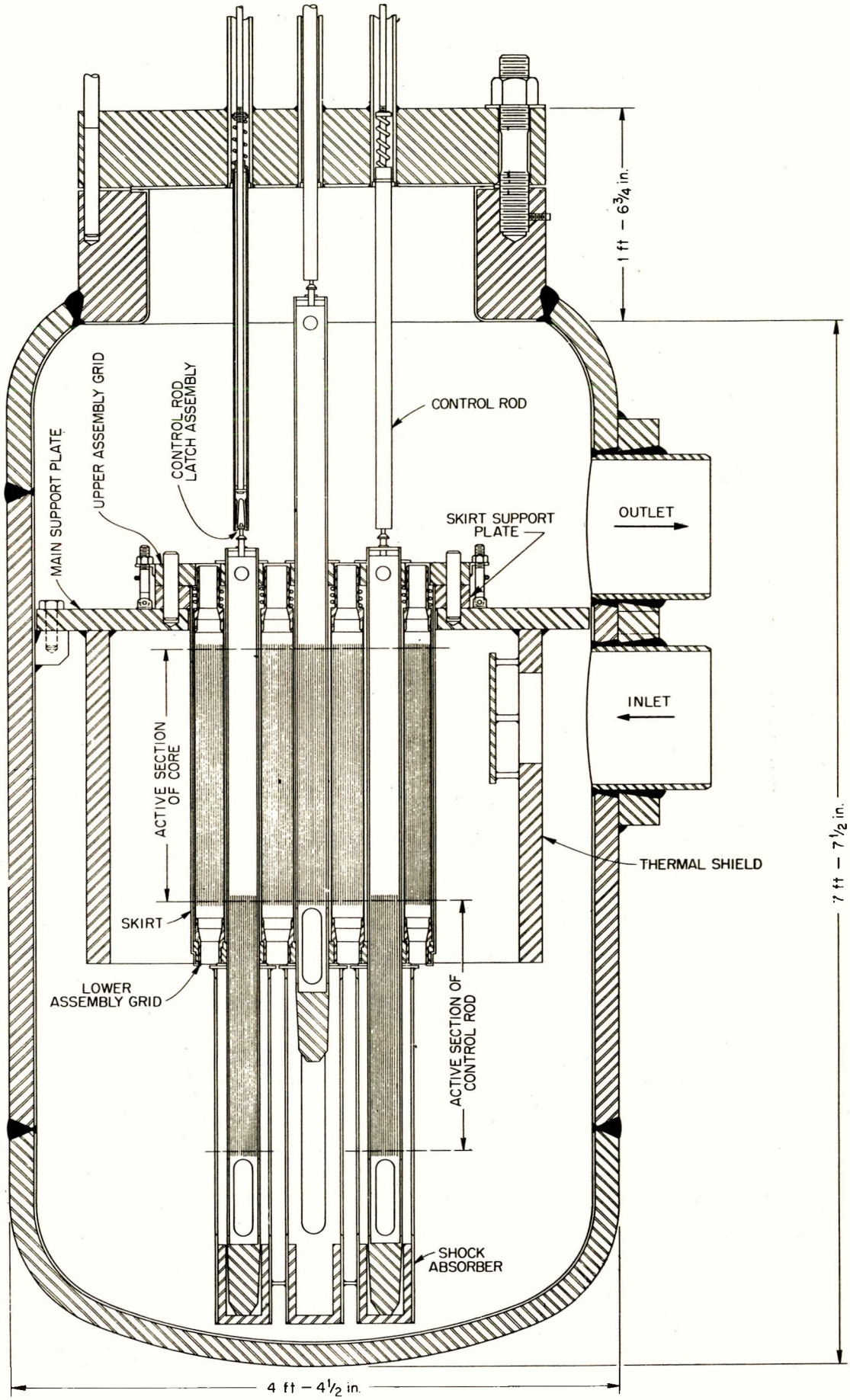

Fig. 11. Reactor Assembly, Vertical Section.

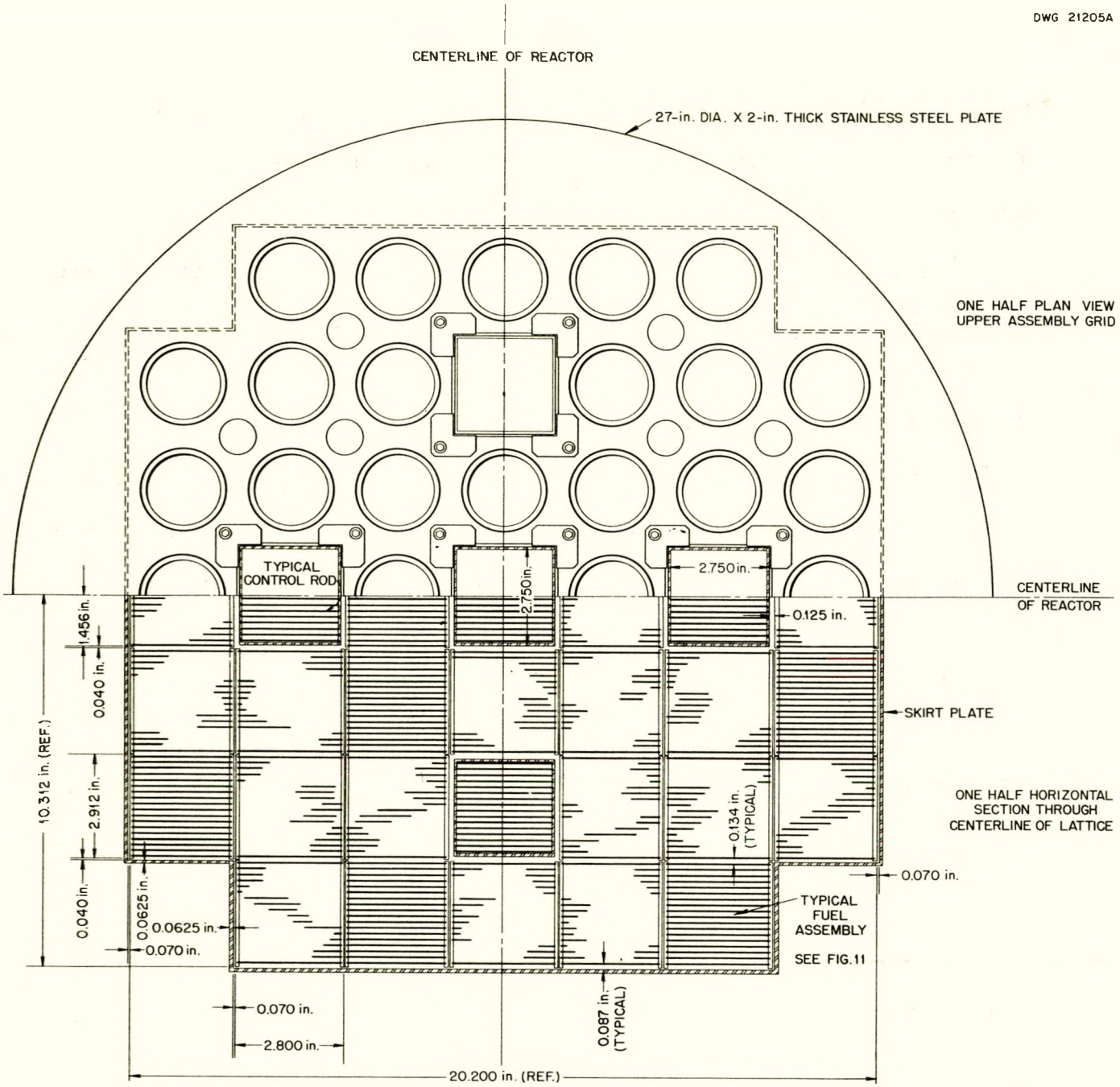

Fig. 12 Reactor Core, Cross Section.

to be held firmly, and still allows for expansion and tolerance limitations. The five square holes in the core assembly grids are for the control rods which extend all the way through the reactor core.

3.1.1 Fuel Assemblies. The reactor is loaded with U-235 fuel enriched to the 93.5% level. The fuel, in the form of uranium dioxide, is incorporated into flat-plate-type fuel assemblies, Fig. 13, which are similar in design to the fuel elements employed in the MTR and STR.

The rectangular fuel plates consist essentially of UO_2 particles uniformly dispersed and imbedded in a matrix of sintered stainless steel powder which is clad on all sides with wrought 304L (low carbon) stainless steel. A small quantity of poison, B_4C, is deliberately added to the fuel mixture to facilitate reactor control.

The core of a fuel plate, when loaded for 15 Mw-yrs, is composed of 17.94 wt % UO_2, 0.18 wt % B_4C, and a matrix of 81.88 wt % sintered stainless steel powder.

Eighteen of these composite plates, each 2.76 in. wide by 23.00 in. long, overall dimensions, are assembled into a single unit which is designated as a fuel element or assembly. The plates with a nominal 0.134 in. water gap space between them are brazed into a pair of stainless steel side plates of 0.050-in. gage thickness. A cross sectional view of the structurally rigid element is shown in Fig. 13. The assembly proper is then equipped on each end with stainless steel castings by plug welding. Each fuel assembly

DWG TD-E-23908

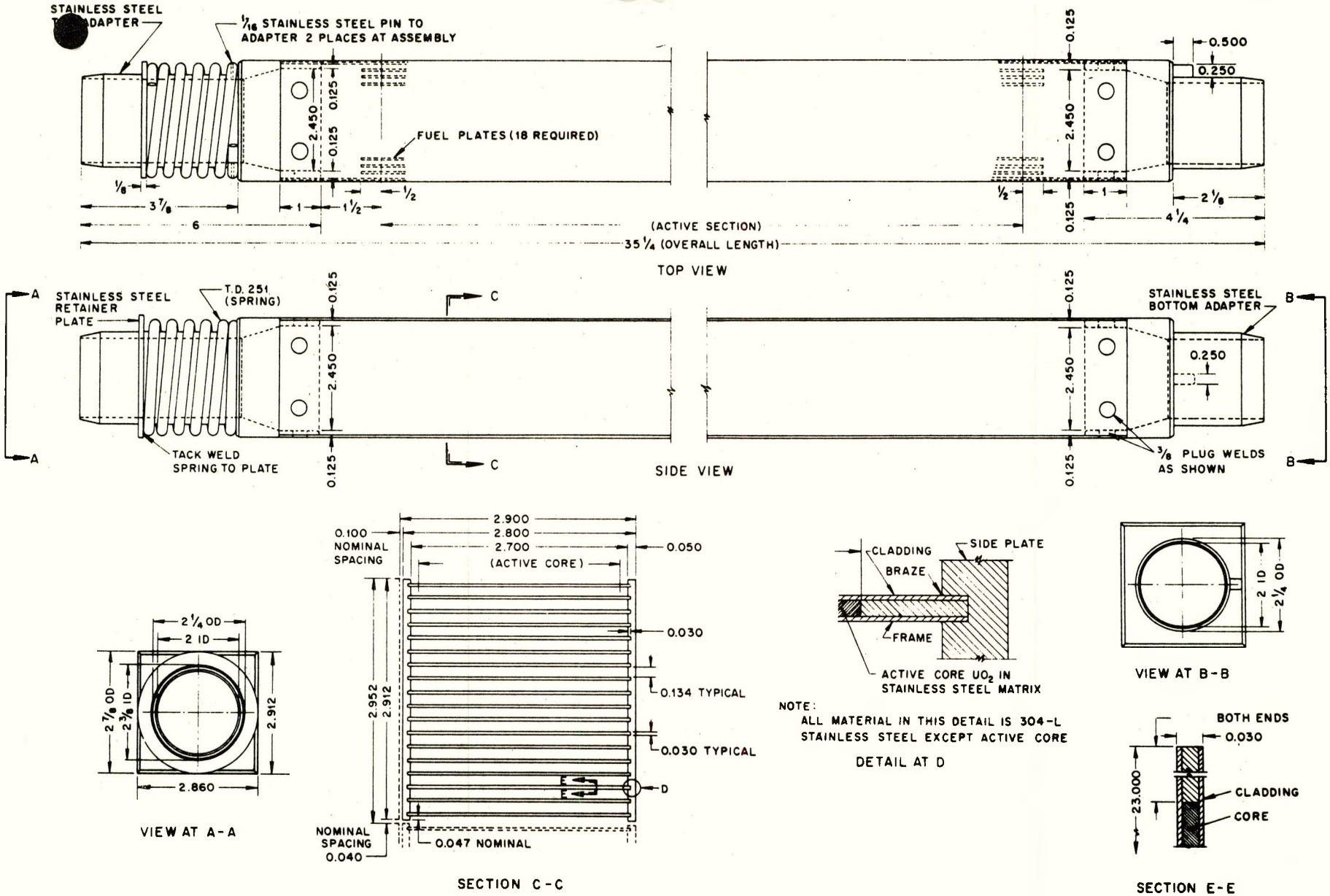

Fig. 13. Fuel Assembly

contains 398 grams of U 235 and 4.95 grams of B_4C; for a 30-Mw-yr loading the figures would be 583 grams of U 235 and 9.61 grams of B_4C.

The purpose of the end fittings is to adapt the unit to the supporting grids which in turn firmly fix the position of the element in the reactor core. A spring is provided on the upper casting to allow for expansion and tolerance limitations. These adaptors also serve as transition pieces which convert the rectangular cross section of the fuel element to the round holes provided in the upper and lower grids; this type of construction greatly simplifies machining of the grid sections. The fittings, of course, are hollow to permit free passage of water through the fuel assembly. The metal-to-water ratio in the active section of the reactor core is 0.27.

The fuel plates are designed to be used in both the fuel assembly and in the fuel section of the shim rod assembly; 0.050 in. of stainless steel is trimmed from the width of the plates to meet the dimensions of the shim rod. Making all plates initially to one specification simplifies fabrication and permits inventory on only one type of plate. The number of fuel plates in both the fuel assemblies and control rods in the reactor core totals 800; they contain 17.7 kg of U 235 for a 15-Mw-yr life, or 26.0 kg for a 30-Mw-yr loading. For more detailed information on the fuel plates refer to Appendix 13.7.

3.1.2. The Control Rods. The reactivity of the reactor is lowered when the control rods are inserted to the "in" position, i.e., resting on their shock absorbers. The rods will overcome the maximum reactivity. The five control rods in the loading are identical, only one rod is used as a regulating rod. The rods are constructed in two segments, jointed by a quick-release connection, Fig. 14. The upper segment contains boron sheet;* this

* Coombs, J. H. and Bomar, E. S., Method of Fabrication of Control and Safety Element Components for the Aircraft and Homogeneous Reactor Components, ORNL-1463.

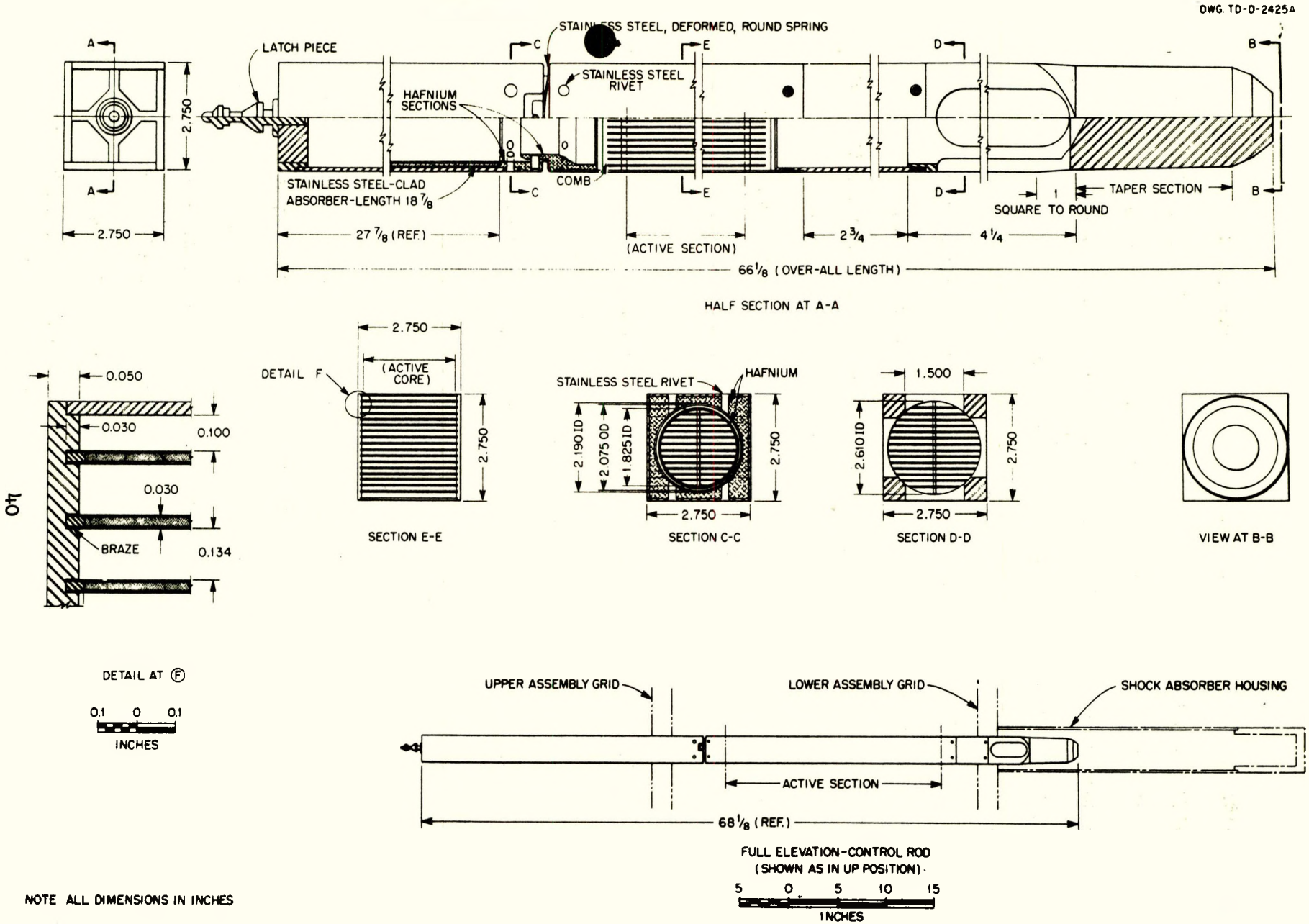

Fig. 14. Control Rod Assembly.

section resides in the lattice when the rod rests in the shock absorbers. The lower segment, containing a fuel element with 16 fuel plates, is raised into the lattice when the control rod is up. The control rods extend from the shock absorber up through the upper assembly grid where they are driven by rack and pinion; a magnetic clutch is released in case of a scram. The control-rod drive mechanism is fully described in Section 3.3.

The segments of the control rod can be uncoupled by rotating the upper segment approximately 30° in relation to the lower segment. This can be accomplished easily while the rod is in the core since, during unloading, the upper assembly grid is removed permitting the upper segment of the control rod to be rotated while the lower segment is contained in the lower assembly grid. The control rod was designed with a quick-release connection for the following reasons:

1. Fabrication and assembly of the rods is simplified.
2. Handling of the rods is easier during reactor unloading. The shielding requirements at the top of the reactor are less rigid during unloading, since the distance that the top of the rod must be raised for removal from the reactor is minimized.
3. One transfer-coffin design is sufficient to handle any of the assemblies in the reactor core.

3.1.3 Grid and Support Structure. The function of the grid and support structure is to position and support the fuel and control assemblies. The structure consists of the skirt support plate, the upper assembly grid, the skirt, the lower assembly grid, and the shock absorbers, Fig. 15. Except for the upper grid, these components are assembled as a unit and lowered into the pressure vessel before the upper section of the vessel is welded into place. A support frame is provided in the pressure vessel to support and hold the core structure in place. The fuel assembly springs are compressed by the

TD-E-2415A

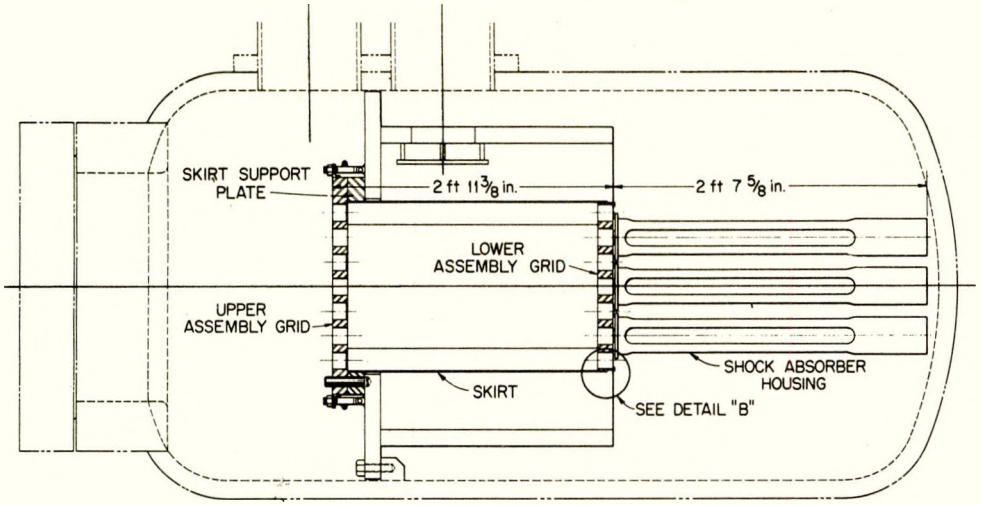

VERTICAL SECTION THRU CENTER LINE OF REACTOR

6 0 6 12 18 24
INCHES

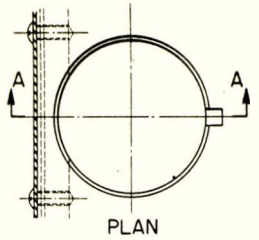

PLAN

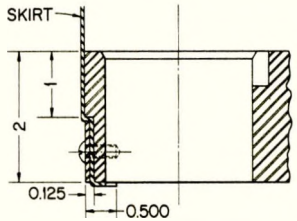

SECTION A-A
DETAIL "B"

0 1
INCHES

NOTE:
DIMENSIONS ARE IN INCHES EXCEPT WHERE OTHERWISE NOTED

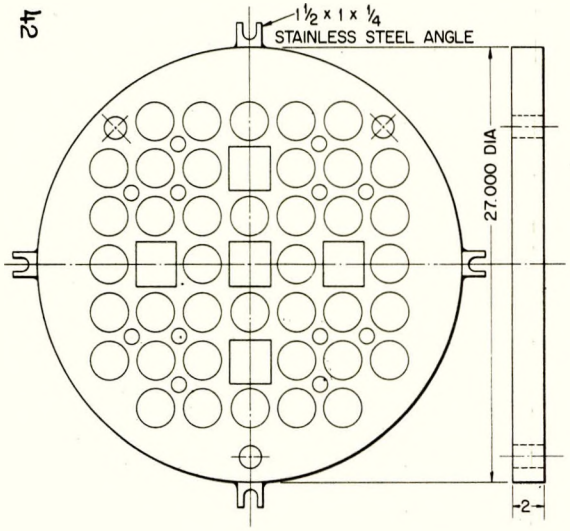

UPPER ASSEMBLY GRID

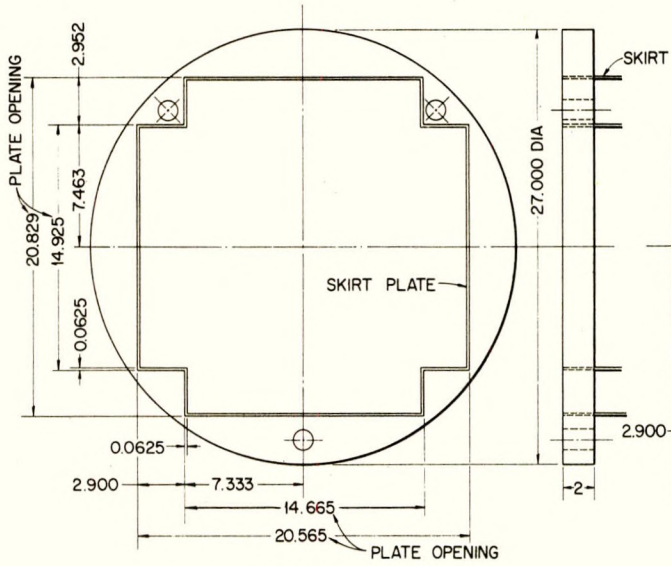

SKIRT SUPPORT PLATE

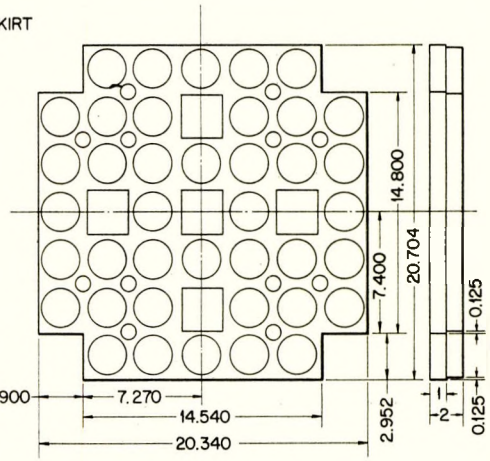

LOWER ASSEMBLY GRID

6 0 6 12 18
INCHES

Fig. 15. Grid and Support Structure.

weight of the upper assembly grid: the assemblies rest on the lower assembly grid. Compression is maintained by bolt latches mounted on the pressure vessel support frame which engage lugs located on the sides of the upper grid.

The grid and support structure also provides bearings and shock absorbers for the control rods; bearings are located in both the upper and lower assembly grids. A bearing assembly, Fig. 16, consists of eight Stellite rollers, two rollers making up one side of a square. The rollers are mounted so as to give a clearance of 1/16". The shock absorbers are simply cylinders which engage the piston-like ends of the control rods and which dissipate the energy of the control rods during a scram or when the rods are driven to their low position. The absorbers are attached to the lower assembly grid and are slotted to insure proper flow of water through the core.

The skirt, which serves the purpose of connecting the upper and lower grids, is made of 1/16" stainless steel sheet. In cross section the skirt is a square with each corner formed in an internal right angle to give added rigidity. The skirt also helps to direct the flow of cooling water through the core.

3.2 Pressure Vessel Design

The reactor pressure vessel was designed according to ASME Standards for Unfired Pressure Vessels, 1952 edition. It has a design pressure of 1250 psi and a design temperature of 650°F. The shell material is ASME Type-SA 212, Grade-B, fire-box quality, boiler-plate steel. This material was selected because of its good welding and mechanical properties.

The vessel is 9 ft 2 1/4 in. high and has a maximum inside diameter of 4 ft, Fig. 17. The cylindrical side wall is 2 1/4 in. thick, including a 125-mil stainless steel cladding, and is welded at the bottom to a standard

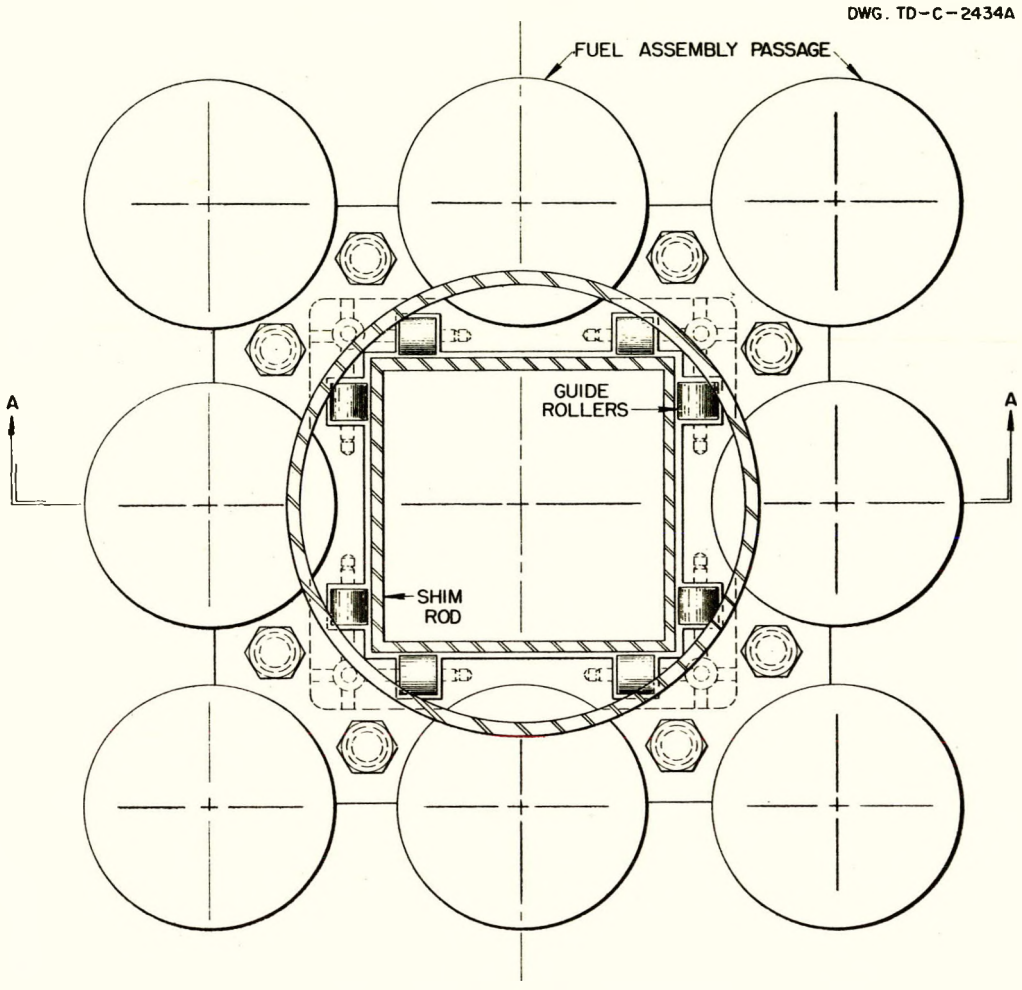

BOTTOM VIEW – LOWER ASSEMBLY GRID

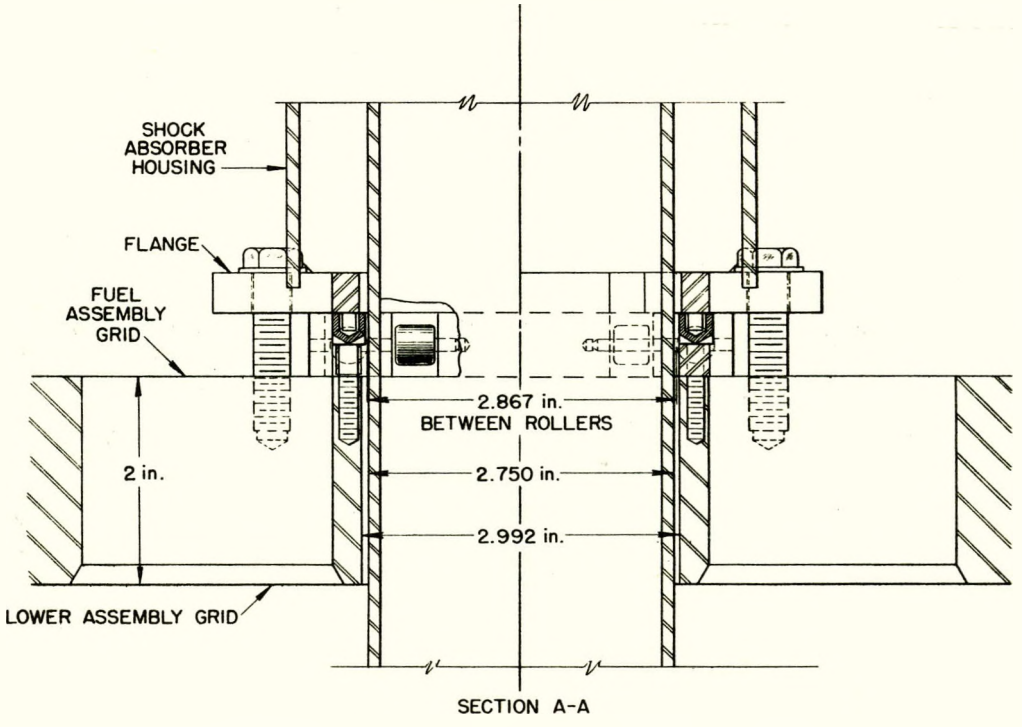

SECTION A-A

Fig. 16 Control Rod Bearing, Lower.

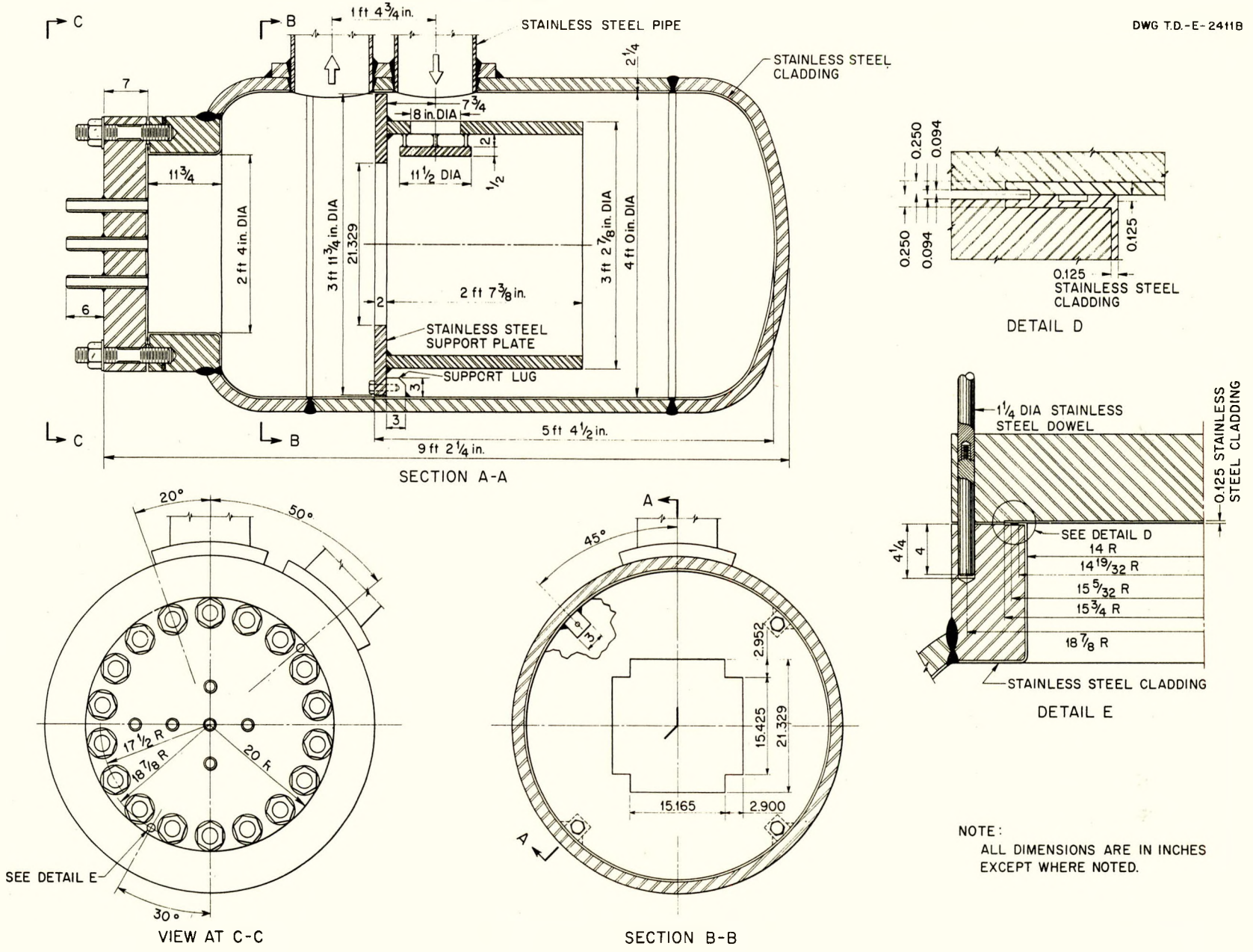

Fig. 17. Pressure Vessel

ASME ellipsoidal head. The cylindrical section is approximately 6 1/2 ft long. The top end of this section is welded to an elliptical head which is, in turn, welded to a 2 ft-4 in.-ID cylinder with a 6-in. wall thickness to provide sufficient area for mounting the studs for attaching the cover plate. Five 1 1/2 in.-diameter stainless steel pipe sleeves are welded into the 7-in. cover plate for mounting the control rod drives. The vessel is to be stress relieved and all weld joints examined by X-ray. The entire surface exposed to the primary coolant is clad with stainless steel, AISI Type 304.

3.2.1 Thermal Shield. The thermal stresses induced by nuclear reactions in the pressure vessel wall were calculated as a function of wall thickness, Fig. 18. After the total stress appeared excessive, a 2-in. thermal shield was included in the geometry and the stresses in the shell opposite the reactor centerline were again calculated, Fig. 19. For operation at 450°F, the 2-in. stainless steel shield reduces the tensile stress in the 2.25-in. vessel wall from 24,000 psi to 17,000 psi. The thermal shield also reduces the thickness of concrete in the radiation shield; the most economical location for a given thickness of thermal shield is adjacent to the reflector.

The cylindrical shield is welded to the upper support plate and extends downward 2 ft 7 1/8 in. from this plate to shield the pressure vessel from the hot core. The support plate and shield are constructed of AISI type 304 stainless steel. An 8-in. diameter baffled opening is placed in juxtaposition to the coolant inlet to permit cooling water to flow downward on either side of the shield before entering the fuel sub-assemblies.

3.2.2 Openings in Pressure Vessel. Two 12-in. Schedule-80 stainless steel pipes are provided in the side of the pressure vessel for the coolant inlet and outlet. The pipes are orientated 45 degrees from one another in the horizontal plane to obtain sufficient welding clearance. In order to

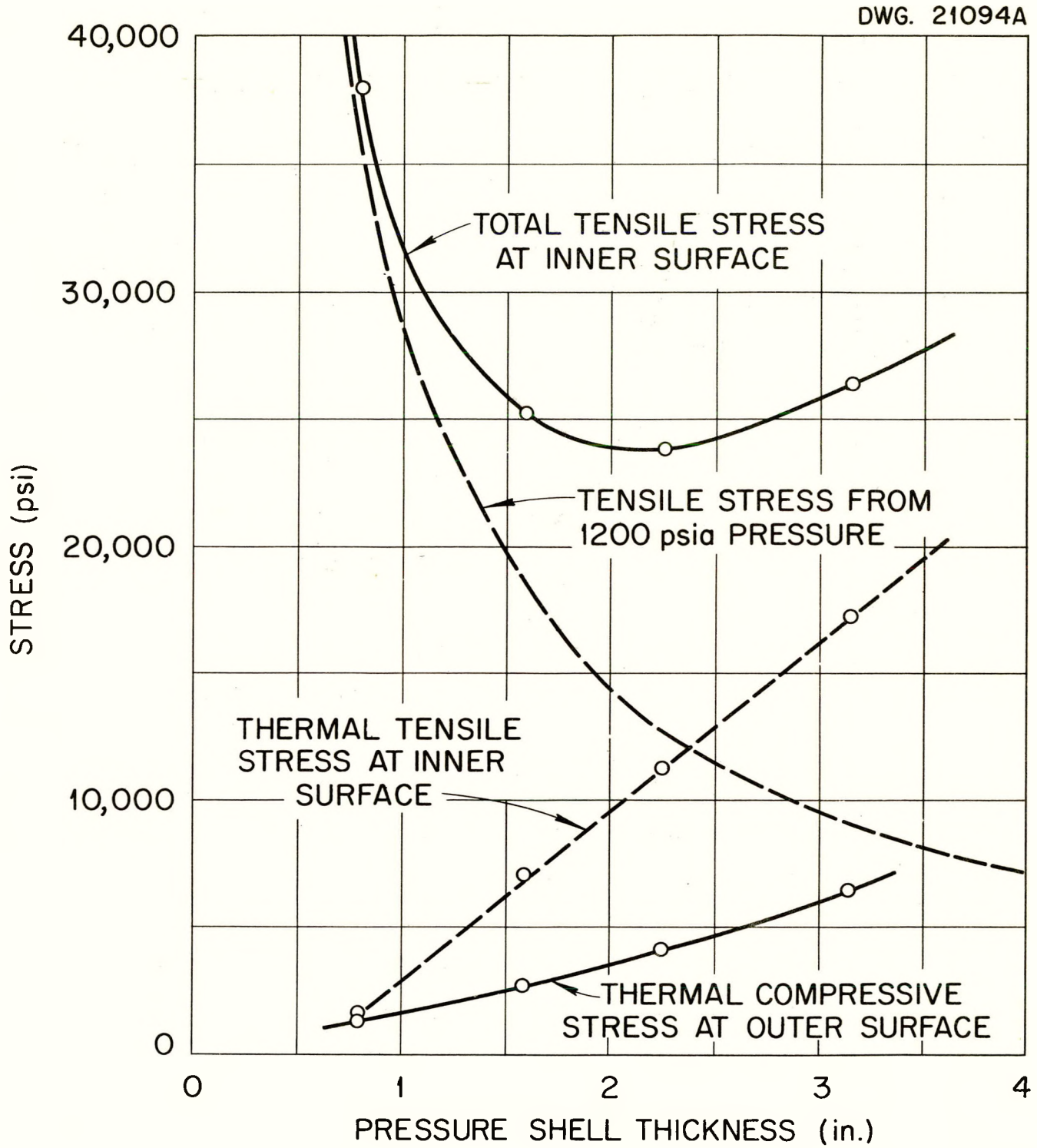

Fig. 18. Stresses in 1200-psia Shells 13 in. from Core; no Thermal Shield; Perfect Insulation at Outside Surface; 10-megawatt Operation.

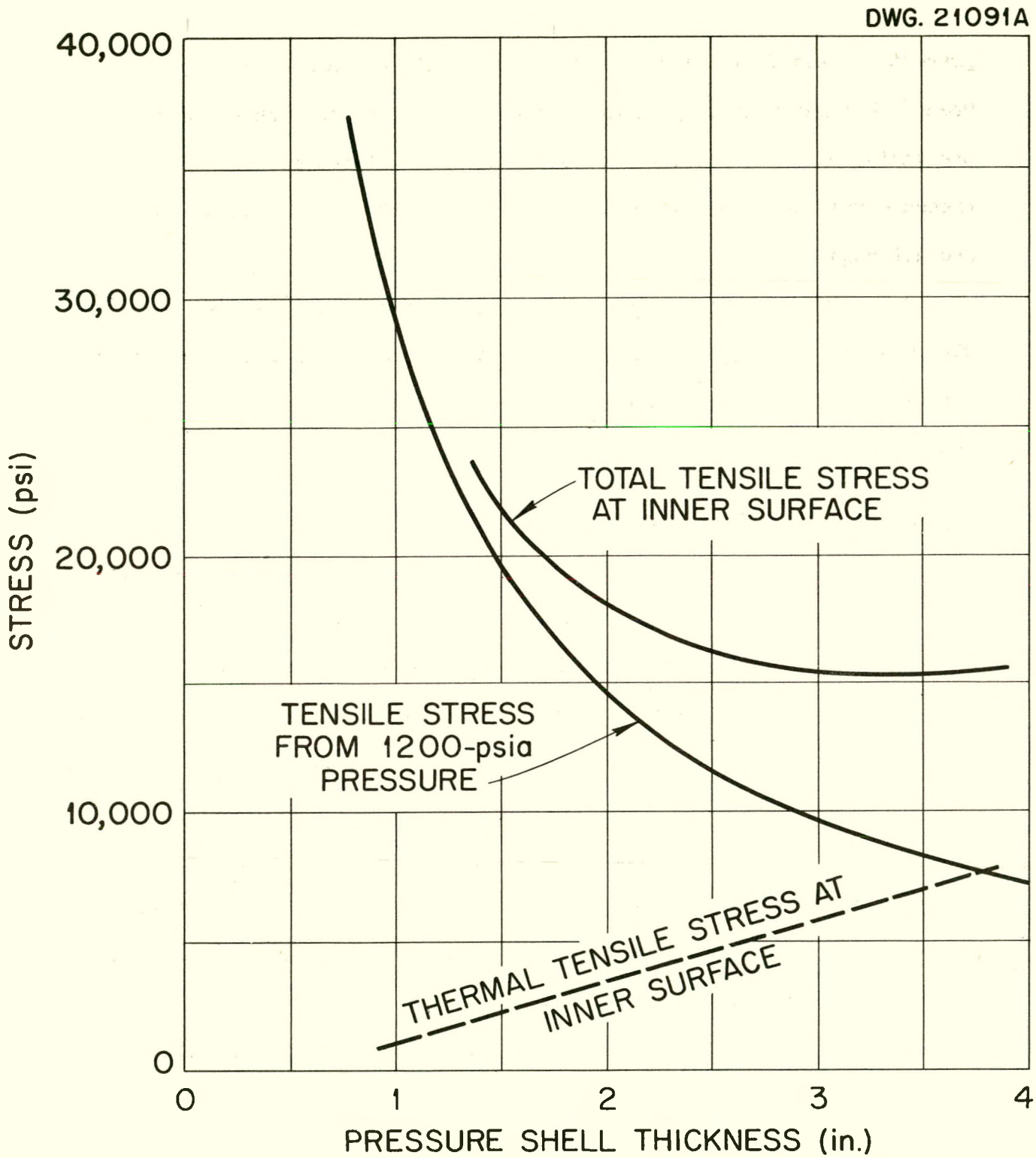

Fig. 19. Stresses in 1200-psia Shells 13 in. from Core and Shielded by 2 in. of Iron Located 7 in. from Core; Perfect Insulation at Outside Surface; 10-megawatt Operation.

prevent the accidental loss of primary coolant no drain cock is provided. When it becomes necessary to drain the water it can be siphoned out. Since the radiation instruments are to be placed against the outside wall of the pressure vessel, parallel to the centerline of the tank, instrument thimbles are not required.

3.2.3 Thermal Insulation. The reactor vessel is insulated thermally with a 4-in. coating of Foamglas. The reactor compartment is ventilated to maintain a temperature less than 150°F. The insulation and ventilation problems are analyzed in Section 6.4.

3.3 Control-Rod Drive Mechanism

In design of the control-rod drive mechanism consideration was given to known technology, reliability, and low cost. The complete design could not be of known technology as well as low cost because the problem of inducing linear motion inside a high pressure vessel from an external source is a relatively new one. The system components are, however, reliable and relatively inexpensive.

The basic solution of the problem is to drive the rod by a rack and pinion located inside the pressure vessel cover. Motion is transmitted to the pinion through a commercial rotary spindle seal. A motor package mounted on top of the reactor cover provides the motive force. The general layout of this design is shown in Fig. 20, and the detailed design is shown in Fig. 21. The unit consists of three main sub-assemblies: the motor unit, the seal assembly, and the rack-latch assembly.

DWG. TD-D-2457

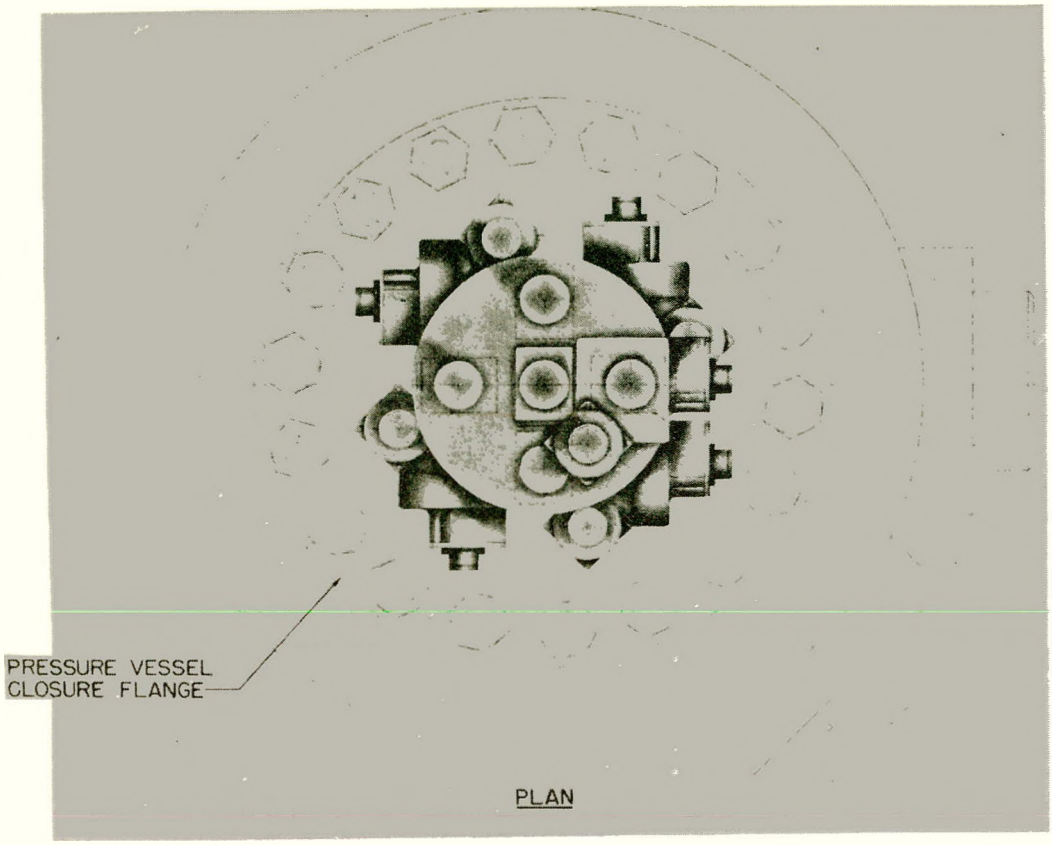

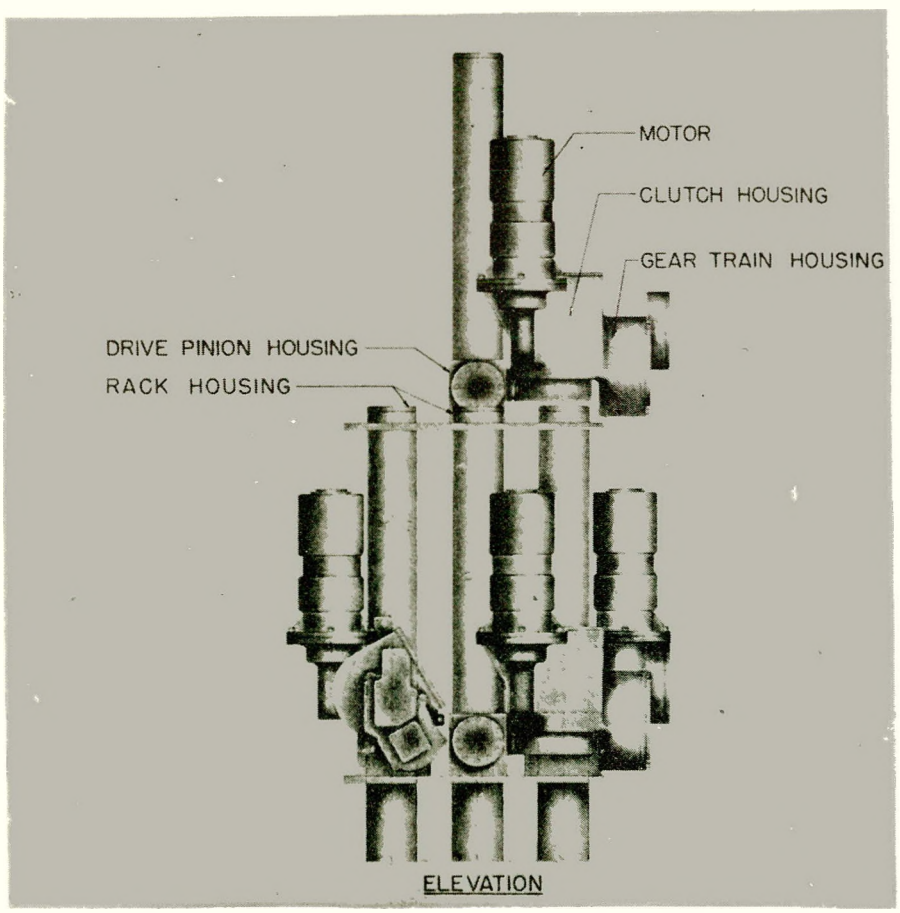

Fig. 20. Control Rod Drive, Plan and Elevation.

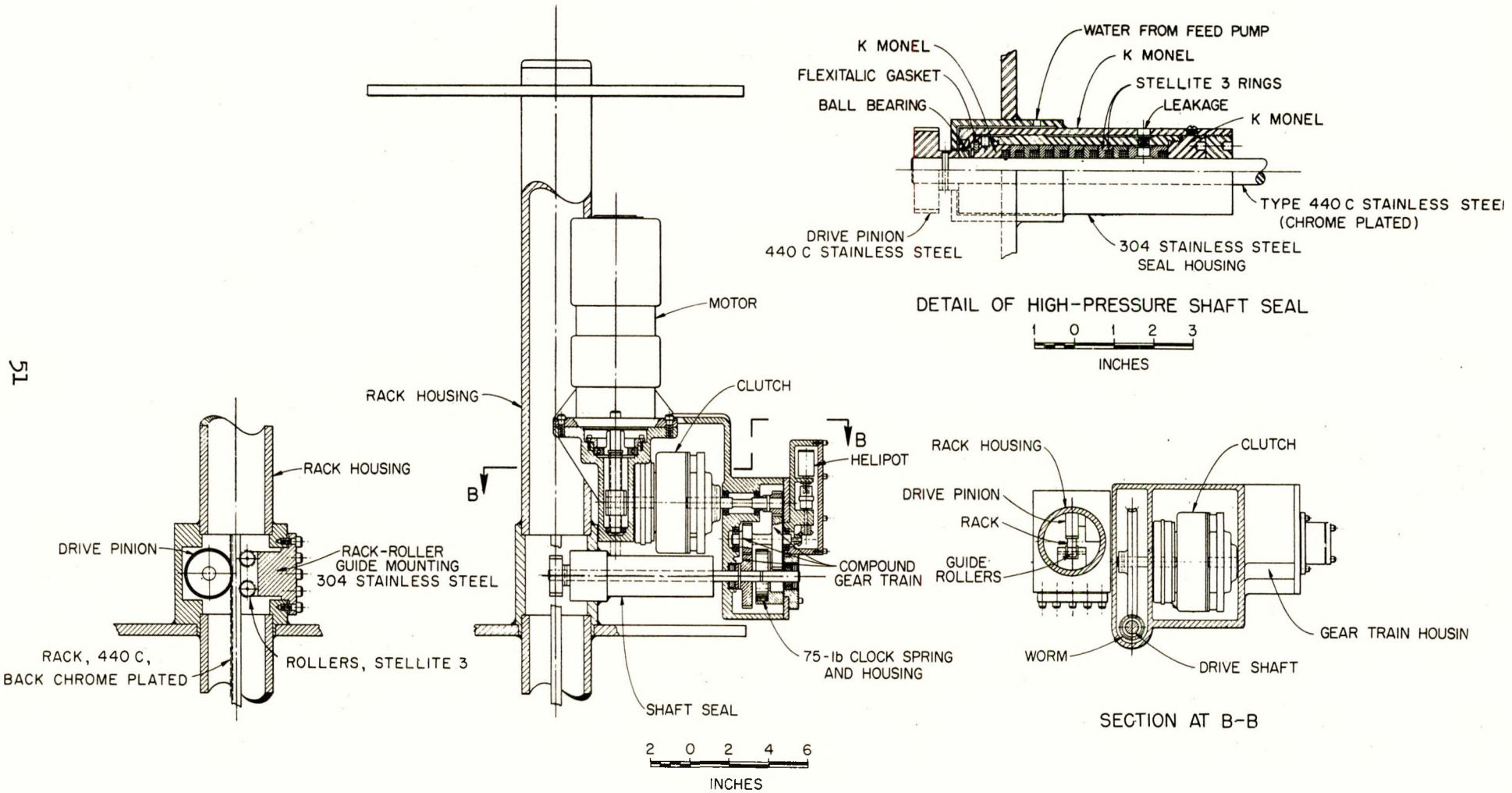

Fig. 21 Control Rod Drive Section and Details

3.3.1 Motor Package Unit. The motor package unit consists of a primary drive, a magnetic clutch, gear box, and an indication system. The design specifications are as follows:

1. Control rod to move up or down with speed of 1 fpm.
2. Rod to move in increments of 0.02 in. by proper switch actuation.
3. Position of rod indicated at all times, including during and after scram, with an accuracy of 0.2%.
4. Automatic scram rods with an acceleration equal to that of gravity.

The primary drive consists of a motor and worm reduction unit, Fig. 21. A Diehl low-inertia servomotor was chosen as the drive motor because of its flexibility. This motor is adaptable to operation from both across-the-line switches and from servo systems. Therefore, the same motor package can be used for either shim control or regulating rod drive. The low-inertia rotor permits the motor to come up to speed quickly and allows the motor to stop with very little coasting after power is removed; this small coast is important since it directly affects the fineness of incremental movement. This motor also contains an integral cooling fan. This is needed since the motor packages are mounted just above the pressure vessel. These fans may be removed if the circulation of air in the reactor compartment will keep motor temperature below 200°F.

The motor shaft is splined to a commercial worm, 24-pitch single thread; the worm wheel has 132 teeth. The worm wheel shaft is keyed to the primary half of a magnetic disc-type clutch, Warner Size-500, 1-25052. Its release time should be 30 to 75 milliseconds. The magnetic clutch is interposed at this point to disconnect the shim rod and permit it to drop in case of a scram. A button on the control panel permits the operator to effect a scram

by cutting power to the clutch. If there is a general power failure or an emergency condition, a scram is effected automatically.

The shaft keyed to the secondary half of the clutch continues through the unit of two sets of reduction gears. The combined gearing reduces the 1700-rpm motor speed to an output spindle speed of 2.2 rpm. This permits the pinion to drive the rack at a speed of 1 fpm. Pinned to the outside spindle, before it enters the seal, is a clock-type torsion spring which is constantly loading the output spindle and pinion and thus tending to drive the rod to the "full in" position. When the rod is "full up" the spring driving load will be 75 lb and when the rod is "full in" the load will still be 30 lb, the load varying linearly with position. The spring is a scram device whose sole function is to overcome the friction in the gearing, seal clutch, and water, so that the rod will drop under the acceleration of its own weight.

The Helipot used in the motor package as a low-cost indication system is an Army-Navy ten-turn model; it is coupled to a take-off shaft geared to the output spindle. In this way indication is never lost since, even during scram, contact is maintained between the rod, rack, pinion, spindle, and Helipot. The Helipot is wired to a meter on the control panel which is calibrated in units of rod travel.

The motor package is designed as a unit which can easily and quickly be replaced. The premise of low cost has been carried throughout the design. All gears, couplings, bearings, and oil seals are commercial items available from stock.

Preliminary test results of the control-rod drive mechanism are reported in detail in Appendix 13.6.

3.3.2 Seal Assembly. The decision to drive the rod through a seal was affected greatly by the fact that the system can tolerate a nominal amount of leakage, provided this leakage could be collected and returned to the system. The seal assembly consists of the seal and leakage collection unit, Fig. 21. The seal is a spindle-type rotary seal developed by the Kuchler-Huhn Company of Philadelphia, Pennsylvania. The seal is a complete breakdown type and is designed for a leakage rate of ten pounds per hour. Calculations were made for a water pressure of 1200 psi and a water temperature of 600°F. These calculations resulted in an overall seal length of 6.00 in. and a shaft clearance of 0.0003 in. It should be noted that the leakage rate varies approximately as the cube of the clearance. The calculated seal operating friction is 3-4 in.-lb and maximum break-away friction is 12 in.-lb.

A fitting included in the design of the seal serves as the outlet for the leakage of the collection unit; tubing runs from each of the five seals to a common receptacle. The seal consists of a number of floating rings, made of Stellite-3 and a series of K-monel guide bushings. These are assembled in a type 304 stainless steel housing. The number of rings as well as the clearance determines the pressure breakdown and resultant leakage. The shaft is 440C stainless steel, chrome plated, and must be ground to close tolerance, ±0.0001 in.

Further development of this type seal has been under way at ANL.* This particular type of seal has also been used in industry by the DeLaval Steam Turbine Division and the Allis-Chalmers Corporation.** The Allis-Chalmers

* Etherington, H., ANL-4455, p. 78 (1950); ANL-4537, p. 72 (1950).

**Personal communication from Mr. Rosmussen, former Chief Engineer, DeLaval Steam Turbine Division, July 10, 1953, and Mr. A. Salzman, Racine, Wisconsin, formerly with Allis-Chalmers Co.

application is for a boiler valve. The seal is on a rotary shaft with an OD of 3/4 in. and the operating steam pressure is 2000 psi. The calculated leakage rate for this seal is 20 lb/hr but the measured leakage rate during operation is only 12 lb/hr. Allis-Chalmers was admittedly skeptical that the close tolerances and sudden rise in temperature in their application would cause some galling and possibly seizing. This condition does not exist however. The seal has been in operation for three years with no overhauling, although the boiler has been down for repair.

If it is necessary to control the leakage of contaminated water from the reactor, the seal design was altered so that clean water, under a pressure somewhat higher than operating pressure, can be introduced into the seal near the pressure end of the seal. In this way the leakage from the seal will be clean water. A simple labyrinth or sealing ring was added to the pressure end of the seal to control the leakage into the reactor resulting from the pressure differential of the clean water and the contaminated water. The high pressure clean water will be supplied by the seal-water pumps.

3.3.3 Rack-Latch Assembly. At the pressure side of the seal a 440C ss pinion is mounted on the shaft. This pinion in turn drives a 440C ss rack which is latched to the control element thus giving the required linear motion. The application of a rack and pinion, Fig. 21, operating in pressurized water has been tested extensively at the Argonne National Laboratory.* The results of these tests show that a 440C ss pinion mating with a 440C ss rack operated for 5 million cycles in water under a pressure of 750 psi and a temperature of 450°-500°F. The teeth of the gears were polished but no

*Etherington, Harold,
ANL-4424, p. 46 (1949)
ANL-4455, p. 81 (1950)
ANL-4504, p. 74 (1950)
ANL-4537, p. 75 (1950)

other damage was perceptible, and the gears were running satisfactorily.

The above results as well as other favorable results reported were contingent on the fact that the water was not oxygenated. Since the system in this design will operate in an excess of hydrogen, it is felt that the corrosion problem of oxygenated water will not be a problem.

In order to meet the rack travel specification of 1 fpm, the pinion was designed to have 32 teeth and a diametrical pitch of 16. The pinion rotates at a speed of 2.2 rpm. The necessary back-up for the rack is accomplished by means of a Stellite-3 roller; the roller rotates on a Stellite-12 roller pin which is mounted in a roller bracket made of type-304 stainless steel. The complete back-up unit is bolted to an opening in the rack housing pipe and can be removed as a unit. It has been shown during preliminary testing that close clearances should be held between the rack and back-up roller. For optimum operation the clearance between the rack and back-up roller should be from 0.005" to 0.010". It is very possible that galling will occur between 440C stainless steel and Stellite-3 under these conditions, especially during a high speed scram. To minimize this possibility the portion of the rack which contacts the roller should be hard-chrome plated.

The latch unit is attached to the lower end of the rack. The latch must be capable of transmitting linear motion to the control rod; it must automatically release the control rod when the rod is in its lowest position, thus allowing removal of the pressure vessel cover while the rod remains in the reactor; and finally, the latch must automatically grip the rod when the pressure vessel cover is replaced. The latch performs its required functions by relative motion between a center rod and an outside sleeve. The upper end of the center rod is attached to the rack while the lower end contains the gripping jaws. The jaws have spring properties and are normally in the open

position. As the outer sleeve moves in relation to the center rod it locks the jaws in the closed position, or allows them to open.

In normal reactor operation, the outer sleeve is held against a flange on the center rod by a strong spring. The opposing force of the spring is taken by a pin through the center rod at its upper end. In this position the rack is latched and locked to the control rod. The control rod, latch, center rod, and latch sleeve move as a single unit. When the control rod has been lowered to approximately 1/4 in. from its lowest position, the motion of the outer sleeve stops due to the engagement of a collar on the outer sleeve with a ring installed in the reactor cover. The center rod and control rod continue to be driven down by the rack, compressing the sleeve spring. When the control rod is in its bottom position it is still latched and locked to the rack. In order to remove the pressure vessel cover the rack must be driven to a lower, overtravel position. This further compresses the sleeve spring and the jaws leave the sleeve and spring open. The vessel cover can then be removed and the control elements remain in the reactor. The position indication gauge in the control room show whether or not the rack is in the overtravel position and if the pressure vessel cover can be removed.

When the pressure vessel cover is replaced the latch is in the open position. Before startup the operator raises the rack from the overtravel position to the normal bottom position. During this operation the jaws are raised into the outer sleeve causing them to be latched and locked to the control rod.

The material used for the components is stainless steel except for the springs which are Elgiloy, a non-corrosive spring material developed by the Elgin Watch Company. The latch described above was developed and built by

American Machine and Foundry Company.*

The latch has satisfactorily withstood a 70,000-cycle test in moist atmosphere and without lubrication.

3.4 Reactor Control System

In considering the feasibility of a nuclear power plant for the routine production of heat and electricity, one of the necessary stipulations is that the operation of the plant be as safe and reliable as the conventional present day power plant. The power output of a fuel-fired boiler is controlled by the rate of fuel delivered to the fire box; this method of control is relatively simple and straightforward. The control of the reactor plant under discussion is, unfortunately, much more demanding in the complexity of control because of several basic differences, namely: (1) the reactor has enough fuel pre-loaded to last for several years of operation; (2) extremely high power surges, limited only by vaporization of the fuel, can occur in a fraction of a second; (3) the speed of response of safety devices must be in the millisecond range to be effective. The control system of a reactor must therefore be capable of maintaining the desired power level and, when necessary, be able to quickly and reliably overcome all the excess reactivity before damage occurs to any of the components.

3.4.1 Requirements of Control System. The control system proposed for this reactor will be capable of meeting the following requirements:

1. The rate of increase of reactivity will be limited to a safe value as determined by the reactor parameters.

2. The neutron flux instrumentation will be such that readings will be available from source level to above full power level.

---

* Charpentier, A. M., American Machine & Foundry Company Report DPEAM-1074, Dec. 6, 1951.

3. At least one instrument must be in range of the existing neutron flux level before startup of the reactor is permissible.

4. The reactor period will be continuously indicated from at least a minimum of 10^{-5} of full power level upwards.

5. The overall time from initiation of the scram signal to the insertion of the safety rods to an effective shutdown position in the reactor will set the maximum rate of k_{eff} increase during startup.

6. All safety circuits will be of the fail-safe type, e.g., in the event of electric power loss the safety rods drop.

7. Changes in steam or electric load demand will automatically set a new power level in the reactor to match the new load conditions.

8. Appropriate process instrumentation will be provided, e.g., pressure, temperature gages, level gages.

9. All components and circuits in the control system will be made as reliable and fool-proof as practical economic limits will allow.

10. The operation procedure for controlling the reactor will be kept as uncomplicated as safety requirements will allow. Training of operators will present a problem which can be alleviated by maintaining a straightforward, consistent operating procedure.

3.4.2 Method of Control. The system used for control of the reactor consists of two sections, namely: (1) control or operational circuits and (2) safety circuits. The basic purpose of the control circuit is to match and maintain the power level of the reactor to the demand level of the load. This will be accomplished by maintaining the temperature of the primary cooling water, leaving the reactor at an approximately constant value of 450°F. This value for the hot-leg temperature of the primary coolant water was determined as a maximum safe temperature at a pressure of 1200 psia; it allows for a 15°F rise in temperature before boiling occurs at hot-spot regions in the core.

The maintenance of the primary coolant temperature at 450°F may be considered the basic function of the automatic control system. The system, Fig. 22, functions as follows: An increase in load demand results in more steam flow and a lower steam temperature; this tends to lower the primary coolant temperature and results in a demand for an increase in reactor power. The lower hot-leg temperature, as indicated on the recorder, effects a rotation of the motor driven demand-level potentiometer and results in a signal to the servo system for regulating rod withdrawal; this increases the reactor power level until equilibrium is again established at a primary coolant temperature of 450°F. A lower load demand would, of course, cause insertion of the regulating rod to lower the reactor power level to match the new load conditions.

A small range of temperature level settings is provided by means of a potentiometer network in the temperature recorder. The demand-level network can be set to any pre-determined maximum power level. A signal proportional to reactor flux is also fed into the demand-level network. If the reactor power level represented by flux level exceeds the maximum setting of the network, the servo system reacts to insert the regulating rod and lower the power level. The temperature is therefore the main controlling factor up to the maximum power setting at which time the neutron flux level becomes the controlling factor and overrides the temperature signal. Such a system will prevent excessive power excursions when the reactor is being adjusted for operation at higher power. A selector switch is also provided to transfer the regulating rod from servo control to manual control.

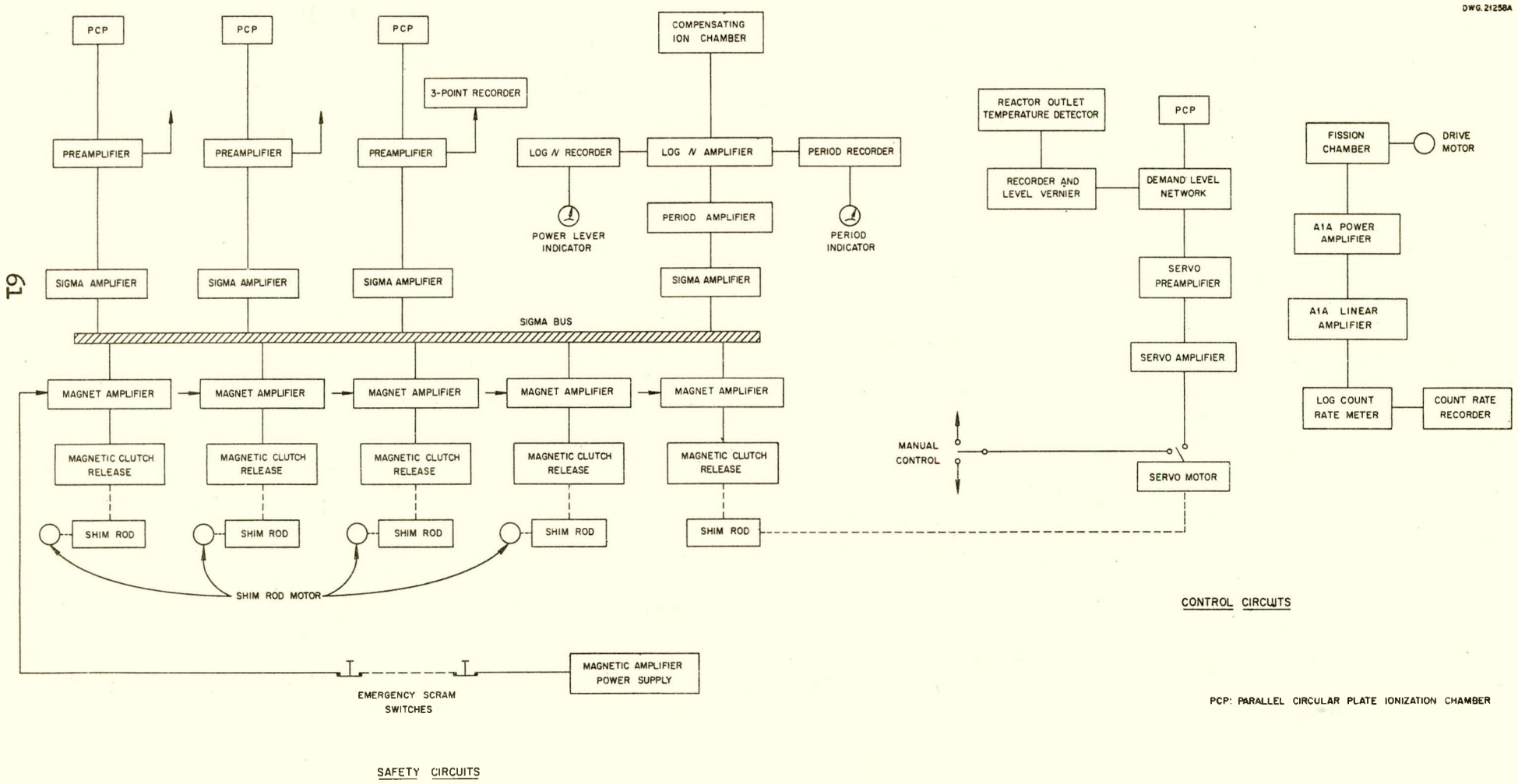

Fig. 22. Control System, Block Diagram.

Preliminary reactor-simulator tests have been completed and are reported in Section 13.5. The results indicate that the reactor is inherently self-regulating as it should be due to its negative temperature coefficient. Pending additional simulator tests, it appears that a fast servo-control system is not at all necessary and even a relatively simple one as described above may prove unnecessary.

The period safety circuit, Fig. 22, consists of a compensated ion chamber feeding into a log-N amplifier.* This amplifier furnishes a signal to a period recorder and indicator, and to a log-N recorder and power level indicator. The signal from the log-N amplifier also feeds a period amplifier which in turn furnishes the signal to a sigma amplifier. The output of this amplifier is connected to all of the magnet amplifiers through the sigma bus which controls the release mechanisms for the safety rods. This system provides protection against raising the power of the reactor on a period faster than can be compensated for by the speed of the reactor controls.

The ultimate safety circuit which can never be over-ridden by operator action is shown on the extreme left side of Fig. 22. This system consists of three parallel-circular-plate (PCP) ionization chambers which transmit a signal through the amplifiers to the sigma bus which in turn controls the current to the magnet amplifiers and consequently the release magnet mechanism. The system is such that an increase in reactor flux lowers the current transmitted to the release magnet; for scram conditions the current is not sufficient to energize the magnet and the rods are dropped. Although one PCP chamber in operation would be sufficient to drop all rods, three are used to insure that at least two are always in operating condition. Being electronic

* Buck, J. H. and Leyse, C. F., Materials Testing Reactor Handbook, ORNL-963 (1951).

in nature this safety system is extremely fast and can be designed to protect the reactor, by neutron-level signal alone, against a very fast period, i.e., 1/30 millisecond. Emergency "scram" buttons will be located at strategic positions throughout the reactor plant for use by personnel in case emergency shutdown of the reactor is required. This latter system would be classified as a slow scram since electromechanical devices are involved which are inherently slower than electronic devices.

For startup conditions the fission chamber used is capable of recording extremely low flux levels. As a safety precaution, operation of the reactor will not be permissible unless the fission chamber is reading; this will insure that at least one instrument is available at the low flux levels. Provision for moving the chamber during startup will be provided so as to increase its effective range.

3.4.3 Instrumentation. The majority of the radiation instruments described below have been developed at the Oak Ridge National Laboratory and are currently available from Radiation Counter Laboratories, Inc., Chicago, Illinois.

The parallel-circular-plate ionization chamber (PCP) is designed for high-speed response to changes in neutron flux level. The active section of the counter consists of a set of graphite disks. Each disk is completely coated with boron-10. Under neutron irradiation the reaction $B^{10}(n,\alpha)Li^{7}$ takes place. An ionization current of approximately 50 microamperes is reached at their operating flux of 10^{10} n/cm^2-sec. The materials used in the construction of the chambers are such that they do not become highly radioactive under neutron bombardment and can be handled without elaborate shielding. This instrument is used for safety and servo circuits and has a power-level range greater than 10^3.

The compensated ionization chamber is designed to give a reliable measurement of neutron flux over a large range, particularly in the presence of intense gamma radiation. The chamber is constructed with two separate volumes. An inner volume is contained between a movable cup electrode and a fixed inner electrode shell; the outer volume is between this inner liner and outer electrode shell. The two volumes are approximately equal, therefore the effect of gamma radiation on the two should be equal. The outer volume is made sensitive to neutron radiation by boron-10 coatings applied to the electrode surfaces. The cup electrode is held at a negative potential and the outer shell electrode at a positive potential with respect to the inner shell; the net current carried by the inner shell will therefore be a measure of neutrons only. Close balance of the two volumes for zero gamma signal is obtained by moving the cup electrode, thus varying the inner volume. The chamber has a range of 10^6 and gives 100 μa current at full operating level of 10^{10} n/cm^2-sec and 10^{-4} μa at the bottom of the range. The instrument is used to supply the signal to the log-N and period circuits.

The fission chamber is designed to give neutron measurements at low flux levels and is used in conjunction with a count rate meter. The chamber which could be used has been developed by Westinghouse. The chamber operates in the following manner: Neutrons absorbed in a U-235 liner produce fission fragments which cause ionization of the gas in the chamber. The voltage pulse created by each fission is amplified and counted. The fission pulses are large and, by proper biasing of the amplifier, can be counted separately from the lesser effects due to gamma and alpha radiation. The neutron flux can therefore be accurately counted even in the presence of intense gamma radiation. The counting rate of the instrument is from 1 to 10^4 counts per second. With the Westinghouse chamber, 1 cps is equivalent to $\sim$1 n/cm^2-sec. On startup,

with the chamber at the closest position to the reactor, a flux of ~10 n/cm^2-sec could be expected from the source; this would be equivalent to ~10 cps. At the full-power condition a flux of ~ 10^{11} n/cm^2-sec could be expected at the innermost position of the chamber. To protect the instrument from the high flux and to extend the range of the instrument, the chamber is moved away from the reactor as power is increased. A distance of ~12 feet is required to attenuate the flux at full power by a factor of 10^7 which would leave 10^4 n/cm^2-sec at the outermost chamber position. The overall range of the fission-chamber count-rate meter is therefore from full power to 10^{-11} of full power.

A summary of the operating instrument ranges is as follows: On startup the fission chamber is used from 10^{-11} of full power up to 10^{-6} which is the beginning of the period instruments. At 10^{-2} the servo and power instruments come in range and all instruments are effective up to full power. The chambers described above have in common the property of being open chambers with continuously flowing gas, with the exception of the fission chamber. Nitrogen is used in the PCP and compensated chambers. The source of neutrons used on startup to check the operability of the fission chamber will be provided by a polonium-beryllium or equivalent source which will be permanently installed inside the reactor shell.

The reactor period and power level instruments are described as follows: The log-N amplifier operates from the output of the compensated ion chamber. It consists of a thermionic diode. The voltage across the diode is proportional to the logarithm of the current passing through the diode over a range of greater than 10^6; thus the output of the amplifier is the logarithm of the reactor power level. The log-N signal is amplified and recorded on the log-N

recorder to give a record of the power level. The log-N amplifier also furnishes a signal which has been passed through an RC differentiator. This signal is inversely proportional to the reactor period and is recorded on the period recorder. The period amplifier differentiates the signal from the log-N amplifier to produce a signal suitable for operation of the safety circuits.

The sigma amplifiers are essentially dc amplifiers which operate in the following manner: The input signal to the sigma amplifier is furnished by a PCP chamber and a pre-amplifier or from a period amplifier. An increase in signal to the sigma amplifier causes the grid of a triode to go more positive. This in turn causes the sigma bus to be driven more positive since the cathode of the triode is connected to the bus. If this action occurs in only one of the four sigma amplifiers, then the cathodes of the other three amplifiers are also carried positive and the tubes tend to cut off. In this manner the amplifier receiving the highest signal can take control and all other amplifiers follow along, assuming the same cathode potential.

The magnet amplifiers receive their input signal from the sigma bus. In operation the magnet current can be set to release the magnet when a certain flux is reached. As the power of the reactor is increased the magnet current remains essentially constant until full load is approached. The magnet amplifier output then decreases as the flux increases until the point is reached where the current is insufficient to support the magnet. The value of neutron flux to initiate a fast scram is usually set at 150% of full-load reactor power. The current which the output tubes of the magnet amplifier supply the magnet is furnished from a separate transformer. The emergency scram switches are connected in series with this circuit providing a convenient means for manually scramming the reactor.

Two types of scram are therefore possible: fast scram by amplifier action and slow scram by interruption of magnet power. An accidental ground on the sigma bus would result in the magnets being de-energized and the rods dropping. If all magnet amplifiers and release magnets were exactly identical in adjustment and operation, all safety rods would be expected to fall in the event a scram were initiated. What will probably happen is that one or more rods will drop before the others and the total number that drop will be dependent upon the duration of the excess flux.

Miscellaneous detectors such as monitrons will be distributed throughout the plant as safety devices for the protection of personnel. Appropriate portable radiation survey instruments will also be provided for use by plant personnel.

4.0 PRIMARY COOLANT SYSTEM

4.1 General Description

The primary coolant system serves the purpose of removing heat from the reactor core and transferring it to the boiling water in the main heat exchanger. The coolant water is forced around a closed loop consisting of the reactor vessel, the circulating pump, main heat exchanger and connecting piping. The system is pressurized to 1200 psia to prevent boiling in the core cooling passages, and yet permit operation at a temperature high enough to generate steam in the secondary system at 200 psia.

Due to the lower design power level in this reactor only one 4000-gpm pump is necessary to circulate the coolant, and relatively low velocities in the system are possible. The lower velocities result in lower pump power requirements, and may also tend to reduce corrosion rates.

The water enters the pressure vessel just below the support plate, Fig. 11, flows downward through the reflector space and upward through the core passages, leaving the vessel just above the support plate. The two 12-inch pipes connecting the pressure vessel to other components of the system pass through a tunnel in the shield to a separate compartment in which the pumps, heat exchanger, pressurizer and check valves are located, as shown in Fig. 3-5.

The pressurizer, Fig. 23, is at the highest level in the system; the water level in it is maintained constant. Steam pressure above the water is maintained constant by immersion-type electric heaters which respond to a pressure control.

DWG. TD-D-2450A

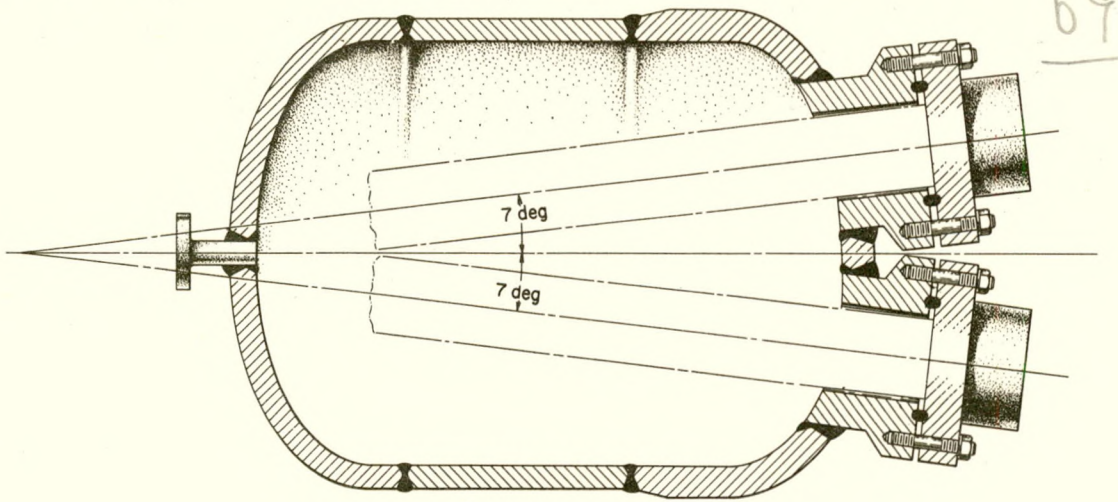

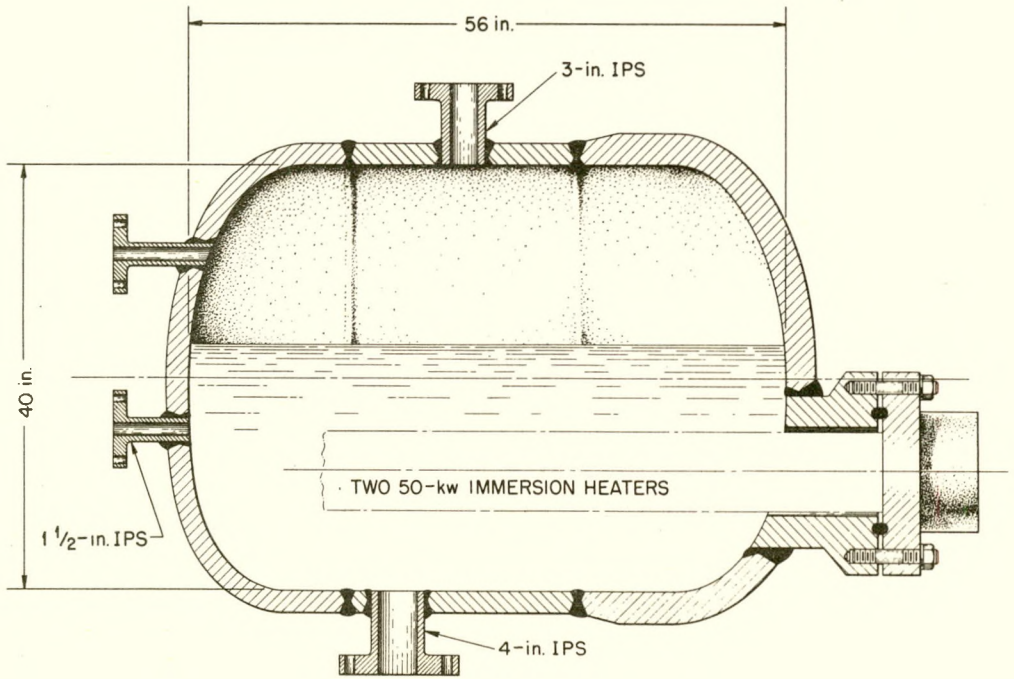

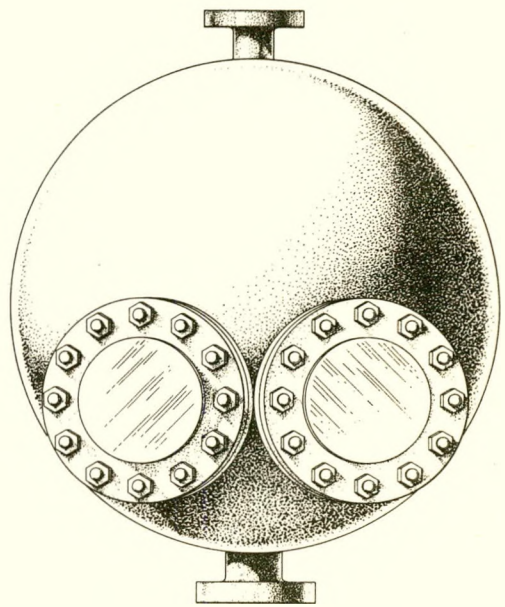

Fig. 23. Pressurizer, Primary Coolant System.

The remainder of the primary coolant system consists of a purification system, and a feed pump described in Section 4.7. The purge rate is controlled by the operator to maintain proper water purity and the make-up pump is controlled by a liquid-level-actuated controller on the pressurizer. Two circulating pumps are provided in parallel, one to be operated while the other is held in standby. The head losses in the primary loop are as follows:

Heat exchanger	ft	8.1
Reactor core	ft	0.98
Piping	ft	4.95
Entrance and exit at pressure vessel	ft	4.98
Total Head Loss		19.01

The calculations of friction losses in the core, piping, and heat exchanger tubes are based on the Fanning equation, with equivalent lengths of piping used for elbows, tees, and valves. Entrance and exit losses are taken as equal to one velocity head. Some of the pertinent data are:

Outside diameter of pipe	in.	12.75
Wall thickness	in.	0.687
Inside diameter of pipe	in.	11.376
Flow area	ft^2	0.705
Reynolds number		7,640,000
Friction factor (f)		0.002
Equivalent length of pipe (L)	ft	235

The Fanning equation is

$$\Delta H_f = \frac{4\ f\ v^2\ L}{2\ g\ D}$$

where ΔH_f = friction head loss, ft of fluid

D = inside diameter, ft

L = length or equivalent length, ft

g = 32.2, ft/sec^2

The friction factor is

$$f = \frac{0.046}{(Re)^{0.2}}$$

where Re = Reynolds number

4.2 Heat Transfer in the Reactor Core

Although the core geometry and composition for this reactor were based on the design by Hallman's group* the design power level is lower, and the total number of fuel plates is greater. In view of these differences in design factors, the following departures were made:

1. The flow rate was reduced from 10,000 gpm to 4,000 gpm.
2. The coolant was allowed to pass through the core only once instead of twice.

These changes result in an average velocity through the core of 4.3 fps instead of 22 fps, and a film coefficient of 2570 $Btu/hr\text{-}ft^2\text{-}°F$ instead of 8000. In an early analysis of the primary coolant system** the effects of flow rate and power level were studied, on the assumption of 4:1 peak to average heat generation rate in the core. It was established that the maximum film temperature drop would be 80° F, the required pressure 1000 to 1200 psia, the steam generator heat-transfer surface 1180 ft^2, and the pump motor power approximately 35 hp.

* Hallman, T. M. et al., Reactor Design and Feasibility Problem, MTR Type Power Producer for a Remote Location, ORNL CF-52-8-220, Aug. 20, 1952.

**Gall, W. R., Package Power Reactor No. 1, Primary Coolant System Calculations, ORNL CF-53-4-284, Apr. 29, 1953.

Due to lack of adequate information as to stability of reactors operating with boiling heat transfer, it was decided to prohibit the occurrence of boiling. This is accomplished by pressurizing the system so that the maximum film temperature is less than the saturation temperature for the system. For the purpose of estimating the maximum film temperature the following assumptions were made:

Ratio of peak-to average generation rate	4:1
Shape of axial distribution of heat generation over 28-in. length	cosine
Total number of cooling channels	800
Effective width of fuel-plate cooling surface	2.5 in.
Average exit temperature	450° F
Actual length of heat generating surface	22 in.

The distribution of temperatures along the hottest fuel channel is given in Fig. 24. The equation for the heat generated per unit area of fuel plate in the hottest channel as a function of axial distance from the center of the channel is:

$$q/A = (q/A)_{max} \cos \frac{\pi z}{28}$$

where q/A = heat generated per unit area, Btu/hr-ft^2
z = distance, in. (at inlet, z = -11; at exit, z = 11)

Since $(q/A)_{av} = 55{,}900$ Btu/hr-ft^2

and $(q/A)_{max} = 4(q/A)_{av}$,

then the above equation becomes:

$$q/A = 223{,}600 \cos \frac{\pi z}{28}.$$

For a flow rate of 4000 gpm through the reactor, the flow through each channel is 2085 lb/hr. The temperature rise of the water at any

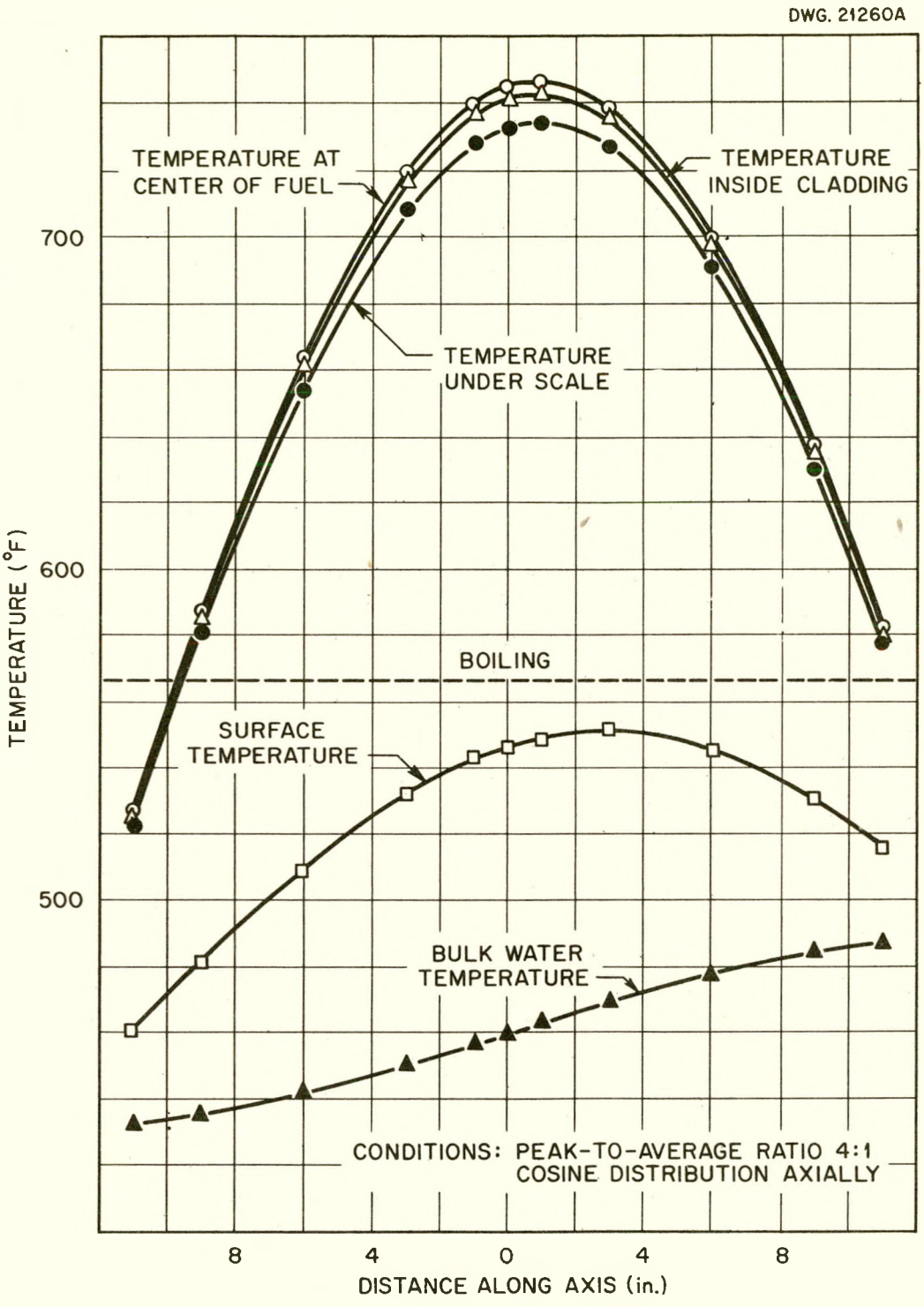

Fig. 24. Temperature Distribution Along Hottest Channel in the Reactor.

point along the channel is:

$$t_z - t_i = \frac{\int (q/A)dA}{2085(1.115)}$$

$$= \frac{223,600}{2085(1.115)} \int_{-11}^{z} \frac{(2.5)(2)}{144} \cos \frac{\pi z}{28} \, dz$$

$$= 29.7 \left(\sin \frac{\pi z}{28} + 0.9436\right)$$

Since $t_i = 431.6$,

$$t_z = 459.6 + 29.3 \sin \frac{\pi z}{28}$$

For a film coefficient of h = 2570 Btu/hr-ft^2-°F, the temperature drop across the film is

$$t_w - t_z = \frac{q/A}{2570}$$

So the surface temperature is given by

$$t_w = t_z + \frac{q/A}{2570}$$

Assuming a scale 0.010 in. thick having a conductivity of 1 Btu/hr-ft^2-°F/ft, the scale coefficient is

$$h_s = \frac{1(12)}{0.010} = 1200 \text{ Btu/hr-ft}^2\text{-°F}$$

Then the temperature at the surface of the metal under this assumed scale is

$$t_m = t_w + \frac{q/A}{1200}$$

The temperature drop across the cladding is

$$t_f - t_m = \frac{(q/A)(0.005)}{k\,(12)}$$

where k = conductivity of cladding material, Btu/hr-ft^2-°F/ft,
= 10.8.

So the temperature at the inside surface of the cladding is

$$t_f = t_m + \frac{(q/A)}{26,000}$$

The temperature distribution inside the fuel matrix is derived from the following differential equation for heat flow across a slab containing a uniformly distributed heat source (neglecting conduction along the slab).

$$\frac{d^2t}{dx^2} = -\frac{S}{k}$$

where S = volume heat source, Btu/hr-ft^2-in.
k = conductivity, Btu/hr-ft^2-°F/in. = 120
x = distance from center of slab, in.
t = temperature, °F

The boundary conditions are:

$$\frac{dt}{dx} = 0, \text{ at } x = 0$$

$$t = t_f, \text{ at } x = 0.010$$

By definition, $S = \frac{(q/A)}{0.010} = 2.236\ (10)^7 \cos \frac{\pi z}{28}$.

Integrating and applying the boundary conditions,

$$t = t_f + \frac{S}{2k}\ (x^2 + 10^{-4})$$

the temperature at the center of the plate is

$$t_a = t_f + \frac{q/A}{(0.010)(2)(120)}\ (10)^{-4}$$

$$t_a = t_f + \frac{q/A}{24{,}000}$$

It is seen in Fig. 24 that the peak of the curve for the surface temperature, t_w, is below the saturation temperature by a margin of approximately 15°F. This is such a narrow margin that a further analysis was made to determine the effects of power level, flow rate, and the peak-to-average ratio on the maximum film temperature. The following equation expresses the relation between these variables.

$$t_w = 450 + \frac{\alpha P}{F}\ 2975 \sin \frac{\pi z}{28} + 1218 + \frac{5590\ \alpha P}{h} \cos \frac{\pi z}{28}$$

where α = peak-to-average ratio
P = reactor power, megawatts
F = coolant flow rate, gpm
h = film coefficient, Btu/hr-ft^2-°F
$= 0.394\ (Re)^{0.8}$
$= 3.4\ F^{0.8}$
Re = Reynolds number
$= 13460\ v$
v = average velocity, fps
$= 0.0011\ F$

Differentiating the above equation with respect to z, it is found that the maximum t_w occurs where

$$\tan \frac{\pi z}{28} = \frac{1.86}{F^{0.2}}$$

In Fig. 25, the maximum values for surface temperature, t_w, are given as functions of α, P, and F, in each case holding the two other variables at design value, that is, α is plotted against $t_{w_{max}}$ for P = 10 Mw and F = 4000 gpm; P is plotted against $t_{w_{max}}$ for α = 4 and F = 4000; F is plotted for α = 4 and P = 10. From this figure it is possible to find the change in flow rate required to maintain a given margin below boiling if either power level or peak-to-average ratio should be different from the assumed values.

4.3 Design of Main Heat Exchanger

The heat removed from the reactor by the coolant is released in the evaporator-type main heat exchanger, Fig. 26. The primary coolant passes through the tube side of the heat exchanger heating the returned condensate from the turbine and the space-heating system to a saturated vapor at 200 psia. In this way the main heat exchanger effectively isolates the primary coolant system from the steam system, with the result that the water in the steam cycle does not become radioactively contaminated . Thus, maintenance of the steam system components of this plant

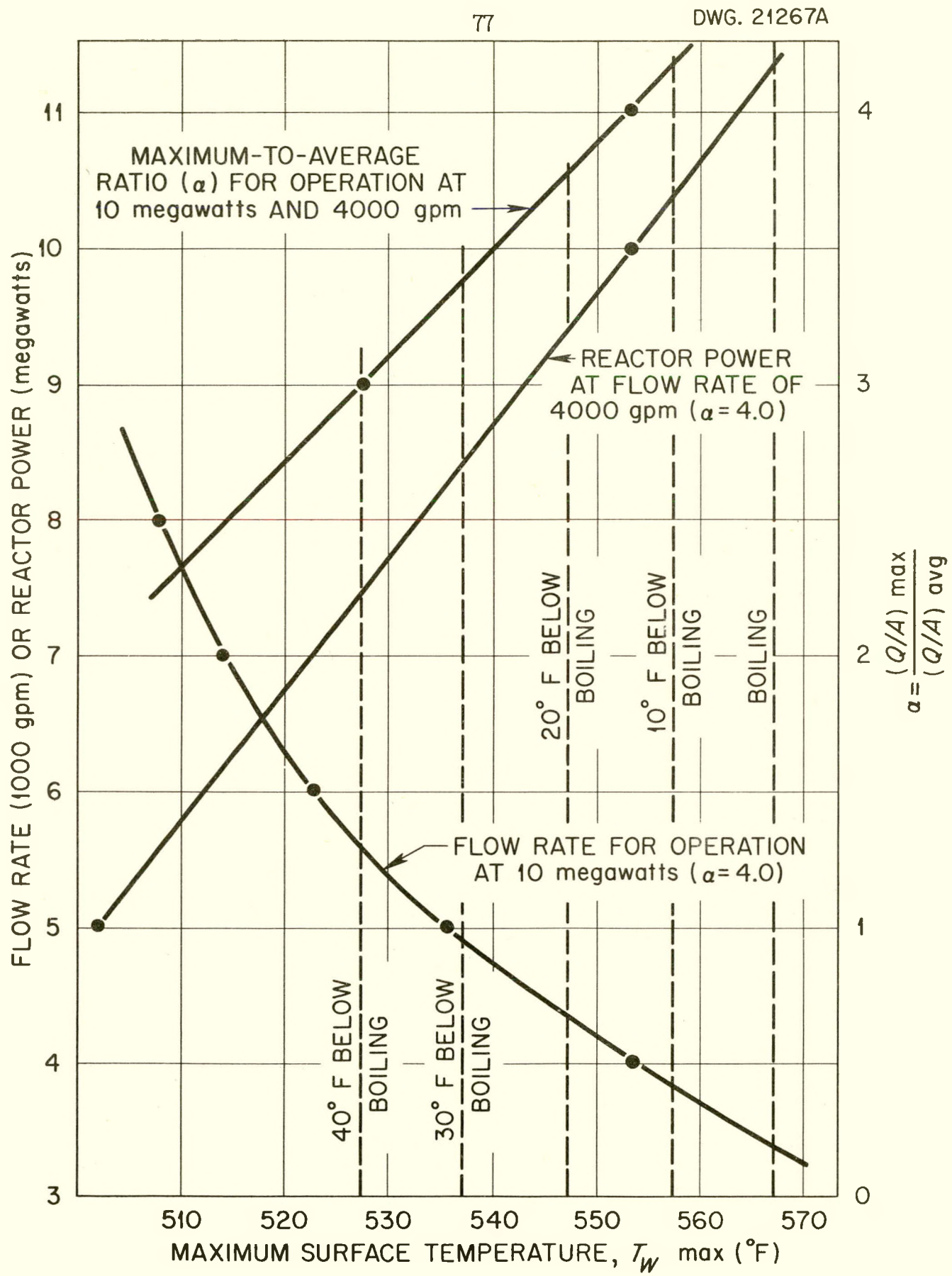

Fig. 25. Effects of Reactor Power and Coolant Flow Rate on Maximum Surface Temperature of Fuel Plates.

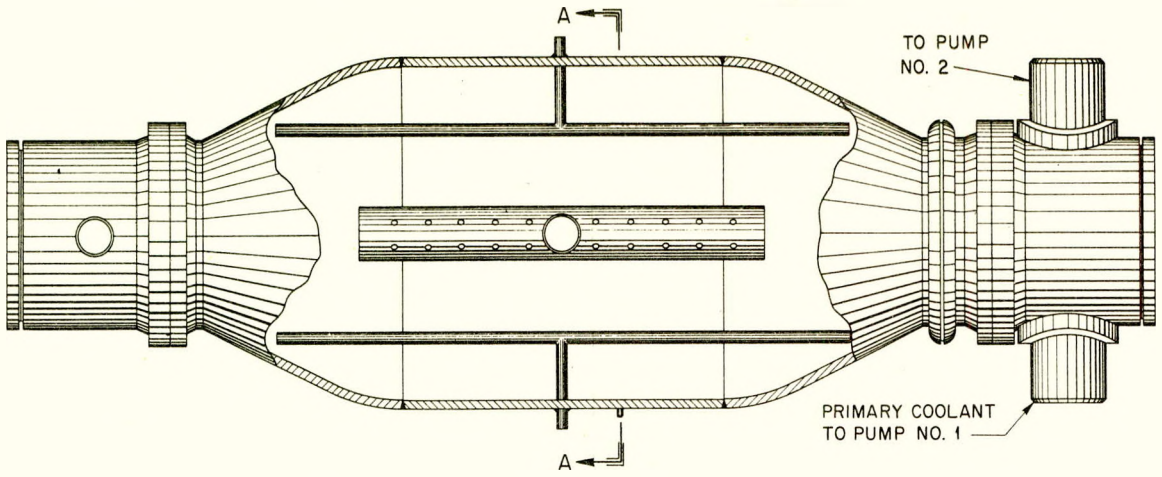

PLAN VIEW

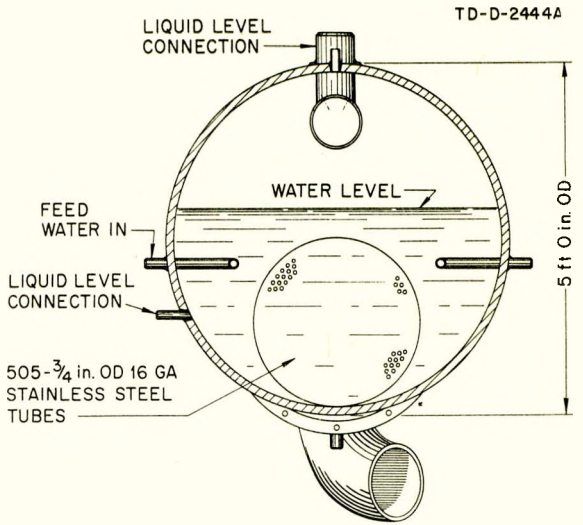

SECTION A-A

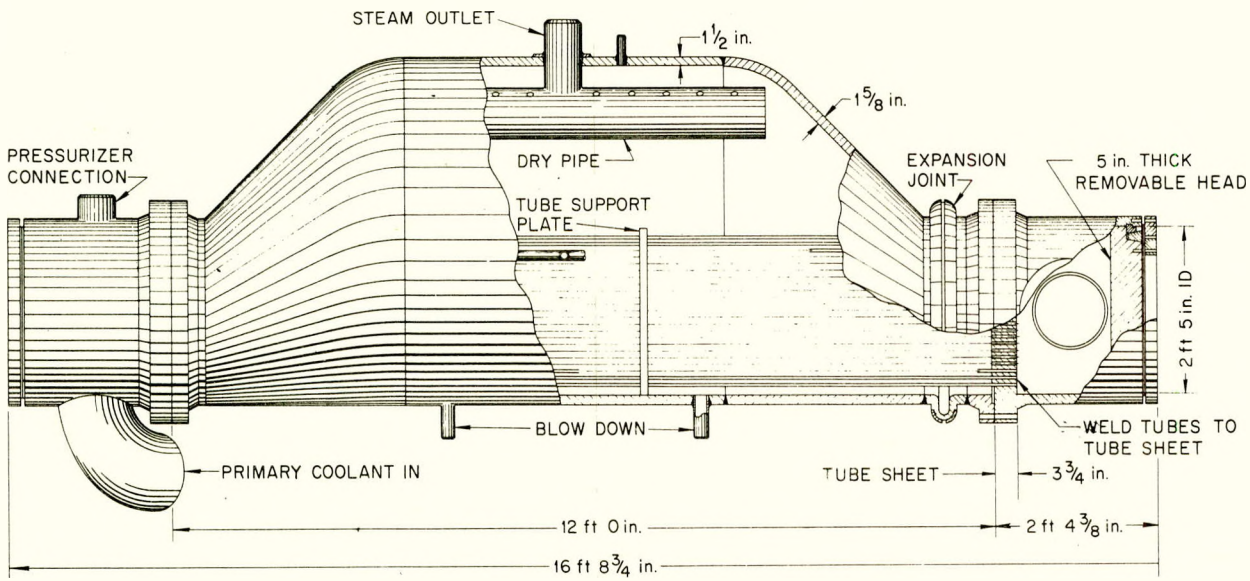

SIDE VIEW

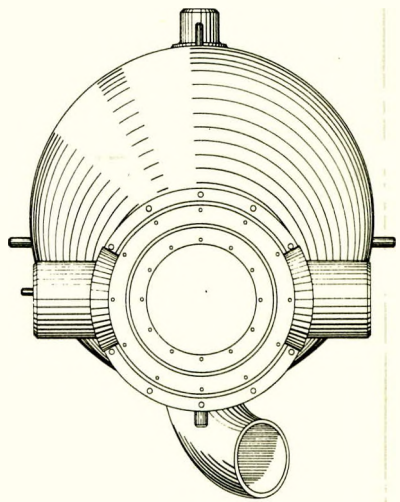

END VIEW

Fig. 26. Main Heat Exchanger for Generation of Steam.

will be essentially the same as in any conventional power plant; also the size of the radiation shield is kept to a minimum.

4.3.1 Heat Transfer Calculations. Heat transfer calculations for the main heat exchanger were presented in generalized form in a previous memo.* In order to reduce the number of variables in the calculations, the following arbitrary assumptions were made for a heat exchanger with Type 304 stainless steel tubes:

Velocity in tubes	fps	8.4
Tube size, OD	in.	3/4
Allowable stress (S) in tube wall	psi	12,000
Corrosion allowance (C) in tube wall	in.	0.020
Steam pressure at design load	psia	200

The tube wall thickness was determined by the following equation:

$$t = C + \frac{PD}{2S}$$

where C = 0.020 in.
P = 1200 psi
S = 12,000 psi
D = approximately 0.70 in.

From these data, t = 0.055 in.

The nearest thicknesses are No. 18 BW gage (0.049") and No. 16 BW gage (0.065"). To preserve the full corrosion allowance of 0.020", the wall thickness is specified to be No. 16 BW gage or 0.065". This makes the inside diameter of the tube 0.62".

If the conductivity, k, for stainless steel at 450°F is assumed to be 130 Btu/hr-ft^2-°F/in., the heat transfer coefficient of the tube wall is 2000 Btu/hr-ft^2-°F.

The Reynolds number inside the tubes is given by

$$Re = \frac{VD\rho}{\mu}$$

* Gall, W. R., Package Power Reactor No. 1, Primary Coolant System Calculations, ORNL CF-53-4-284, April 1953.

where V = velocity of the fluid = 8.4 fps
D = diameter of the tube = 0.62/12 ft
ρ = density of the fluid = 52 lb/ft^3
μ = viscosity of the fluid = 0.295/3600 lb/ft-sec

So Re = 275,400.

The film coefficient inside the tubes is given by:

$$h_i = (0.023)\ (Re)^{0.8}\ \left(\frac{C_p \mu}{k}\right)^{0.3}\ \frac{k}{D}$$

where C_p = specific heat of the fluid = 1.115 Btu/lb-°F
k = thermal conductivity of the fluid = 0.39 Btu/hr-ft-°F

So h_i = 3710 Btu/hr-ft^2-°F

The method of determining heat transfer surface is described by Segaser.* It is shown that at a constant rate of heat transfer, the film coefficient, h_o, for boiling water on the outside of tubes varies as the 0.25 to 0.4 power of the absolute pressure. Assuming the lower exponent, this may be expressed as follows:

$$h_o = h_{atm} \frac{(P)^{0.25}}{P_{atm}}$$

Also, Segaser shows (his Fig. 2) that h_o is a straight line function of Δt_b on log-log coordinates between values of 5° and 40°F for Δt_b, where Δt_b is the temperature drop across the film. From values in this chart, corrected for pressures of 150, 210, and 215 psia, the curves in Fig. 27 were plotted. It is seen that values from the chart for 200 psia may be used for 150 to 215 psia, with little discrepancy.

Since the curve is a straight line on log-log coordinates, it may be written:

$$h_o = a(\Delta t_b)^b$$

From the curve it is found that

$$b = 1.453$$
$$a = 74.2$$

* Segaser, C. L., Heat Exchanger Analysis for the Homogeneous Power Reactor Pilot Plant - Study I, ORNL CF-49-8-231, Aug. 1949.

Segaser, C. L., Heat Exchanger Design Study for the ISHR, ORNL CF-52-10-195, Oct. 22, 1952.

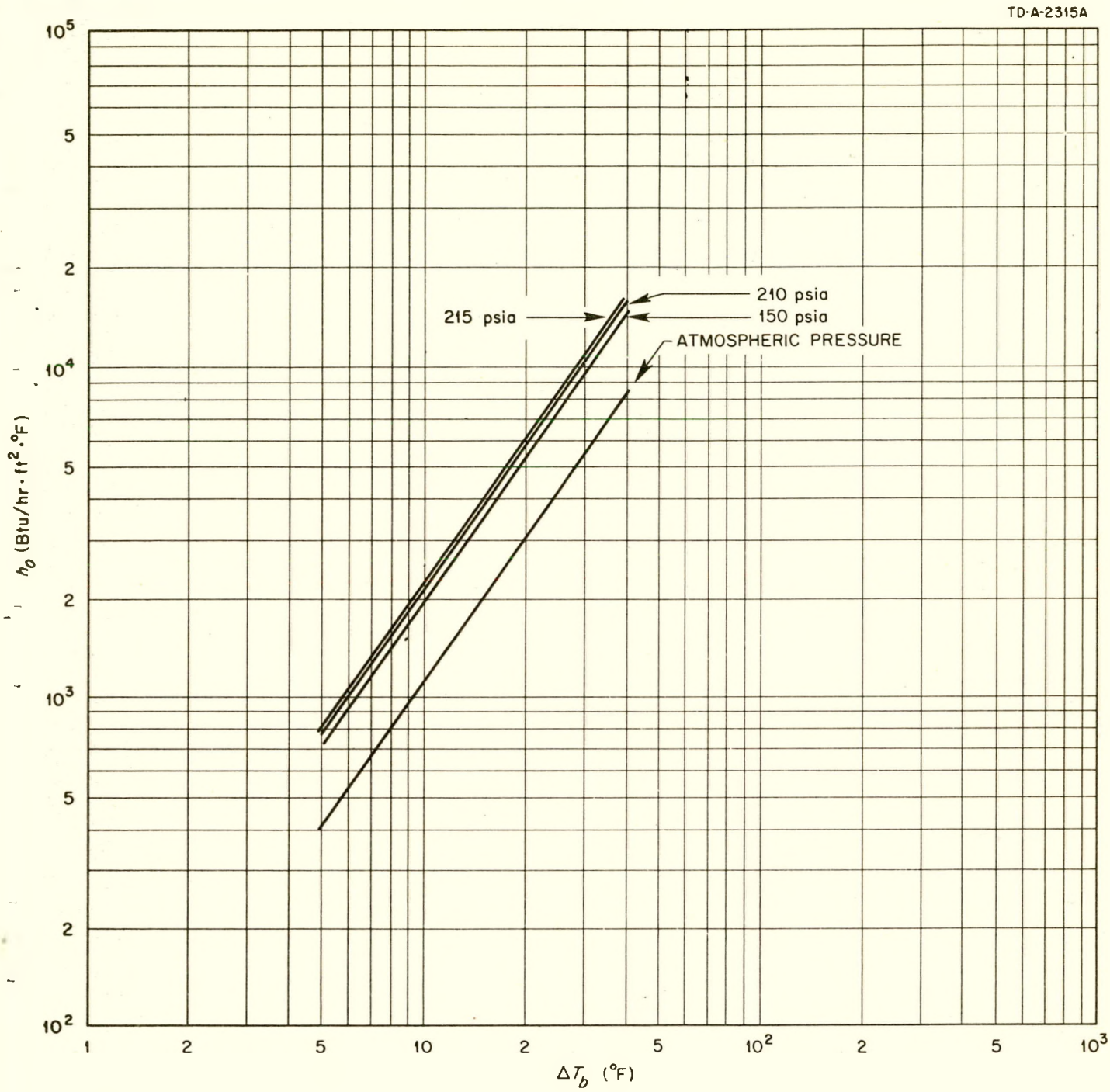

Fig. 27. Heat Transfer Coefficients for Natural Convection of Boiling Water on Outside Surface of Horizontal Tubes.

Thus $$h_o = 74.2\ (\Delta t_b)^{1.453}$$

The heat transfer per unit area is

$$q/A = h_o\ \Delta t_b = 74.2\ (\Delta t_b)^{2.453}$$

at $\Delta t_b = 5°$ F, $q/A = 3285$ Btu/hr-ft^2

at $\Delta t_b = 40°$ F, $q/A = 623{,}000$ Btu/hr-ft^2

So the limits in q/A for which the equation for h_o is applicable are 3825 to 623,000 Btu/hr-ft^2.

Solving (1) for Δt_b in terms of heat flux,

$$\Delta t_b = 0.172\ (q/A)^{0.408}$$

This is the film temperature drop outside the heat exchanger tubes.

To determine the heat transfer area in the heat exchanger, let A be the outside area of the tube, so that (q/A) represents heat flux per unit of outside tube area.

The overall temperature drop from fluid inside the tube to fluid outside the tube is:

$$(t_c - t_b) = \frac{q}{A_i h_i} + \frac{q}{A_i h_{Si}} + \frac{q}{A h_w} + \frac{q}{A h_{So}} + 0.172\ (q/A)^{0.408}$$

where A_i = inside surface area of tube, ft^2
h_i = inside film coefficient = 3710 Btu/hr-ft^2-°F
h_{Si} = inside scale coefficient= 4000 Btu/hr-ft^2-°F
h_w = wall coefficient = 2000 Btu/hr-ft^2-°F
h_{So} = outside scale coefficient = 2000 Btu/hr-ft^2-°F
t_c = temperature of fluid inside tube, °F
t_b = temperature of fluid outside tube, °F
A_i/A = 0.62/0.75
A_i = 0.83 A

Substituting

$$(t_c - t_b) = \frac{q}{A}\left[\frac{1}{0.83\ h_i} + \frac{1}{0.83\ h_{Si}} + \frac{1}{h_w} + \frac{1}{h_{So}}\right] + 0.172\ (q/A)^{0.408}$$

$$= \frac{q}{A}\left[\frac{1}{0.83(3710)} + \frac{1}{0.83(4000)} + \frac{1}{2000} + \frac{1}{2000}\right] + 0.172\ (q/A)^{0.408},$$

$$(t_c - t_b) = 0.00163\ (q/A) + 0.172\ (q/A)^{0.408} \qquad (2)$$

Equation (2) is plotted in Fig. 28.

The equation for heat transfer surface* is:

$$A = W\ Cp \int_{\Delta t_2}^{\Delta t_1} \frac{d(t_c - t_b)}{U(t_c - t_b)} \qquad (3)$$

where W = flow through tubes, lb/hr = 415 F
F = flow rate, gpm

By definition,

$$U(t_c - t_b) = q/A \qquad (4)$$

Differentiating equation (2),

$$d(t_c - t_b) = 0.00163\ d\ (q/A) + 0.0702\ (q/A)^{-0.592}\ d\ (q/A) \qquad (5)$$

Substituting (4) and (5) in (3),

$$A = W\ Cp \int_{(q/A)_2}^{(q/A)_1} \left[\frac{0.00163 + 0.0702\ (q/A)^{-0.592}}{(q/A)}\right] d(q/A)$$

Integrating and substituting limits:

$$A = W\ Cp \left[0.00163\ \ln \frac{(q/A)_1}{(q/A)_2} + \frac{0.119}{(q/A)_2^{0.592}} - \frac{0.119}{(q/A)_1^{0.592}}\right] \qquad (6)$$

Then $t_{c1} = 450°$ F, $t_{b1} = t_b = 381.8°$ F

So $\Delta t_1 = 450 - 381.8 = 68.2°$ F

From Fig. 28, for $(t_c - t_b) = 68.2°$ F,

$$(q/A)_1 = 33{,}200 \text{ Btu/hr-ft}^2$$

$$(q/A)_1^{0.592} = 477$$

and

$$\frac{0.119}{(q/A)_1^{0.592}} = 2.495 \times 10^{-4}$$

*Segaser, C. L. Heat Exchanger Analysis for the Homogeneous Power Reactor Pilot Plant - Study I, ORNL CF-49-8-231, Aug. 23, 1949.

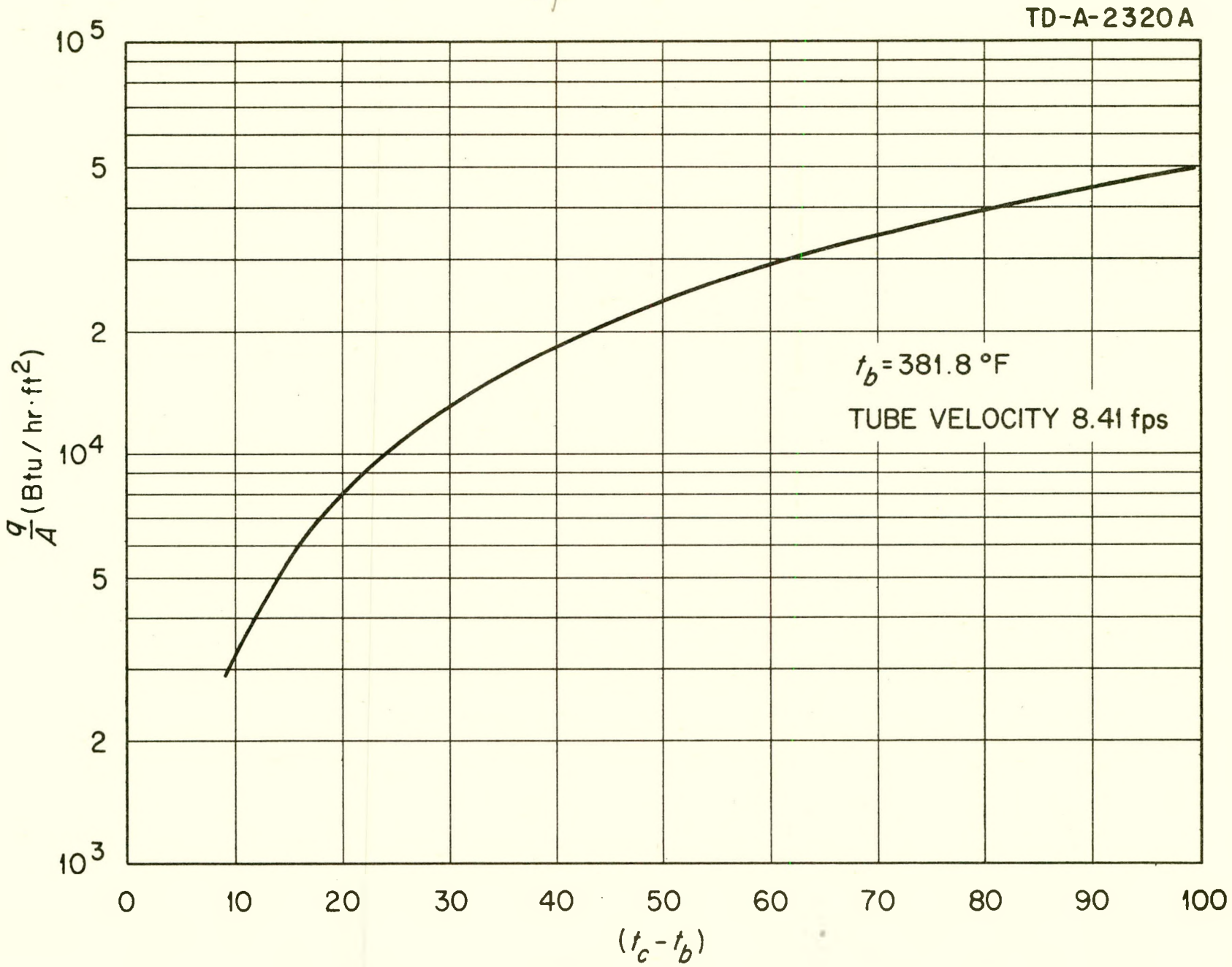

Fig. 28. Heat Flux, as a Function of Temperature Drop across Tube Wall.

$$W = \frac{F(60)(51.75)}{7.48}$$

$$W = 415\ F$$

$$Cp = 1.115$$

So: $$W\ Cp = 463\ F$$

To determine $(q/A)_2$, Δt_2 must be known for entry into Fig. 28. Since $t_{b2} = t_b$, it is only necessary to find t_{c2}. This may be found from

$$Q = 463\ F\ (t_{c1} - t_{c2})$$

$$t_{c1} - t_{c2} = Q/463\ F$$

or, if Q is expressed in megawatts

$$(t_{c1} - t_{c2}) = \frac{Q(3.415)(10)^6}{463\ F} = 7376\ Q/F$$

For $Q = 10$ Mw, and $F = 4000$ gpm,

$$(t_{c1} - t_{c2}) = 18.4\ ^\circ F.$$

Since the temperature of the coolant entering the heat exchanger is taken as a constant, values may be substituted in (6) as follows:

$$A = 463\ F \left[0.00168 \ln \frac{33{,}200}{(q/A)_2} + \frac{0.119}{(q/A)_2^{0.592}} - 2.495(10)^{-4} \right] \quad (7)$$

Thus, the heat transfer area required is a function of the flow rate and the heat flux at the exit of the heat exchanger. To determine the exit heat flux, the temperature rise of the water corresponding to the selected flow rate and power is calculated. For 4000 gpm and 10 Mw, it is 18.4° F, as previously calculated.

Then, since $t_{c1} - t_{c2} = 18.4$ and $t_{c1} = 450$,

$$t_{c2} = 431.6^\circ F$$

The boiling water temperature t_b = 381.8° F

So $t_{c2} - t_b = 49.8°$ F

Using the value $t_{c2} - t_b = 49.8°$ F in Fig. 28, it is found that

$$(q/A)_2 = 23{,}400 \text{ Btu/hr-ft}^2$$

Substituting these numbers in equation (7),

$$A = 1190 \text{ ft}^2$$

4.3.2 Tube Design

Number of Tubes Required

The flow area required for a velocity of 8.4 fps is

$$\frac{F \times 2.228 \times 10^{-3}}{8.4} \text{ ft}^2$$

The flow area per tube is

$$0.0021 \text{ ft}^2$$

So, the number of tubes is

$$N = 0.126 F$$

For F = 4000 gpm,

$$N = 505$$

Length of Heat Exchanger Tubes

The outside area of the heat exchanger tubes is

$$A = \frac{N\pi dL}{12}$$

where d = outside diameter of tubes, in., = 0.75
L = effective length, ft

So $$L = \frac{12\,A}{N\pi(0.75)} = 5.094\,\frac{A}{N}$$

For 4000 gpm and 10 Mw,

$A = 1190 \text{ ft}^2$

$N = 505$

So $L = 11.9$ ft

Head Loss in the Heat Exchanger

The Fanning equation for loss of head due to friction is

$$\frac{\Delta H_f}{L} = \frac{4fv^2}{2gD}$$

where f = friction factor = $\frac{0.046}{(Re)^{0.2}}$

L = length, ft
D = inside diameter, ft, = 0.62/12
v = velocity, fps, = 8.4
Re = 275,400

So f = 0.00375

Then the head loss due to friction in heat exchanger tubes is

$$\underline{\Delta H_f = 0.3185\ L}$$

For L = 11.9 ft, $\underline{\Delta H_f = 3.8 \text{ ft}}$

Assuming the head losses to be one velocity head at the exit and one-half velocity head at the entrance of the tubes, the combined loss is:

$$\frac{1.5(8.4)^2}{2\ g} = 1.647 \text{ ft}$$

The total head loss in the heat exchanger consists of losses due to friction in the tubes, entrance to and exit from the tubes, and entrance to and exit from the tube headers. Treating the entrance as a sudden contraction and assuming the diameter of the header to be 30 inches, the diameter ratio for 12-inch pipe is 2.5. Referring to Cameron Hydraulic Data, the losses are 0.88 ft of fluid for exit and 1.44 ft for entrance. So, for the case of 12-inch pipe at 4000 gpm, the total loss due to entrance and exit is 2.32 ft. Thus the friction drop in the single-pass heat exchanger is

$$\Delta H = 1.647 + 0.3185\ L + 2.32$$

For 4000 gpm and 10 Mw

$$\underline{\Delta H = 8.1 \text{ ft}}$$

In Fig. 29, heat exchanger design data calculated by this method are presented as functions of flow rate through the system for three different reactor design power levels. Performance as a function of reactor load is given in Fig. 30.

4.3.3 Shell Design. The diameter of the heat exchanger was selected on the basis of obtaining the maximum boiling surface in order to reduce turbulence and carry-over, and yet have the condensate level in the evaporator of a sufficient height to cover the tube bundle at all times. A standard 60" ID shell (TEMA Sect. A-3.111) was selected.

A tube bundle 28 1/2" in diameter is required to accommodate the 505 tubes on a 1 1/8" square pattern. A standard shell size of 29" ID (TEMA A-3.111) was selected. The larger shell thickness, designed according to Section UG 27 of the ASME Standards for Unfired Pressure Vessels, 1952, becomes:

$$t = \frac{PR}{SE - 0.6\,P}$$

where t = minimum required thickness of shell plate, in.
P = design pressure, psi
R = inside radius of shell, in.
S = maximum working stress, psi
E = efficiency of longitudinal joint

$$t = \frac{(500)(30)}{(16{,}000)(0.85) - (0.6)(500)} = 1.129 \text{ in.}$$

With allowance made for corrosion, a 1 1/2" thickness was selected.

In a similar manner, the minimum thickness of the small shell including corrosion allowance is 5/8".

From Section UG 32 (ASME Standards), the thickness of the toriconical section was determined to be 1 5/8", including corrosion allowance.

The tube sheet thickness was determined according to TEMA Sections A-7.161 and A-7.162.

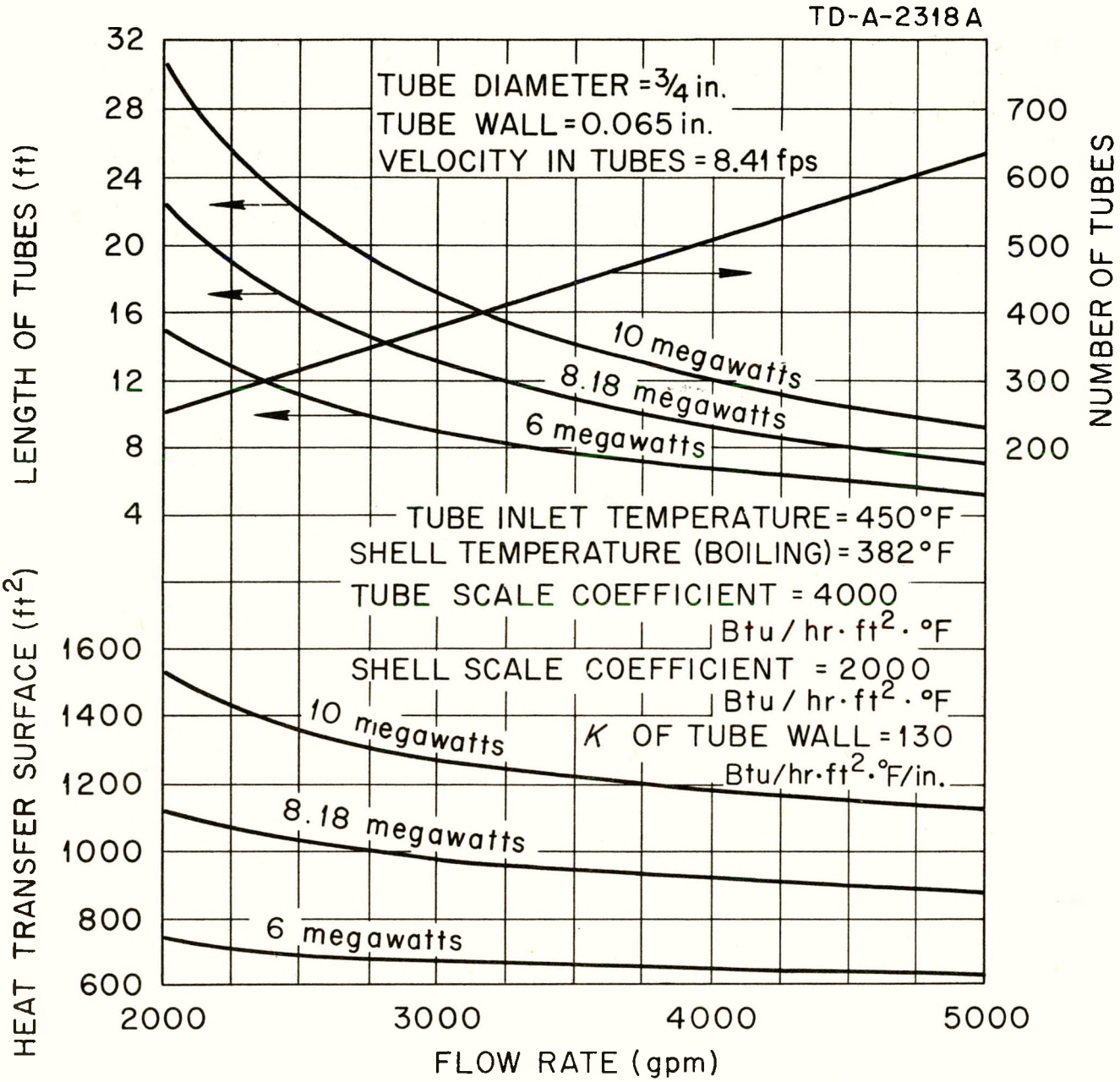

Fig. 29. Heat Exchanger Design Data, as Affected by Flow Rate.

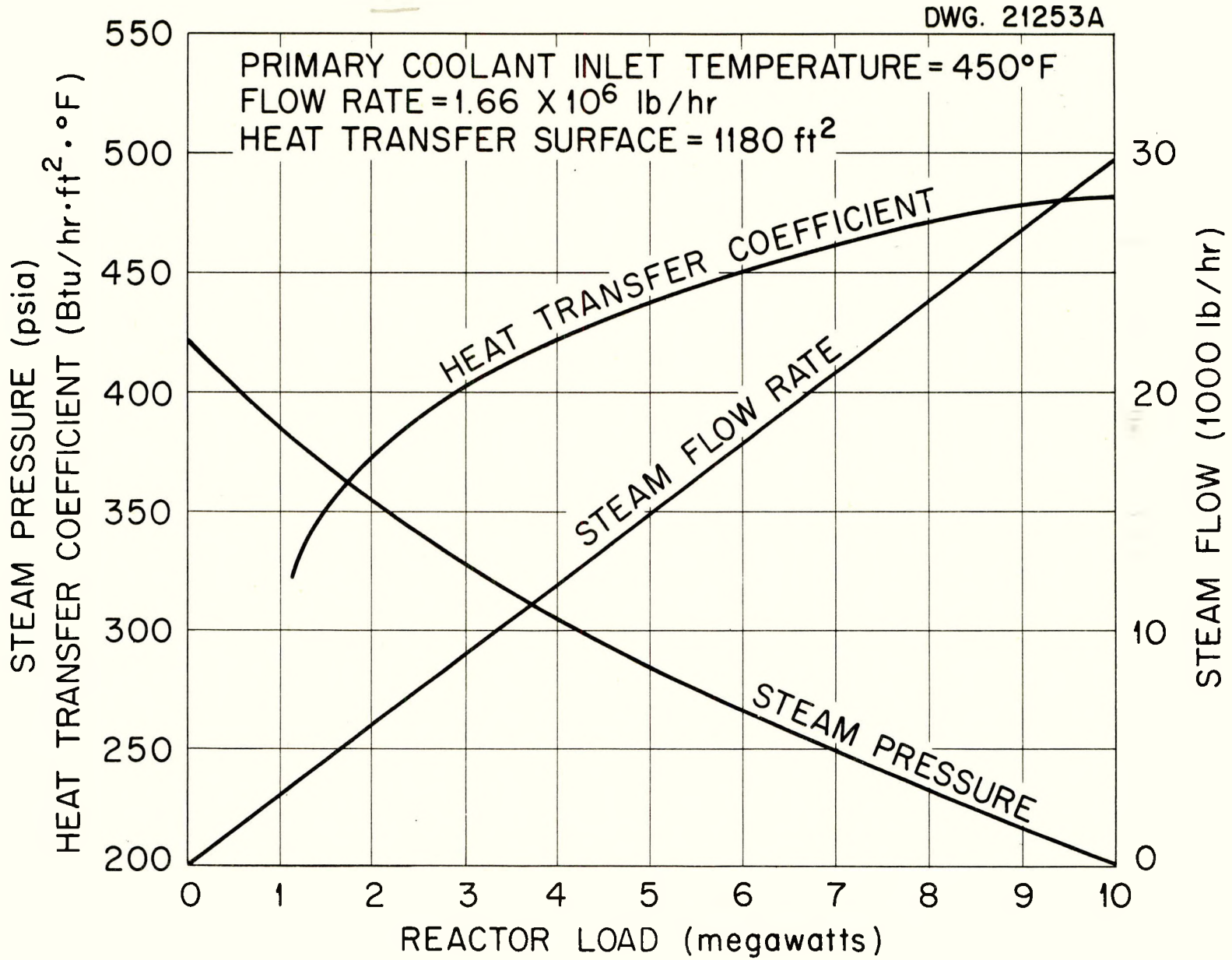

Fig. 30. Main Heat Exchanger Performance.

$$t = FG \sqrt{\frac{(0.25)\ P}{S}}$$

where $F = \sqrt{\frac{2 + K}{2 + 3K}}$

G = inside diameter of tube sheet header, in.

$K = \frac{E_s t_s\ (D_1 - t_s)}{E_t N_2 t_t (d_o - t_t)}$

E_s = elastic modulus of shell, psi

E_t = elastic modulus of tubes, psi

D_1 = inside diameter of shell, in.

d_o = outside diameter of tubes, in.

t_s = shell thickness, in.

t_t = tube wall thickness, in.

N_2 = number of tubes in shell

Then $K = \frac{(26 \times 10^6)(0.75)\ [29 + 0.875]}{(27 \times 10^6)(505)(0.65)\ [0.75 - 0.065]} = 0.964$

$$F = \sqrt{\frac{2 + 0.964}{2 + 2.89}} = 0.78$$

$$t = (0.78)(31.62)\ (\frac{(0.25)(1200)}{17,000})^{1/2} = 3.27 \text{ in.}$$

With allowance for corrosion, a 3.75" thick tube sheet was selected.

The removable channel cover was designed according to TEMA Section A-8.21 in which the thickness is given by:

$$T = F\ G \sqrt{\frac{CP}{S}}$$

where $F = 2.1 \frac{\sqrt{S}}{E^{1/3}} = 1$ for carbon steel

G = mean gasket diameter

C = a constant dependent on bolting and gasket proportions (from Section UG 34 ASME Code C = 0.3.)

P = design pressure

S = allowable working stress

$$T = 29 \sqrt{\frac{(0.3)(1200)}{17,000}} = 4.65 \text{ in.}$$

With allowance for corrosion, a 5.0" thick cover was selected.

The channel and tube sheet could be made of an integral stainless steel forging with the tube sheet either welded or bolted to the heat exchanger shell. A clad channel and tube sheet would be satisfactory if the fabrication problems could be solved. The differential expansion is provided for by either an expansion joint in the shell of the heat exchanger or by uniformly warping the tubes.

Inlet and outlet connections for both the primary water cycle and the steam cycle are provided. To simplify the piping, two outlet connections are used on the primary cycle, each feeding one of the main circulating pumps. The pressurizer is connected to the inlet side by a 6" pipe.

4.3.4 Summary of Design Data. The following represents a summary of design data for the main heat exchanger, and conforms to "Standards of Tubular Exchanger Manufacturers Association", Third Edition, for Class-A type heat exchangers.

		Tube Side	Shell Side
Material, 16 ga		304 ss	Carbon steel
Diameter	in.	3/4 (OD)	60 (ID)
Pressure, design	psi	1200	500
Temperature, design	°F	450-431.6	450
Velocity	fps	8.41	
Number of tubes		505	
Length of tubes, effective	ft	11.9	
Pitch of tubes arranged on squares	in.		1 1/8

4.4 Circulating Pumps

The primary coolant system was designed with low velocities throughout so that head loss would be low. The flow rate through the system, 4000 gpm, is exactly equal to the rated flow capacity of pumps developed for the STR. However, the low head requirement of this system results in a much lower pump power requirement.

The pump for this system requires only ~ 35 hp.

The pump specified for the proposed reactor is the "canned-rotor" type used in the STR; all rotating parts of both the pump and the motor are contained in a stainless steel can with the motor stator on the outside. Thus no shaft seal is required and therefore no leakage occurs. As an alternate it may be possible to use a pump with a shaft seal of the same type as that being specified for the control rod drives. In that case the motor could be located outside the shield and some leakage through the seal would have to be allowed. Before final design of the reactor is completed a comparison should be made of the two types of pumps to determine which is more economical, consistent with reliability requirements.

Although a centrifugal-type pump is shown herein, it is possible that an axial-flow type is more suitable for this low-head application. The centrifugal pump has the advantage of smaller volume, whereas the axial-flow type would offer less resistance to the natural convection flow which would provide cooling after shutdown.

4.5 Pressurizer System

The purpose of the pressurizing system is to maintain a constant pressure of 1200 psia in the primary coolant system, to remove gases

from the primary coolant, and to provide a surge tank which will minimize the effect of large fluctuations in the power requirements of the steam generating system. The pressurizing system consists of a large tank connected to the main heat exchanger and located above it at the highest point in the primary system. Two 50-kw immersion type electric heaters are placed near the bottom of the tank. Since the pressurizer tank is thermally isolated from the primary loop in that there is no appreciable flow between them, the immersion heaters are able to maintain the water at a temperature which will be in equilibrium with steam at a pressure of 1200 psia.

An abrupt increase in the temperature of the fluid in the primary loop would result in the following series of events: The expanded coolant would flow into the pressurizer. Since the water in the pressurizer is at 567° F, the influx of several cubic feet of water at only 450° F would result in the condensation of some of the steam in the vapor space. The final equilibrium condition would be at some lower temperature and pressure. However, as soon as the pressure had dropped sufficiently to actuate the heat controls, the two electric heaters would return the water temperature to 567° F and thereby restore the pressure to the required 1200 psia. In the meantime, since the amount of water in the pressurizer increased, the level controller would have deenergized the make-up pump until the original level has been restored by drainage through the constant bleed.

The case of a decrease in the temperature of the primary coolant would result in the following action: The contraction in volume of the primary coolant would cause water to flow out of the pressurizer tank

thus lowering the pressure. This would result in the heater controls energizing the heaters which would raise the temperature of the remaining water and bring the pressure back to the required value. Meanwhile, the level controller would energize the make-up pump to return the water level to normal.

The size of the pressure vessel is based on a capacity that is adequate to accept any sudden drop in power requirement without allowing either the pressure in the primary loop to drop more than 50 psi or the water level in the pressurizer to rise appreciably. This, together with the volume required for water to insure covering the heaters under any conditions, constitutes the volume requirements for the pressurizing tank.

This tank is 3 ft in diameter inside and has an overall length of 61 in. It is designed according to the ASME Code for Unfired Pressure Vessels, 1952 Edition, and is fabricated of carbon steel with an inner liner or cladding of Type 304 stainless steel. The cylindrical part of the tank is 1 7/8 in. thick including the stainless steel cladding. Two flange connections are provided for mounting the immersion heaters. Two safety valves are attached at the top and one to the coolant inlet on the bottom. At the top of the pressurizer a relief valve is connected to the off-gas stack to allow the operator to manually control the pressure.

In the event of instantaneous loss of full load, the primary system pressure will fall about 50 psi. The size of the pressurizer heaters is great enough to restore the primary system pressure within 2 minutes.

4.6 Primary Coolant Piping

The primary coolant piping is required to carry water at 1200 psi and 450° F at a flow rate of 4000 gal/min. To minimize corrosion, the piping is to be fabricated of Type 304 stainless steel (see Section 4.11). This material has an allowable working stress of 12,750 psi at this temperature*.

Twelve-inch pipe was selected on the basis of calculations made in a previous report**. In a comparison of three different pipe sizes at various flow rates, Fig. 31, it was found that, at a flow rate of 4000 gpm, 12 in. pipe requires almost twice the pump horsepower as the 16-in. pipe. Since the power requirement is less than 50 hp for 12-in. pipe, the smallest size considered, economic reasons dictated its choice for this system.

Wall thickness was determined by the use of the following formula***:

$$t_m = \frac{PD}{2S + 0.8\,P} + C$$

where P = design pressure = 1200 psi
D = OD of the pipe = 12.75 in.
S = allowable stress for welded pipe = 12,750 psi
C = allowance for corrosion = 0.065 in.

$$t_m = \frac{1200 \times 12.75}{25{,}500 + 0.8(1200)} + 0.065 = 0.643 \text{ in. minimum}$$

The heaviest weight in which stainless steel pipe is normally furnished is Schedule 80S. For a pipe of 12-in. nominal diameter this represents

---

* ASME Code for Pressure Piping, ASA B31.1, 1951, p. 21.

** Gall, W. R., Package Power Reactor No. 1, Primary Coolant System Calculations, ORNL CF-53-4-284.

*** ASME Code for Pressure Piping, ASA B31.1, 1951, p. 11.

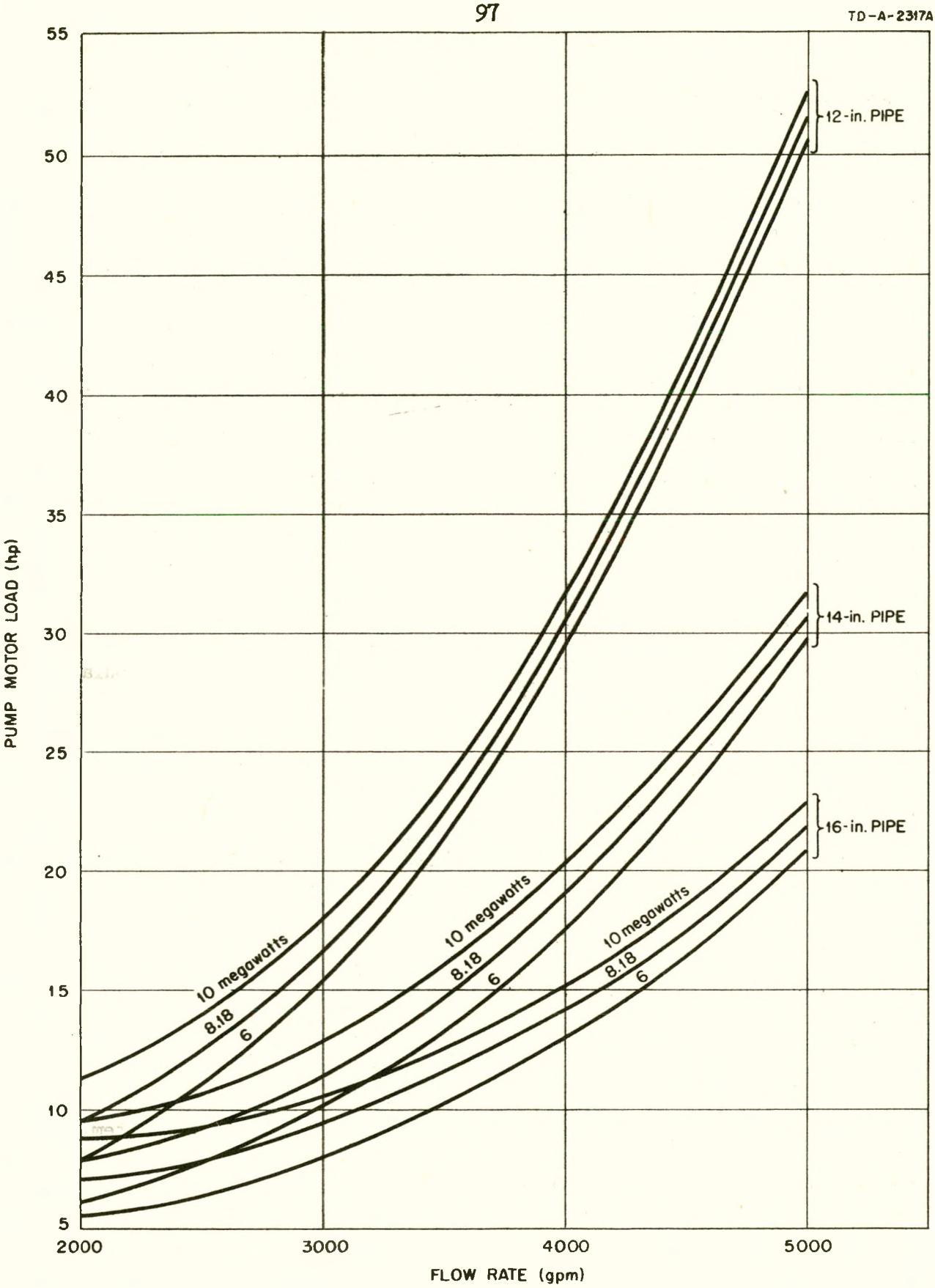

Fig. 31. Primary Coolant Flow Rates vs. Pumping Power.

a wall thickness of 0.500 inches. For economic reasions it appears desirable to consider using fabricated pipe, i.e., with a longitudinal welded seam. By doing this, it is possible to specify a wall thickness more nearly in line with the desired value. All welds should be X-rayed and inspected with Zyglo.

A potentially serious situation exists in the expansion of the primary loop as it is heated to operating temperatures. The section of pipe that conveys the primary coolant from the reactor to the heat exchanger is about 15.5 ft long. Consequently, it will increase in length about 0.729 in. due to thermal expansion. If the ends of this section are constrained, a bending moment will be applied to the straight lengths of this piece with a torsional moment appearing at the ends where the pipe is connected to the heat exchanger and the reactor. If the stress is calculated for the case where all strain occurs in one segment of the pipe, it can be assumed that no one of the actual stresses will be as large. This is equivalent to the moment required to deflect a 10-ft section of the pipe 1.021 in. and produces a maximum fiber stress of 39,100 psi which is approximately equal to half the yield strength of the material. Thus, it is apparent that some means of alleviating this condition must be provided. A possible method is to mount the heat exchanger in such a manner that it is free to move as the pipe expands.

It will be noted that the primary coolant loop is a completely closed system. All joints are welded; the circulating pumps have no shaft seals; and the only valves in the system are check valves which allow the circulating pumps to operate individually without by-passing the coolant through the inoperative pump. This closed system keeps the total number of possible sources of leakage of the radioactive primary coolant as small as possible.

This also contributes to a simpler, less expensive system with lower head losses. The location of the pumps above the reactor facilitates repair or replacement. If it becomes necessary to remove a pump, all that needs to be done is to drain the system until the pumps are dry, the reactor core still remains covered with water. The pump can then be replaced simply by cutting it loose from the rest of the system and welding another pump in its place. STR experience indicates that after a few days waiting period, the pumps can be handled without extensive precautions from the radioactivity standpoint.

4.7 Water Purification and Feed System

The purity of water is measured by either its resistivity or by its total dissolved solids. Of the two quantities, the resistivity is most easily measured and will give the best indication of the ionic content of the water from the corrosion point of view. A knowledge of the amount of dissolved solids is helpful in calculating the amount of demineralization required to effect high purity.

The relationship between resistivity and total dissolved solids is not a fixed one since the resistivity is a function of ion activity which may vary from one type of ion to another. In order to establish a working relationship between the two, selected known relationships between resistivity and total dissolved solids were plotted, Fig. 32. A relationship covering the range in which the expected calculations will fall was estimated.

Water in the primary loop will be maintained at 2 ppm (330,000 ohm-cm from the graph). The rate of decrease in resistivity in the system running

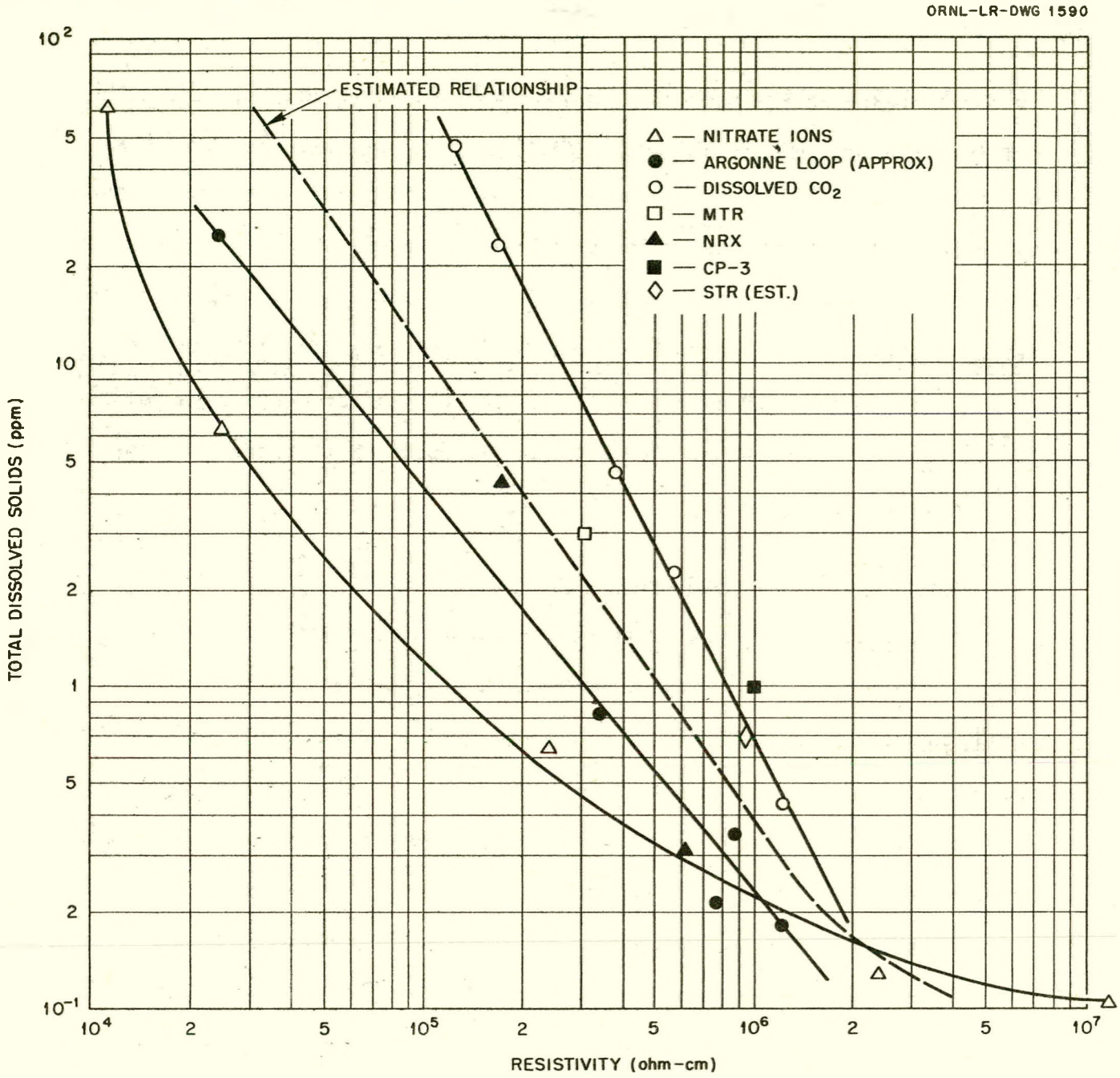

Fig. 32. Resistivity as a Function of Dissolved Solids.

without demineralizer has been selected as a basis for the determination of the rate of impurity increase as shown in the following table:

EQUILIBRIUM RESISTIVITY WITHOUT DEMINERALIZATION

Loop Condition	5 cc O_2/L 100-150 cc H_2/L Time (hrs)	Temp. (°F)	Resistivity (meg-cm)	0.38 cc O_2/L 100-150 cc H_2/L Time (hrs)	Temp. (°F)	Resistivity (meg-cm)
Startup	0	150	1.2	0	150	1.3
H_2 added	0.8	150	1.2	0.8	150	1.1
Start of 1st Const.Temp.	1.9	412	0.51	2.1	412	0.61
End of 1st Const. Temp.	2.4	412	0.48	2.8	412	0.57
Start of 2nd Const.Temp.	3.0	500	0.34	3.3	500	0.50
During 2nd Const. Temp.	3.5	500	0.30	3.7	500	0.50
End of 2nd Const. Temp.	7.2	495	0.30	881.	500	0.44-0.48

In a test without hydrogen, the resistivity dropped to within less than 0.1 megohm-cm before temperature was reached.

From the above it can be seen that under operating conditions approaching that of the reactor, the resistivity drops off from 1.3 megohm-cm to 0.44-0.48 megohm-cm in 77 hours which is, from Fig. 32, equal to about 1 ppm.

If it is intended that the water be maintained at 2 ppm and if non-deionized water has its impurity increased by 1 ppm in 77 hours, then it would be necessary to completely replace the water in the system with water of 1 ppm purity in 77 hours. Thus the make-up water would have to be:

$$\text{Volume of loop in gallons} = 1365$$

$$\text{make-up } \frac{1365}{77} = 17.8 \text{ gal/hour}$$

It has been estimated by Sevitz and Scheibelhut at Argonne that 1 gram equivalent of solids requires 1 liter of cation resin and 2 liters of anion resin. A gram equivalent of the total dissolved solids has been

estimated by calculating the average molecular weight of dissolved solids in a typical water sample at the Argonne pilot channel at Oak Ridge as follows:

Material	ppm	Mole. Wt.	%	Weighted %
(OH)	1.00	17	33	5.8
SO_4	0.3	80	10	8.0
Cl	0.2	36	7	2.5
NO_3	1.0	62	33	21.0
Ca	0.03	40	1	0.4
K	0.03	40	1	0.4
Si	0.02	28	1	0.3
Na	0.03	23	1	0.3
Remainder	0.39	50(assumed)	13	
Total Dissolved Solids	3.00			45.2 Average Molecular Weight

The water as received from the evaporator has been estimated at 5 ppm. Since it is necessary to make up water at the rate of about 18 gph of 1 ppm solid content, it is necessary to remove 4 ppm of the solids from the water initially containing 5 ppm.

$$\frac{0.004}{45.2} = 8.8 \times 10^{-5} \text{ equivalents/liter}$$

$$= 6.0 \times 10^{-3} \text{ equivalents/hour}$$

at 8750 hours/year

$$= 52.5 \text{ equivalents/year}$$

at the rate of 3 liters/gram equivalent

$$= 157.7 \text{ liters of resin/year}$$

A commercial demineralizer, such as the Barnstead Model MM-2, will supply the needs as follows: The unit will provide 1300 gallons of water whose mineral content has been reduced from 10 grains/gallon to 10 ppm. The demineralization is therefore

$$10 \text{ grains/gallon} = \frac{10}{7000 \times 8.3}$$

$$= 170 \times 10^{-6} \text{ lb/lb}$$

$$= 170 \text{ ppm}$$

The net solids removal is then 160 ppm, and 1300 gallons with a 160 ppm removal is equivalent to

$$1300 \times \frac{160}{4} = 52{,}000 \text{ gallons of water with 4 ppm removal}$$

at the make-up rate of 18 gph then

$$\frac{52{,}000}{18} = 2900 \text{ hours}$$

$$= 129 \text{ days}$$

The demineralizer would have to be regenerated every 120 days.

It is of interest to note that the use of a by-pass recirculating system would require the removal of 1-2 ppm solids by the demineralizer instead of 4. This could either have the effect of reducing the size of the demineralizer to almost 1/3 size or it would permit the use of the suggested demineralizer without regeneration for one year instead of 4 months. In order to properly evaluate the purge system against the by-pass recirculating system, several advantages of the former must be taken into account. If a purge system is used, the demineralizer will never become radioactive and will require no shielding. Further, no heat exchanger will be required to cool the water from 450° F to 100° F to permit it to go through the resin beds. The system up to the feed pump can be operated at low pressure, about 35 psi for the MM-2. If the purge system is used, the recharging of the demineralizer will consume 50 pounds of hydrochloric acid and 25 pounds of sodium hydroxide per year.

In this discussion of the capacity of the demineralizer, the effect of the initial cleanup of the system on the resin bed has been neglected.

It is possible that auxiliary filtering devices may have to be used temporarily to remove the debris that usually is associated with the fabrication and assembly of a large system such as this. It is expected that the initial fill of water will be continuously recirculated through the demineralizer and filters prior to reactor startup until the concentration of soluble impurities and suspended solids has been reduced to 2 ppm.

The purification system for the primary coolant is composed of two mixed-bed type ion exchangers, two filter beds employing micrometallic filters, and a storage tank. The demineralizers are in series with the filter beds and are used alternately. Water from the steam system passes into the storage tank and from there through an ion exchanger and its associated filter bed. The impurities in the water at this point should be less than 1 ppm.

The demineralized water is pumped into the primary coolant system by two sets of pumps. One pump will deliver about 8 gph through the seals in the control rod drives to provide a positive pressure inward through the seals and thereby prevent the leakage of contaminated water. These pumps operate continuously. A second set of pumps, each of about 60 gph capacity, supply the primary loop directly.

Coolant water is expelled from the primary system either continuously through a capillary or periodically through a valve. This removal of water causes the level in the pressurizer to fall and signals the second set of feed pumps to feed in the high purity water. When the upper limit of the pressurizer has been reached, the feed pumps automatically shut off.

The amount of purging, presently estimated at between 18 and 30 gph, will be definitely established during operation to maintain the required

water purity. The make-up pump is believed to be of sufficient size to meet any expected drop in water purity in the loop.

4.8 Instrumentation and Control

Because of the initial premise of low cost for this plant, all non-vital instruments were omitted. The instrumentation was designed to meet the needs of a power plant and not that of a research facility. It is felt that the following information concerning the facilities of process water and cooling air should satisfy the most important operating requirements.

Primary coolant outlet temperature

Coolant water flow rate

Coolant water inlet temperature

Pressurizer liquid level

Primary system pressure

Liquid level in make-up water storage tank

Integrated flow through the demineralizer

Reactor pit air temperature

The temperature of the primary coolant is probably the most important information for the reactor operator. Undue changes in temperature or flow of this water can result in damage to the reactor just as serious as undue changes in neutron level. The process water outlet and inlet temperatures as well as the flow rate are three of the most critical factors to control.

To maintain the power output in step with the steam power demand under constant water flow conditions, only the proper Δt need be maintained. This permits the control of either the inlet or outlet reactor water temperature

while the other uncontrolled temperature will adjust itself to meet the demand. The reactor outlet water temperature was selected as the controlled quantity in order to limit the maximum reactor temperature to 450° F. In effect, the coolant temperature is controlled by controlling the temperature of the fuel plate. This is accomplished as follows.

A temperature-sensing device is placed in the coolant outlet line, as close to the reactor as possible and still accessible for maintenance. The sensing device should be accurate and have a high response speed. For this application a Foxboro Dynatherm resistance bulb may be used. Resistance bulbs are more stable than thermocouples due to the elimination of cold junction compensation. The output of the resistance bulb is fed to the input of the regulating rod servosystem. As the outlet water temperature increases, the signal received by the servosystem indicates to the system that the regulating rod must be driven down. The system then drives the rod down, decreasing the flux density, decreasing the fuel temperature, and returning the coolant to its proper temperature. If the coolant falls below the desired temperature, the signal is to raise the rod, reversing the procedure. In this way the outlet water temperature is maintained constant.

The outlet coolant temperature is also recorded for power reference. The recording instrument activates signal lights to inform the operator that the temperature has exceeded predetermined limits, enabling him to take proper action if the automatic system has not done so already.

The coolant water flow information is needed since any change in flow directly affects the temperature of the coolant. A recording instrument operates signal lights to inform the operator that the flow has exceeded or fallen below predetermined safe limits. If no action is taken by the

operator and the flow continues to deviate from the safe range, the current to the magnetic clutch is automatically turned off and the control rods drop, shutting down the reactor. The inlet water temperature is also recorded to allow calculation of the reactor power. A direct-reading power meter would be most desirable.

For convenience of recording, calculation, and storage, all three quantities are recorded on the same instrument. This instrument may be of the Foxboro Multi-record Dynalog type using three pens and containing Foxboro Rotax signal controls. Each pen controls a set of Rotax switches. The outlet temperature Rotax control actuates signal lights when the temperature deviates a predetermined amount, in either direction, from 450° F; the flow control Rotax signals when the flow rate exceeds 110% that of normal or falls to 85% of normal; and the inlet temperature Rotax switches signal when the inlet temperature has fallen below a safe limit for full load. Each of the three recorded quantities have their own sensing devices. The outlet temperature is recorded from a Dynatherm resistance bulb in the reactor outline, separate from that used to signal the servosystem. A Dynatherm type resistance bulb is also placed in the inlet reactor line as the inlet water temperature sensing device. The flow is determined from the pressure drop measured across an orifice in the primary line by an electrically operated differential pressure cell, manufactured by Foxboro and other instrument manufacturers.

Since the pressurizer is physically located at the high point of the primary loop, it is assured that the primary loop is filled as long as there is a liquid level in the pressurizer. This level can be maintained automatically by an indicator-controller instrument such as the Foxboro Rotax

indicating controller. The level is sensed by a differential pressure cell and the signal to the control instrument actuates the Rotax switches which automatically starts or stops the make-up pumps supplying water to the primary loop. At predetermined values the instrument energizes signal lights to inform the operator that the level has exceeded or fallen below safe level limits.

Another quantity to be sensed and controlled at the pressurizer is the pressure in the primary system. The signal from the fluid pressure cell is sent to a Foxboro indicating controller-type instrument in the control room. The Rotax switches in the instruments are arranged so that additional heaters are energized in the pressurizer as the pressure decreases. The heaters can be energized or de-energized in as many steps as is deemed convenient. Signal lights also indicate when the pressure has deviated past safe upper and lower limits.

The liquid level in the makeup water tank is indicated in the control room by means of a differential pressure cell, operating another Foxboro instrument. This instrument indicates the liquid level and actuates signal lights when the water falls below the desired level. The tank is then filled by manually operated valves.

Since the resin bed used in the demineralizer must be reactivated after a given amount of usage, the flow through the bed must be indicated. The pipe line leading to the demineralizer passes along the operations deck where it is convenient to install a Rockwell-type water meter, which indicates total gallons flowing to the demineralizer. After a predetermined volume of water has been treated, the demineralizer should be reactivated.

The temperature of the air in the reactor pit is important because of the presence of instruments and motors which limits the maximum allowable ambient temperature. Outside air is circulated through the pit by an air blower. The temperature is indicated by a filled thermal system; a thermal bulb feeds into an instrument which may be of the Foxboro-type electrically operated Rotax controller. The control portion of the instrument is used only for signal light control. If the air temperature rises above normal the light signals the operator, who then adjusts the ventilation controls.

4.9 Emergency Cooling

After any shutdown of the reactor, it is necessary to remove fission-product decay energy from the core; even during a normal scheduled shutdown some form of cooling must be provided. A careful study of this design was made to insure that temperatures of the fuel plates will not be high enough at any time to damage them. Relative locations of the reactor core and the steam generator tube bundle are such that, with the coolant circulating pump shut down, natural convection will be adequate to keep the reactor cool after shutdown.

By virtue of the fact that the coolant is also the moderator, this reactor is fundamentally safe in an emergency in which failure of pumps occurs. If the circulating pump fails during full-power operation without an immediate scram, the water in the core will reach the boiling temperature within 3 or 5 seconds. The boiling will itself cause the reactor to become subcritical. During the interval required to bring about boiling, the maximum heat flux is 223,600 Btu/hr-ft^2. Since the flow rate is reduced,

boiling occurs on the surface of the plates; very high heat fluxes are then possible. Recent tests at ANL* indicate, however, that in a flat-plate geometry very similar to that used in this reactor, burnout occurs at a continuous heat flux of approximately 220,000 Btu/hr-ft^2 at atmospheric pressure. Hence, for continuous heating at the full-power rate, a very dangerous situation exists, and it is important that shutdown occur very rapidly after failure of the pump. Although the shutdown will be brought about by the rise in temperature and boiling of the water, interlocks are provided on pump motor current and on coolant flow rate to scram the reactor.

One second after shutdown, the maximum heat generation rate is down to 12,280 Btu/hr-ft^2, Fig. 33. For this heat flux the temperature drop in the plate is only 4.92° F. Therefore, within one second after shutdown the heat is safely transferred from the plates to the water.

Flow by natural convection from the core to the heat exchanger and return is adequate to remove all after-heat from the reactor if a supply of water to the shell of the steam generator is maintained. It has been established that for steady state generation of 750,000 Btu/hr, the flow rate by natural convection is 4.9 x 10^5 lb/hr, with the heat being utilized to generate steam in the steam generator at 200 psia. Under these conditions, the temperatures of water entering and leaving the core are 382° F and 392.6° F respectively. The velocity in the core is 0.123 fps, giving a Reynolds number of 1500. This is near the transition between laminar and turbulent flow, but on the laminar side. From equations for heat transfer with laminar flow the film coefficient in the core is 303

*Personal Communication, Paul A. Lottes to P. C. Zmola, Sept. 9, 1953.

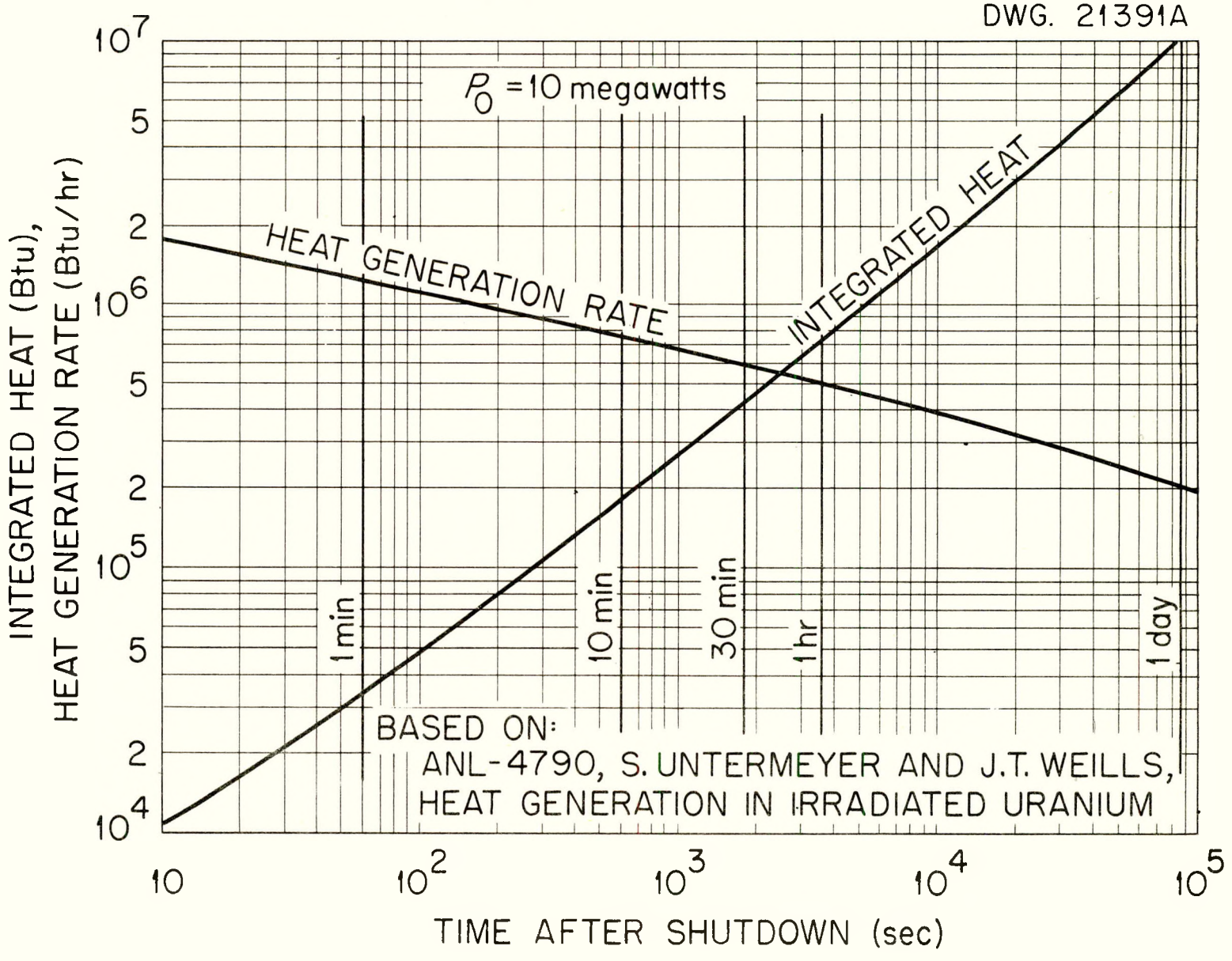

Fig. 33. Reactor Heat After Shutdown.

Btu/hr-ft^2-°F. The maximum heat flux ten minutes after shutdown is 4905 Btu/hr-ft^2, so that the temperature drop is 16.2° F. This yields a plate surface temperature of approximately 416° F, indicating that boiling is not taking place at this time.

A small steam-driven, piston-type boiler feed pump is provided for pumping water into the steam generator during shutdown, independent of any supply of electric power.

The thermal capacity of water in the primary coolant system and in the steam generator insures cooling of the core for a period of approximately 26 hours after shutdown. The total volume of water in the primary coolant system is 180 ft^3, or 9400 lb. The average temperature is 440.8° F. To raise the average temperature to the boiling point at 1200 psia requires 152.7 Btu/lb. So, before any net boiling occurs 1,434,000 Btu are absorbed. The volume of water above the tops of the fuel plates is 100 ft^3, or 5216 lb. The heat of vaporization at 1200 psia is 611.7 Btu/lb. So before the fuel plates are exposed, 3,200,000 Btu additional are absorbed. Furthermore, this evaporation process cannot take place as long as the heat exchanger tubes are submerged in water. The volume of water in the heat exchanger shell is 114.7 ft^3 which, at 54.4 lb/ft^3, is 6230 lb. Since the water is initially at 200 psia, saturated, and since 500 psia is required to open the safety valve for steam to escape, 849 Btu/lb are required to evaporate water in the exchanger shell. So a total of 5,290,000 Btu are absorbed in drying out the heat exchanger. This makes a grand total of 9,924,000 Btu which can be absorbed by the system before the fuel plates are exposed, neglecting heat losses. This is the amount of after-heat generated in the first 22.5 hours after shutdown.

Heat losses amount to 42,000 Btu/hr, giving approximately 1,000,000 Btu for 24 hours. Adding this to the previous total brings it to 10,924,000 Btu, which is equal to the decay heat for approximately 26 hours. Thus, if no cooling water were available, or if the feed pump were inoperable, a period of 26 hours is available in which to make repairs.

4.10 Insulation

It is necessary to provide adequate thermal insulation of all high-temperature components in order to keep heat losses to a minimum, to keep the ambient air temperature inside the shield below 150° F for protection of motors and other electrical components, and to avoid heating the concrete to temperatures in excess of 200° F. The insulation chosen should have, in addition to a low thermal conductivity, a high resistance to radiation damage from neutrons and gamma radiation, and a low absorption capacity for water. The material tentatively specified for use inside the shield is Foamglas manufactured by Pittsburgh-Corning Corporation. It consists of a mass of small sealed glass bubbles of air, so formed that only the bubbles at the outer surface which are broken in the cutting process are open to the atmosphere. Thus, in event of a spill, only a small amount of liquid is absorbed by the insulation, and that may be removed by washing or scraping.

Heat loss calculations are based on an assumed thickness of 4 in. of Foamglas on all piping and equipment inside the shield, except motors. The average thermal conductivity of insulation on the primary coolant system is 0.565 Btu/hr-ft^2-°F/in., and on the steam system it is 0.54. In air at 150° F, this yields average heat losses of 46 and 34 Btu/hr-ft^2 from the primary coolant system and the steam system respectively. Based

on these data, heat losses in Btu/hr from the various major components inside the shield are:

Primary coolant piping pumps and valves	20,700
Reactor pressure vessel	6,760
Pressurizer	6,500
Steam generator, shell	5,770
Steam generator, headers	7,000
Steam line	1,070
Total Btu/hr	47,800

For high temperature equipment outside the shield ordinary steam-pipe insulating material may be used, such as 85% magnesia. Danger of radioactive contamination is lower outside the shield, and in the event of such an accident, the insulation is more readily removed and replaced than that inside the shield.

4.11 Analysis of Materials

The suitability of any material of construction for a reactor is based upon these prime factors:

It must have the proper physical properties to perform its function over long periods of time.

It must resist radiation damage and perform satisfactorily under radiation and in contact with transport materials which have been irradiated.

It must withstand the corrosive action of contact with and sub-submersion in water at 500° F.

On the basis of information generally available in the literature on materials and on the basis of extensive investigations and tests run at atomic energy installations such as Hanford, Oak Ridge, Argonne,

Babcock and Wilcox, Battelle, Brookhaven, North American, General Electric, Westinghouse, and others, it has been possible to compile data and evaluate materials in the light of the above requirements.

Among the materials which have been investigated are the following:

304 ss	Monel
304L ss	K-Monel
316 ss	Inconel
347 ss	Inconel-X
410 ss	Armco 17-4 PH
440L ss	Armco 17-7 PH
Stellite-3	USS 322 W
Stellite-6	A-Nickel
Stellite-12	Hastelloy C
Graphitar-14	Vascoloy-Ramet 166
Chrome Plate	

The results of the investigation are reported in more detail in Appendix 13.3.

A list of specific suggestions for the various components has been supplied, together with a range of materials, to enable the designer to select an alternate if for some reason the selected material is unavailable. The effect of irradiation upon the materials can all but be discounted, since its effects are generally to toughen and harden the material.

Stainless steel 304 has been selected as the basic material to be used except in certain special instances. Most of the reactor and corrosion loops to date have employed 347 ss as the basic corrosion resistant material. The state in reactor technology has been reached where it is becoming more important to select an optimum material rather than just the "best" material. The selection of such an optimum material is a function of the ability of the material to perform what is required of it, based on lowest cost, availability, control, etc. Since 347 ss costs more (about 25%), contains the strategic material, columbium, and is only slightly

better under some conditions than 304 ss, the selection of 304 ss is justified.

The materials for the primary loop are then as follows:

1. Reactor Vessel

   304 ss clad to A.S.M.E. Type-SA 212 Grade-B fire-box quality steel. Gasket - dead soft nickel or monel. Studs - 304 ss, nuts - 303 ss.

2. Piping

   304 ss, Weld 304L ss or 25-20 ss.

3. Fuel Elements

   Cladding - 304 or 304L ss; matrix - 304 or 304L ss sintered with suitable fuel.

4. Control Mechanisms

   Rack and gear 440C ss
   Seal - discs Stellite 3; diaphragm - K-monel
   Shaft - Armco 17-4 PH or 440C chrome-plated
   Bearing - rollers and races - Stellite 3
   Retainers - Armco 17-4 PH
   Springs - Inconel-x

5. Heat Exchanger

   Tubes and headers - 304 ss

6. Pumps

   Canned rotor
   Frame, block and position indicator - 347 or 304 ss
   Bracket and bearing carrier 304 ss
   Shaft - 410 or 440C ss chrome-plated
   Lamination ring - monel

7. Valves - gate

   Body - 347 or 304 ss, Stellite 3 runners
   Gate - Armco 17-4 PH

8. Valves - check

   Body - 347 or 304 ss
   Pin - Stellite 3
   Facing-Stellite 3

It should be noted that the 304 ss can be replaced by 304L, 316, 321, or 347 ss if necessary.

4.12 Gases in Solution

The presence of gases normally found dissolved in water has been found to be undesirable in the primary loop. The quantity of these gases, primarily carbon dioxide, nitrogen and oxygen, should be kept low. Carbon dioxide forms carbonic acid and lowers the pH and the specific resistivity of the system water. Carbon dioxide can be removed by the anion resin of the demineralizer but this shortens the effective life of the demineralizer. Nitrogen under irradiation can form either ammonia if hydrogen is present, or nitrates, and nitric acid. All of these compounds lower the specific resistance of the water and increase the corrosion potential.

Oxygen is undesirable because it combines with the metals to form oxides and with carbon to form carbon dioxide and with nitrogen to form nitrates. It is also one of the elemental constituents of water and is therefore difficult to exclude from the water.

Hydrogen, on the other hand, in a minimum quantity of 50 cc/liter of water has been found to inhibit overall corrosion in general and crevice corrosion in particular. It has also been found to inhibit the formation of oxygen, to reduce wear, and to assist in the maintenance of higher water purity.

4.12.1 Hydrogenation. The hydrogenation of water in a purge and make-up system, such as is proposed, offers a somewhat different problem than is encountered with a reactor whose primary coolant is sealed in and continually recirculated. Continuous bleeding of primary coolant plus losses in gasketed closures and seals requires a continuous influx of make-up water for which hydrogen must be provided. Assuming that a

concentration of 50 cc/liter is required in the coolant and that the rate at which make-up water is introduced is 30 gph, the hydrogen requirement will be 136 liters/day at standard conditions of temperature and pressure. If the hydrogen is introduced into the low pressure section of the make-up line, i.e., upstream from the feed-water pump, a gas cylinder can be used until its pressure is reduced to approximately 200 psi; under these conditions it will last 39 days. Thus, for one year of operation ten standard 2660 $in.^3$ cylinders of hydrogen gas will be required. The hydrogen should always be added to the water before heating the system.

4.12.2 Degasification. The operations of degassing and hydrogenating the primary coolant are at cross purposes. In the one case the object is to remove dissolved gases from the water and in the other to add a dissolved gas as a corrosion inhibitor. It is obvious that these two processes cannot go on simultaneously.

It is felt that degasification as such is unnecessary. The gases introduced into the primary loop with the make-up water are considered negligible because of the distillation process and the demineralization which removes any CO_2 still remaining. It is known, however, that oxygen and hydrogen will be formed by dissociation of the water due to irradiation. The presence of stoichiometric quantities of O_2 and H_2 will likewise result in some recombination of these elements. The net result in terms of the gas remaining is somewhat in doubt. It is known, however, that an excess of hydrogen will inhibit the formation of oxygen. It is estimated that the resultant oxygen concentration in the water will be about 0.25 cc/liter of water. Because of the circulation of the water it is possible for some of the gases to be eventually transferred to the

pressurizer, where, some of the gases will leave solution and add their partial pressure to the steam. Eventually, equilibrium between the gas and liquid phases will be reached and no further degasification should take place. The presence of these gases in the pressurizer can be detected by noting the difference between the theoretical boiling temperature at the existing pressure and the actual temperature in the pressurizer.

The presence of a concentration of hydrogen greater than the 50 cc/liter which is required as a corrosion inhibitor does present a problem on shutdown, however.

Allowing the hydrogen to come out of the solution and form gas pockets as the water is cooling might lead to difficulties during the next startup period. Perhaps the most serious result of gas pockets in the system might be the entrapment of gas in the tubing connecting the primary system with differential pressure cells used to give indications of flow or liquid levels. These devices are very sensitive to small changes in pressure and it is important that no gas accumulate on one side of the diaphragm which forms the sensing element.

Inspection of the proposed package reactor primary system leads to the conclusion that the hydrogen will collect not only in the pressurizer, but at several points in the primary loop such as the top of the reactor, the check valves, the pump housings, and the headers at either end of the heat exchanger. As soon as the circulating pump is started for a subsequent run, primary coolant will sweep this collected gas around the system and as the temperature and pressure increase, the gas will be reabsorbed in the water. The only precaution that need be taken is that

gas should not be allowed to accumulate in the lines leading to the flow and pressure measuring instruments. This can be accomplished by judicious venting of the lines and the use of valves to isolate these instruments on shutdown.

14.3 Accessibility for Maintenance

It would be impractical to design this plant in such a way as to make any component inaccessible for repairs. The principal difficulties to be overcome are the radiations from fission products in the core and from induced activities in other parts of the system. Accessibility to the core is provided by a water shield over the pressure vessel, which is drained during operation. All work performed in the reactor compartment must be done remotely, working through the water shield. It is not desirable to flood the control rod drive motors; when the motors are in place over the vessel, the water level above the vessel lid should not exceed 2 ft. This depth, plus the thick sheet of the vessel lid makes it possible to work from the top of the shield with long tools.

The pumps, heat exchanger, pressurizer, check valves, and fan are separated from the core by sufficient shield so that activation by neutrons is negligible. Some activity may build up, however, due to corrosion products deposited from the water. Since activation of the water is low, all components in the heat exchanger compartment will be accessible within a short time after shutdown. Removal of all components except the heat exchanger and reactor vessel is practical.

The heat exchanger is positioned so that tube headers are adjacent to outside walls of the compartment and removable shield blocks are placed

in the wall beside them. Thus, it is possible to open the shield wall and the end of the heat exchanger in order to plug or repair any tubes that may develop a leak.

Access to the pressurizer for replacement of electric heaters or the safety valves is from above by removal of the shield plugs.

5.0 PHYSICS

The physical characteristics of the package reactor core have been evaluated by the use of three-group and modified two-group diffusion theory. A program of multigroup calculations, involving the use of high speed computers, is also in progress, but is not sufficiently advanced to be discussed in detail here.

Some general features of the core behavior may be predicted by qualitative analysis or by analogy with other somewhat similar reactors:

1. It is clear that if the core contains, in addition to its critical mass, enough fuel for several years of operation, the reactivity may be quite high, especially if the core is cooled to room temperature. In order to reduce the initial reactivity, it is planned to incorporate boron in the fuel matrix as a burnable poison.

2. Multigroup calculations* of a number of hydrogenous reactors with fuel-to-moderator ratios in the range expected for the package reactor indicate than an appreciable fraction of fissions will be caused by neutrons with energies up to a few hundred electron volts. This resonance absorption is not properly described by the usual two-group diffusion theory.

3. The ANP calculations* also indicate that the leakage of neutrons from the core occurs predominantly at energies above 100 kev. Consequently, the loss of neutrons by leakage and the critical value of the infinite multiplication factor will be nearly independent of fuel and poison concentrations in the core.

5.1 The Modified Two-Group Theory

In view of the appreciable resonance absorption of the package reactor core, it was considered advisable to use at least three groups to describe the neutron flux. The ANP calculations referred to above indicate the resonance group should extend from thermal energy (lethargy

*Mills, C. B., The General Methods of Reactor Analysis used by the ANP Physics Group, ORNL-1493, Sept. 1953.

u = 19.23) to about 450 ev (u = 10, where u = 0 at E = 10^7 ev). Since there is very little probability of a neutron scattering from group 1 to group 3 directly, the equations describing the neutron flux in the core may be written

$$D_1 \nabla^2 \varphi_1 - \Sigma_1 \varphi_1 + (1-p) k_2 \Sigma_2 \varphi_2 + k_3 \Sigma_3 \varphi_3 = 0 \qquad (1)$$

$$D_2 \nabla^2 \varphi_2 - \Sigma_2 \varphi_2 + \Sigma_1 \varphi_1 = 0$$

$$D_3 \nabla^2 \varphi_3 - \Sigma_3 \varphi_3 + p \Sigma_2 \varphi_2 = 0$$

However, since the age from 450 ev to thermal energy is only about 12% of the age of fission neutrons to thermal energy, the slowing down distribution of a single fast group extending from u = 0 to u = 19.23 is affected very slightly by the resonance absorption. With little loss of generality, therefore, the three groups may be reduced to two, with multiplication in the fast group:

$$D_1 \nabla^2 \varphi_1(\bar{r}) - \Sigma_1 \varphi_1(\bar{r}) + (1-p) k_1 \Sigma_1 \varphi_1(r) + k_2 \Sigma_2 \varphi_2(r) = 0 \qquad (2)$$

$$D_2 \nabla^2 \varphi_2(\bar{r}) - \Sigma_2 \varphi_2(\bar{r}) + p \Sigma_1 \varphi_1(\bar{r}) = 0$$

Here, k_1 is the resonance multiplication factor, k_2 is the thermal multiplication factor and p is the resonance escape probability. All constants in equation (2) are described below.

The conclusion that the three-group and modified two-group treatments should yield comparable values of the critical mass was verified by applying both methods to an equivalent bare reactor. The results were indistinguishable. The modified two-group treatment was therefore employed because of its greater simplicity.

5.2 The Group Constants

5.2.1 Cross Sections. The cross sections used in computing the group constants were taken chiefly from the compilation of the ORNL Reactor Calculations Group. The resonance cross sections of uranium were taken from BNL-170B*. In view of the present uncertainty in the energy dependence of the quantity $(1 + \alpha) = \frac{\sigma_a}{\sigma_f}$ in the low energy range a choice must be made whether to use the fission or the capture cross-section curves. Above 1 ev, both the fission and the absorption cross-section curves were used. Below 1 ev only the fission cross-section curve was used and $(1 + \alpha)$ was assumed to be 1.184 throughout this range. It was determined that the resonance integrals discussed below are insensitive to the detailed shape of the cross-section curves.

The average thermal-fission cross section of U 235 was obtained by numerical integration of the cross-section curve in BNL-170B over a Maxwell distribution at 450° F. The resulting average cross section was normalized to agree with the assumption that $(1 + \alpha)$ is constant below 1 ev. The average absorption cross section is then $1.184\,\sigma_f$. A similar average was obtained for the cross section of Xe 135, taken from TAB-84**.

Values of the average cross sections used are shown in the following table.

---

* Neutron Cross Sections, Supplement 2, BNL-170B, Apr. 1953.

** Greuling and Goertzel, Temperature Dependence of Xenon 135 Cross Section, TAB-84, Aug. 1950.

$\frac{T}{(°F)}$	$\frac{\sigma_f}{(\text{barns})}$	$\frac{\sigma_a \text{ (U 235)}}{(\text{barns})}$	$\frac{\sigma_a \text{ (Xe 135)}}{(\text{barns})}$
68	509.0	602.7	2.87×10^6
450	372.3	440.8	2.66×10^6

All other absorbers were assumed to have 1/v cross sections*, and their average cross sections over a Maxwell distribution at the core temperature were used.

5.2.2 Inelastic Scattering. Because of the rapid decrease of the n-p scattering cross section with increasing energy in the range from 1 to 10 Mev, the inelastic scattering of neutrons by metals in the core may play an important role in moderating neutrons in this energy range. In computing the age and the average diffusion coefficient of fast neutrons in the core, inelastic scattering was accounted for by adding to the hydrogen scattering cross section a fictitious cross section, σ', given by

$$\sigma' = \sigma_i \, \bar{\xi} \, \frac{N_{SS}}{N_H} \qquad (3)$$

where σ_i is the compound-nucleus scattering cross section of stainless steel, $\bar{\xi}$ is the average logarithmic energy decrement in inelastic scattering, and N_H and N_{SS} are the average numbers** per cm^3 of atoms of hydrogen and of the elements in stainless steel, respectively. Chromium and nickel are assumed to have the same inelastic scattering effects as iron.

* Compilation of the AEC Neutron Cross Section Advisory Group, AECU-2040.

**Materials in the core are treated as if homogeneously distributed throughout the core volume; N_x is the total number of atoms of material x in the core, divided by the total core volume.

The inelastic scattering cross section of iron, σ_i', is computed from*

$$\sigma_i'(E) = AC(E) \sum_{j=1}^{N} (E - E_j)^{1/2} \qquad (4)$$

where E is the incident neutron energy and E_j is the excitation energy of the j^{th} state of the iron nucleus. N is determined by the requirement $E_N < E$, and C(E) by: $C(E) \times \sum_{j=0}^{N} (E - E_j)^{1/2} = 1$. The constant A was determined by comparison of (4) with experimental results for the inelastic cross section of iron**.

The quantities σ_i and $\bar{\xi}$ in (3) were computed from the formulae:

$$\sigma_i = AC(E) \sum_{j=o}^{N} (E - E_j)^{1/2} = A$$

$$\bar{\xi} = \frac{\sum_{j=o}^{N} \ln\left(\frac{E}{E - E_j}\right)(E - E_j)^{1/2}}{\sum_{j=o}^{N} (E - E_j)^{1/2}}$$

It was found that $\sigma_i = 1.5$ barns is in good agreement with experiment, and that $\bar{\xi}$ is rather close to 0.6 over a broad energy range above the first excited state. The excited states of iron are found*** at E_j = 0.85, 1.40, 2.10, 2.60, and 3.0 Mev. Above 3 Mev, the levels were assumed to be 0.5 Mev apart.

---

* Feld, B. T., Phys. Rev. 75, 1115 (1949).

** Barschall, et.al, Phys. Rev. 72, 881 (1947).
Stelson and Preston, Phys. Rev. 86, 132 (1952).
Graves and Rosen, Phys. Rev. 89, 343 (1953).

***Elloit and Deutsch, Phys. Rev. 64, 321 (1943).
Day, Phys. Rev. 89, 908 (1953).

For the core described in this report, at 450° F,

$$\sigma' = 0.30 \text{ barns for } E > 0.85 \text{ Mev}$$

$$= 0 \text{ barns for } E \leq 0.85 \text{ Mev}$$

5.2.3 The Energy Dependence of the Flux. The fast-group diffusion coefficients, D_1, in the core and in the reflector are flux-averaged values; that is,

$$\bar{D} = \frac{\int_{u_1}^{u_2} D(u)\cdot\varphi(u)\,du}{\int_{u_1}^{u_2} \varphi(u)\,du} \qquad (5)$$

Implied in this expression is the assumption that the space dependence and the lethargy dependence of the flux are separable, i.e., $\varphi(\bar{r},u) = \psi(\bar{r})\cdot\chi(u)$. This assumption breaks down at thermal energies, because of the reflector. However, preliminary multigroup calculations indicate that the assumption is good down to very low energies, and that even at thermal energies, it breaks down only within a few centimeters of the reflector.

The integral equation for the lethargy dependence of the flux may be written

$$\left[D(u)\cdot B^2(u) + \Sigma_a(u) + \Sigma_{SH}(u)\right]\varphi(u) = f(u) + \int_0^u \Sigma_{SH}(u')\varphi(u')e^{u'-u}\,du' \qquad (6)$$

$D(u) = 1/3\ \lambda_{tr}(u)$, λ_{tr} is the transport mean free path, $B^2(u) = \left(\frac{\pi}{R_e}\right)^2$, where R_e = R + 6 cm (reflector savings) + 0.71 λ_{tr} (u); $\Sigma_a(u)$ is the macroscopic absorption cross section, Σ_{SH} (u) is the macroscopic scattering cross section of hydrogen, and f(u) is the fission spectrum. (Macroscopic cross sections throughout this discussion, except where

noted, refer to averages over the entire reactor volume.). Equation (5) rests on the assumption that all scatterers in the core, other than hydrogen, may be considered to have infinite mass.

The flux is given by the solution of (6)

$$\varphi(u) = \Lambda^{-1}(u) e^{-\int_0^u [1-g(w)]dw} \left\{ \int_0^u \left[f(u') + f'(u') \right] e^{\int_0^{u'} [1-g(w)]\,dw} \, du' \right\} \qquad (7)$$

where $f'(u) = df/du$

$$\Lambda(u) = \Sigma_{SH}(u) + \Sigma_a(u) + D(u)\, B^2(u)$$

$$g(u) = \Sigma_{SH}(u) \times \Lambda^{-1}(u)$$

In the reflector, the fission spectrum f(u) is replaced by the core leakage spectrum, $L(u) = D(u) \times B^2(u) \times \varphi(u)$.

The value of D_1 is not greatly changed if leakage and absorption are neglected in equation (6), yielding a simpler expression for the flux:

$$\varphi(u) = \Sigma_{SH}^{-1}(u) \int_0^u \left[f(u') + f'(u') \right] du' \qquad (7a)$$

Equation (7) and the similar expression for the reflector, describe the slowing-down flux and are applicable only to the fast group In the thermal group, the flux is, as usual, assumed to have a Maxwell distribution.

5.2.4 Diffusion Coefficients. The fast-group diffusion coefficient D_1 was computed from equation (5)

with $u_1 = 0$

and $u_2 = 19.23$ at 450° F
$u_2 = 19.8$ at 68° F

The thermal-group diffusion coefficient is given by

$$D_2 = 1/3 \left[\Sigma \text{ tr } (H_2O) + \Sigma \text{tr } (S.S.) \right]^{-1} \qquad (8)$$

In computing Σ tr (H_2O), the transport cross section of water, account must be taken of the fact that the hydrogen is bound in H_2O molecules. This has been done by A. Radkowsky*, whose results are presented as values of $L^2 = (3\Sigma_a \Sigma_{tr})^{-1}$ for water as a function of temperature. The values used were L (H_2O) = 2.70 cm at 68° F, and L = 4.07 cm at 450° F.

5.2.5 Age. The mean squared slowing-down length of fission neutrons in the core was calculated by a method described by C. W. Tittle** The method involves calculating mean free paths for the first few collisions with hydrogen, assuming a lethargy change of one in each collision; below about 100 kev, age theory is employed. Inclusion of inelastic scattering in the age calculation reduced the age about 10%.

For the age in water the experimental value at 68° F*** was multiplied by a density correction factor, $(\frac{\rho_{68° F}}{\rho_T})^2$.

5.2.6 Resonance Integrals. Since there are relatively few absorptions of neutrons at energies above 450 ev, the resonance properties of the reactor are described by integrals from 450 ev to thermal energy.

The resonance escape probability is given by the Wigner formula

$$P = \exp\left[-\int_{u=10}^{u_{th}} \frac{\Sigma_a \, du}{\xi (\Sigma_a + \Sigma_s)}\right] \qquad (9)$$

---

* Radkowsky, A., Temperature Dependence of Thermal Transport Mean Free Path, ANL-4476.

** Tittle, C. W., Nuclear Shielding Studies, I, NP-1418.

*** Reactor Handbook, Vol. I, p. 525.

However, in the package reactor core, Σ_a is always much smaller than Σ_s, even at resonance peaks, so that (9) is well approximated by

$$P = \exp\left[- \int_{u=10}^{u_{th}} \frac{\Sigma_a(\text{U 235}) + \Sigma_a(B^{10})}{\Sigma_{SH}} \, du \right] \qquad (10)$$

The multiplication factor for neutrons absorbed in the resonance region is

$$k_1 = \frac{\nu \int_{u=10}^{u_{th}} \Sigma_f(u)\, \varphi(u)\, du}{\int_{u=10}^{u_{th}} \left[\Sigma_a(\text{U 235}) + \Sigma_a(B)\right] \varphi(u)\, du} \qquad (11)$$

where ν is the average number of neutrons per fission, = 2.48.

The resonance multiplication factor is substantially greater than the thermal multiplication factor, which is

$$k_2 = \frac{\nu \Sigma_f(\text{U 235})}{\Sigma_a(\text{total})} \qquad (12)$$

and a significantly lower estimate of critical mass is obtained if the resonance absorption is taken into account. The modified two-group method gave a critical mass 15% smaller than the usual two-group method.

5.2.7 Self-Shielding. Because of the heavy concentration of absorbers in the fuel plates, the neutron flux in the fuel is somewhat lower than in the moderator. The reactor may be treated as if it were homogeneous by applying a factor, less than one, to the macroscopic cross sections of all constituents of the fuel matrix. This factor, calculated on the assumption that the flux entering the fuel plate is isotropically distributed, is given by

$$F = 1 - 0.321\, \Sigma_a t \qquad (13)$$

In Equation (13) $\underline{t}$ is the full thickness of the fuel matrix and Σ_a is the true macroscopic cross section of absorbers in the matrix, obtained by dividing the cross section of all atoms of absorber in the matrix by the volume of the matrix material in the core.

5.2.8 Summary of Group Constants. The group constants used for the core and the reflector are given below and in Figs. 34-38.

Constant	Core		Reflector	
	68° F	450° F	68° F	450° F
D_1	1.21	1.44	1.54	1.85
τ	35.5	48.9	31.4	45.6
Σ_1	0.0341	0.0294	0.0490	0.0406
k_1		(Cf Fig. 34)	0	0
p		(Cf Fig. 37)	1.0	1.0
D_2	0.166	0.229	0.143	0.204
L_2^2		(Cf Fig. 38)	7.29	16.56
Σ_2		D/L^2	0.01957	0.01232
k_2		(Cf Figs.35,36)	0	0

Graphs of the quantities k_1, k_2, p, and L_2^2, which depend on fuel concentration, are given at 450° F to illustrate a way of presenting the information to facilitate the critical calculations.

5.2.9 Burnout Rate of Fuel. The burnup of the fuel was calculated on the basis of 193 Mev of heat energy per fission. Since radioactive capture competes more strongly with fission in the resonance region than at thermal energies, the burnup rate depends on the fuel concentration in the core. In the package reactor core the burnup is very close to 500 grams/mw-yr over the whole range of fuel concentrations to be considered.

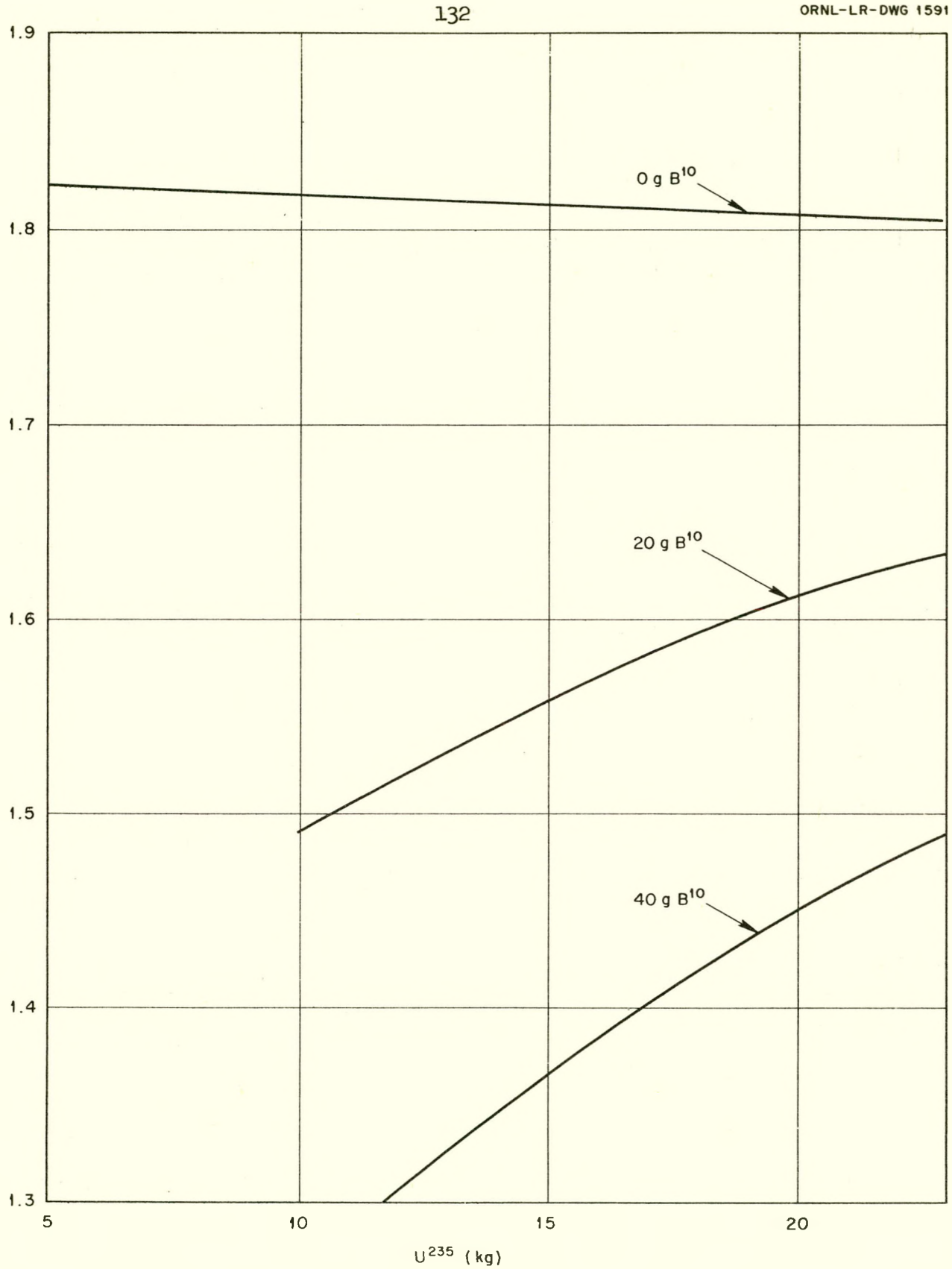

Fig. 34. Resonance Multiplication Factor, k_1. T = 450°F.

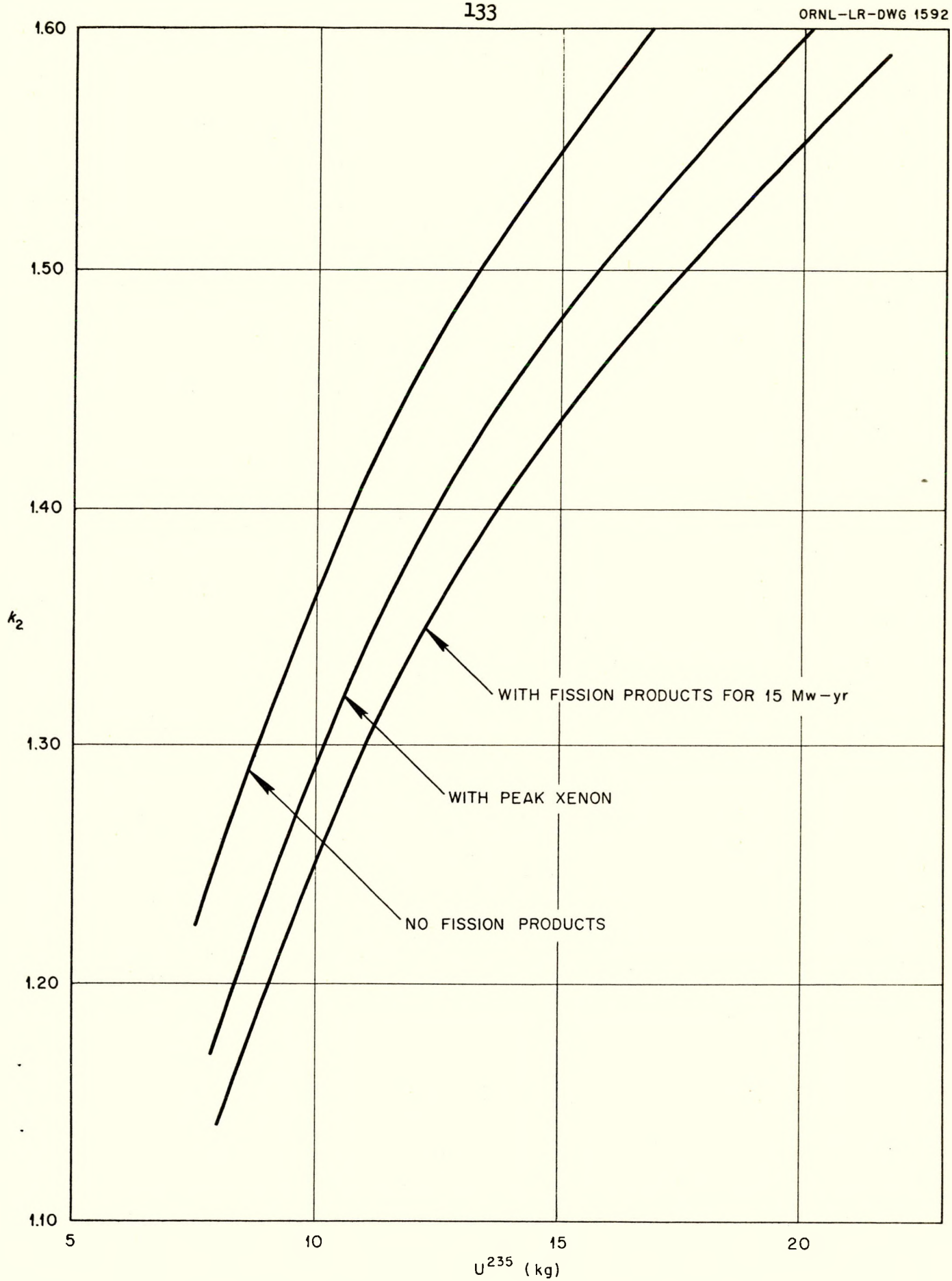

Fig. 35. Thermal Multiplication Factor, Without Boron. T = 450 °F.

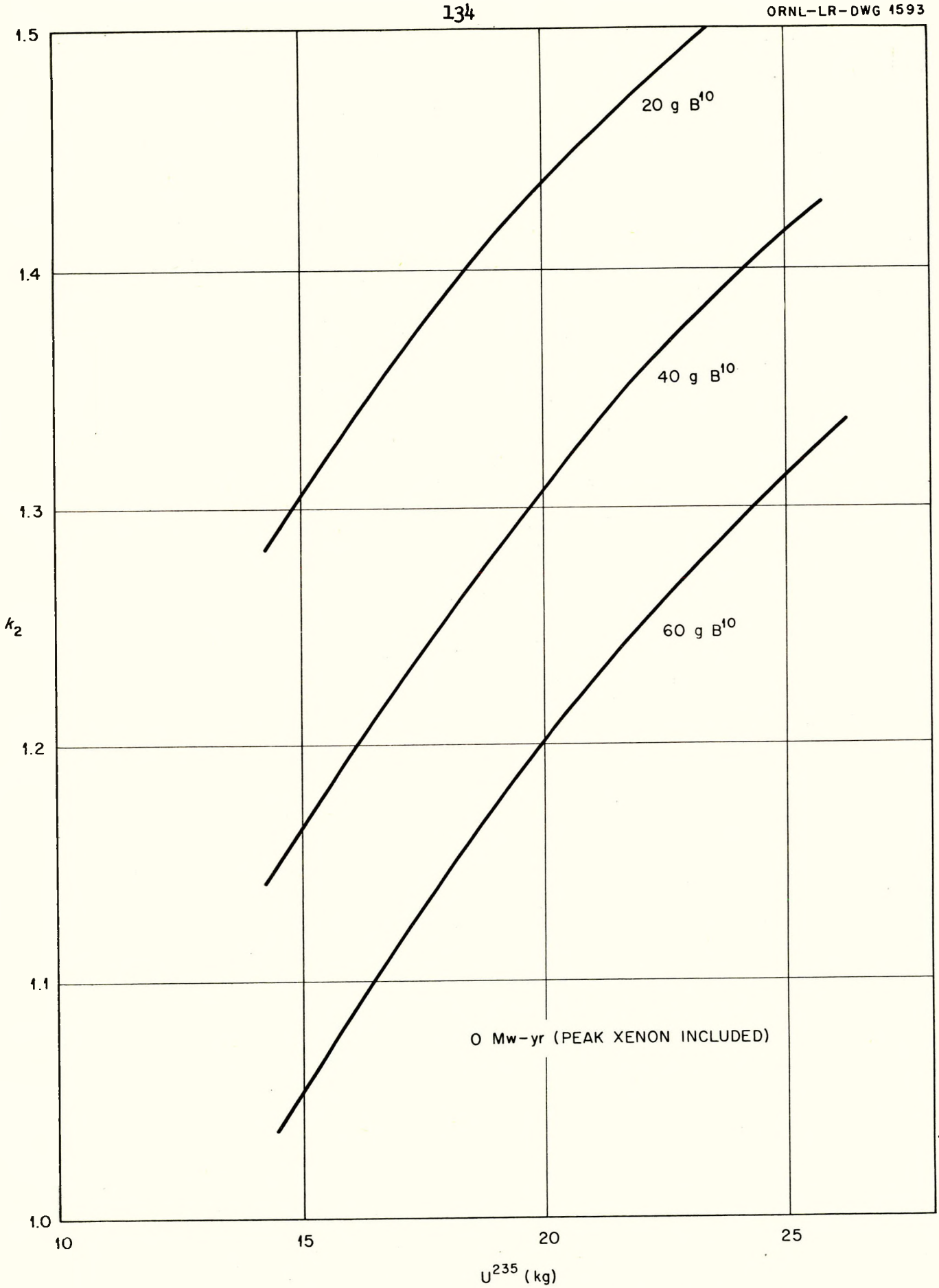

Fig. 36. Thermal Multiplication Factor, With Boron. T = 450 °F.

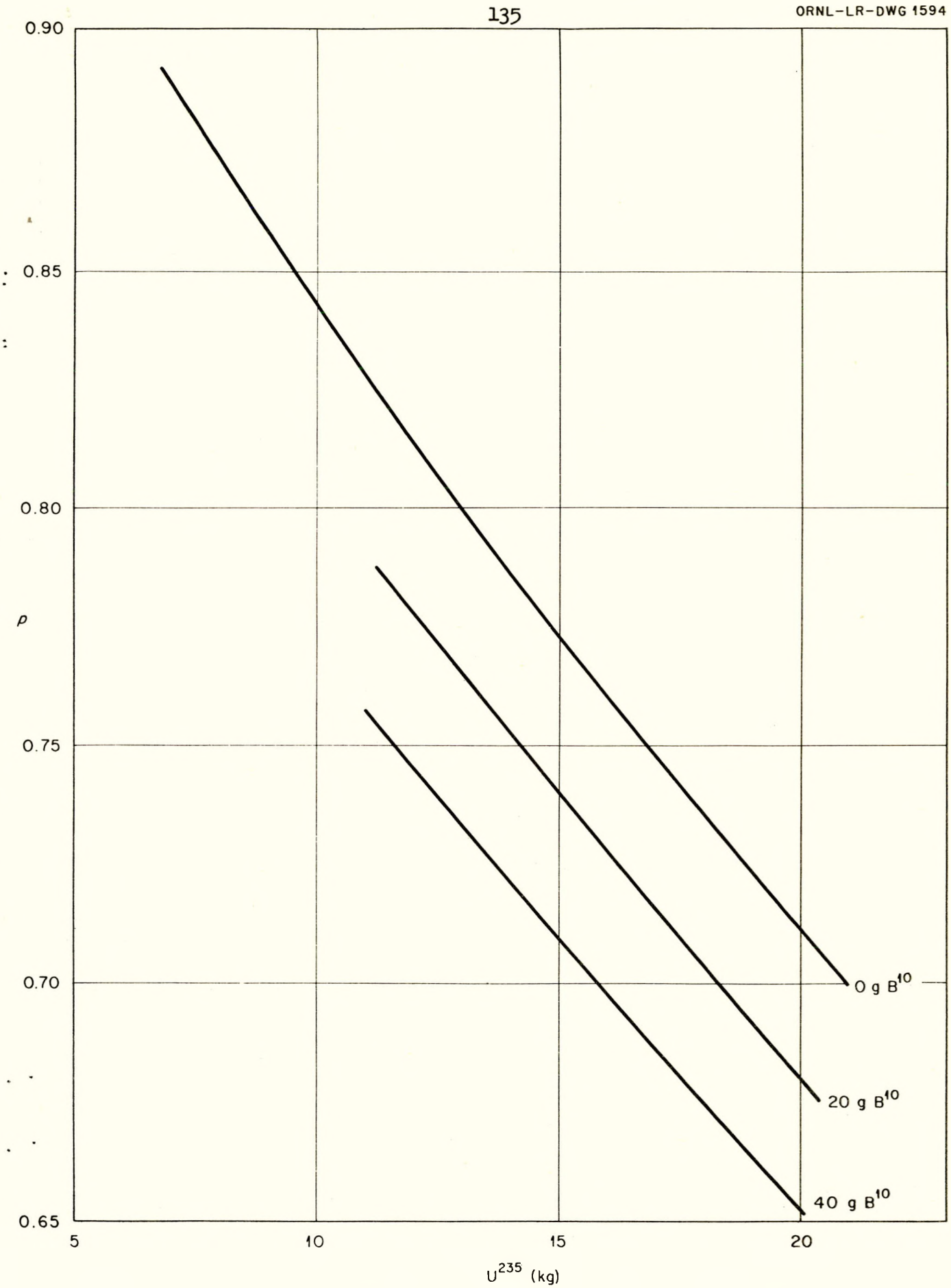

Fig. 37. Resonance Escape Probability. T = 450°F.

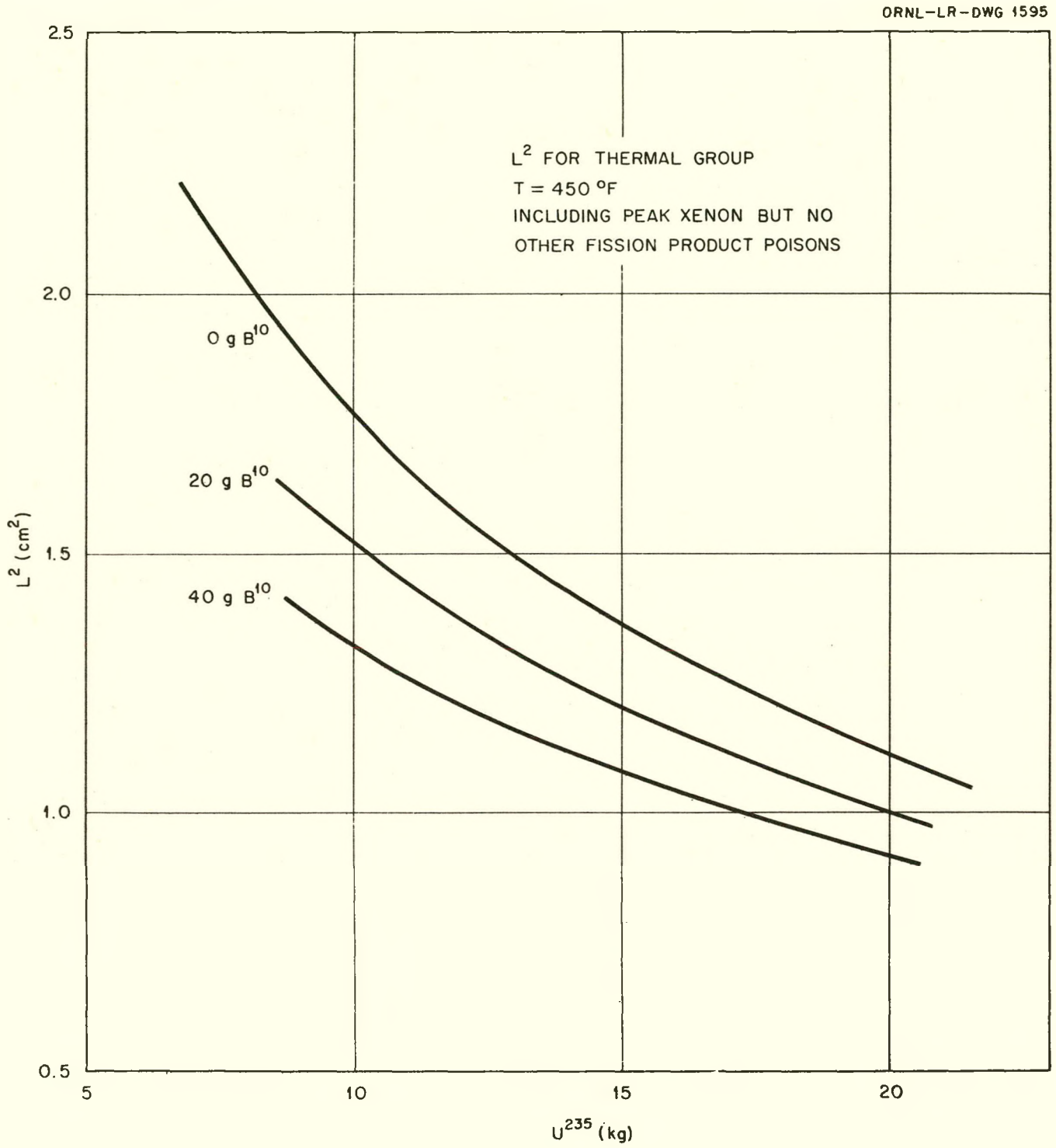

Fig. 38. Thermal Diffusion Length, L.

5.2.10 Burnout Rate of Boron. The concentration (B) of boron-10 at a time t is related to the initial concentration and to the fuel concentration (U) by the expression:

$$\frac{B(t)}{B(0)} = \left[\frac{U(t)}{U(0)}\right]^{g} \qquad (14)$$

In the absence of resonance absorption, the exponent g is given by the ratio of the thermal absorption cross sections

$$g = \frac{\sigma_{th(B)}}{\sigma_{th(u)}}$$

Since the cross sections of the fuel and of the boron depend differently upon neutron energy, the exponent g will, with resonance absorption, vary somewhat with the fuel and boron concentrations. However, over the range of concentrations encountered in the package reactor the exponent g is approximately constant at a value of 5.8

5.2.11 Fission-Product Poisons. The accumulation of fission-product poisons was studied by obtaining for each product, of known or estimated cross section*, the solution of the differential equation describing its production as a result of fission and its removal as a result of neutron absorption, radioactive decay, or both. At 68° F the combined cross section of fission product poisons, other than Xe 135, expressed in terms of barns per uranium atom fissioned, ranges from over 100 barns/fission for small fractional burnup of fuel to 50 barns/fission after 15 mw-yr. At 450° F, the value used was 38 barns/fission. Critical mass estimates were also made with the fissionproduct cross section arbitrarily increased 50%, to 57 barns/fission.

*Webster, J. W., Low Cross Section Fission Product Poisons, IDO-16100.

5.3 Critical-Mass Calculations

As far as the critical determinant is concerned, the modified two-group theory is the same as the usual two-group theory. By separating out the quantities that depend strongly on the fuel concentration, the critical equation may be written

$$\alpha = \frac{(S_2\mu_f - S_3\mu_s)\,\beta\gamma + (S_3 - S_1)\,\mu_s\,\beta\delta + (S_1 - S_2)\,\mu_f\mu_s\gamma\delta}{(S_2 - S_1)\,\beta + (S_1\mu_f - S_3\mu_s)\,\gamma + (S_3 - S_2)\,\mu_s\,\delta} \qquad (15)$$

$$\alpha = X'(R)/X(R) \qquad \delta = Z_2'(R)/Z_2(R)$$

$$\beta = Y'(R)/Y(R) \qquad \mu_f = D_1 r/D_1 c$$

$$\gamma = Z_1'(R)/Z_1(R) \qquad \mu_s = D_2 r/D_2 c$$

The rest of the notation is that of Glasstone and Edlund*.

In the modified two-group treatment, the eigenvalues of the buckling are given by the usual two-group expressions (equations 8.45.2 and 8.45.3 of Glasstone and Edlund) except that τ_c and k are replaced by

$$\tau_c' = \tau_c \left[1 - (1-p)\,k_1\right]^{-1} \text{ and } k' = k_2 p \left(1 - (1-p)\,k_1\right)^{-1}$$

The coupling coefficients, S_1 and S_2, differ from Equations 8.47.5 and 8.48.2 of Glasstone and Edlund only by an extra factor p in the numerator, while S_3 is the same as in two-group theory.

5.3.1 Results of Critical Calculations. The results of the modified two-group theory are summarized below. The calculations were made for a reflected sphere and for a side-reflected, bare-ended cylinder, whose volumes, in both cases, were taken equal to the package reactor volume. In the case of the cylinder, an estimate of reflector savings was needed for the bare ends, in order to calculate the axial buckling. The critical

*Glasstone and Edlund, Elements of Nuclear Reactor Theory, D. Van Nostrand Co., New York, 1952.

value of μ found in the spherical case was inserted in the expression $\mu^2 = (\frac{2.405}{R})^2 + (\frac{\pi}{H})^2$, and R set equal to H/2. (In the physical cylinder, R = 0.504 H). The resulting value of H is used to compute the axial buckling, $(\pi/H)^2$.

	Sphere (kg)	Cylinder (kg)
Critical mass, cold, clean core	7.13	7.26
Critical mass, hot, clean core	8.21	8.44
Hot, with peak xenon	9.28	9.51
With fission products for 15 Mw-yr	9.92	10.16
Fission products, except Xe, multiplied by 1.5	10.30	--
Fuel burnup in 15 Mw-yr	7.5	7.5
Initial fuel loading	17.4	17.7
Boron poison content (B^{10})	0.0334	0.0324

5.3.2 Reactivity vs. Time. Because the boron burns out more rapidly than the fuel, the reactivity of the core at first increases with time. The time dependence of the effective multiplication factor of the core is shown in Fig. 39. In the cold core, the excess multiplication reaches 15%, which the control rods must be capable of holding.

5.4 Control Rods

The reactivity value of the central control rod was determined by the use of modified two-group theory, applied to an equivalent bare cylinder. The control rod was assumed to be a cylindrical boron shell of perimeter equal to that of the design rod, filled with water at the same temperature as the reflector.

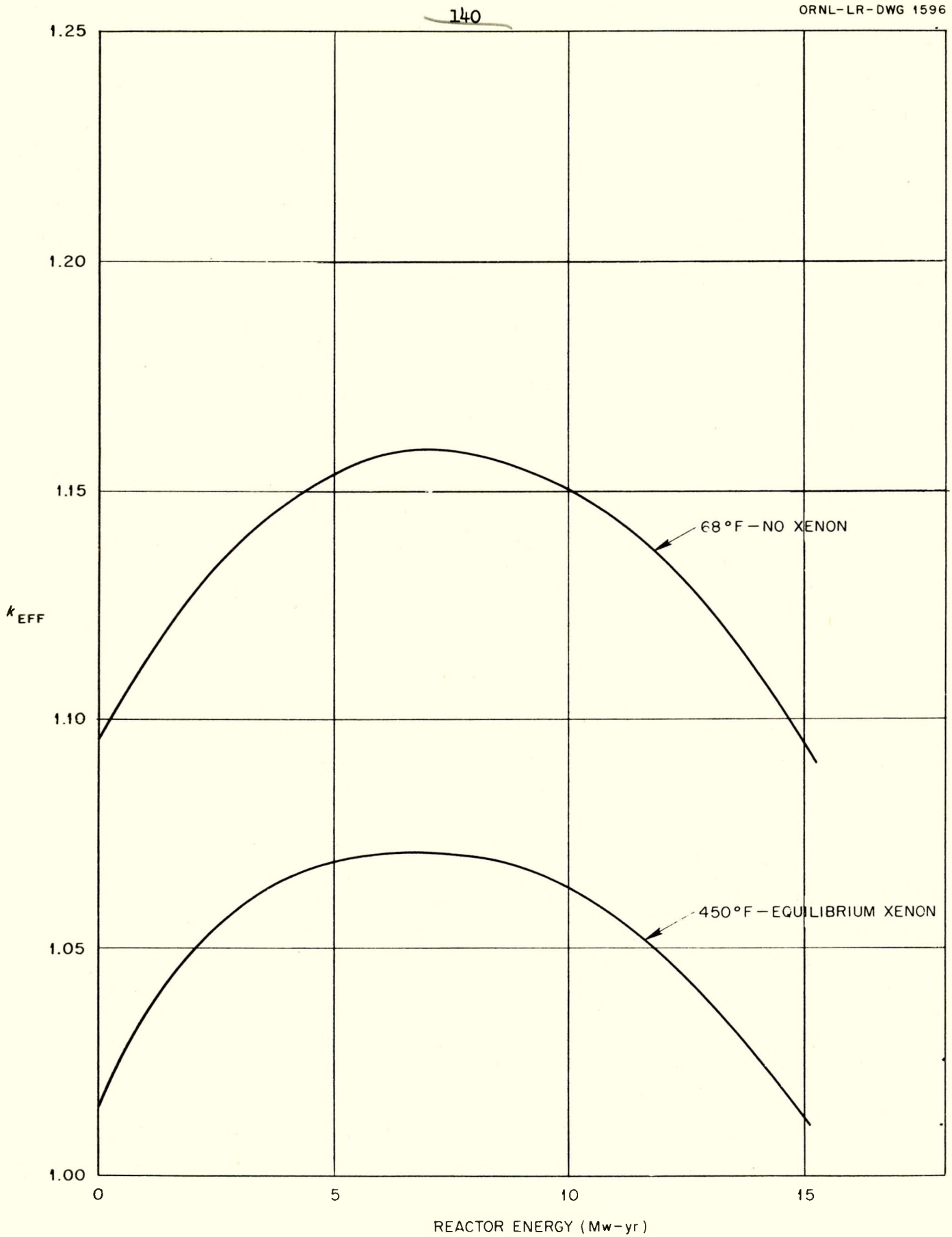

Fig. 39. Multiplication Factor vs. Time.

The conventional Nordheim-Scallettar method of calculating critical conditions with control rods was considered to be inappropriate for the package reactor. First it was recognized that over-estimates of rod effects are inherent in the method because of the large apparent fast-neutron current into the rod that arises from the condition that the fast flux is finite at the origin. Second, it was desirable to take proper account of the moderation of neutrons in the water core of the rod, and of the response of resonance neutrons to the boron shell.

A detailed comparison was made between the results of three-group and modified two-group theories of a reactor with a central control rod; this comparison yielded the conclusion that the modified two-group theory is adequate. A study of the effect of the reflector on cores with and without a central rod indicated that it was sufficiently accurate to perform all calculations of rod effects with an equivalent bare reactor. The fast group was assumed to be moderated in the rod as in the case of an internal reflector. The boron shell was taken to be transparent to fast neutrons, but opaque to thermals. In the critical condition used, no approximations relating to the rod size were made; the fast-group extrapolation length into the rod was taken as:

$$d_1 = \frac{D_{1c}}{D_{1r}} \frac{I_0(\kappa'_1 b)}{\kappa'_1 I_1(\kappa'_1 b)}$$

where κ'_1 is the inverse slowing down length in the rod, and b is the rod radius.

The critical determinant can be put in the form

$$\frac{J_0(\mu' R)}{Y_0(\mu' R)} = \frac{\begin{vmatrix} \frac{J_0(\mu' b)}{d_1} + \mu' J_1(\mu' b) & \frac{K_0(\nu' b)}{d_1} + \nu' K_1(\nu' b) \\ S_1\left[\frac{J_0(\mu' b)}{d_2} + \mu' J_1(\mu' b)\right] & S_2\left[\frac{K_0(\nu' b)}{d_2} + \nu' K_1(\nu' b)\right] \end{vmatrix}}{\begin{vmatrix} \frac{Y_0(\mu' b)}{d_1} + \mu' Y_1(\mu' b) & \frac{K_0(\nu' b)}{d_1} + \nu' K_1(\nu' b) \\ S_1\left[\frac{Y_0(\mu' b)}{d_2} + \mu' Y_1(\mu' b)\right] & S_2\left[\frac{K_0(\nu' b)}{d_2} + \nu' K_1(\nu' b)\right] \end{vmatrix}}$$

$$\mu' = \left[\mu^2 - \left(\frac{\pi}{H}\right)^2\right]^{1/2}$$

$$\nu' = \left[\nu^2 + \left(\frac{\pi}{H}\right)^2\right]^{1/2}$$

$$\kappa_1' = \left[\kappa_1^2 + \left(\frac{\pi}{H}\right)^2\right]^{1/2}$$

H is the height of the cylindrical core, including reflector savings; μ; ν, and κ_1, have their usual definitions.

The value of the central rod in reducing the multiplication factor of the cold reactor was found to be 0.059 in δk_{eff}, both at the start of the cycle and at the end of 7.5 Mw-yr operation.

Since the counterpart of the method described above was not available for a system of several rods, an investigation of the effect of a system of rods was made by the Nordheim-Scallettar method. The critical determinant for a system consisting of a central rod and an annular ring of four rods, according to Garabedian*, is

---

*Garabedian, H. L., Control Rod Theory for a Cylindrical Reactor, WAPD-18.

$$
\begin{vmatrix}
S_1 & S_2 & S_1 Y_0(\mu' a) + \frac{2}{\pi} S_2 K_0(\nu' a) & S_1 Y_0(\mu' b) + \frac{2}{\pi} S_2 K_0(\nu' b) \\
S_1 J_0(\mu' a) & S_2 I_0(\nu' a) & \frac{S_1}{4}\left[Y_0(\mu' b) + L_{oo}\right] + \frac{S_2}{4}\frac{2}{\pi}\left[K_0(\nu' b) + H_{oo}\right] & S_1 Y_0(\mu' a) + \frac{2}{\pi} S_2 K_0(\nu' a) \\
J_0(\mu' R) & 0 & J_0(\mu' a)\, Y_0(\mu' R) & Y_0(\mu' R) \\
0 & I_0(\nu' R) & \frac{2}{\pi} I_0(\nu' a)\, K_0(\nu' R) & \frac{2}{\pi} K_0(\nu' R)
\end{vmatrix} = 0
$$

where b' is the extrapolated radius* of the control rods

a is the radius of the ring of rods

R is the radius of the equivalent bare reactor.

$$L_{oo} = \sum_{n=2}^{4} Y_0(\mu' \rho_{1n})$$

$$H_{oo} = \sum_{n=2}^{4} K_0(\nu' \rho_{1n})$$

ρ_{1n} is the distance from rod #1, in the outer ring, to rod #n in the outer ring.

The rods are treated as right-circular cylinders, of perimeter equal to the perimeter of the design rectangular rods. The radius of the cylinder is reduced by an amount related to the transport mean free path* in the core, to yield the effective radius b'; in the present case

---

*Davison and Kushneriuk, Linear Extrapolation Length for a Black Sphere and a Black Cylinder, MT-214, March 1946.

b' = 4.04 cm. Rods for which b' = 3.50 and 3.00 cm were also considered. Values of the rods, in δk_{eff} are given below:

Number of Rods	b' = 3.00	b' = 3.50	b' = 4.04
1	0.052	0.075	0.11
5	0.235	0.339	$\gg$ 0.35

For b' = 3.00 cm, the value of one central rod, calculated by the Nordheim-Scallettar method, is close to that obtained for the central design rod by the method described above, which uses a more realistic boundary condition on the fast flux. An estimate of the value of a central rod, $\delta k_{eff} = 0.059$, is multiplied by the ratio of the value of five rods to that of one rod, as given by Nordheim-Scallettar method. It is concluded that the five design rods will shut down the reactor if $k_{eff} < 1.27$.

5.5 Flux Distribution

The flux distribution given in Fig. 40 was calculated on the modified two-group model for a spherical reactor. The peak-to-average thermal flux ratio is 2.0. It is realized that the flux distribution in the design reactor may be quite different from that shown, especially near the corners. No method has yet been adopted for computing the flux distribution in the actual core geometry.

5.6 Temperature Dependence of k

To determine the temperature coefficient of reactivity, the multiplication constant of the reactor was calculated with the UNIVAC by using a 30-group age-diffusion theory (Medusa Code). This multiplication constant was determined at concentrations of materials corresponding to 210°, 230°, 250° C. The temperature coefficient of reactivity at 450° F was 3.35×10^{-4}

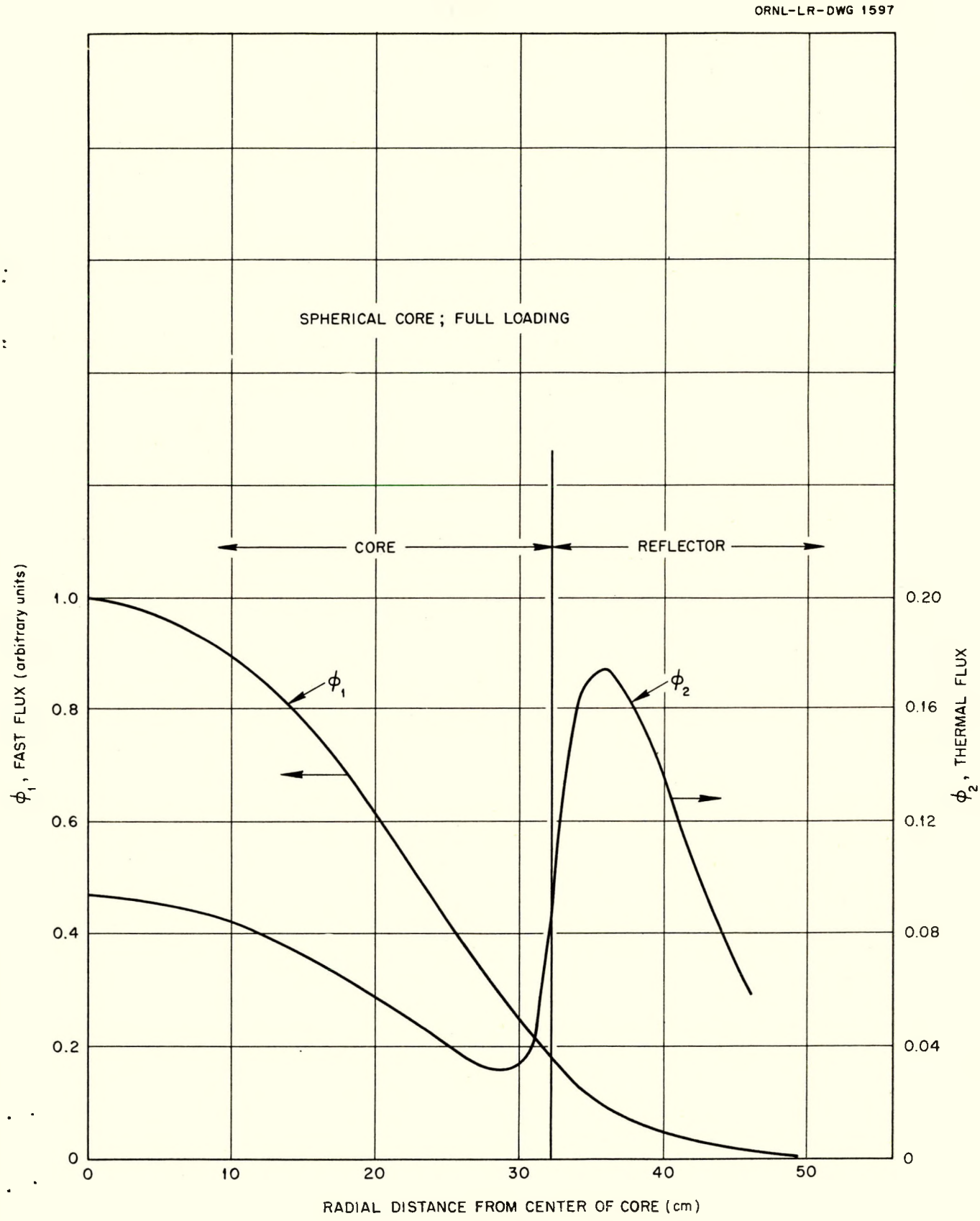

Fig. 40. Flux Distribution.

per °F. From modified two-group calculations at 68° F and 450° F, the average temperature coefficient between these two temperatures was 1.68×10^{-4} per °F. Because of the shape of the density vs temperature curve for water the latter figure is considerably smaller than the coefficient at 450° F.

5.7 Matters for Further Investigations

There are several matters which have not been fully investigated at this writing: the effect of spatially non-uniform burnup of the fuel and of the boron poison; the effect of particle size of the B_4C powder; heating of the control rods by neutron and gamma-ray absorption; and a thorough parameter study to determine the optimum size and configuration of the reactor. Further work is needed on the important question of the neutron flux distribution, with emphasis on the power density at the corners of the core and in that portion of the fuel section of a partially inserted control rod that extends into the reflector. The assumed peak-to-average ratio, four, may be enough higher than the ratio, two, calculated on a spherical model, to allow for uncertainties due to geometry. However, further analytical work or measurements in connection with proposed critical experiments will place this matter on a firmer basis.

6.0 SHIELDING

The biological shielding requirements for a remotely-located reactor power plant will depend largely upon the location of the plant. If ground excavation is practical, large savings in shielding material may be accomplished by burying or partly burying the reactor and primary coolant equipment. Similarly, proximity of the plant site to a mountainside may permit material savings if the plant may be constructed against a cliff. The concrete shield proposed for this plant is designed with the assumption that ground excavation and rock shielding are impractical; hence the design is applicable for any location. It is assumed that water and aggregate are locally available so that only cement need be shipped. The specific gravity of concrete is assumed to be 2.33.

The general configuration of the biological shield around the reactor and components is shown in Figs. 2-5. It forms two compartments, the reactor compartment and the steam generator compartment. The reactor is separated from other components of the primary coolant system in order to prevent activation of those components. Primary coolant pipes joining the reactor and the steam generator pass through a tunnel in the shield wall which is located off-center relative to the reactor to prevent streaming of radiation through it.

A metal lining is provided in the reactor compartment, sealed to the pressure vessel near the top. This makes it possible to flood the well over the reactor when loading the core. For shielding over the top of the reactor during operation, concrete slabs totaling 6 ft 10 in. thick are placed in the top of the well. Removable slabs are also placed above the pumps and heat exchanger. Additional openings in the shield wall are provided where necessary for maintenance accessibility, the openings being filled with removable

shielding blocks.

Overall dimensions of the shield structure are ~27 ft wide, 32 ft long, and 19 ft high. The height is measured from the building floor elevation. Actually the bottom of the reactor compartment extends 5 ft below the building floor level and will require either a 5-ft excavation below grade or an extra 5 feet of fill under the entire building.

The pit in which the reactor vessel is located is only 6 ft in diameter but is enlarged to an 8-ft octagon, located eccentrically above the top of the reactor to provide space for coffins and handling tools during unloading operation. A water-filled well along side the reactor vessel provides for storage of spent fuel elements and also acts as a sump into which leakage from seals and other places could be drained.

All shielding calculations are based on a continuous reactor power of 10 Mw. Tolerance is arbitrarily defined as 300 mrep absorbed over a 50-hour working week, or 5.36 mrep/hr. Estimated dosage rates are plotted as a function of concrete thickness, and shielding requirements are specified for various locations to obtain ten, one, and one-tenth times tolerance. Conservatism has governed all estimates in the calculations. In addition to the calculations of biological shielding requirements when the reactor is operating, estimates of the dose rate were made for a number of conditions that may occur during the shutdown period following full operation.

A detailed analysis of the biological and thermal shielding requirements is presented in ORNL CF-53-10-81* and a study of water activation and component shielding requirements is contained in ORNL CF-53-10-168.**

---

* Pearce, W. R., Analysis of Biological Shielding and Thermal Shielding Requirements for the ORNL Package Reactor, CF 53-10-81 (1953).

** Pearce, W. R., Water Activation and Component Shielding Requirements for the ORNL Package Reactor, CF-53-10-168 (1953).

6.1 Primary Shield Calculations

The similarity of this reactor to the Bulk Shield Reactor permits extensive use of modified BSR data. A preliminary estimate of shielding requirements indicates that the necessary thickness of concrete would be most dependent upon the magnitude of hard gamma radiation entering the shield. It seems advisable, therefore, to approximate the gamma spectrum with four energy groups and to separately attenuate these groups through iron, water, and concrete by using appropriate build-up factors. Both gamma and neutron dosages were examined at the time of reactor burn-out, when thermal flux and capture gamma production are greatest.

The magnitude of total gamma radiation and fast and thermal neutron flux as a function of distance from the BSR have been measured.* This data, adjusted for lower water density, geometry, and power level, was used to determine the flux at the edge of the reflector and at points of interest above the reactor.

The gamma spectrum from the BSR was calculated as a function of distance in standard water from the known spectrum at 96.6 cm** and from build-up factors plotted as a function of distance and energy,*** Figs. 41 and 42. Corrections were applied to the flux for each selected energy group in consideration of the greater amount of self-absorption in the core and the difference in capture gamma production.

---

* Blizard, E. P., Introduction to Shield Design I and II, CF-51-10-70, (1952).

** Aircraft Nuclear Propulsion Project Quarterly Progress Report, for period ending June 10, 1952, ORNL-1294.

*** Goldstein, H. and Wilkins, J. E., "Notice of Systematic Calculations of Gamma Ray Penetrations", NDA Memorandum 15C-2, Feb. 10, 1953.

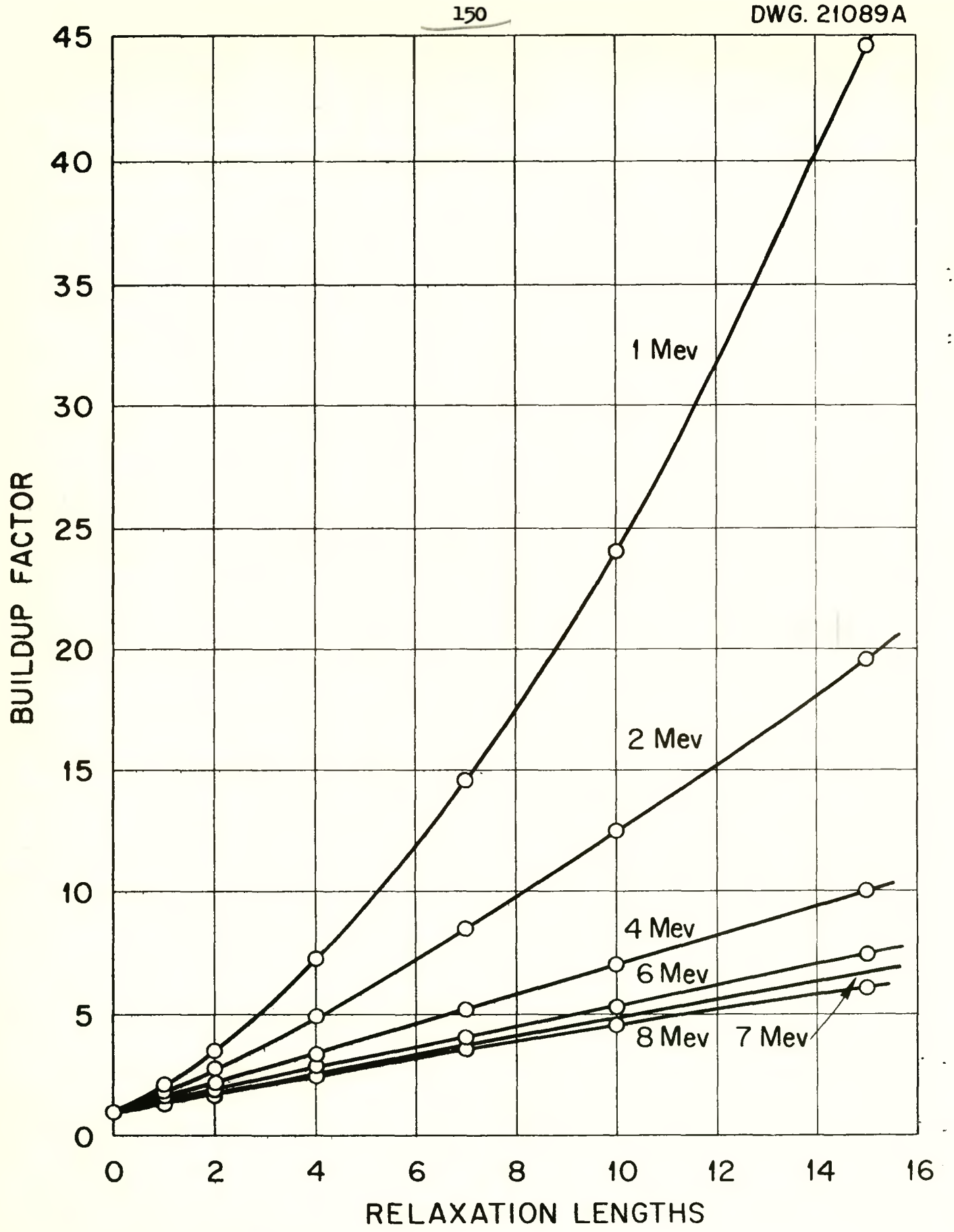

Fig. 41. Buildup Factors for Water (7 Mev Interpolated).

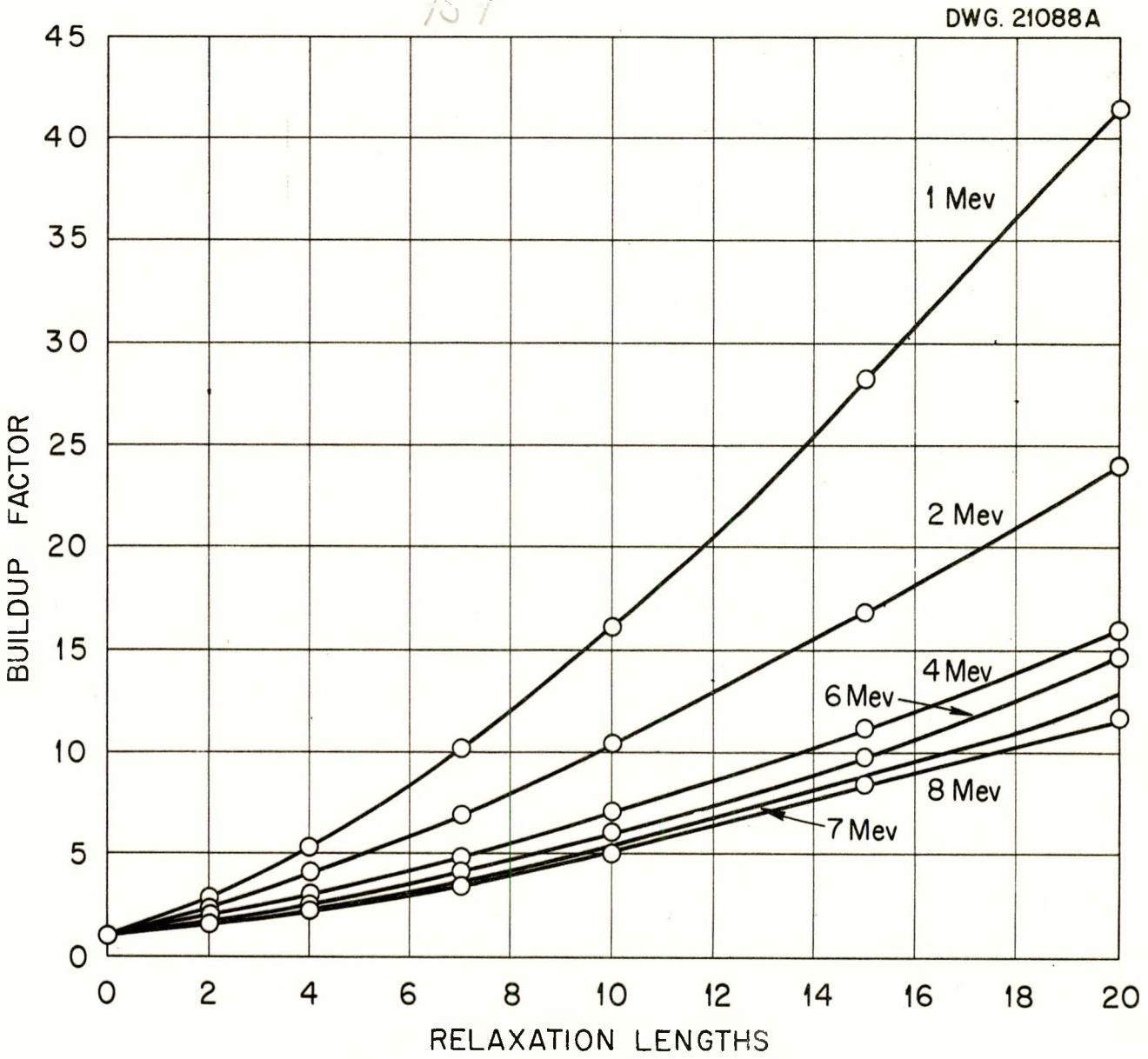

Fig. 42. Buildup Factor in Iron (7 Mev Interpolated).

From the composition, size, and temperature of each reactor, the relative leakage of fast and thermal neutrons was obtained and corrections were made to the values of neutron flux obtained from the work sheet. Capture gammas in the lid, shell, and top spider were computed by assuming slab geometry and uniform thermal neutron flux through the thickness of each member. The thermal-neutron flux used in each case was the average of the exponential flux obtained for slab geometry from diffusion theory. Only the 7.64-Mev gamma was considered in capture by steel. With these methods and an attenuation through the wall of the pressure vessel, the fluxes were obtained for each radiation at the top and sides of the vessel.

6.1.1 Radial Shielding. A spherical source was assumed with surface source strength equal to the fluxes obtained at the inner surface of concrete and with radius equal to the radial distance from the core axis to the shield. The dosage rates determined at a point opposite the reactor centerline are plotted as a function of concrete thickness in Fig. 43. Tolerance is obtained with a thickness of 8.5 ft, provided a thermal shield is present. The specified centerline thicknesses are:

For ten times tolerance	7.6 ft
For tolerance	8.5 ft
For one-tenth tolerance	9.5 ft

The shield is designed so that a maximum of ten times tolerance is obtained at the hottest surface of the radial shield and no greater than one-tenth tolerance is obtained at any surface in the control room.

6.1.2 Axial Shielding. During operation the reactor is shielded axially by 3 feet of water, a 7-in. steel vessel lid, a void, and a concrete plug. Since the lid of the pressure vessel does not extend fully across the access well and since a portion of the gamma rays consequently do not pass through the lid, it is assumed that only 5 in. of steel is present.

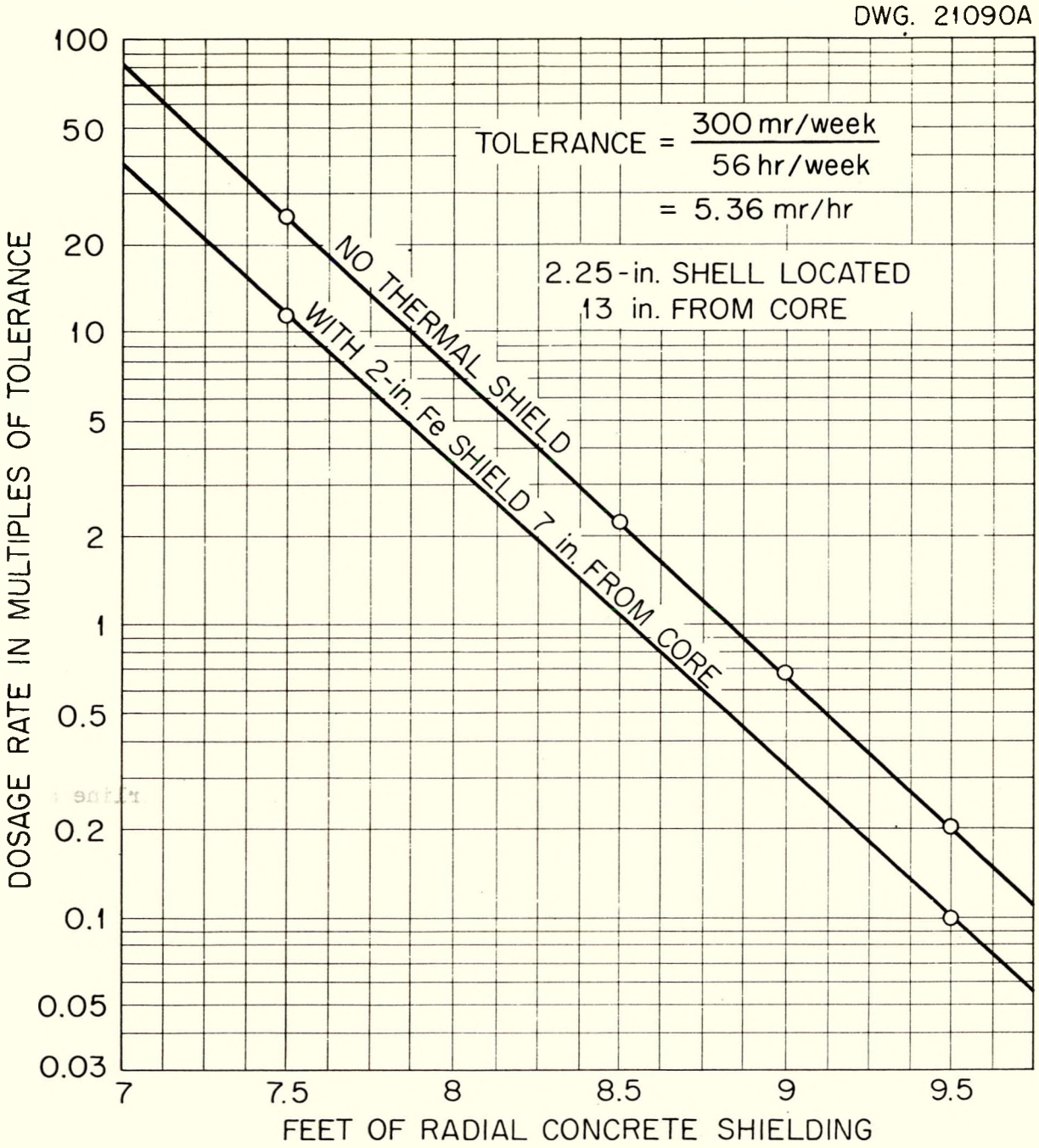

Fig. 43. Dose Rate at Edge of Radial Shield for 10-megawatt Operation.

The most penetrating radiation at the top of the reactor is found to be the 7-Mev gamma rays from neutron capture in iron in the core and upper grid. The dosage rates at the top of the concrete plug are plotted for varying thicknesses of concrete, Fig. 44. The specified thicknesses are:

For ten times tolerance	5.8 ft
For tolerance	6.9 ft
For one-tenth tolerance	7.9 ft

A 6.9-ft plug is specified above the reactor to reduce dosage to tolerance at the hottest surface.

6.1.3 Water Shield after Shutdown. Dosage rates at the top of the access well are determined for the several situations which may follow in some sequence during the reloading operation. The tentative reloading demands that no more than 2 ft of water be present above the pressure vessel lid when the concrete plug is lifted and the nuts are removed from the lid. The lid and attached motors are then lifted out and the access well is flooded with an additional 12 ft of water to permit transfer of elements over the lip of the pressure vessel and into the fuel storage area. After shutdown the only activity is from the decay of fission products and the decay of induced activity in the iron structure and the reactor coolant.

The power from gamma decay of fission products for short times of decay after shutdown following long periods of continuous reactor operation is approximately $6.3\ t^{-0.2}$ Mev/sec per fission/sec*, where t is measured in seconds after reactor shutdown. Where all fission-product activity is assumed to be from 1-Mev gamma radiation and the temperature of shield and core water is 180°F after shutdown, the estimated initial dosage rates at the top of the

* Buck, J. H. and Leyse, C. F., Materials Testing Reactor Handbook, ORNL-963, (1951).

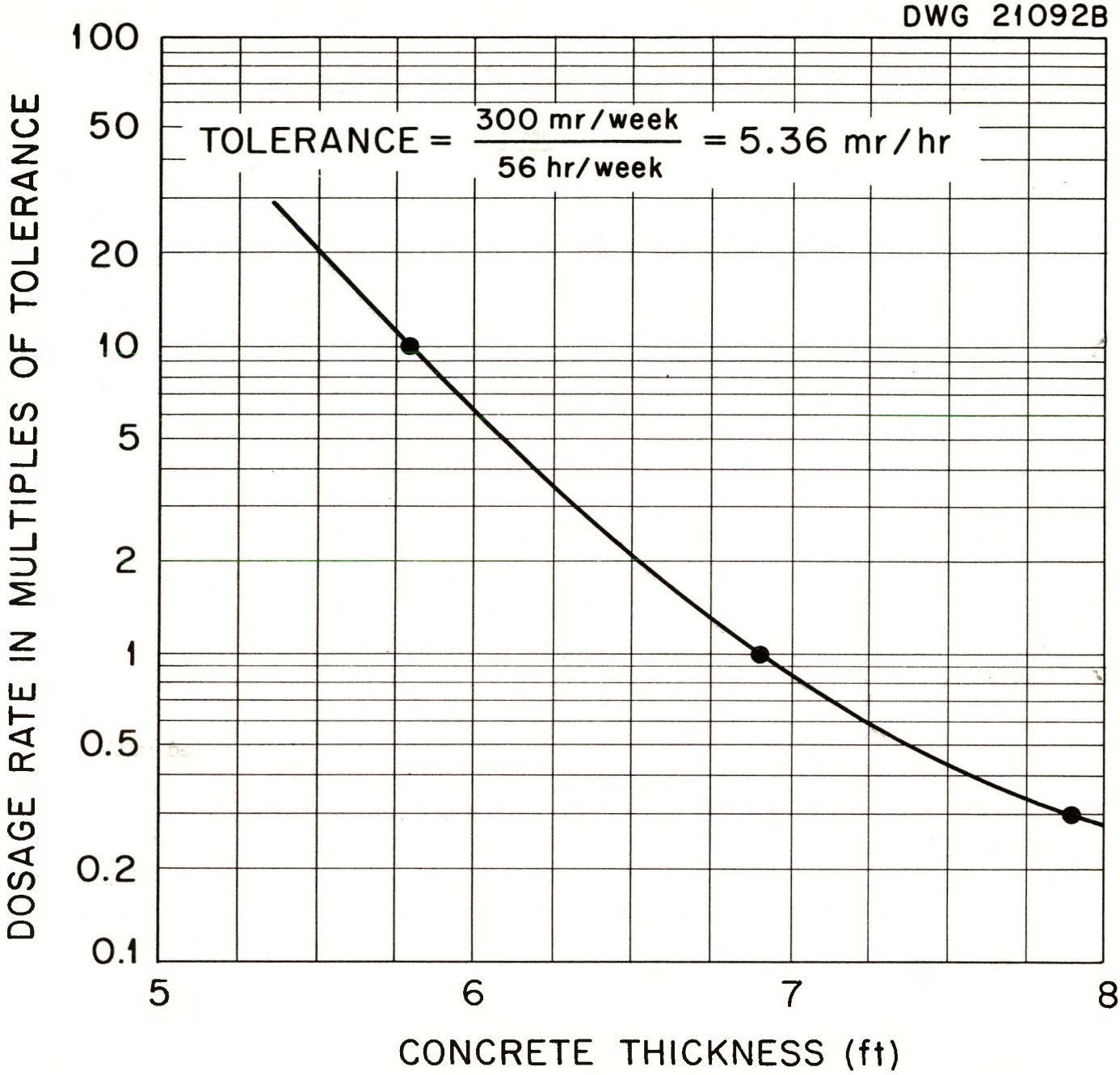

Fig. 44. Dose Rate at Top of Concrete Plug for 10-megawatt Operation; Access Well Not Flooded.

access well with the concrete plug removed are as follows:

Geometry	Multiple of Tolerance		
	1 sec after shutdown	1 hr after shutdown	1 wk after shutdown
With lid removed; well contains 2 ft of water	47,000	9,120	3,300
With lid removed; well contains 4 ft of water	2,200	429	155
With lid removed; well contains 6 ft of water	920	178	64.5
With lid in place; well contains 2 ft of water	3.9	7.5	2.7
With lid in place; well contains 4 ft of water	5.9	1.2	0.4

These values are in approximate agreement with extrapolated values of after-shutdown gamma measurements in the BSF.* Provided the well is flooded after the lid nuts are removed and provided operations are resumed one hour after shutdown, the tentative reloading procedure should produce an exposure of no greater than 100 mr/hr. If the well is gradually flooded as the lid is withdrawn, in order to keep the motors and leads dry, a somewhat higher dose rate will be received momentarily when the lid is lifted from its seat.

The vessel lid is exposed to a thermal neutron flux of 3×10^8. The initial activity at the surface of the lid will be several r/hr, depending upon the manganese content of the steel. After 24 hours the 2.6-hr manganese activity will have decayed, leaving a dosage rate of less than 100 mr/hr from the iron itself.

Calculation of the dosage rate received 2 ft from a 55-gal sphere of hot pressurized coolant water indicates that the convection of radioactive water from the core to the surface of the flooded access well may produce intolerable

* Hullings, M. K. and Blosser, T. V., After-Shutdown Gamma Measurements at the BSF, ORNL CF-53-6-1 (1953).

dosages. The exposures from the hot sphere, with self shielding and time decay of each activity separately considered, are:

10 Mw activity	387 mr/hr
1 hr after removal	300 mr/hr
12 hr after removal	20 mr/hr
24 hr after removal	4 mr/hr
36 hr after removal	2 mr/hr

Low-energy gamma and beta radiation have been neglected.

6.2 Secondary Shield Requirements

Due to the build-up of radioactivity in the reactor coolant, all components in the primary coolant circuit must be shielded. A detailed analysis of the secondary shielding requirements is presented elsewhere.*

The sources of radiation from the components will be the activity induced in pure water, in normal water contaminants, in corrosion products, and the radioactive recoil atoms which escape into the coolant. An analysis of similar studies in water activation reported by Passarelli** and by Branyan*** permit most of the possible activation reactions to be neglected.

It is assumed that the initial charge of water is treated with a total carry-over of solids no greater than 2 ppm by number and that make-up water is of the same degree of purity. A conservative corrosion rate of 0.05 mg/cm^2-mo is assumed to the entire surface area of the primary water circuit. The purge rate for the system is 30 gph. The estimated maximum concentrations of those elements, present in the water as natural contaminants or corrosion products, which will be most responsible for water activity are listed in Table I.

---

* Pearce, W. R., Water Activation to Component Shielding Requirements for the ORNL Package Reactor, CF-53-10-168 (1953).

** Passarelli, W. O, Study of the Ventilation Requirements for Power Reactor Compartments, AECD-3228 (1951).

*** Kroeger, H. R. et al., A 1000-kw Reactor Power Plant, Bendix Aviation Corporation Research Laboratory Report No. 610, June 15, 1953.

TABLE I: SOURCES OF ACTIVITY IN PRIMARY COOLANT*

	Parts per Million, by weight	% Abundance of Parent Isotope	Reaction	Atoms, Parent Isotope/cm^3 H_2O (sp. gr. = 0.828)
Water				
Oxygen	8.8×10^5	99.76	$O^{16}(n,p)N^{16}$	2.79×10^{22}
		0.037	$O^{17}(n,p)N^{17}$	1.03×10^{19}
		0.204	$O^{18}(n,\gamma)O^{19}$	5.59×10^{19}
Natural Contaminants				
Sodium	0.06	100	$Na^{23}(n,\gamma)Na^{24}$	1.24×10^{15}
Chlorine	0.10	24.6	$Cl^{37}(n,\gamma)Cl^{38}$	3.56×10^{14}
Calcium	0.20	0.185	$Ca^{48}(n,\gamma)Ca^{49}$	4.75×10^{12}
Magnesium	0.02	11.29	$Mg^{26}(n,\gamma)Mg^{27}$	4.68×10^{13}
Corrosion Products				
Nickel	0.20	1.0	$Ni^{64}(n,\gamma)Ni^{65}$	1.75×10^{13}
Manganese	0.055	100	$Mn^{55}(n,\gamma)Mn^{56}$	4.55×10^{14}

* Kroeger, H. R. et al., A 1000-Kw Reactor Power Plant, Bendix Aviation Corporation Research Laboratory Report No. 610, June 15, 1953.

Neutron reactions in the outer layer of fuel-element cladding will cause recoil atoms of Fe, Cr, Ni, and Mn to be ejected into the coolant. Those reactions which produce a radioactive recoil nuclide emitting decay of gamma rays of greater than 1 Mev are of greatest interest. The significant reactions in their probable order of importance are:

$$Mn^{55}(n,\gamma)Mn^{56}$$
$$Fe^{56}(n,p)Mn^{56}$$
$$Cr^{52}(n,p)V^{52}$$
$$Ni^{64}(n,\gamma)Ni^{65}$$
$$Fe^{58}(n,\gamma)Fe^{59}$$

Only the first of these reactions is considered since the rest appear to contribute collectively less activity and since the 2-Mev decay gamma from Mn^{56} will be less effectively attenuated by concrete than will the lower energy gammas from the other reactions. The average range of manganese recoils is assumed to be 10^{-5} cm. It has been indicated experimentally* that this range is conservative. For continuous operation at full power and for the specified purge rate, the density of manganese disintegrations is 10^{5}/cc-sec.

The saturated activity of the water, normal contaminants, and corrosion products at the core exit will be:

$$\gamma\text{'s/cc-sec} = N \sigma \phi \frac{1 - e^{-\lambda R T_c}}{1 - e^{-\lambda T_c}} \times \text{Yield}$$

where N = concentration of target nuclide, atoms/cc
σ = thermal neutron absorption cross section of target
ϕ = activation flux
λ = decay constant
R = fraction of cycle time during which target is exposed to ϕ
T_c = cycle time
Yield = photons/disintegration

* Briggs, Sisman, and Manowitz, Activity from Stainless Steel in Pile Water, Monsanto-Clinton Laboratory (now ORNL) Report MonN-36, Nov. 1945.

The effective neutron energy thresholds for activation of O^{16} and O^{17} which take into account the potential barrier are 11.2 and 10 Mev respectively.* In this reference the rates of production of N^{16} per O^{16} atom and N^{17} per O^{17} atom are computed. Assuming that the flux beyond 10 Mev includes only virgin neutrons, the relative activity is nearly proportional to the fission density. With this assumption the production rates are:

$$\sigma\phi = 1.28 \times 10^{-15} \text{ sec}^{-1} \text{ for } N^{16}$$

$$\sigma\phi = 2.29 \times 10^{-15} \text{ sec}^{-1} \text{ for } N^{17}$$

It is assumed that all targets are exposed to a thermal flux of 2.7×10^{13} during residence in the core and reflector (R = 0.084) and that O^{16} and O^{17} are activated only during residence in the core (R = 0.021). (R = fraction of cycle time, see Table II.)

The cross section, half life, and specific activity of each reaction are given in Table III. The radiation from the 7.4-second N^{16} appears to be both most energetic and most abundant. Since less than three half lives will elapse during the cycle time, it is evident that all but N^{16} may be neglected in the determination of shield thickness about the steam generator compartment.

The total cycle time of the primary circuit is 20.5 seconds. The volumes and relative periods of coolant residence in the various components are listed in Table II. The components of the circuit external to the primary shield are grouped into five units as described in this table and the dosage rate from these components is determined for a position at the outer surface of the secondary shield. For the position selected, radiation from the heat exchanger

* Taylor, J. J., WAPD-23 (1951).

TABLE II: VOLUMES AND RESIDENCE TIMES IN PRIMARY WATER CIRCUIT COMPONENTS

	Volume (liters)	Time of Residence (fraction of cycle-time)
Components Outside Primary Shield		
Reactor exit line	167	0.032
Heat exchanger	745	0.145
Pump and check valve	321	0.064
Vertical leg, reactor inlet line	244	0.047
Horizontal log, inlet leg	197	0.040
Total	1674	0.328
Components within Primary Shield		
Reactor inlet line	100	0.019
Bottom header and thermal shield	1426	0.274
Core	107	0.021
Reflector	320	0.063
Top header	1424	0.276
Reactor exit line	100	0.019
Total	3477	0.672

Total volume of circuit	5151 liters
Flow rate	4000 gal/min or 252 liters/sec
Total cycle time	20.5 seconds

TABLE III: REACTIONS, RADIATIONS, AND RELATIVE ACTIVITIES IN PRIMARY COOLANT

Parent and Product Nuclide	Cross Section (barns)	Half Life	γ Energy (Mev)	Yield (%)	Photons/cc-sec at reactor exit
Water					
$O^{16} - N^{16}$	1.4×10^{-5}	7.4 s	6.7	(80)	1.3×10^{6}
$O^{17} - N^{17}$	0.01	4.1 s	1.0*	(100)	1.7×10^{3}
$O^{18} - O^{19}$	2×10^{-4}	29 s	1.6	(70)	2.25×10^{4}
Natural Contaminants					
$Na^{23} - Na^{24}$	0.6	15 h	1.4 2.8	(100) (100)	1.7×10^{3} 1.7×10^{3}
$Cl^{37} - Cl^{38}$	0.56	38 m	2.1 1.6	(50) (30)	226 135
$Ca^{48} - Ca^{49}$	1.1	5.8 m	2.7	(100)	12
$Mg^{26} - Mg^{27}$	0.05	9.6 m	1.0	(120)	6
Corrosion Products					
$Ni^{64} - Ni^{65}$	2.6	2.6 h	1.5	(50)	51
$Mn^{55} - Mn^{56}$	13	2.6 h	2.0 1.0	(40) (100)	5.4×10^{3} 1.35×10^{4}
Recoil Products					
$Mn^{55} - Mn^{56}$	13	2.6 h	2.0 1.0	(40) (100)	6×10^{4} 1.5×10^{5}

* Neutrons

and from the vertical leg of the reactor inlet line will be least attenuated by concrete. Hence these two components are represented by a finite disk source and an infinite line source, respectively. For each of the three remaining components, an effective center of radiation is conservatively located and each center is regarded as a point source of radiation.

Assuming a mass absorption coefficient of 0.063 cm^{-1} for the N^{16} radiation in concrete, tolerance is obtained with 3.8 ft of shielding. The fast neutrons from N^{17} are attenuated with a relaxation length of $\sim$11 cm in concrete and are found to contribute a negligible dose. It is specified that the secondary shield be 46 in. in thickness to obtain tolerance at the face of the steam generating compartment. It is assumed that radiation from the core is attenuated by a factor of ten in traversing this compartment; hence a minimum thickness of 56 in. of concrete between the reactor and steam generator compartments is specified, giving an additional dosage through the secondary shield of one-tenth tolerance.

6.3 Shield Ventilation

As stated in the previous discussion of insulation, it is necessary to maintain air temperature inside the shield below 150°F for protection of electrical components and to keep the concrete temperature below 200°F. In addition to insulating the high temperature components it is necessary to circulate enough air through the shield to remove the lost heat.

Where the inlet air temperature is 0°F and the exit air temperature is 150°F, the heat removal rate is 141 Btu/hr-cfm. Heat losses from equipment and piping were estimated to be 47,800 Btu/hr. In addition, approximately 410,000 Btu/hr is generated in the shield by absorption of radiation. Where this must be removed at the inside surface of the concrete, the total heat to

be absorbed by the air is 457,800 Btu/hr; at 500,000 Btu/hr, the air flow required is then 3550 cfm.

Since some radioactive argon is formed as air passes through the compartment, it is necessary to discharge the air through a stack. For a 100-ft stack made of 12-in. Schedule-10 pipe the friction head loss in the stack is 2 in. of water. A total pressure drop of 3 in. of water should be adequate for the entire system.

The control-rod drive motors are located in a space above the reactor vessel which is to be flooded for shielding during reloading operations. In order to provide for air flow through this space and still make it possible for it to be flooded, the air is brought through the foundation into the bottom of the reactor compartment. It then flows through vent pipes to the upper part of the compartment, just below the under surface of the shield plug. It leaves the compartment through a 12-in. pipe and gate valve in the wall between the reactor and heat exchanger compartments. When the well over the pressure vessel is flooded, the vent pipes can be plugged with stoppers and the 12-in. gate valve closed.

The air is exhausted from the heat exchanger compartment by a fan located in the compartment and discharging through a duct which passes through an outer wall into the adjacent stack. The stack is shielded with concrete to a height 10 ft above the top of the reactor shield. The fan drive shaft extends through to the outside of the shield where the drive motor is located.

7.0 THE STEAM SYSTEM

The steam system has been designed for a net electrical output of 1000 kw and a maximum reactor power level of 10 Mw. The plant auxiliary power requirement is estimated at 300 kw and the plant steam usages and losses are estimated to require about 1150 lb/hr (2 gpm) raw water make-up as a maximum. A total of about 3535 kw of heat (12,065,000 Btu/hr or 50,271 sq ft EDR) is available for the heating system when the peak electric load exists and the reactor power level is 10 Mw.

A flow diagram of the steam system is shown in Fig. 1. The steam system equipment layout is shown in Figs. 7-9. Detailed explanations of sources of turbine performance data, condition curve plots, equations with sample calculations, tabulated data, and design considerations, have been included in Memorandum ORNL CF-53-9-33.*

7.1 Steam Generation

Steam is generated in the primary coolant heat exchanger at 200 psia under full load conditions. A simple dry-pipe arrangement is used to provide dry steam at the outlet. Under partial loads the steam generator pressure is greater than 200 psia, ranging upwards to a maximum of 423 psia at no load, Fig. 30. The steam pressure at the turbine throttle is maintained constant at about 192 psia at all loadings by means of a pressure-reducing valve in the steam line. A pressure-reducing valve, set at 60 psia, will supply steam to the heating system directly from the steam generator. No superheat is available for the steam to the turbine throttle.

---

* Robertson, R. C., Design Calculations for Package Reactor Steam System, ORNL CF-53-9-33.

7.2 Main Components

7.2.1 Steam Turbine-Generator. Electricity at 4160 v, 3-phase, 60 cycle is provided by a straight, geared, condensing, steam turbine-generator, rated at 1250 kw at 0.8 power factor. The unit has a direct-connected exciter, open generator, and is arranged with one non-automatic extraction nozzle for 30-psia steam to be used for feed-water heating. Frequency is automatically controlled by a regulator acting through an oil-relayed constant speed governor actuating the multi-valve steam-flow control. An over-speed governor protects the unit and emergency stopping is accomplished by a trip valve in combination with the throttle valve. An oil system consisting of the reservoir, pump, filters, and cooler (using steam condenser coolant), and the usual appurtenances, such as, pressure gages, temperature indicating devices, voltage regulator, speed indication, and synchronizer, is provided. The unit is mounted on a common bedplate located on top of the reactor shielding, thus eliminating the considerable concrete and forming required for a turbine-generator foundation.

7.2.2 Steam Condenser. The steam condenser is of the two-pass, horizontal, shell-and-tube type. It is rigidly mounted on the side of the shielding with a flexible connector in the exhaust line to the turbine. The condenser may be cooled either by water, if available at the site, or by an antifreeze solution, such as ethylene glycol. In the latter case the antifreeze gives up its heat to the atmosphere in two horizontal cooling coils located outside the building. A 12-ft-diameter propeller-type fan driven by a 40-hp electric motor drives air over the 18 x 20-ft faces of the coils. A by-pass arrangement in the coolant line prevents the antifreeze solution from entering the condenser tubes at temperatures low enough to freeze the condensate. A two-stage steam-jet air ejector with intercooler is used to maintain the

condenser vacuum at 2 in. Hg during the winter months. When outside temperatures are high the condenser pressure must be allowed to increase (i.e., the vacuum decrease) to provide high enough condenser-cooling-fluid temperatures to adequately transfer the heat to the atmosphere. The maximum condenser pressure is estimated to be 5 in. Hg at mean maximum summer temperatures.

If condensing water is available at the site, the condenser can be maintained at a lower pressure with considerable improvement in efficiency. The steam jets for the vacuum system are supplied with 192-psia steam and the intercooler uses condensate from the hot well for condensing, with the outflow from the intercooler returned to the hot well through a drainage loop. No aftercondenser is employed, the second-stage jet discharging directly into the open feed-water heater. An air-cooled steam condenser has been investigated and is covered in this report in Section 7.5.2.

7.2.3 Feed-Water Heater. The condensate from the main steam condenser and from the heating system, together with all other recoverable condensates, is collected in a tray-type deaerating feed-water heater rated at 35,000 lb/hr outflow capacity and with ability to reduce oxygen concentration to 0.005 cc per liter. This heater is mounted on top of a 100-gal insulated storage tank. Heating steam for the heater is extracted from the turbine at about 30 psia and is admitted through a pressure-regulating valve set to hold the heater pressure at about 17 psia, with the temperature of the outflow to feed-water pump suction 220°F at all load conditions. Air is vented from the top of the heater through a vent condenser cooled by the incoming condensate flow. The level in the storage tank is maintained by a float control regulating the incoming condensate flow. A float control admits steam to the make-up evaporator to maintain adequate water supply in the heater storage tank. High- and low-water alarms are provided and an overflow connection prevents flooding of

the heater. The storage capacity serves as a surge tank; as an approximate 15-minute emergency supply at full load; as a source of enough evaporated water to completely refill the steam system, should this be necessary; and as an assured source of cooling water for the reactor primary coolant during the reactor cooling-off period after shutdown.

7.2.4 Pumps. With the exception of the small steam-driven duplex pump used during the reactor cooling-off period, all pumps in the steam system are electrically driven. Sizes and capacities are as follows:

	Number	Actual Pumping Load (gpm)	Capacity Each (gpm)	Rated hp Each
Boiler feed	2	68	75	20
Hot well	2	47	50	2
Circulating	3	1380	900	20
Condensate return	2	21	75	2
Reactor cooling	1	-	2	(steam driven)

Standby pump capacity is provided in all cases.

7.2.5 Evaporator. An evaporator with a 1050-lb/hr outflow capacity is needed to provide make-up water for the system. Raw water is evaporated at about 25 psia and the resulting steam used for heating feed water in the deaerating feed heater. The steam used by the evaporator is taken from the 192-psia source and the condensate cascaded into the deaerating heater. The maximum estimated make-up requirement of 1150 lb/hr (2 gpm, or 2880 gal/day) includes the requirement of 30 gph for the primary coolant system, 100 lb/hr for evaporator blowdown, 200 lb/hr for steam generator blowdown, and liberal amounts for plant and heating system leakages.

7.2.6 Condensate Return Unit. A standard condensate return unit consisting of a 100-gal receiver and two 75-gpm pumps, with alternator to distribute the pump wear, is used to collect the heating system condensate at the low

point and return it to the steam cycle. The condensate return pumps are three times oversize to prevent excessively short cycling.

7.2.7 Blowdown Equipment. The steam generator and the evaporator are provided with combination blowdown and positive-seating valves. The discharge is into a small blowdown tank fitted with an atmospheric vent and drain.

7.2.8 Miscellaneous. All pressurized equipment is fitted with spring-loaded safety valves, the main steam condenser with a blowout disk. The safety valves, together with all air vent lines, discharge into a venting stack within a heated area to assure that the openings will not become clogged with ice. All drains are into a common sump, also within a heated space. A steam hose may be used to keep this sump open. All piping is steel, Schedule-40, with welded joints wherever practicable, and covered with standard thickness of insulation, where required.

7.2.9 Control. Control over the system is as follows: An increase in the electric load causes the constant speed mechanism on the turbine to admit more steam, increasing the rate of steam flow from the steam generator. Both the pressure and the water level in the steam generator tend to fall, causing the feed water regulator to admit more water and more heat to be transferred from the primary coolant, followed by an increase in reactor power level.

A sudden loss in the electric load causes the steam flow to the turbine to be interrupted by the overspeed governor. A sudden loss of condenser coolant flow causes the steam pressure in the condenser to rise, resulting in the low-vacuum trip stopping the turbine with the same result as above. Pressures in excess of the safe values on the condenser shell are relieved by a blowout disk. Should the water level in the condenser rise to a point where the

turbine might be endangered, the turbine vacuum breaker admits air to the condenser, shuts off the condenser coolant flow, and stops the turbine by means of the low-vacuum trip.

Either recording or remote-indicating equipment is provided in the control room for all major variables in the system, as indicated in the flow diagram, Fig. 1.

7.3 Performance

The thermal efficiencies and steam flow rates for typical loads on the electric and heating systems are shown in Table IV. The relationship between these loadings and the reactor power level is shown in Fig. 45. These values reflect the drop in turbine and generator efficiency at partial loads, Fig. 46, the rise in exhaust pressure with outside temperature, Fig. 47, and the increased enthalpy of the steam to the turbine throttle due to the pressure rise in the steam generator at partial loads, Fig. 30.

The temperature of the condensate returning from the heating system affects the estimated performance of the steam cycle. In the absence of actual data based on experience at arctic bases, a value of 100°F has been assumed for all loads.

The water losses for the steam system have been estimated as shown in Table V. These losses have been assumed constant at all loads, but undoubtedly would show some decrease for partial load operation since in the summer months the heating system leakage should be essentially zero.

Distribution of the energy in the steam cycle at full net electric load of 1000 kw and full reactor power output of 10 Mw to the heat exchanger is shown in Table VI.

TABLE IV: PARTIAL LOAD PERFORMANCE PACKAGE REACTOR STEAM SYSTEM

			Steam Flow, lb/hr				Thermal Efficiencies		
Gross Turbine Load, kw	Heating System Load, kw	Exhaust Pressure In. Hg Abs.	To Heat Exchanger	To Turbine Throttle	To Heating System	Extracted	Reactor Power Level, Mw	Net Power* Generation percent	Net Heat** and Power percent
1300	3800	2	34,645	21,345	11,317	2450	10.24	15.5	46.9
1300	3535	2	33,780	21,784	10,513	2350	10.00	15.4	45.4
1300	1800	3.3	29,492	22,242	5,267	1528	8.74	14.4	32.0
1300	0	5	25,015	23,032	0	651	7.43	13.5	13.5
875	3800	2	28,358	15,078	11,297	1664	8.40	12.5	52.1
875	1800	3.3	22,808	15,567	5,258	795	6.77	11.6	35.1
875	0	5	18,133	16,150	0	0	5.40	10.6	10.6
500	3800	2	22,487	9,227	11,277	938	6.67	7.0	59.9
500	1800	3.3	17,033	9,797	5,253	169	5.06	6.1	39.5
500	0	5	12,443	10,460	0	0	3.71	5.4	5.4
300	3800	2	19,860	6,600	11,277	614	5.89	0	64.5
300	1800	3.3	14.036	6,800	5,253	0	4.17	0	43.2
300	0	5	9,353	7,370	0	0	2.79	0	0

$$\text{T. Eff.}^{*} = \frac{\text{Net Elec. Power}}{\text{Reactor Heat - Heat Sys. Load}}$$

$$\text{T. Eff.}^{**} = \frac{\text{Net Elec. Power + Heat Sys. Load}}{\text{Reactor Heat}}$$

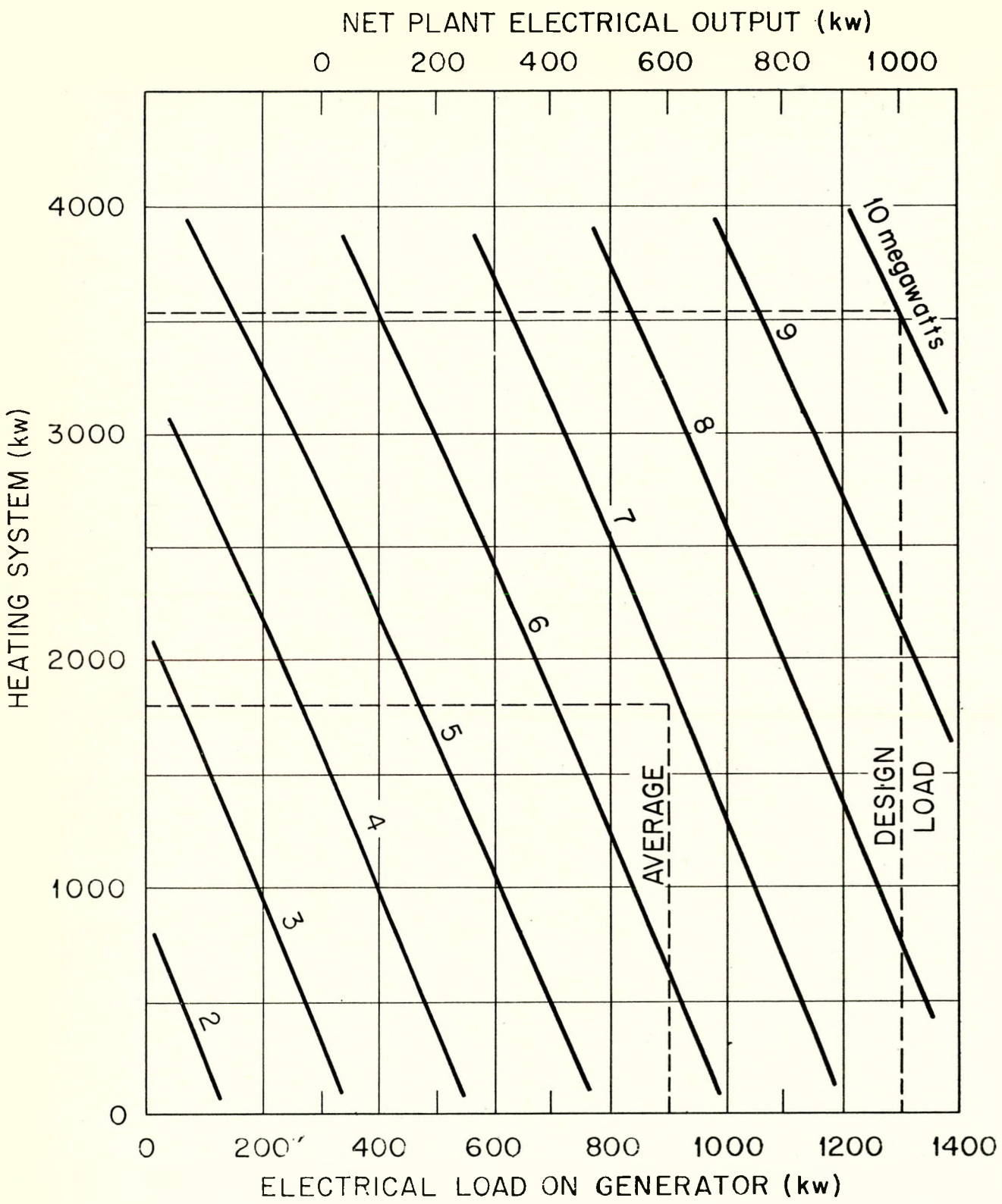

Fig. 45. Reactor Power Level at Various Electrical and Space-heating Loads, Based on Performance of 1250-kw Geared Condensing Turbine-generator; Plant Heat Losses and Steam Usage, ~265 kw; Plant Auxiliaries, 300 kw.

DWG. 21257A

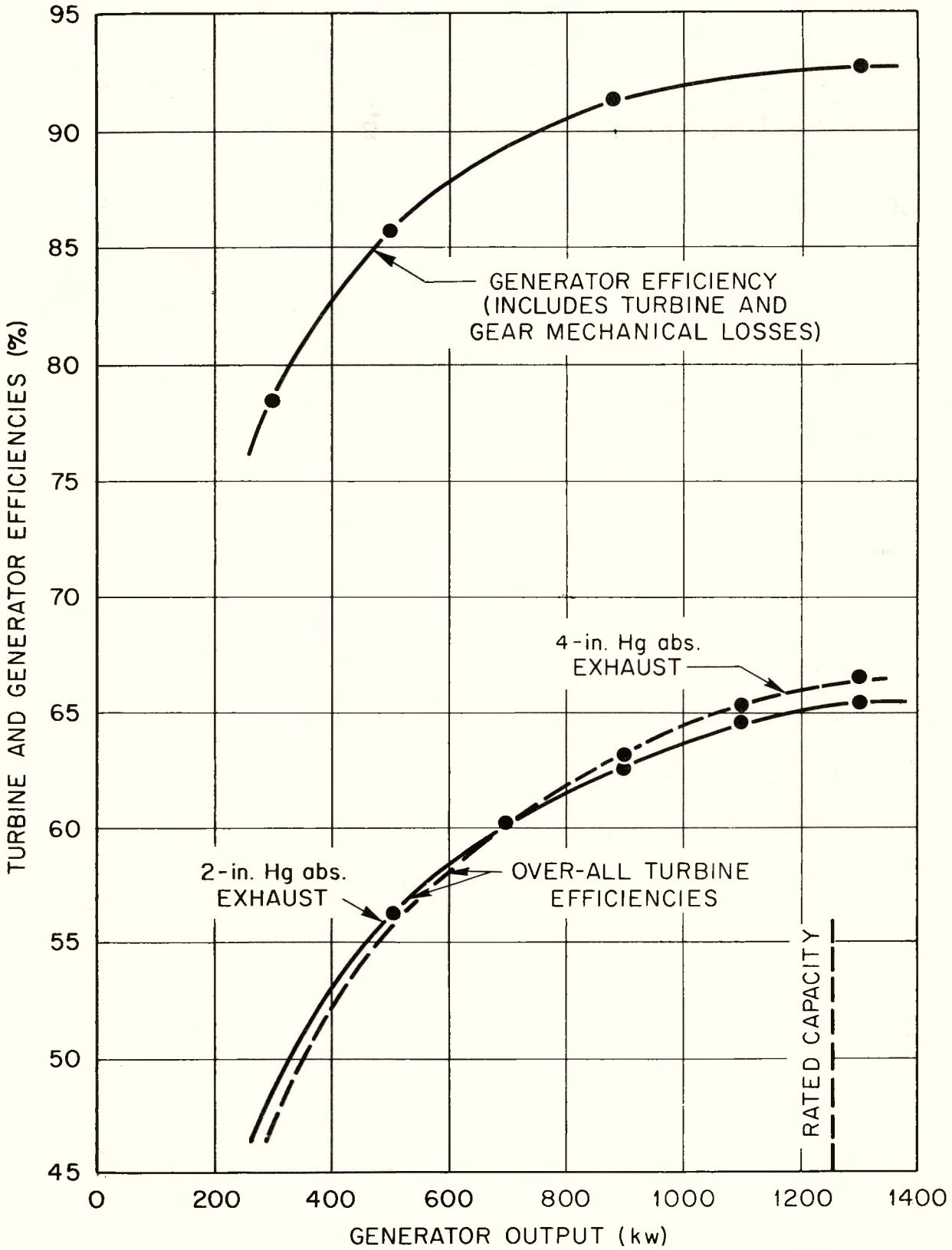

Fig. 46. Turbine and Generator Efficiencies, 1250 kw Unit.

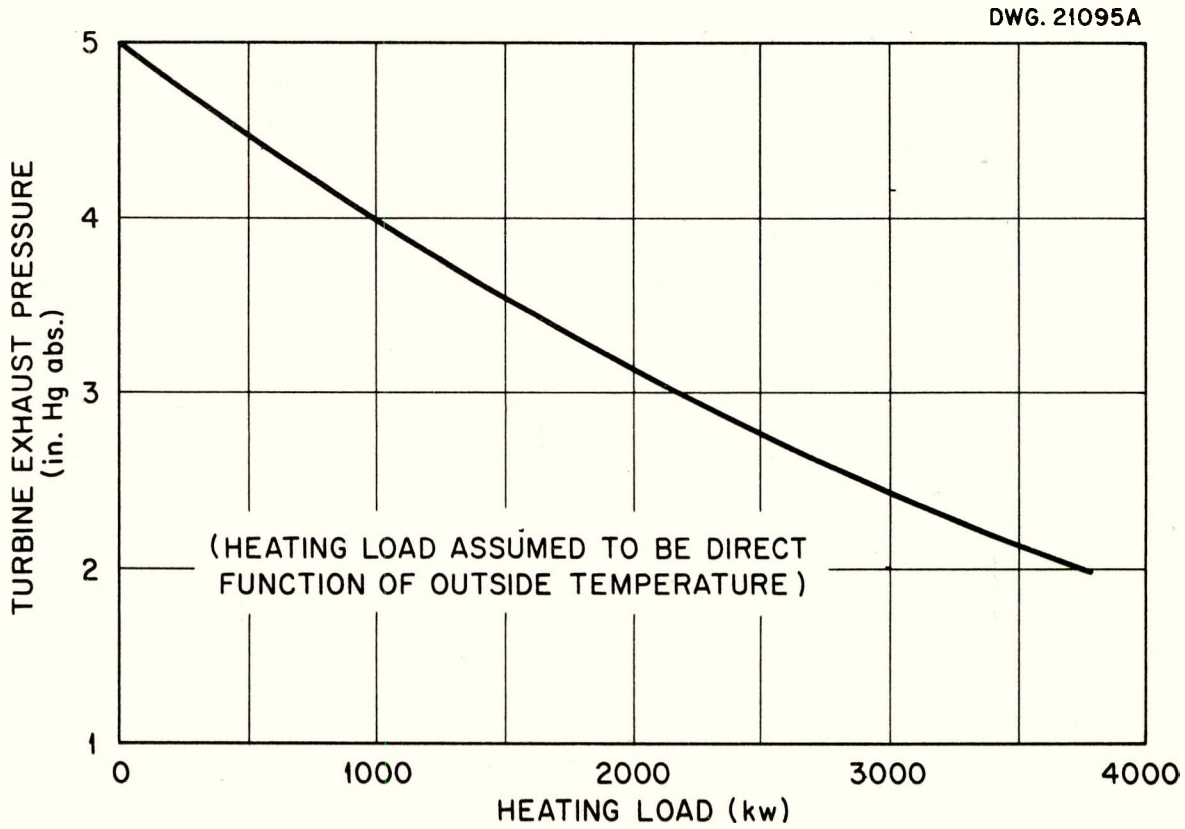

Fig. 47. Turbine Exhaust Pressure as a Function of Space-heating Load.

TABLE V: ESTIMATED WATER AND HEAT LOSSES FROM STEAM SYSTEM

Loss	lb/hr	Btu/lb	Btu/hr
Boiler blow down	200	355.4	71,080
Evaporator blow down	100	208	20,800
Turbine glands	165	1198.4	197,736
Calorimeter	35	1198.4	41,944
Heating steam	150	1198.4	179,760
Heating condensate	150	68	10,200
Demineralizer make-up	250	68	17,000
Pump leak-off	100	188.7	18,870
Total losses	1,150		577,870

TABLE VI: ENERGY BALANCE, STEAM SYSTEM*

	Btu/hr		kw	
Heat Added to System				
Reactor heat	34,130,000		10,000	
Make-up water	32,200		9	
Boiler feed pump	20,441		6	
		34,182,641		10,015
Heat Removed from System				
Turbine Work				
Turbine mechanical losses	23,891		7	
Gear loss	47,782		14	
Generator loss	279,866		82	
Generated output to distribution system	3,413,000		1,000	
Generated output to plant auxiliaries	1,023,900		300	
		4,788,439		1,403
Rejected by System				
Heating System**	12,063,655		3,535	
Condenser coolant	16,917,829		4,956	
Water losses	377,630		111	
Heat loss in condensate	23,652		7	
Unaccountable	11,436		3	
		29,394,202		8,612
		34,182,641		10,015

* At 1000 kw net electric load and 10 Mw reactor power level.

** Includes 150 lb/hr steam leakage from heating system.

As may be noted in Table IV, at low electric and heating loads the extraction steam requirement reduces to zero and at very low loads there is more steam available from the make-up water evaporator and from the steam jet ejectors than is needed for feed-water heating. This steam is wasted to the main steam condenser rather than complicate the equipment with a vent condenser.

The moisture in the turbine exhaust at full load and at 2 in. Hg exhaust pressure is estimated to be 14 to 15%, values slightly higher than the maximum of 12 to 13% generally recommended by turbine manufacturers. No development of a special turbine should be required, however, and standard routine blade inspection procedures should be followed.

7.4 Design Considerations

The basic criteria used in design of the steam cycle for the package reactor steam system is that it must be simple, reliable, and require an absolute minimum of transportion and construction effort. The proposed cycle has been reduced to bare essentials, employing one stage of feed-water heating because of the necessity for deaeration, and throttling the heating steam directly from the steam generator rather than extracting from the turbine. At the more accessible bases, changes in the proposed cycle will be justified by the better efficiencies obtained. The most promising of these modifications to the cycle are now discussed.

7.4.1 Condenser. The reduced condensate return flow from the heating system in summer requires less extraction steam for feed-water heating, with the result that more steam flows through the low-pressure stages of the turbine. This effect is further amplified in the summer due to the increased

exhaust pressure. Estimated condensing loads at full net electric load of 1000 kw are as follows:

Heating Load (kw)	Exhaust Pressure (in. Hg)	Condensing Load (Btu/hr)
3535	2	17,078,000
1800	3.3	18,725,000
0	5	20,188,000

When heat is rejected to the atmosphere the outside maximum temperatures are of importance. The average mean daily maximum, by months, for 27 arctic stations* is 58.5°F, occurring in July; for Galena, Alaska, it is 69°F. An average daily maximum of 70°F has been assumed as a design value.

Several arrangements of the condensing equipment are possible. The system proposed for the package reactor consists of a standard shell-and-tube condenser with pumps for circulating an antifreeze solution through an outside liquid cooler. Variations of this arrangement are to use condensing water in the shell-and-tube condenser the year around; to use the liquid cooler in winter and condensing water in summer; to use liquid cooler in winter and water with cooling tower in summer; to use liquid cooler in winter and summer and spray outside surfaces of cooler with small amounts of water in summer. Another possibility is an air-cooled condenser.

Temperature and water supply permitting, it would be desirable that all condensing be accomplished by a standard shell-and-tube condenser using water as the coolant. The turbine exhaust pressure would thus be lower, particularly in the summer season; the steam condensing equipment would be less bulky;

* Climatic Data for Various Selected Stations in Alaska, Canada, Newfoundland, Labrador, and Greenland, Headquarters, Air Weather Service, Directorate of Climatology, prepared at the request of Nuclear Power Division, IT and R, OCE, July 1953.

and the power requirement for the cooling-water circulating pumps would probably be less than the power required for an air-cooled condenser.

The proposed basic design for the package reactor condensing system may be modified to fit any of the following site conditions:

Condensing water available at site year around.
Condensing water available in summer months.
Limited water available in summer.
No water available.

If the antifreeze solution referred to above were ethylene glycol of about 60% concentration, by weight, it would have a specific heat of about 0.70 Btu/lb-°F. There would thus be some advantage to storing the antifreeze in summer and circulating water in the liquid-cooler system.

An air-cooled steam condenser would have the advantage of simplicity; elimination of one of the heat exchanging processes, permitting slightly lower condensing pressures for a given outside temperature; and would dispense with the necessity of storing and supplying antifreeze. The bulk and weight of equipment probably would not be materially less than the system described for the package reactor steam system, since the coils would be quite large; there is no cost advantage. At the present time, few companies manufacture air-cooled steam condensers. The package reactor condensing requirement would possible necessitate development work by these manufacturers, particularly in regards to effective air removal for low-vacuum operation. Of chief concern, however, is the danger of freezing the condensate in the coils. Experiences with air-cooled steam condensers in below-freezing temperatures indicate that this is a real danger since condensate drainage velocities in the tubes are quite low, particularly at low condensing loads, or in event of sudden shutdown. A by-pass arrangement, whereby air is recirculated to keep the temperature of air entering the coil above 32°F would be the best

guarantee against freezing, although the air ducts would be large.

The use of sub-freezing air as a coolant, either in the above-mentioned air-cooled steam condenser, or in the air-cooled liquid cooler proposed for the package reactor system, presents special problems of operation. The circulating fan may become unbalanced by ice formation on the blades, and the bearing exposed to the cold air stream will require special treatment. It is possible that at very low outside temperatures and with brisk winds operation of the fan will not be required, or a natural draft tower might be used to promote air circulation without use of the fan. It is believed that vagaries of wind direction and velocity minimize the value of a vertical coil depending solely on the windage effect.

With regard to condensing-water supply systems, there is such a wide variance between stations, e.g., distance and elevation water must be pumped, intake and screening structures required, and necessary discharge flumes, that generalized statements as to cost without regard to location would have little significance. In the United States the values range between about $1.00 and $70 per installed kilowatt of generating capacity. Estimated first costs, not including freight and erection costs, for various condensing arangements are listed in descending order of thermodynamic efficiency:

Year around cooling-water supply. Use of shell-and-tube condenser.	$15,000, plus condensing-water-supply works cost.
Summer condensing-water supply. Use of shell-and-tube condenser, air-cooled liquid cooler for winter.	$34,000, plus condensing-water-supply works cost.
Limited summer water supply. Use of cooling tower, shell-and-tube condenser, air-cooled liquid cooler for winter.	$50,000 plus water-supply cost.
No water supply. Use of air-cooled steam condenser.	$40,000

No water supply. Use of shell-and-tube condenser, air-cooled liquid cooler. $34,000

The proposed arrangement for the package reactor, listed last above, uses standard equipment that has been fully developed, is easily adapted to all situations that might exist at arctic bases, minimizes the freeze-up danger, is comparable in costs to other methods, and is presented in this report as a method applicable to the largest number of bases. Each station with its different design requirements should, however, be considered separately.

7.4.2 The Steam Cycle. The steam cycle proposed for the package reactor system was selected to minimize the erection time and transportation effort problems. Improvement to the thermal efficiency of the cycle could be realized by use of one or more closed feed-water heaters in addition to the deaerating heater, and by extraction of the heating steam from the turbine. Closed feed-water heaters are relatively simple to install and add only slightly to the boiler feed pumping head. A heater for the package reactor application is estimated to cost about $3500 with attendant fittings, not including freight and erection cost.

Extracting the heating steam requires an automatic extraction-type steam turbine that maintains a constant steam pressure at the extraction nozzle regardless of the electric load on the generator. Because of the added steam flow rate through the turbine throttle and high pressure stages, the automatic extraction turbine is larger and heavier than a conventional unit. The turbine efficiency is also slightly less, about 64.6% as compared with 65.6%. The estimated additional cost for automatic extraction is about $15,000, not including the extra freight and extra installation cost. A pressure-reducing valve to supply heating steam directly from the steam generator will be required even though the extraction source is used, to furnish heating steam when the turbine

is inoperative and under extreme temperature conditions. Automatic extraction equipment has been developed fully to a point of reliability equal to that of the turbine, and maintenance demands are small.

Performance of four different cycle arrangements were estimated for comparison purposes, by using the simplified flow diagram shown in Fig. 1. Losses and plant usage of steam have been estimated as equivalent to 1983 lb/hr of additional steam from the steam generator with 1633 lb/hr of this steam useful in the open heater for heating feed water. Credit on the heating load was taken for 150 lb/hr of steam leaked from the heating system. Comparisons were made at average load conditions of 875-kw gross electrical load and 1800 kw of heating load and also at full electric load of 1300 kw gross and a reactor power output of 10 Mw. These values are presented in Table VII.

From the values in Table VII it will be noted that the capability of the package reactor to furnish steam to the heating system can be markedly increased by use of the additional equipment. For sites where it is anticipated that the load on the heating system will increase, it would be possible to add the closed feed-water heater at a later date, as required, provided that the turbine originally installed had the extra opening for an extraction nozzle.

The economies of the various cycle arrangements shown in Table VII may be compared by using the average load conditions and assuming a burn-up rate of ~1.4 gm/Mw-day and a fuel cost of $20/gm. These values are shown in Table VIII. Judged by conventional power plant standards, any and all of the above improvements to the cycle would be economically justified and should be considered for the more accessible bases. However, extra transportation and construction costs for the package reactor installation at an arctic base are not included in the above estimates of savings, and the net savings represent only a very small portion of the total investment and operating costs.

TABLE VII: PERFORMANCE OF VARIOUS STEAM CYCLE ARRANGEMENTS

Steam Cycle	Full Load			Average Load		
	To Heating System (kw)	Net Power* Therm. Eff. (%)	Heat Power** Therm. Eff. (%)	Reactor Power (Mw)	Net Power* Therm. Eff. (%)	Heat Power** Therm. Eff. (%)
a. Straight, extraction at 30 psia for open feed-water heater, heating steam straight from steam generator.	3535	15.4	45.4	6.77	11.6	35.1
b. Straight, ext. at 60 psia for closed feed-water heater and at 30 psia for open feed-water heater, heating steam straight from steam generator.	3698	15.9	47.0	6.70	11.8	35.5
c. Automatic ext. at 60 psia for heating steam and non-auto. at 30 psia for open feed-water heater.	4493	18.2	54.9	6.52	12.2	36.5
d. Auto. ext. at 60 psia for heating steam and closed feed-water heater and non-auto. at 30 psia for open feed-water heater.	4515	18.3	55.2	6.44	12.4	36.9

The above values are based on:
Avg. loads: 600 kw net elec., 1800 kw heating.
Full loads: 1000 kw net elec., 10 Mw reactor power.
Turbine Eff: Avg. load: straight: 62.6%; Auto. Ext: 61.0%
Full load: straight: 65.5%; Auto. Ext: 64.6%
Generator Eff: Avg. load: 91.4%; Full load: 92.7%

Losses and plant steam usage equivalent to 1983 lb/hr from steam generator, with 1633 lb/hr useful for feed-water heating. Heating steam leakage of 150 lb/hr considered useful for building heat.

* Thermal Eff. = $\frac{\text{Net Elec. Power}}{\text{Reactor Power - Heat Load}}$

** Thermal Eff. = $\frac{\text{Net Elec. Power + Heat Load}}{\text{Reactor Power}}$

TABLE VIII: SAVINGS DERIVED FROM MODIFICATIONS TO PROPOSED STEAM CYCLE

Steam Cycle	Avg. Reactor Power Level (Mw)	Reduction in Reactor Power (Mw)	Fuel Saving ($/yr)	First Cost Add. Equip. ($)	Net Saving ($/yr)	Years to Pay for Itself
a. Straight, ext. at 30 psia for open feed-water, heating steam straight from steam generator.	6.77	-	-	-	-	-
b. Straight, ext. at 60 psia for closed feed-water heater and ext. at 30 psia for open feed-water heater, heating steam from steam generator.	6.70	0.07	714	3,500	425	8.3
c. Auto. ext. at 60 psia for heat steam and non-auto. ext. at 30 psia for open feed-water heater.	6.52	0.25	2546	15,000	1300	11.5
d. Auto. ext. at 60 psia for heat steam and closed feed-water heater and non-auto. ext. at 30 psia for open feed-water heater	6.44	0.33	3367	18,500	1838	10.0

The above values based on:
First cost does not include transportation and erection at arctic base.

Interest cost per year = $\frac{Y + 1}{2Y} \times I \times FC$

where: Y = 15-year depreciation period
I = 3-percent interest rate
FC = First cost

All savings referred to the simple cycle, a, in above table, proposed for the package reactor.

All values computed at the yearly average loads of 600 kw net electric load and 1800 kw heating load.

7.4.3 Variable Pressure to Turbine Throttle. At partial loads the steam pressure in the steam generator will increase with decrease in load, see Fig. 30. The proposed steam system for the package reactor system reduces this pressure to a constant 192 psia at the turbine throttle regardless of the load. This throttling process with its loss in availability is thermodynamically undesirable. If the steam from the steam generator were supplied directly to the turbine throttle at 265 psia at average electric and heating loads, the reactor power required would be 6.49 Mw as compared with 6.77 Mw when the steam is first throttled to 192 psia. At the estimated burn-up, a savings of $2,860/yr would be effected. The throttle end of the turbine casing would, however, have to be heavier to withstand a maximum pressure of approximately 400 psia, with a resulting increase in cost and weight of the turbine. The increased cost is estimated at about $5,600, and with an interest rate of 3% and amortization period of 15 years, the net savings would be $2,397/yr, taking over two years to pay for itself. This rate of return would certainly justify its use but, with the emphasis on savings in weight and first cost, it was not incorporated in the initial design of the package reactor. The quality of the exhaust steam would be decreased further if the higher pressure steam were used, but this factor is not of importance unless condensing water is available at the site year-around.

8.0 ELECTRICAL SYSTEMS

The electrical systems associated with the plant are of proven, conventional design incorporating high reliability, safety, and simplicity of operation. Approved practices are used in the installation and construction of all electrical facilities. Adequate grounding of all equipment is observed for the protection of personnel and equipment. Appropriate shielding and grounding arrangements are made to reduce electronic instrument background interference to a minimum.

The transformer room is adequately protected by a CO_2-fog system, or the equivalent, and the insulating oil used in transformers and switch gear is of the non-flammable type, such as Pyranol or Askarel.

8.1 Plant Electrical System

The proposed synchronous generator is rated as follows:

Voltage	volts	4160
Phase		3
Power Factor		0.80
Output	kw	1250
	kva	1560
Frequency	cps	60

The usual generator protective and operating equipment consisting of overload relays, indicating instruments, etc., is provided. A standard synchronizing device is used for paralleling the generator output with the standby unit or the existing network.

The load distribution system within the plant, Fig. 48, is as follows. The 4160-volt output of the generator is fed through an oil circuit breaker to a 4160-volt bus. This bus divides and connects to three oil circuit breakers, namely, the OCB to the standby supply or existing network, the OCB which feeds the station auxiliary load, and the OCB which supplies the main load. Such an arrangement allows the standby unit to feed the plant auxiliaries during startup conditions and also to supply part or all of the main load, depending upon the size of the standby unit.

The plant auxiliary OCB output feeds a stepdown transformer rated at 4160 to 460 volts. The output of this transformer divides into three circuits as shown. Circuits 1 and 2 consist primarily of pump motors and blowers which are large enough to warrant 460-volt, 3-phase service. Circuit 3 is stepped down in voltage by a transformer from 460 to 208/120 volt service. Circuits 1, 2, and 3 are protected by air circuit breakers. The oil and air circuit breaker ratings shown in Fig. 48 are for calculated load conditions; no attempt was made to determine the actual size needed by taking into account short-circuit ratings and other pertinent considerations. The voltage of 4160 for the main load was selected to agree with existing military transmission-line values. All of the major auxiliary components and breakers are operated from a central control panel located in the control room.

All vital units of plant auxiliary equipment are provided with a standby unit, e.g., there are two primary coolant pumps where one is sufficient to carry the load; in the event of breakdown the reactor continues to operate with the standby unit in service. Circuits 1 and 2 in Fig. 48 are designed so that either circuit can carry the pumps and blowers

DWG. 21259A

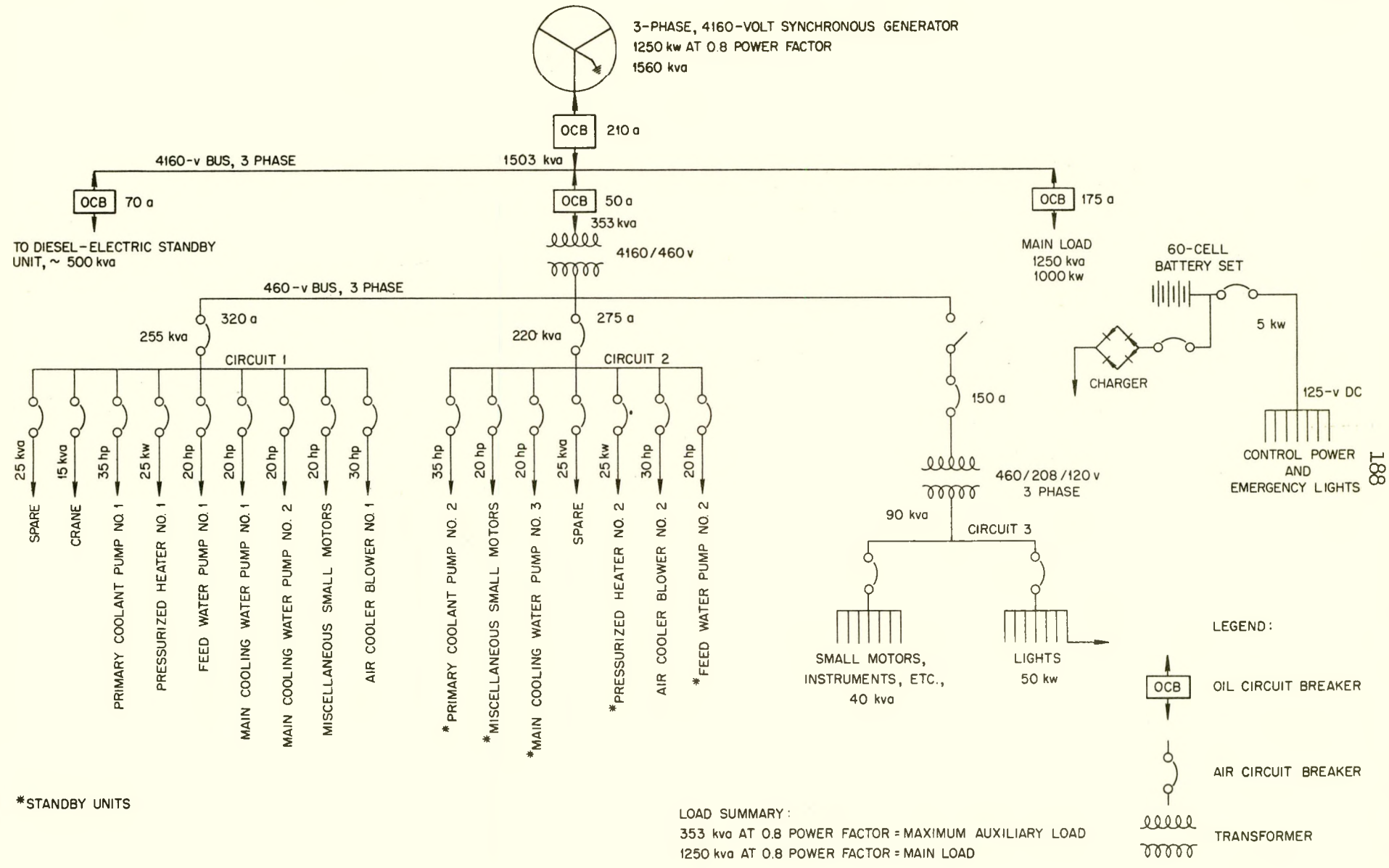

Fig. 48 Electrical Load Distribution.

necessary for plant operation. Circuit 3 provides power for all lighting, outlets, and reactor control-drive motors and instruments. Voltage regulating transformers are used in circuits requiring stable voltage for operation.

The maximum estimated auxiliary load for plant operation is 353 kva. This figure combined with the main load adds up to 1503 kva, which is well within the rating of the generator.

8.2 Emergency Lighting System

In the event of an electrical failure and until such time as standby power can be obtained, emergency lighting and control power for the operation of the generator breakers is provided by a battery set. This lighting system consists of fixtures located only at the vital areas throughout the plant; the system is completely separate from the conventional lighting. A time delay of perhaps 5 seconds exists from the time of loss of power to the energizing of the emergency system.

9.0 BUILDING AND AUXILIARY EQUIPMENT

9.1 Control Center

All major functions of the reactor power plant are controlled and monitored from a single control room, Fig. 49. This room contains the following instrumentation and control components.

1. A reactor control panel from which the operator can monitor and manually control the operation of the reactor. All of the important reactor indicators, such as the reactor period, power level, rod positions, are continuously displayed on this board. Controls for emergency scram, individual or ganged operation of the rods, fission chamber position setting, and manual or automatic operation of the reactor are all available on this console.

2. The various nuclear instruments and recorders are mounted on racks back of the control panel and are visible to the operator from his position at the control desk.

3. All recorders and indicators connected with the steam and water systems are rack-mounted to the right of the control desk.

4. A switch panel for the control of critical pump motors, blowers, heaters, etc., associated with the plant steam and water systems is mounted adjacent to the process instrumentation panel.

5. The remaining panel is for the control and indication of the generator output and associated distribution equipment. A system is also included for synchronizing the generator output with the existing electrical network.

All instruments and controls are arranged so that the operator can easily and quickly detect faulty operation and apply corrective action. Off-range conditions for all important functions, such as water flow and temperatures, are called to the operator's attention by alarms as well as indicating lights. The position of the control room, Fig. 50, provides for convenient access to equipment requiring inspection.

DWG. 21641

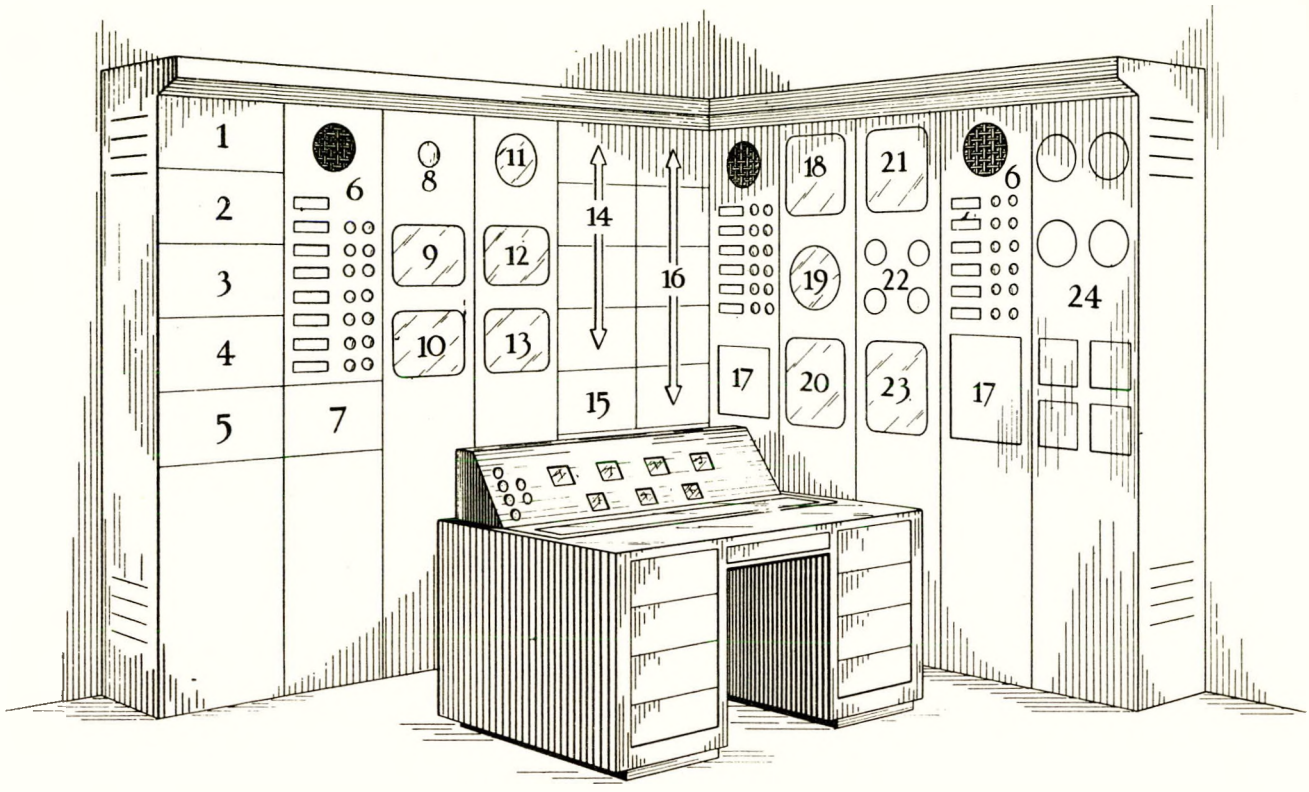

1. SERVO AMPLIFIER
2. POWER SUPPLY
3. COUNT RATE METER
4. PERIOD AMPLIFIER
5. LINEAR AMPLIFIER AND PREAMPLIFIER
6. ANNUNCIATOR PANELS (3)
7. COMPENSATED ION-CHAMBER POWER SUPPLY
8. REACTOR "ON" SIGNAL
9. COUNT-RATE RECORDER
10. THREE-POINT-LEVEL RECORDER
11. CLOCK
12. "LOG N" POWER-LEVEL RECORDER
13. PERIOD REACTOR
14. SIGMA AMPLIFIERS (4)
15. CLUTCH-AMPLIFIER POWER SUPPLY
16. CLUTCH AMPLIFIERS (6)
17. SWITCH PANELS (2)
18. PRIMARY COOLANT INDICATION
19. PIT TEMPERATURE
20. REACTOR TEMPERATURE-IN-TEMPERATURE-OUT RECORDER
21. STEAM CYCLE INDICATION
22. BEARING TEMPERATURES
23. STEAM CYCLE TEMPERATURE RECORDER
24. SWITCH GEAR PANEL

Fig. 49. Power Plant Control Center.

TD-E-2423A

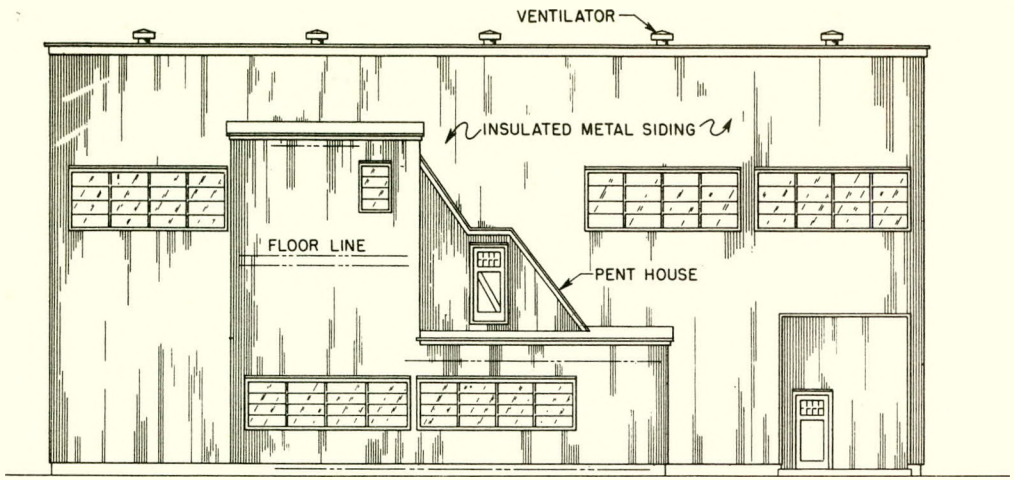

SIDE ELEVATION

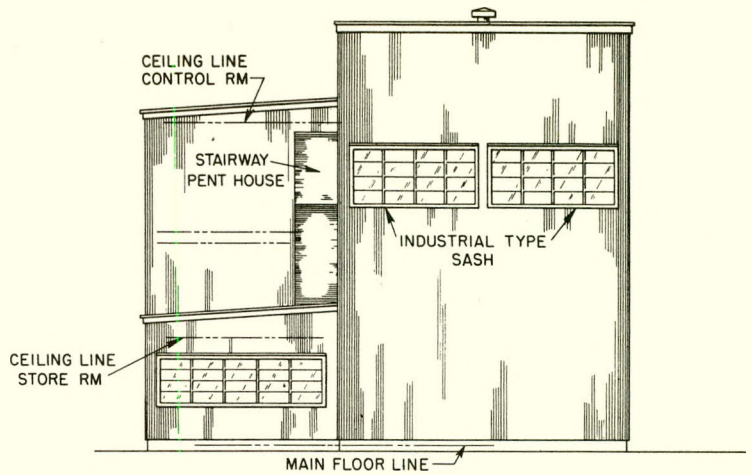

END ELEVATION

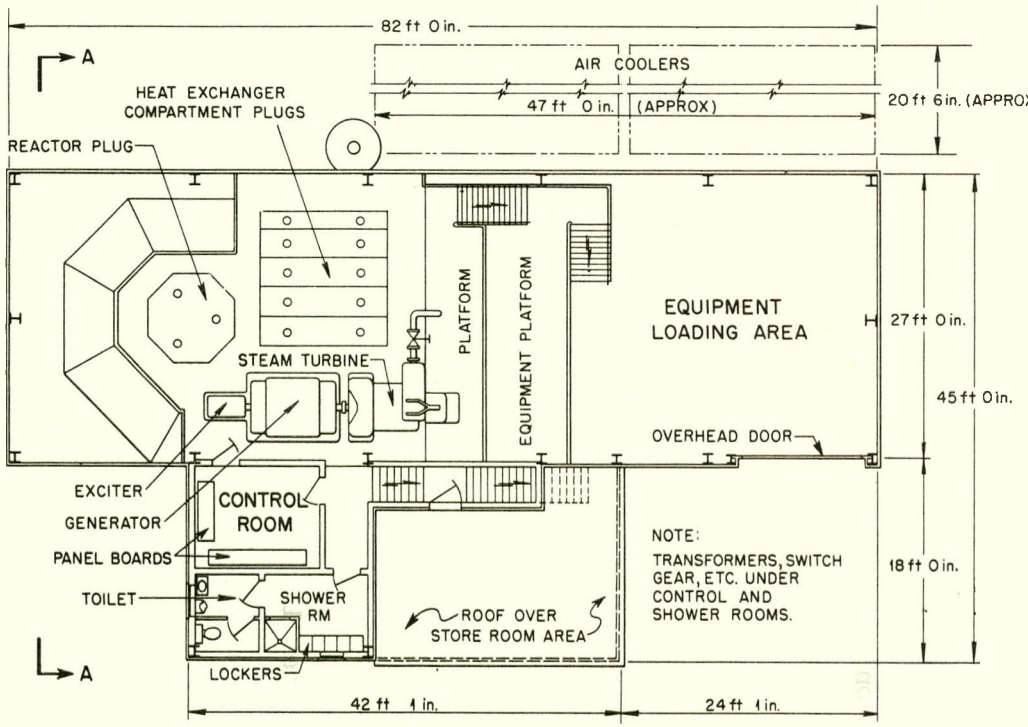

FLOOR PLAN

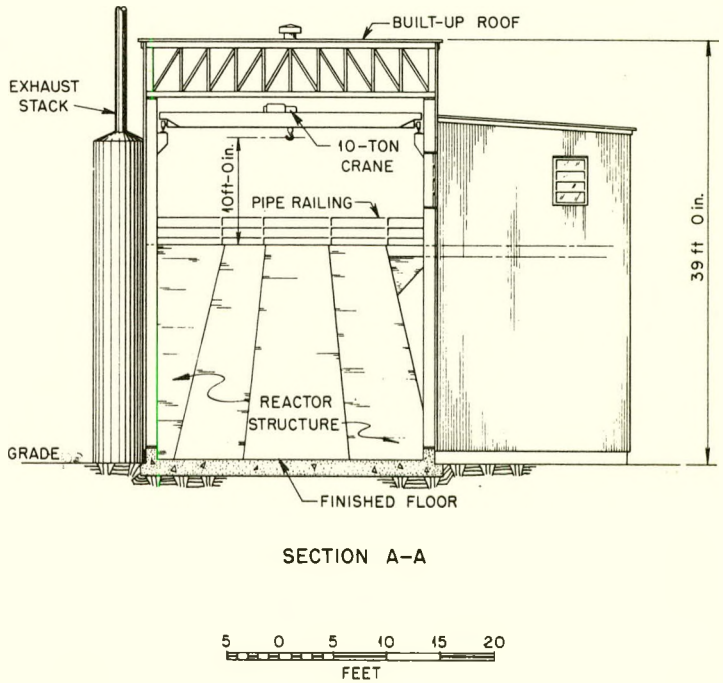

SECTION A-A

5 0 5 10 15 20
FEET

Fig. 50. Building Layout.

192

A minimum of two people will be required for the operation of the plant in addition to maintenance personnel. It is anticipated that three or four people will constitute an operating shift, including maintenance technicians.

9.2 Building

The building is, of necessity, a compromise design incorporating at least one important feature of each of the various design criteria. The components should be placed for ease of maintenance and yet the plant should be compact to save shielding and building costs. Building materials should be of low weight to allow transportation by air, but should also be of low cost in keeping with the primary premise of this plant. The building should be of the prefabricated type to permit rapid erection yet rugged enough to be readily adaptable to meet all arctic climatic conditions. It can easily be seen that if the building were designed to be optimum for one set of conditions it would entirely neglect a second set of conditions, therefore, the need of this compromise design.

The overall dimensions of the building are 82 ft long, 45 ft wide, and 39 ft high. The block of concrete which houses and shields the reactor and primary loop components takes up the major portion of the building. The block is $\sim$32 ft long, 27 ft wide, and 19 ft high.

The height of the building is determined by the requirements of the main building crane. The hoist of the crane has a capacity of 10 tons, and the hook is 10 ft above the reactor plug top when at its highest position. The upper limit of travel is governed entirely by the height necessary to permit hoisting the reactor cover over the top of the shielding. The hoist on the crane has enough cable to provide a 50-ft lift, which is sufficient for lifting objects from the floor level. The working latitude of the

crane permits servicing the entire building area.

The reactor block is compartmentized to house the various reactor components. The thickness of the concrete making up the walls of each compartment varies, depending on the intensity of radiation being emitted. To maintain short piping runs and a general compact layout, the components have been stacked, one above the other, rather than spread out in one plane. Fig. 5 and 6 show a side elevation of component placement.

The walls of the building, shown in Fig. 50, are constructed from a light-weight prefabricated type of siding. The siding consists of 1 1/2 inches of Fiberglas insulation sandwiched between two fluted 18-gauge galvanized steel sheets. The prefabricated siding slabs provide for ease of transportation while being readily adaptable to arctic conditions. The roof is of the flat-deck, built-up type, also provided with 1 1/2 inches of insulation. The steel framing of the building forms columns for the support of rails for the 10-ton overhead service crane.

The building is of sufficient length to permit a truck to be wholly contained within the building on the loading ramp. This allows uninterrupted service in spite of outside weather conditions.

The control room and change house are located alongside the building proper to insure optimum conditions for the operation of all instruments. At this point, vibration and background level are minimum. The control room is at the same elevation as the top of the reactor shield, at the second level, to insure that the operator is protected in full measure by the longest distance through the shield, since the reactor is located at floor level.

In actual construction, the building should be so placed that the end containing the air coolers is exposed to the prevailing winds. This is to minimize the possibility of snowdrifts interfering with operation of the coolers.

9.3 Waste Disposal System

In the design as presented in this report no specific provisions are made for disposal of radioactive waste. Under normal conditions the only waste material to be handled is the purge water from the primary coolant system. The purge rate is $\sim$30 gal/hr. The exact method of removal from the high pressure system is not yet determined. However, some of this waste will be collected in a sump inside the shield. The storage capacity of this sump should be equal to approximately one day's flow, or 1000 gallons. Activity of the water after one day will be low enough that it can be pumped to a second holdup tank and after further decay transferred to drums and hauled away in trucks to a dumping ground. The only long-life activities are those due to corrosion products, but the concentrations of these are very low at this purge rate.

Estimated dose rates are given below for a distance of 3 ft from the center of a 55-gal spherical container filled with primary coolant water at various times after removal from the reactor. Activities are based on operation of the reactor at 10 Mw.

Time (hr)	Dose (mr/hr)
0	387
12	16
24	2.8
36	1.35

9.4 Water Supply and Storage

Raw water makeup requirements for the reactor plant amount to about 1150 lb/hr (about 2.3 gal/min). The make-up replaces water bled from the primary coolant cycle in order to maintain a low concentration of corrosion products, as well as such losses in the steam cycle as pump leakage, turbine gland leakage, and blowdown from the evaporator and main heat exchanger. This amount represents the very minimum water requirement, not including personnel use, on which the plant can be operated. If necessary, this water can be hauled to the installation by truck. It would then be necessary to provide a storage tank at the installation site, the size of which would be determined by the reliability of truck service, but probably not less than 25,000 gallons.

The turbine condenser is cooled by a fluid (ethylene glycol and water) circulating in a closed system between the condenser and a bank of air coolers. This would certainly represent the case at any installation which was located where a large supply of fresh water is not available. The possibility does exist that the reactor plant may be located near a river or large body of fresh water. In this case, it would be a great advantage to be able to pump the water directly through the condenser. In addition to eliminating the necessity for expensive air coolers, it would also eliminate the need for electrical energy to drive the large fan motors with which the air coolers are equipped. With the turbine under full load, the condenser will require approximately 1400 gallons of 60°F water per minute.

9.5 Heating and Ventilation Requirements

It is estimated that in the winter the heat given up by the power plant equipment is sufficient to maintain an inside temperature of at least 65°F when the outside temperature is -50°F. The control room and the shower and locker rooms require about 32,500 Btu/hr of supplemental heat from unit heaters.

The above estimate is based on the use of a prefabricated siding, consisting of 1 1/2-inch Fiberglas insulation sandwiched between two fluted 18-gauge galvanized steel sheets, having an overall heat transfer coefficient of 0.18 Btu/hr-ft^2-°F. The roof is of the built-up type having 1 1/2" insulation. In winter the windows are covered with an insulated storm shutter so that the heat loss per ft^2 is estimated to be equivalent to that of the wall. Air leakage in winter is estimated at 1/2 air change per hour. Estimated heat losses are as follows:

Estimated Heat Losses from Building

	Area ft^2	Trans. Coeff. Btu/hr-ft^2-°F	Temperatures, °F Inside	Outside	Loss Btu/hr
Power Plant					
Walls	9,131	0.180	65	-50	189,000
Roof	2,641	0.173	73	-50	56,400
Floor	2,965	0.10	65	0	19,300
Air leakage	(850 cfm)		65	-50	132,500
Total					397,200
Control Room & Shower					
Walls	540	0.180	70	-50	11,700
Roof	324	0.173	70	-50	6,720
Air leakage	(140 cfm)		70	-50	4,040
Total					32,460

The heat losses from equipment into the building are estimated as follows:

	Btu/hr
Electric generator, at average load of 875 kw	179,500
Steam leakage, at 200 lb/hr	240,000
	419,500

In addition to the heat released into the building due to steam leakage there are significant amounts of radiation and convection from the reactor shielding and the steam system. It is therefore estimated that no heating equipment is required in the building except for the control room and shower room. In event of an emergency shutdown it is presumed that oil-burning portable heating equipment could be used.

In the summer, with 70°F outside temperature and 80°F inside temperature, about 50,000 cfm ventilating air is required to remove excess heat lost from the equipment, amounting to about 30 air changes per hour. A total of 285 ft^2 of openings is needed at the top and near the floor to provide adequate ventilation without use of motor-driven exhausting equipment. The roof ventilators and opened windows should take care of this requirement.

10.0 REACTOR LOADING PROCEDURE AND EQUIPMENT

At the end of a specified period, the reactor is shut down for a maintenance check and unloading. The aim is to unload the reactor safely and simply, with as many operations being performed manually as possible.

10.1 Tools

The equipment required for loading and unloading the reactor is:

1. Crane. An overhead crane with a capacity of 10 tons is used for the majority of the loading and unloading procedure. The length of travel of the crane affords service to the truck loading area and the temporary storage area for the concrete plug blocks.

2. Nut-Removal Tool. This modified impact wrench is used to remove the nuts which hold down the reactor cover. With the aid of the crane, the operator lowers the tool on a nut. After the nut is loosened, it is retained by means of a magnet while it is being lifted out of the reactor pit. The tool is a wrench similar in design to the Ingersoll-Rand type impact wrench. One modification is an extension added between the drive mechanism and the wrench socket to eliminate the danger of lowering the drive mechanism deep enough to damage the conrol-rod drive assembly.

3. Upper-Assembly-Grid-Unlatching Tool. The upper assembly grid is equipped with a hold-down mechanism which must be unlatched prior to removal of the assembly. The tool must unscrew a nut far enough to permit the latching rod to drop out of the latch slot. The tool consists of a socket wrench, an extension rod, and a handle which the operator turns manually.

4. Upper-Assembly-Grid-Removal Tool. The upper assembly grid has three handles to facilitate removal of the assembly. The tool consists of a hook, extension rod, and upper handle which will be attached to the crane lifting hook. Three of these tools are used to remove the upper assembly grid, the upper handles of the tools being attached to a common crane hook.

5. Fuel-Element Removal and Transport Tool. The fuel elements are lifted out of the core and transported to the storage racks. The tool consists of the operator's handle, an extension rod, and a gripping mechanism. The gripping is accomplished by means of retractable pins inserted radially into the snouts on the ends of the fuel assemblies. The operator's handle permits locking the pins in an open or closed position.

6. Shim-Rod Unlatching and Removal Tool. This tool disconnects the upper half of the shim rod and transports this segment to the storage racks. The rod is disconnected by rotating the upper section approximately 30 degrees. Grapples actuated by a toggle mechanism engage the cross member at the top of the rod and permit the operator to rotate and transport the upper segment.

7. Shim-Rod Removal - Lower Segment. The gripping mechanism of this tool is similar to that of the fuel element removal tool. The tool is longer due to the lower position of the element in the pressure vessel.

8. Underwater Light Assembly. A watertight steel housing with a transparent plastic lens encases the sealed-beam lights to prevent accidental breakage. It is estimated that three lights will give sufficient illumination for loading and unloading the reactor.

10.2 Carrier Design

The thicknesses of lead walls required for a transfer coffin containing four irradiated fuel assemblies were computed* to be ~9 in. for the sides, the top, and the bottom. The exposure from assemblies that have remained in the basin for one year is then 200 mr/hr at the surface of the coffin.

The inside dimensions of the coffin are 8 in. square and 36 in. high. The inside is divided into four sections by steel plates covered with 2 mils of cadmium. The outside dimensions of the coffin, including the cover are 26 in. square and 54 in. high. The corners of the coffin are rounded to the required shield thickness in order to reduce its weight. The estimated weight of the coffin is 8.6 tons.

10.3 Unloading Procedure

The reactor is not unloaded until after it has been shut down for 24 hours. The sequence for unloading is as follows:

1. The plug blocks are removed by means of the overhead crane and stacked on the building floor so as to form a wall.

* See Appendix 13.4: Carrier Design Calculations.

2. Water is added in the pit to a level of 2 ft above the pressure vessel. The nuts holding down the reactor vessel cover are removed in the following manner. The nut-removal tool is attached to the crane and gradually lowered into the pit. Care must be taken while lowering the tool so as not to damage the control-rod drive mechanism. When the tool is lowered so that the socket is engaged with the nut, the wrench may be actuated and the nut removed from the bolt. The tool is then raised, carrying the nut with it, and the nut is deposited behind the wall of concrete plug blocks. This procedure is repeated for each nut.

3. The pressure vessel cover is basically an assembly consisting of the cover proper and an upper deck attached to the cover. The five control-rod drive mechanisms are mounted on the upper deck. There are three eyes on the cover to which the crane hooks may be engaged. The initial lifting should be done slowly and carefully since the control-rod latches will be in the open position, and these should remain plumb. When the cover has been raised approximately 3 in., each control mechanism should be driven to its top position. The latches are then in a safer position for handling. The cover should then be raised out of the reactor pit and placed behind the wall of concrete-plug blocks.

4. Once the control-rod drive mechanisms have been removed from the reactor pit the water level of the pit should be raised to a height of approximately 2 ft below floor level.

5. Since the fuel rods must be removed before the control rods, the next operation is to remove the upper assembly grid which holds down the fuel elements. The assembly grid is held in place by means of pivoted bolts and hold-down nuts. The procedure is to loosen the nut far enough to let the bolt and nut fall out of a slot in the assembly grid. The assembly-grid-unlatching tool is used to accomplish this.

6. Once the assembly grid has been unlatched, the three grid-assembly removal tools are used to engage the three eye bolts on the top of the assembly. The tops of the three tools are attached to the common crane hook and lifting can proceed. The initial lifting should be done carefully, keeping in mind that the control-rod bearings are still engaged with the control rods and plumbness is essential. The assembly grid should also be placed behind the concrete wall.

7. For the initial unloading the fuel elements are removed from the reactor by the fuel-element removal tool. The elements are placed in underwater storage racks adjacent to the reactor. For succeeding unloadings the fuel elements that have been in the storage racks must be removed. A transport coffin is lowered into the pit. The coffin top is removed with an upper-assembly-grid-removal tool. Four fuel elements are placed in the coffin and the coffin top replaced. The crane removes the coffin and loads it on an awaiting truck. The procedure is repeated until all the elements in the storage racks have been removed. The fuel element unloading then proceeds as outlined above.

8. The control rods have been designed as two independent segments joined by a quick-disconnect coupling. Both segments of a rod should be removed from the reactor before the unloading of another rod is begun. The unloading of these rods is accomplished with the two control-rod-removal tools. The unlatching and upper removal tool engaged the top of the rod. A rotation of approximately 30 degrees disconnects the rod segments. It should be remembered that, although the upper segment of the rod is free to rotate, the lower segment is restrained from rotation by the lower assembly grid, thus allowing the relative motion needed for the disconnection. The upper segment is then placed in the storage racks. The long rod-removal tool is used to remove the lower segment and place it in the storage racks. On succeeding unloadings the storage racks are first emptied as outlined in the preceding paragraph. The coffin is designed to accommodate either fuel or control rod segments.

10.4 Loading Procedure

The loading procedure is the reverse of the procedure outlined above and the same tools are used in loading as in unloading. The loading sequence is as follows:

1. The connected control rods are placed in the reactor.
2. The fuel elements are next loaded into the reactor core.
3. The upper assembly grid is lowered into place, care being taken when engaging the assembly grid over the control rods.
4. The assembly grid is bolted in place.
5. After the assembly grid is in place and prior to replacing the pressure vessel cover, the water level in the pit should be lowered to the level of two feet above the top of the reactor.
6. The pressure vessel cover is lowered onto the reactor.
7. The nut-removal tool is used to replace and tighten the nuts.
8. The control-rod drive mechanisms are driven to their lowest position.
9. The concrete plug blocks are replaced.

11.0 COST ANALYSIS

11.1 Bases of Cost Estimates

In all of the following estimates the best information available from various sources was used. All major plant components were engineered sufficiently to enable several reliable manufacturers to quote realistic construction costs. In the absence of direct quotations from manufacturers, costs were estimated by comparing the component to similar, existing items.

A very wide discrepancy existed in the two quotations received on the heat exchanger, a difference of $75,000. The higher figure was used because of the superior product offered. It is conceivable that, after further investigation, considerable money can be saved in the major components in the primary coolant system. The urgency of issuing the report did not allow time to obtain other competitive bids. It is probable that the cost of this system can be reduced $50,000 to $100,000.

The costs shown are believed to be realistic for construction at a developed site similar to Oak Ridge, Tennessee. No attempt was made to estimate the costs for construction of the plant at an arctic base where labor costs could be expected to run approximately three times that for eastern United States. The estimated cost for the plant, $1,703,000, includes a 10% engineering charge. Additional costs would be required to cover any development deemed necessary.

11.2 Reactor Plant Cost Estimate

Reactor		$148,000
Reactor vessel (1)	$37,500	
Core fuel assemblies (45)	41,500	
Core structural supports	5,000	
Control rods and guides (5)	25,000	
Control-rod drive, release and indicating mechanisms (5)	25,000	
Thermal shield (1)	3,000	
Reactor vessel insulation	5,000	
Leakage collection system (1)	6,000	
Primary Coolant System		357,000
Main coolant pumps (2)	180,000	
Main coolant check valves (2)	12,000	
Heat exchanger (1)	102,000	
Main coolant piping	63,000	
Steam System		171,000
Turbo-generator set (1250 kw) (1)	100,000	
Main condenser (1)	20,000	
Condensate pumps (2)	2,000	
Feed-water pumps (3)	4,000	
Valves (40)	14,500	
Condensate return unit (1)	1,500	
Piping and lagging	29,000	
Main Condenser Cooling System		61,500
Pumps (3)	4,000	
Valves (14)	8,000	
Piping	17,000	
Air coolers and fans	30,000	
Storage tank (1)	2,500	
Evaporator System		22,000
Evaporator (1)	4,500	
Deaerator feed-water heater and storage tank (1)	6,500	
Valves (6)	3,500	
Piping	7,500	

Primary Coolant Water Purification System		$ 32,000
Filters (2)	$ 1,000	
Purification tanks (2)	6,000	
Pumps (4)	9,000	
Storage tank (1)	3,000	
Valves (20)	6,000	
Piping	7,000	
Pressurizer System		40,500
Pressurizer tank and heaters (1)	20,000	
Valves (5)	2,500	
Piping	8,000	
Off-gas stack	10,000	
Instrumentation and Controls, Reactor		82,000
Safety and control circuits, instruments and indicators	70,000	
Control panels	8,000	
Fission chamber drive	4,000	
Instrumentation and Control, Process		38,500
Steam system	17,000	
Water systems	15,500	
Miscellaneous systems	6,000	
Electrical Systems		82,000
Generator switchgear and distribution equipment	44,000	
Electrical distribution and lighting in plant	30,000	
Metering and controls	8,000	
Building (including crane, platforms, and ventilating equipment)		260,000
Reactor Shielding (500 cu yd)		70,500
Lubrication System		4,000
Core Handling and Replacement Equipment		20,000
Compressed Air System		6,000
CO_2 Fire Protection System		12,000
Contingencies, 10%		140,700
Engineering, 10%		155,300
TOTAL PLANT COST		$1,703,000

11.3 Installed Plant Costs per Kilowatt

The reactor will produce 1000 kw net electrical power and 12.065×10^6 Btu/hr (3,535 kw) in the form of steam for heating purposes. An analysis of the plant costs indicates that 45% can be charged to steam and 55% to electric power.

55% of \$1,703,000 = \$936,650 (electric power)

45% of \$1,703,000 = \$766,350 (steam heat)

The costs per installed kilowatt are, therefore:

$$\frac{\$936,650}{1000} = \$936/\text{kw net electric power}$$

$$\frac{\$766,350}{3535} = \$216/\text{kw steam heat}$$

11.4 Kilowatt-Hour Costs

In calculating the costs per kilowatt-hour for net steam and electricity delivered the following assumptions were used:

The plant amortization rate would be 13.5%.

The fuel inventory rate would be 10%.

\$20 per gram of U 235 would be charged for burn-up.

\$3.00 per gram would be charged for chemical reprocessing of the fuel.

The initial fuel loading would be approximately 18 kg of U 235.

The operating costs would be based on a 15-Mw-yr core life, before refueling.

1.4 gm of U 235 would be used per megawatt-day of reactor operation.

\$150,000 per year would be allowed for operations and routine maintenance of the reactor plant.

Capital Costs	Rate	Mills/kw-hr 60% Average Load Electric	Steam	100% Average Load Electric	Steam
Complete plant	13.5%	24.06	5.57	14.43	3.34
Fuel inventory	10.0%	3.76	0.87	2.25	0.52
Sub Total		27.82	6.44	16.68	3.86
Operating Costs					
Fuel burn-up		6.42	1.49	6.42	1.49
Fuel fabrication		1.78	0.41	1.78	0.41
Chemical reprocessing		1.58	0.37	1.58	0.37
Labor and maintenance		15.70	3.63	9.42	2.18
Sub Total		25.48	5.90	19.20	4.45
Total Costs		53.30	12.34	35.88	8.31

It is realized that the rates and charges used in the above analysis of costs are subject to question.

11.5 Summary of Costs

A summary of the above estimates is as follows:

Plant construction costs $1,703,000

Installed plant cost per kilowatt

Electric $ 936
Steam $ 216

Cost per kilowatt-hour (70% average load)

Electric 5.33 cents
Steam 1.23 cents

Cost per kilowatt-hour (100% average load)

Electric 3.59 cents
Steam 0.83 cents

12.0 FUTURE PROGRAM

The reactor study presented in the foregoing was undertaken to assess the feasibility of designing and constructing a reactor suitable for the production of electrical energy and steam heating for a remote location. An attempt was made to provide a complete conceptual design of this reactor and its auxiliary equipment, and to investigate the engineering details in certain key portions of the system in order to estimate the amount of further development required and to provide a basis for establishing sound cost estimates. It is believed that the study has provided a feasible reactor design and realistic cost estimates.

It is expected that this report will provide the basic specifications an architect-engineer firm or other suitable group will need for proceeding with the actual engineering and construction of the reactor power plant.

12.1 Variation from Present Specifications

Now that the reactor design presented in this report is established, it is possible to consider the effect of variations of certain of the specifications on price and performance without a major new investigation for each case.

12.1.1 Lower Power. Some uses for remote power at a level considerably below the 1000 kw of electricity and 3500 kw of heat of the present design have been suggested. The group has made an extrapolation of the present plant costs to one with a total reactor heat rating of 4500 kw and a peak output of 1900 kw of steam for heating along with 400 kw gross electric power. The cost of such a plant is estimated at $1,270,000.

12.1.2 Higher Power. A study has also been made of the present plant

extrapolated to a total reactor heat rating of 30,000 kw, utilizing the present core and pressure shell. The peak output rating is estimated at 4240 kw of gross electric power and 9370 kw of steam for heating purposes. The cost of such a plant is estimated at $2,591,000. The present plant extrapolated to 30,000 kw of reactor heat as a producer of 6000 kw of electric power only is estimated at $2,771,000.

12.1.3 Heat Only. The possibility of using a reactor to produce heat only and not electrical energy could conceivably place the nuclear plant in a more favorable position with respect to conventional equipment. This would require, of course, a suitable location for utilization of large amounts of heat. The present plant with an output of approximately 10,000 kw of 330°F, 60-psia steam would cost about $1,216,000.

12.2 Other Reactor Types at 10-Megawatts Gross Heat

Obviously there are many possibilities for nuclear reactor types besides the one described in this report. A number of these other types were or are being investigated by students of the Oak Ridge School of Reactor Technology. There are as follows:

Aqueous Homogeneous Circulating-Solution Reactor

Heterogeneous Boiling Reactor

Homogeneous Boiling Reactor

Los Alamos-Type Water Boiler

Gas-Cooled Reactor with Ceramic Fuel Elements

Fused-Salt Reactor

In addition, a study of a water-cooled, boiling, graphite-moderated reactor has been prepared by the Bendix Corporation. A study of a helium-cooled, graphite-moderated reactor has been prepared by North American Aviation, Inc. The possibility of making a low pressure boiling reactor from

aluminum has been suggested by ANL; if this is indeed feasible, significant cost reductions might become practicable. It is believed by the authors that none of the above systems offer any large short-range savings or any important reductions in operating costs over the reactor described in this report; however, continuing studies will be made of these types in an effort to establish their feasibility and the cost reductions which might be anticipated.

12.3 Other Reactor Types at Higher Power

Nuclear power producers in the range of 3,000 to 30,000 kw of developed electricity may be important for certain special applications. While the reactor described in the present report deserves careful consideration at the low end of this scale, it is almost certain that a different reactor type could be used more advantageously at the high end.

13.1 APPENDIX A: REACTOR PLANT WEIGHTS

The following table is a summary of the weights of the important components. The weights of sand and gravel required for the building and shield are not included. The overall dimensions of the larger components are also tabulated. The total weight of the complete plant is approximately 540 tons.

	Size (larger pieces)	Weight (lb)
Reactor		
Reactor vessel	(10' x 4' -5" x 5' -0")	18,800
Core, fuel assemblies		900
Core, structural supports		630
Control rods and guides		300
Control-rod drive release and indicating mechanisms		600
Thermal shield		2,560
Reactor vessel insulation		100
Leakage collection system		750
		24,640
Primary Coolant System		
Main coolant pumps (2)	(7' -8" x 4' -0" x 4' -0")	17,600
Main coolant check valves (2)		2,400
Heat exchanger	(16'-10" x 5'-7" x 7'0")	15,200
Main coolant piping		3,000
		38,200
Steam System		
Turbogenerator set	(22' x 6'-7" x 8'-2")	45,800
Main condenser	(14'-6" x 6'-2" x 4'-6")	9,500
Condensate pumps		600
Feed-water pumps		3,400
Valves		2,570
Condensate return unit		1,350
Piping and lagging		4,440
		67,660

	Size	Weight (lb)
Main Condenser Cooling System		
Pumps		3,000
Valves		3,490
Piping		6,000
Air coolers and fans	(4'-0" x 20' - 0" x 2'-0")	33,800
Storage tank		1,990
Ethylene glycol, 550-gal		5,600
		53,880
Evaporator System		
Evaporator		3,400
Deaerator feed-water heater and storage tank	(5'-6" x 14'-0" x 4'-0"	4,000
Valves		310
Piping		500
		8,210
Primary-Coolant-Water Purification System		
Filters		100
Purification tanks	(2'-0" x 2'-10" x 10'-0")	1,400
Pumps (4)		800
Storage tank	(6'-0" x 4'-6" x 4'-6")	1,990
Valves		250
Piping		200
		4,740
Pressurizer System		
Pressurizer tank and heaters	(83" x 56" x 46")	7,000
Valves		540
Piping	(22'-0" x 1'-2" dia)	500
Exhaust stack (100 ft)		4,000
		12,040
Instrumentation and Controls (Reactor)		6,500
Instrumentation and Controls (process)		3,500
Electrical Systems		35,000
Building*		220,000
Shielding*		600,000
Miscellaneous Systems		6,000
		1,080,370
		540 tons

* Sand and gravel not included

13.2 APPENDIX B: OPTIMUM REFUELING CYCLE

The total fuel and related costs plotted in Fig. 51 are arrived at by adding costs of uranium actually burned, inventory charges on unburned uranium held up in the core, core fabrication costs, shutdown costs, transportation costs, and chemical processing costs for the uranium remaining in the burned out core. Fuel burnup cost is based on a charge of $20.00/gm U 235 fissioned. The amount of U 235 required initially is shown in Fig. 52 as a function of operating time. Thus, for a 15-Mw-yr cycle, 18 kg of U 235 are required as initial loading. It is assumed that after the burned out core is chemically processed, the unburned uranium would be sold back to the Atomic Energy Commission at a value which would be the same as that of partially enriched fuel with an equivalent percentage of U 235*. Annual inventory charges are assumed to be 10% of the value of the uranium held up**. This holdup period was estimated at one and one-sixth years beyond the actual fuel cycle length; it includes time spent in fabrication and chemical processing plus one year cooling period for the burned-out core. The core fabrication cost is estimated to be $42,500. Shutdown costs are based on an estimate of labor requirements for a shutdown of two weeks. Chemical processing costs represent a charge of $3.00/gm of uranium remaining in the burned-out core**. There are indications that this charge will be decreased as a result of development work currently underway in the fuel-plate processing field.

---

* Lane, J. A. et al, Feasibility and Economics of Aqeous Homogeneous Reactors, December 10, 1951. ORNL-1096.

** Lane, J., personal communication, August 12, 1953.

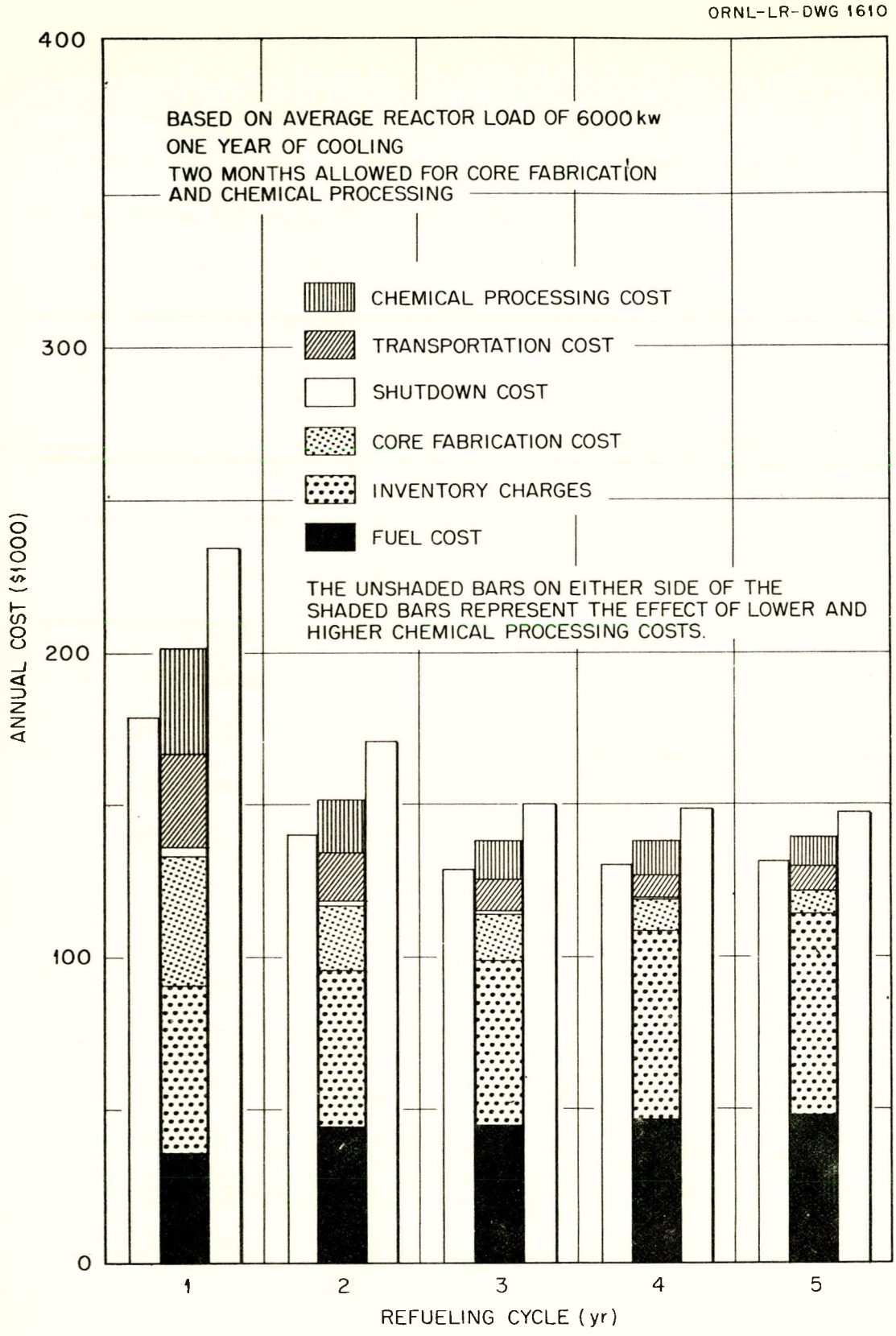

Fig. 51. Effect of Fuel Cycle-Length on Fuel Costs.

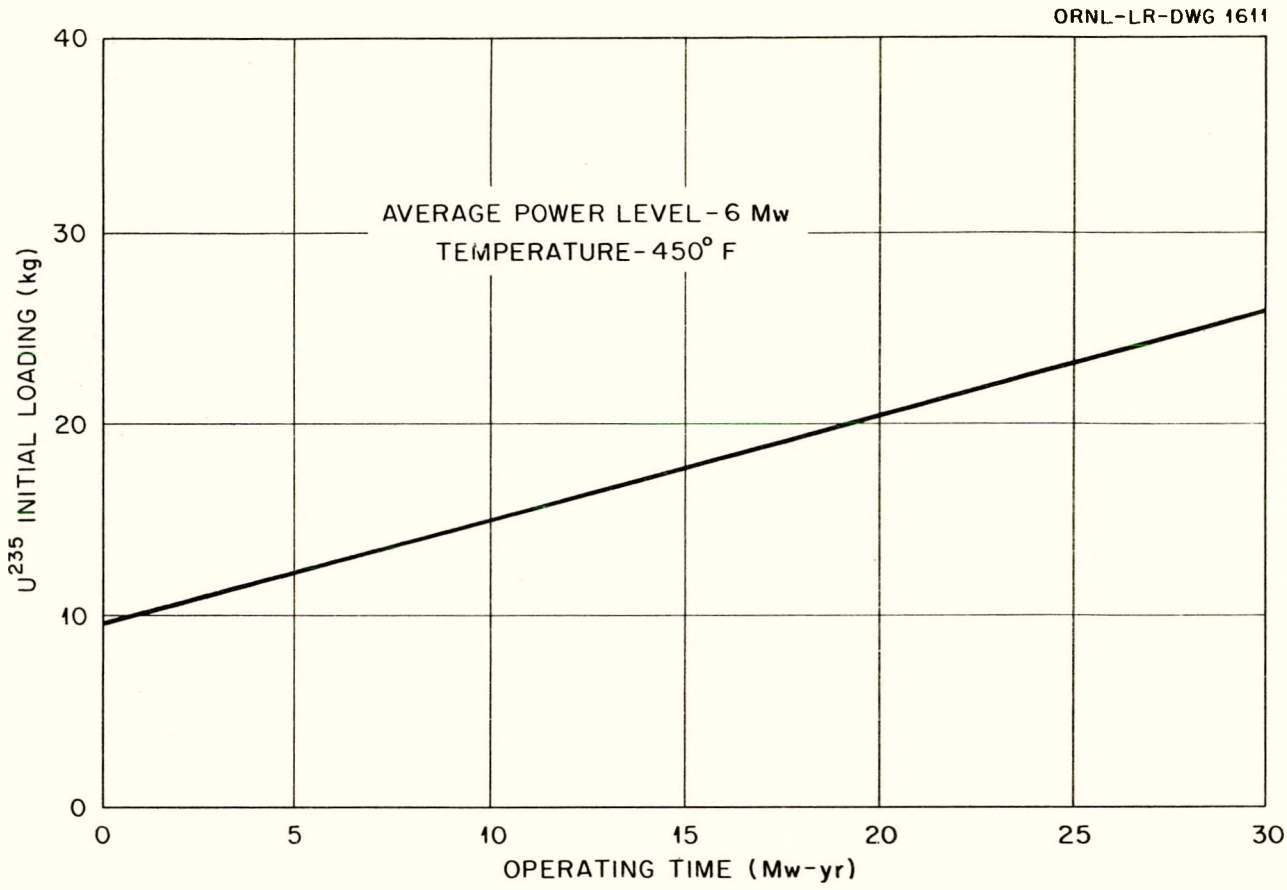

Fig. 52. U^{235} Loading Required vs. Operating Time.

The shaded bars of the graph in Fig. 51 represent the various cost components mentioned above, as well as the total fuel cost, as a function of the length of the refueling cycle. They are based on a power level of 6 Mw and indicate that from the standpoint of fuel costs, the optimum refueling cycle length, is four years. In order to show the effect of lower and higher fuel processing costs the two unshaded bars have been added. They represent the total fuel cost if fuel processing charges are $1.00 and $6.00 per gram of uranium, respectively. It should be noted that the optimum fuel cycle length is affected significantly by these costs.

13.3 APPENDIX C: REACTOR MATERIALS

13.3.1 The Problem of Material Selection

Introduction. The material requirements for a water cooled and moderated reactor, as compared with the needs of either the chemical industry with its high corrosion rates, on one hand, and the aircraft industry with its high temperature requirements, on the other, are not very stringent. The urgency that proper materials be selected is based on the unique combination of the following circumstances:

a. The materials must have the proper physical properties to function for long, maintenance-free periods.

b. The materials must perform satisfactorily under irradiation and in contact with transport materials which have been irradiated.

c. The materials must withstand the corrosive action of contact with, and submersion in, water between 450° F and 550° F.

The need for the basic data, to permit the selection of materials to meet the above requirements, was encountered first for the STR in 1948 and, as a consequence, an extensive investigation was launched at various research centers, including Oak Ridge, Hanford, Babcock and Wilcox, Westinghouse, General Electric, Battelle Memorial Institute, and others.

It was felt that if this information could be tabulated, together with other known corrosion data, and then analyzed, the following could be accomplished for the package reactor:

a. Eliminate the need for basic experimental research on materials and so keep the development costs on the package reactor to a minimum.

b. Arrive at specifications for proper materials to give trouble-free operation of the readily accessible equipment for a minimum of three to five years, and to give lifetime operation for the remainder of the equipment.

c. To arrive at the proper operating conditions required for realizing (b).

The results of such a compilation will be issued under separate cover in the near future. This appendix is an abbreviation of the above report, wherein the actual tabulation of the corrosion data has been omitted. The averaged corrosion rates are, however, included.

Basis for Material Selection. The package power reactor is composed of two basic components: the reactor itself with its primary loop and the power plant and its associated equipment which might be considered a secondary loop. This report is mainly concerned with the primary loop, since this loop contains the potentially radioactive liquids, and is consequently the most probable source of trouble. The corrosion in the secondary or steam-cycle loop can be treated in the same manner as any conventional steam turbine plant.

On the basis of the materials selected for testing at the various atomic research centers and on the basis of the materials actually selected for use in the STR, an evaluation was made of the following materials:

304 ss	Monel
304L ss	K-Monel
316 ss	Inconel
317 ss	Inconel-X
410 ss	Armco 17-4 PH*
440C ss	Armco 17-7 PH
Stellite-3	USS 322 W
Stellite-6	A-Nickel
Stellite-12	Hastelloy C
Graphitar 14	Vascoloy-Ramet 166
Chrome plate	

*Precipitation-hardening

Physical Properties. The physical properties of the materials of construction are the first criteria upon which to base the selection of such material. Since it is not the purpose of this report to attempt any detailed design of the reactor, it was considered sufficient to have supplied a sufficient number of materials of varying characteristics so that any physical property, such as hardness, ductility, strength, can be obtained by proper selection from the group listed. The analysis of the materials of construction, in light of their physical properties, was therefore limited to an investigation of underwater bearing materials, since information on such applications are not normally available in the literature. Wear tests were conducted on various materials at ANL on the Falex machine which rotates a pin against a V-block. Some of the more favorable combinations are listed below:

TABLE IX: WEAR RATES AND FRICTION COEFFICIENTS OF MATERIALS AS DETERMINED ON FALEX MACHINE, ONE-HOUR RUNS

Water at 500° F

Material	Hardness	Wear (in.)	Pressure (psi)	Appearance	Apparent Coefficient of Friction
Pin, Stellite-6	Rc 44	0	728	Burnished	0.28
V-Block, Stellite 6	Rc 42	0.0002		Smooth	
Pin, Stellite-6	Rc 44	0.0001	2420	Scratched	0.21
V-Block, Stellite-6	Rc 22	0.0001		Some Score	
Pin, Cr Plate USS/W	R15,N86	0.0001	389	Smooth Wear	0.42
V-Block, Stellite-6	Rc 41	0.0001		Fine Scratch	
Pin, Cr Plate USS/W	R15,N86	0.0001	707	Smooth Wear	0.28
V-Block, Stellite-6	Rc 41	0.0001		Fine Scratch	
Pin, Cr Plate USS/W	R15,N86	0.0001	2380	Smooth Wear	0.20
V-Block, Stellite-6	Rc 41	0.0003		Smooth Wear	
Pin, Stellite-6	Rc 41	0.0001	342	Fine Scratch	0.71
V-Block, SS 347	Rc 13	0.0009		Deep Scratch	
Pin, Stellite-3	Rc 53	None	398	Burnished	0.71
V-Block, USS/W	Rc 46	0.0005		Deep Scratch	
Pin, 347 Cr Plate(0.0005)		None	715	Fine Scratch	0.37
V-Block USS/W		0.0003		Smooth Wear	

From other tests run on the Falex machine the following combinations showed wear of 0.0005" or less and an apparent friction coefficient of 0.4 or less:

TABLE X: LOW WEAR AND LOW FRICTION COMBINATIONS

Water at 500° F

Pin	Hardness		V-Block	Hardness
Stellite-6	Rc 40	vs	Vascoloy - Ramet-166	Rc 55
Stellite-3	Rc 45	vs	Vascoloy - Ramet-166	Rc 54
Vascoloy - Ramet-166	Rc 43	vs	Stellite-3	Rc 52
SS 410 HT	Rc 37	vs	Stellite-3	Rc 49
Stellite-21	Rc 33	vs	Stellite-21	Rc 21
SS 347	R15,N71	vs	Stellite-6	Rc 39
Stellite-12	Rc 40	vs	Stellite-6	Rc 30
USS/W PH	R15,N86	vs	Stellite-6	Rc 41
Stellite-6	Rc 43	vs	Bachrach alloy	Rc 55
Stellite-3	Rc 53	vs	SS 440C HT	Rc 52
SS 347 Cr plate	R15,N73	vs	Stellite-6	Rc 43
Armco 17-4 PH Cr plate	R15,N84	vs	Stellite-6	Rc 40

Westinghouse has run wear tests and has evolved a wear factor based on loads per million cycles. Many of the combinations which are of possible interest are listed in Table XI.

TABLE XI: WEAR FACTORS AT 500° F IN WATER

Weight Loss in Milligrams per Pound Load per Million Cycles as Established in WAPD-MA-1020

P-C = Piston and Cylinder J-S = Journal and Shaft

Materials	Oxygenated P-C	Oxygenated J-S	Hydrogenated P-C	Hydrogenated J-S
17-4 vs 17-4			460	
17-4 vs Cr plate 17-4 PH, honed	20		13	
USS 322W PH vs 322 PH	470			
USS 322 W PH vs 304 or 347	1040			
USS 322W PH vs 17-4 PH Cr plate	21			
304 or 347 vs 17-4 PH	475			
304 or 347 vs USS 322W	880			
304 or 347 vs 17-4 Ph Cr plate,honed	65			
304 or 347 vs 304 or 347	3200			
17-4 Cr plate vs 17-4 PH		7.8		
17-4 Cr plate vs USS 322W PH		4.7		
Stellite-3 vs 17-4 PH	150	47	25	1.4
Stellite-3 vs USS 322W PH	130	310	11	
Stellite 3 vs Cr plate 17-4,honed	8.3	6.1	0.3	8.5
Stellite-6 vs 17-4 PH	62	320		100
Stellite 6 vs 17-4 PH Cr plate,honed	65		24	
Haynes 21 PH vs 17-4 PH	25			
Haynes 21 PH vs 17-4 PH Cr plated		80		
S-monel vs USS 322W PH	340	970		
S-monel vs 304 or 347 SS	420	180		350
S-monel vs 17-4 PH Cr plate		420		2
440C vs USS 322W PH		59		
440C vs 17-4 PH Cr plate, honed	92	47		
Lead vs 304 or 347		2730		4.1
USS 322W PH vs Stellite 3	220		136	
17-4 PH nitrided vs 17-4 PH Cr plate	40			
17-4 PH Cr plate, honed vs Stellite-3			37	
17-4 PH Cr plate,honed vs Stellite-6	74		50	
17-4 PH Cr plate,honed vs KR monel PH	81		1.1	

Materials	Oxygenated P-C	Oxygenated J-S	Hydrogenated P-C	Hydrogenated J-S
Stellite-3 vs Stellite-3	71		34	
Stellite-3 vs Stellite-6	59			
Stellite-3 vs Stellite-12	155			
Stellite-3 vs KR monel PH	170		31	
Wall Colmonol 6 vs Stellite-3	61		60	
Stellite-3 vs 410	16	140		
Stellite-3 vs graphitar 14			43	
410 vs 410		380		145
416 vs 416		165		49
Nitrided Cr C_3 vs nitrided Cr C_3	0.0			
Nitrided 17-4 PH vs nitrided 17-4 PH	9.9			

13.3.2 Radiation Effects on Physical Properties

The problem of radiation damage on materials of construction has been fairly extensively investigated at many of the national laboratories. These studies included investigations of the effects of radiation on such physical properties as hardness, tensile strength, elongation, ductility, creep strength, and density changes.

The effects of irradiation upon the hardness of the selected materials was investigated at Oak Ridge, Hanford, NRX (Chalk River) and Brookhaven; results are shown in Table XII.

TABLE XII: EFFECT OF IRRADIATION ON HARDNESS OF MATERIALS

Material	Hardness-Rockwell Before	After	Facility	Irradiation (nvt x 10^{19}) Thermal	Fast	Time (hours)	Temp. (°F)
304 annealed	B72-76	B72-76	ORNL	1	-	3240	500
347 annealed	B89-90	B81-90	Hanford	30	-		540
440C hardened	A75	A77-79	Hanford	4	5		540
440C hardened	C54-55	C53-55	NRX	37	51	3000	70
USS/W hardened	C48-49	C47-49	NRX	37	51	3000	70
17-4 annealed	C33-35	C48-52	Hanford	4	-		540
17-4 hardened	A73	A74	Hanford	3	-		540
17-7 hardened	C50-51	C45-50	Hanford	4	-		540
Hastelloy C	C16-20	C15-20	Brookhaven	4.8	-	-	270
Stellite-3,Cast	A77-78	A78-79	Hanford	1.3	-	-	70-140
Nickel A	F64-68	F82-91	ORNL	1	-	1800	500
Monel	B81	B95	Hanford	4	5		70-140
K-monel	C24-28	C25-28	Hanford	4	-		540

In most instances the hardness increased, the nickel-base alloys showing the greatest increase. It is generally believed that the hardness increase is induced by the neutron bombardment. It has been proven in other tests at Hanford that the hardness increase can be eliminated by annealing. The irradiation of 347 ss caused an increase in hardness from Rockwell B75 to B98. The hardness was reduced to B75 again by annealing and increased back to B98 by a second irradiation. The welds and heat-affected zones associated with welds, upon irradiation, showed hardness increases similar to those of the parent metal.

The effect of irradiation on the tensile properties is generally to alter these properties in the same manner that cold working would. Tensile samples irradiated at Oak Ridge showed the following comparisons with non-irradiated samples:

TABLE XIII: EFFECT OF IRRADIATION ON TENSILE PROPERTIES

Material	Ultimate Strength (psi)	Yield 0.2% Offset (psi)	Elongation (%)
304 irradiated	92,000	43,500	58.5
304 non-irradiated	95,000	48,500	41.0
304 non-irradiated	92,500	44,000	70.8
309 irradiated	99,000	43,500	51.0
309 non-irradiated	95,000	38,500	54.0
316 irradiated	89,500	36,500	66.5
316 non-irradiated	90,000	35,000	70.0
347 irradiated	103,000	42,500	54.5
347 non-irradiated	99,000	37,500	56.6

at 1 x 10^{19} nvt slow, 3200 hours, 400°-500° F.

Other tensile specimens run at Chalk River and Hanford showed the following changes upon irradiation:

TABLE XIV: EFFECT OF IRRADIATION ON TENSILE PROPERTIES

Material	Ultimate Strength, (psi) Non-irrad.	Irrad.	Yield 0.2% offset Non-irrad.	Irrad.
316 annealed*	79,500	151,000		
USS/W*	113,000	134,500		
440C hardened**	199,000	240,000	185,000	205,000
440C hardened**	211,000	240,000	185,000	200,000

* 3000 hours 3.7×10^{20} nvt slow, 5.1×10^{20} nvt fast, 75° F, Chalk River.

** 4×10^{19} nvt slow, 5×10^{19} nvt fast, Hanford.

Other test samples of nickel-based alloys likewise showed improvement in tensile strength.

TABLE XV: EFFECT OF IRRADIATION ON TENSILE PROPERTIES OF NICKEL-BASE ALLOYS

Material	Ultimate Strength, (psi) Non-irrad.	Irrad.	Elongation in 2", % Non-irrad.	Irrad.
Monel unnotched	85,000	96,000	33	10
Monel notched	129,000	---	--	--
K-monel unnotched	123,000	134,000	11	3
K-monel notched	211,000	226,000	--	--
Inconel unnotched	106,000	116,000	31	29
Inconel notched	151,000	172,000	--	--
Inconel-X unnotched	126,000	133,000	20	12
Inconel-X notched	174,000	203,000	--	--

Radiation tests on springs made on Inconel and Inconel-X showed only minor decreases in free length and insignificant changes in spring constants.

The effect of irradiation on the density and the dimensions of most materials has been found to be negligible and within the measurement error. Changes in electrical resistivity and magnetic susceptibility have also been found to be slight with some tendency towards increased values.

Creep test specimens of SS 347 run at Hanford, loaded at 10,000, 15,000, 20,000 and 25,000 psi were irradiated at Hanford at 1 x 10^{20} nvt slow and 1.5 x 10^{20} nvt fast. All changes were within the experimental error. Other tests at ORNL indicate that irradiation may increase the creep rate somewhat.

The basic pressure vessel material which is to be clad with SS 304, which is proposed for the reactor,

is ASME SA-212 Grade-B firebox quality steel. Irradiation results of this material follows:

TABLE XVI: REACTOR PRESSURE VESSEL MATERIAL

SA-212 Grade-B Firebox Quality Irradiated at Hanford at 5 x 10^{19} nvt Slow
4 x 10^{19} nvt Fast

Material	Hardness Rockwell B Before	After
Parent metal	B75	B89
Weld	B65	B89

	Yield, (psi) Before	Yield, (psi) After	Ultimate, (psi) Before	Ultimate, (psi) After	Elongation, (%) Before	Elongation, (%) After
Weld only	43,000	71,000	62,000	75,000	14	6.8
Unnotched	42,000	70,000	64,000	82,000	00	---
Notched			124,000	141,000	19.2	14.5

Specimens of this same material, seam welded with E6010 rod and stressed relieved at 620° C, were also exposed at 4 x 10^{19} nvt. The samples showed an increase in hardness from 40 to 47 Rockwell A; 63% increase in yield strength, a 20% increase in ultimate strength, and a decrease in elongation at rupture, from 17% to 14%.

13.3.3 Corrosion Resistance

Of the three reactor material selection criteria, the corrosion resistance of the material is the most important; the major effort on materials at the atomic energy installations has been directed at corrosion evaluation. Corrosion is of concern for the following reasons:

a. Corrosion may break down protective clads and coatings such as the stainless steel cladding on the fuel elements and the chrome plate.

b. Corrosion will damage and shorten the life of moving mechanisms such as the control-rod drives and the break-down seals.

c. Corrosion may form films on heat transfer surfaces and reduce efficiency.

d. Corrosion may form solid transport materials which may clog passages, hinder operation of fine mechanisms, and differentially coat out on heat transfer systems to lower the heat transfer efficiency.

e. Corrosion may cause leaks in the high-pressure closed-primary loop.

Although the mechanism of corrosion is generally accepted as an electrochemical process, it is agreed that many variables affect and in turn are affected by the continually changing equilibrium of the corrosion process. After a study of the test methods and results, the corrosion phenomena were identified as follows:

a. Effect of dissolved gases (O_2, H_2, CO_2, N_2, degassed).

b. Effect of welding, heat treatment, and sensitizing.

c. Effect of fluid flow, including mechanism of transport materials formation.

d. Effect of irradiation of materials.

e. Effect of irradiation of water on gases in solution and corrosion of materials in the water.

f. Effect of water purity.

g. Effect of stress.

h. Effect of pH.

i. Effect of inhibitors and additives.

j. Effect of crevices and galvanic couples.

k. Effect of surface finish.

l. Effect of acid cleaning and passivation.

The evaluation of these effects constitutes the main basis for the corrosion section of the report to follow. The corrosion behavior of about 1000 specimens of the selected materials was evaluated. Individual charts of the various materials were made and the test conditions and the corrosion rates are listed so that many of the above effects of the variable conditions can be substantiated with actual corrosion figures.

The results of tabulation have been summarized in Tables XVII through XXI, following.

TABLE XVII: AVERAGE CORROSION RATES OF MATERIALS

($mg/cm^2/mo$)

Water at 400° F to 600° F

Material	With Oxygen		With Hydrogen		Degasses		With Alkali		Irradiated	
	Samples	Rate	Samples	Rate	Samples	Rate	Samples	Rate	Samples	Rate
304	48	0.04	57	0.03	11	0.09	27	0.03	1	0.02
304L	32	0.07	27	0.03	6	0.07				
347	44	0.09	78	0.04			3	0.04	14	0.08
316	63	0.08	24	0.02	14	0.11	18	0.04		
17-4 PH	38	0.09	33	0.17	13	0.27			4	0.05
17-7 PH	29	0.11	8	0.38	15	0.19			9	0.16
440C	28	0.41	9	0.66	9	0.41	6	0.48		
410	27	0.63	10	0.52			9	0.23		
Monel	18	1.10	7	0.03	6	0.37	8	0.08	2	0.50
K-Monel	37	0.27	14	0.04			15	0.08	15	0.08
Inconel	51	0.31	39	0.01			11	0.02	1	0.11
Inconel-X	8	0.70	16	0.03	4	0.04	3	0.03	1	0.15
Hastelloy C	4	0.22			3	0.03			2	0.18
A-nickel	16	0.27	6	0.02	3	0.19	3		2	0.10
Vascoloy - Ramet-166	7	1.04							2	0.11
Stellite-3	7	0.11	5	0.04			3	0.58	10	0.11
	8	20.60								
Stellite-6	20	0.17			4	0.19	3	0.05	3	0.13
	21	12.13								
Stellite-12	12	0.18			1	0.18				
322W	26	0.60	9	0.15	5	0.28			10	0.05
Graphitar-14	5	6.40			3	3.84				

TABLE XVIII: AVERAGE CORROSION RATES OF MATERIALS

($mg/cm^2/mo$)

Water at 4000° F to 6000° F

Material	Fluid Flow 0.01 fps		Fluid Flow 10 fps		Fluid Flow 20 fps		Fluid Flow 30 fps		In Autoclave	
	Samples	Rate	Samples	Rate	Samples	Rate	Samples	Rate	Samples	Rate
304	46	0.03	11	0.03	12	0.04	52	0.05	19	0.02
304L	24	0.04					31	0.06		
347		0.04	9	0.038	10	0.02	63	0.07	32	0.06
316	43	0.03	3	0.03			49	0.12		
17-4 PH	11	0.12	4	0.02			32	0.22	23	0.12
17-7 PH	15	0.08					15	0.30	14	0.15
440C							8	0.29		
410	7	0.14	2	0.23			11	0.26		
Monel	12	0.46					14	1.46		
K-Monel	26	0.16					22	0.20		
Inconel	29	0.06	3	1.20	5	0.052	45	0.12		
Inconel-X	7	0.07					15	0.37		
Hastelloy C										
A-nickel	8	0.13					8	0.15		
Vascoloy - Ramet-166									2	0.11
Stellite-3	6	0.20					6	26.84		
Stellite-6			2	0.07			5	0.19	20	0.10
Stellite-12									13	0.18
322 W	21	0.07					19	0.17		
Graphitar-14										

TABLE XIX: AVERAGE CORROSION RATES OF MATERIALS

($mg/cm^2/mo$)
Water at 400° F to 600° F

Material	As Welded		Quenched at 1900°		Machined		Vapor Blasted		Hardened		Annealed	
	Samples	Rate	Samples	Rate	Samples	Rate	Samples	Rate	Samples	Rate	Samples	Rate
304	20	0.03	10	0.02	12	0.06						
304L	3	0.05					10	0.17				
347	28	0.17	27	0.07	44	0.54	5	0.15				
316	14	0.05	12	0.04	4	0.01	20	0.21				
17-4 PH					4	0.07			29	0.14		
17-7 PH									19	0.09		
440C									16	0.42		
410									10	0.58	10	1.10
Monel												
K-monel									14	0.34	21	0.09
Inconel	6	0.15			1	0.07	6	0.19				
Inconel-X											4	0.21
Hastalloy C												
A-nickel												
Vascoloy - Ramet-166												
Stellite 3												
Stellite 6	9	0.12										
Stellite 12												
322 W	4	0.02							12	0.06		
Graphitar 14												

TABLE XX: AVERAGE CORROSION RATES OF MATERIALS

($mg/cm^2/mo$)
Water at 400° F to 600° F

Material	Polished		Chrome Plated		Malcomized		Tensile 10,000 psi		Ground		Sensitized	
	Samples	Rate	Samples	Rate	Samples	Rate	Samples	Rate	Samples	Rate	Samples	Rate
304	8	0.01			8	0.19					12	0.05
304L					10	0.47	1	0.01				
347												
316												
17-4 PH			6	0.04	6	0.16						
17-7 PH					9	0.16						
440C									16	0.53		
410			1	0.32					9	0.75		
Monel												
K-monel							2	0.12	1	0.01		
Inconel												
Inconel-X												
Hastalloy C			2	0.18								
A-nickel			1	0.07								
Vascoloy - Ramet-166												
Stellite 3												
Stellite 6	9	0.12										
Stellite 12												
322 W					7	4.10	2	0.11				
Graphitar 14	6	6.75										

TABLE XXI: GRAND AVERAGE CORROSION RATES FOR CONDITIONS OF TABLES XVII THROUGH XX

In Water 400° to 600° F

Material	Number of Samples Averaged	Corrosion Rate ($mg/cm^2/mo$)
304	116	0.04
304L	66	0.05
347	122	0.05
316	101	0.07
17-4 PH	84	0.14
17-7 PH	52	0.17
440 C	46	0.45
410	37	0.60
Monel	31	0.77
K-Monel	41	0.25
Inconel	80	0.20
Hastelloy C	7	0.14
Inconel-X	28	0.22
A-Nickel	27	0.18
Vascoloy-Ramet 166	7	1.04
Stellite-3	12	0.08(no O_2)
Stellite-6	24	0.17(no O_2)
Stellite-12	13	0.18
322 W	40	0.46
Graphitar 14	8	4.40

13.3.4 Effects of Dissolved Gases on Corrosion

The presence of dissolved gases in water has long been known to affect the corrosive effects of the water. Oxygen, nitrogen, carbon dioxide and hydrogen are normally dissolved in waters obtained from natural sources. Oxygen and nitrogen are mostly dissolved from the atmosphere. Some of the carbon dioxide is absorbed from the atmosphere and the remainder is obtained from the decomposition of plant and animal life in the water. Hydrogen is probably produced from decaying vegetation and is normally present in the water in a non-ionic state to a very small extent. Both the hydrogen and the oxygen in a reactor may be augmented by the dissociation of the water caused by irradiation.

Much of the corrosion testing has concerned the precise evaluation of the effects of varying quantities of these gases upon corrosion. Of these, the studies of the effect of both hydrogen and oxygen in water have been most significant. Since most of the products of corrosion are oxides, oxygen is suspected to be the principle corrosive agent. Conversely, since hydrogen is an effective depolarizing agent, its presence ought to inhibit corrosion. From an analysis of data from many corrosion tests, it was noted that some such general effect is indeed apparent.

A summary of these tabulations is given in Tables XVII-XXI; a specific analysis of gas conditions appears in Table XVII. The values are gross averages in which a large number of samples are employed to average out any peculiar results which may be caused by the different techniques of the various investigators. A qualitative evaluation of the effect of hydrogen and oxygen on the corrosion of sundry materials was also made by

Argonne and is shown in Table XXXVIII. In general, the results show that the austenitic stainless steels resist corrosion almost equally well in either medium. The other materials almost universally show good corrosion resistance in hydrogenated water. The corrosion rates of the materials other than the austenitic stainless steels show a variation depending upon the particular investigation. Most of the results show a fair corrosion rate for these materials in oxygenated water. However, tests at ORNL produced extremely high corrosion rates for the stellites and for chrome plate, and tests at the Naval Engineering Experimental Station produced high corrosion rates for the high nickel alloys in oxygenated water.

Crevice Corrosion. The corrosion of materials which occurs in close-fitting places is most potentially serious in systems which contain precision moving parts since the presence of the corrosion products will tend to bind and score the close-fitting surfaces of the mechanism. Such binding will take place particularly in machinery which is left idle for periods of time, such as in the control-rod drives. Investigations conducted by Battelle indicate that the presence of oxygen in water promotes the formation of corrosion products at crevices of immersed materials.

In tests run by Battelle, SS 347 was combined with SS 410 and immersed in 600° F degassed water. The crevices between the two materials were 0.0005, 0.001 and 0.005 in. After six months no seizing between the two materials was evident. The experiment was repeated under the same conditions except that 60 cc of oxygen per liter of water was added. Again no seizing occurred after the same period of time although more rust was apparent.

However, in experiments run at 600° F and 300 cc oxygen per liter of water, couples of the following materials with 0.0005" clearance, showed these effects after eight weeks:

SS 410	vs	SS 410	Severe seizure
SS 347	vs	SS 347	Slight seizure
SS 430	vs	SS 430	Severe seizure
Armco 17-4	vs	Armco 17-4	No seizure

The same materials at 600° F, with 385 cc H_2 per liter, and with the same clearance, showed the following after 12 weeks submersion:

SS 410	vs	SS 410	No seizure
SS 347	vs	SS 347	No seizure
SS 430	vs	SS 430	No seizure
Armco 17-4	vs	Armco 17-4	No seizure

Argonne reported crevice corrosion in tests run in water at 500° F containing 30 cc oxygen per liter of water, as follows:

Couple	Crevice Width	Comments
SS 410 vs Stellite 3	0.0027	Partial freezing
Armco 17-4 vs Stellite 3	0.0024	Frozen
SS 410 vs Stellite 3	0.0021 to 0.0084	No freezing
Armco 17-4 vs Stellite 3	0.0028	Frozen

It is apparent that the presence of oxygen promotes the build-up of crevice corrosion products particularly in some of the less corrosion-resistant materials which may be used. The presence of hydrogen seems to alleviate this condition for long periods of time. Tests at Babcock and Wilcox on hydrogenated water samples showed no metal embrittlement attributable to the hydrogen.

The effects of other inhibitors and the effect of crevice width on crevice corrosion is discussed later in the report. The presence of oxygen in the water also adversely effects the wear rates of bearing surfaces as shown on Table XI. X-ray examinations of the oxide films at the crevices seem to indicate that the normal film is composed of Fe_3O_4 and alpha Fe_2O_3.

The results of the tests in degassed water are erratic and in many instances they show a higher corrosion rate than similar samples in oxygenated water. The questionable nature of the results may be attributed to the fact that it is hard to keep a system degassed, particularly in a radioactive zone (see Section 13.3.8). Some investigators have found that the presence of 0.2 cc O_2/liter of water has a more corrosive effect than larger concentrations of oxygen and any attempt at degassification may well lead to this lower oxygen concentration.

The effect of carbon dioxide in the water is to make it acidic and to promote pitting corrosion (see Section 13.3.11). Also, the CO_2 is collected by the deionizer and tends to deplete this unit.

Nitrogen dissolved in the water is converted to nitrates or nitric acid and promotes corrosion. This occurs to a small extent.

13.3.5 Effects of Welding and Heat Treatment on Corrosion

The effect of the application of heat to engineering materials by annealing, tempering, hardening, and welding, and the subsequent potential changes in crystal structure, are of primary concern. The effect of welding on the grain structure is of particular concern since the metal is subjected to temperatures up to the melting point. The unstabilized austenitic stainless steels, when heated in the range between 900° F and 1600° F, tend to precipitate chromium carbide at the grain boundaries. It is postulated that the depletion of chromium from the alloy makes the metal immediately adjacent to a crevice susceptible to corrosion. Heating the welded structure to about 1900° F, followed by quenching, tends to redissolve the chromium and prevent its precipitation. However, in the assembly of large welded pipe sections in the field, post-weld heat treatment is not feasible. As a consequence, in most installations, the stabilized stainless steels such as Type 347 and Type 321 are employed in the pipe lines and pressure vessels, since the presence of columbium and titanium in these alloys prevents the precipitation of chromium carbide. Since a low-cost reactor is sought, the use of the least expensive and most commonly available austenitic stainless steel, namely 304 ss, would be preferred. No proof was found in the literature that any precipitation of chromium carbide, if it takes place, has affected the corrosion rate of the 304 stainless steels in the reactor temperature range. Likewise, no correlation was found between any of the heat treatments and the corrosion rates. Tests at Babcock and Wilcox, see Table XXII, indicate that no effect is evident from either welding or sensitizing the materials.

TABLE XXII: WELDED AND SENSITIZED STAINLESS STEELS CORROSION RATES ($mg/cm^2/mo$)

Conditions - 1350 hours, Water at 500° F

Material	pH-10 1.7 cc O_2/L 30 fps	pH-10 1.7 cc O_2/L 1 fpm	pH-7, 2.1 cc O_2/L 30 fps	pH-7, 2.1 cc O_2/L 1 fpm
304 ss	-0.05	0.01	-0.06	0.01
304 ss welded	-0.04	0.02	--	0.04
304 ss sensitized at 1250° F	-0.04	0.01	-0.06	0.04
316 ss	-0.07	0.01	-0.04	0.01
316 ss welded	-0.06	0.00	-0.05	0.02
316 ss sensitized at 1250° F	-0.05	0.00	-0.04	0.02

Other tests at Argonne show that the effect of quenching to dissolve any precipitated carbides does not give any better corrosion results than the samples left as welded.

TABLE XXIII: WELDED AND QUENCHED STAINLESS STEEL CORROSION RATES In Water

Material	Temp.	Time-hrs.	Condition	Corrosion Rate ($mg/cm^2/mo$)	Rating
304 welded to 304, as welded	600	2930	240 cc O_2/L	0.010	Good
304 welded to 304 quenched at 1900° F	600	2930	240 cc O_2/L	0.021	Good
304 welded to 304, as welded	600	2301	70 cc H_2/L	0.010	Good
304 welded to 304 quenched at 1900° F	600	2301	70 cc H_2/L	-0.021	Good
304L welded to 304	600	257	30 cc O_2/L	0.016	Good

Other weldments of 316 ss to 316 ss, tested under the same conditions, showed similar results. The stabilized stainless steels welded together, such as 347 ss and 321 ss, also showed good results. Cross-welding of two dissimilar stainless steels also showed no unusual corrosion effects.

The Babcock and Wilcox Company and Westinghouse have further supplied Argonne with samples of 304 ss varying in carbon content from 0.08 to 0.27% for dynamic corrosion testing in oxygenated water (5-6 cc O_2/L) at 315° C for the purpose of studying the extent of intergranular corrosion on samples that have been sensitized at 650° C for 2 hours and others at 24 hours. The first test period of 1480 hours was completed with the following results:

a. All samples exhibited an adherent dull bluish tarnish with a yellow-brown discoloration at the edges.

b. The corrosion rates, calculated from the weight changes, were very low, about ±0.04 mg/cm^2/mo, and seem to have no correlation with the carbon content or the heat treatment.

In his book Metals at High Temperatures, F. H. Clark points out that intergranular corrosion of stainless steels in water does not start until the water reaches 800° F. The nature of this corrosion at higher temperatures has been investigated by Battelle.

Some of the results of this investigation follow:

TABLE XXIV: CORROSION OF MATERIALS IN SUPERCRITICAL WATER
Degassed

Material	800° F		1000° F		1350° F	
	Days	(mg/cm^2/mo)	Days	(mg/cm^2/mo)	Days	(mg/cm^2/mo)
17-7 PH	82	0.01	148	0.00	132	0.10
17-4 PH	82	0.03	---	----	132	0.20
302	82	0.03	148	0.19	132	1.00
309	82	0.02	148	0.03	132	0.20
310	82	0.03	148	0.01	132	0.20
347	82	0.00	148	0.02	132	0.20 pits
410	82	0.03	148	0.02	132	0.40
Inconel-X	82	0.00	109	0.25	104	0.95
Hastelloy F	82	0.00	58	0.07	132	0.13

From these figures, it would appear that the Armco 17-4 and Armco 17-7 as well as Hastalloy F 309 and 347 offer the best in materials in operations at temperatures above 1000° F.

13.3.6 Effects of Fluid Flow on Corrosion

A definite relationship between the rates of fluid flow in a water loop and the corrosion rate of the materials composing the loop could not be discerned in the study of the various corrosion testing loops. From the compilations, Tables XVII-XIX, it may be predicted, in a very general way, however, that the higher the fluid velocity the greater will be the corrosion rate. This general pattern can be illustrated by the following typical set of experiments run at Babcock and Wilcox.

TABLE XXV: EFFECT OF FLUID FLOW ON CORROSION

	Corrosion Rate (mg/cm^2-mo)			
	pH-10		pH-7	
	30 fps	1 fpm	30 fps	1 fpm
304	-0.05	+0.01	-0.06	+0.01
304 welded	-0.04	+0.02	--	+0.04
304 sensitized at 1250°F	-0.04	+0.01	-0.06	+0.04
Monel	-0.15	-0.01	-0.46	-0.14
440C	-0.17	--	-0.09	--
K-Monel annealed	-0.04	0.00	-0.45	+0.01
K-Monel hardened	-0.18	0.00	-0.44	-0.05
Inconel	-0.02	0.02	-0.22	+0.01
316	-0.07	0.01	-0.04	+0.01

Analysis of the effect of flow upon corrosion of 304 ss with oxygen dissolved in the water and with hydrogen dissolved in the water from the tabulation of about 120 samples is shown in graphical form in Fig. 53.

The analysis of the remainder of the materials appears in Tables XVII AND XX. The effect of higher fluid velocities is also apparent in the Argonne evaluation shown in Table XLIII. The typical corrosion rate-fluid velocity table above (Table XXV) and all other compilations show that high fluid velocities do not appreciably affect the corrosion rates

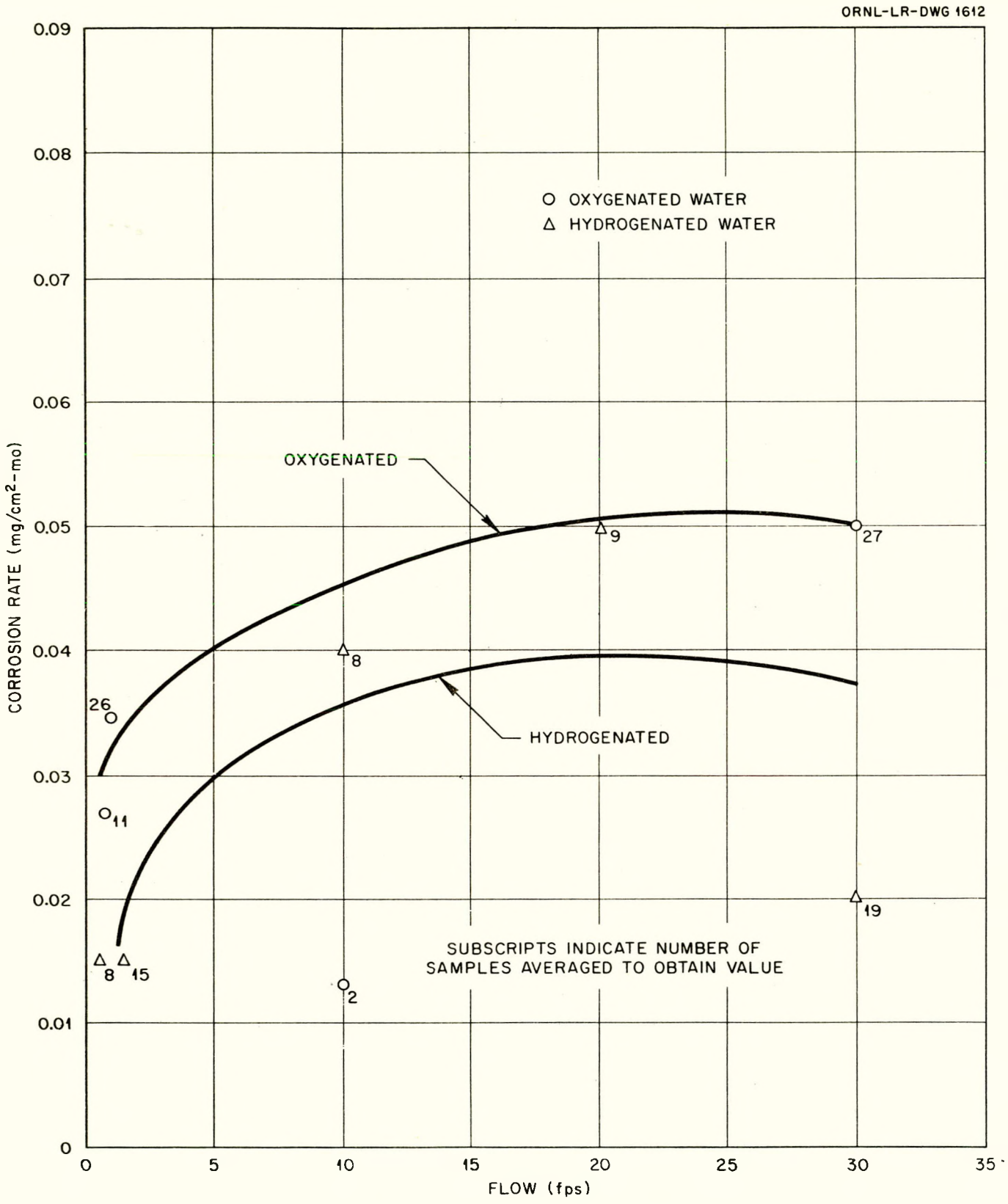

Fig. 53. Corrosion of Type 304 Stainless Steel vs. Fluid Flow.

of the austenitic stainless steels. The corrosion rates of the martensitic and the ferritic stainless steels and the cobalt and high nickel alloys do show a more marked relationship to fluid velocity changes.

Transfer Products. A secondary effect of fluid flow is the transport of corrosion products from one point in the system to another. This transfer not only bares the corroded surface for renewed attack but it also affects the remainder of the circuit as follows:

a. Particles may become radioactive and deposit in unshielded areas.

b. Particles may form scale on heat transfer surfaces and so lower the effective heat transfer coefficient.

c. Particles may restrict flow in confined places such as tubes and orifices.

d. Particles may injure wearing surfaces and precision equipment.

The transported material may be dispersed for redeposition in several ways; it may travel in solid particles or flocculates, or it may be carried in solution.

Tests by Battelle indicate that the solubility of many of the metals comprising the alloys and of the alloy corrosion products is not very high in water. These solubilities ranged in the neighborhood of 0.03 to 0.05 ppm for stainless steel; most of the corrosion products must necessarily be carried in the undissolved state. Moreover, the presence of loosely adhering corrosion products in nearly all test loops suggests the probability that this material is transported by suspension rather than by solution.

At the generally accepted corrosion rate of 0.05 mg/cm^2-mo the formation of the products of corrosion in the primary loop having a surface area of 4×10^6 cm^2 would be:

$$0.05 \text{ mg/cm}^2\text{-mo} \times 4 \times 10^6 \text{ cm} = 0.200 \times 10^6 \text{ mg/mo}$$
$$= 200 \text{ gm of corrosion products per month.}$$

If the solubility of the corrosion products is accepted as 0.05 ppm then the portion of the corrosion products in solution would be:

5150 liters in system = 5,150,000 cc or $\sim 5 \times 10^6$ gm H_2O

5 x 0.05 = 0.25 gm of corrosion products in solution in loop.

The largest portion of the corrosion products apparently is not in solution.

It is rather difficult to estimate what portion of the solid corrosion materials formed circulates and what portion remains on the surface where formed. A study of the corrosion rate charts indicate that a negative corrosion rate, or loss of material, occurs in the more rapidly flowing channels, and a positive corrosion rate, or material buildup, occurs in the more quiescent parts of the loop. If it is assumed that 50% of the corrosion products find their way to the stream, then the material introduced into the loop would be:

0.5 x 200 = 100 gm/mo

A study of the materials deposited on heat transfer surfaces and on fuel elements indicates that corrosion products preferentially coat out on surfaces of high energy exchange. The exact mechanism of such deposition--whether it be from solution or by electrical charge of the solid materials, or both--is in doubt, and is presently being investigated.

At Westinghouse, it was found that local boiling or high temperature can cause corrosion deposition, while adjacent cooler areas are free of such deposits. Cooler portions of the hot zone have a less adherent covering of black magnetic oxide, while a brown or red-brown adherent hematite deposit is found in the hotter zones.

It is obvious that the corrosion products must not be permitted to accumulate in the loop. The purification of the water is based on the ionic content of the water, see Section 13.3.9. In the proposed purification system, water is purged from the primary loop at a minimum rate of 18 gph and the loop is replenished with deionized water. This purge and make-up will reduce the amount of transport corrosion products in suspension to one-tenth the value previously given, or 10 gm, at any one time in the entire system. Furthermore, this quantity will not be cumulative. The purge system will also remove 2.5 gm/mo of corrosion products in solution.

The effect of the solid transport materials can further be alleviated by the consideration of the following particle flow characteristics:

a. At fluid flows of less than 10 fps, particles of 0.5 microns to 0.1 microns will deposit out.

b. Fine particles tend to migrate from rapidly flowing streams toward areas of low turbulence. Larger particles remain suspended only in rapidly flowing streams.

c. Irradiation seems to have a coagulative effect on positively charged metal oxide particles.

It is therefore possible, by proper flow design, by proper purge outlet location, and by the use of filters, to eliminate much of the remaining transport materials.

13.3.7 Effects of Irradiation of Materials on Their Corrosion Rates

The effect of irradiation of materials on their corrosion rates, as distinct from the effect of such irradiation on the physical properties, has been undertaken at some of the national laboratories. Most of the data were obtained at Hanford where an irradiated loop was early established. Some of the early results at Hanford show the following effects of irradiation on corrosion.

TABLE XXVI: CORROSION IN ARGONNE LOOP AT HANFORD
Water at 540°F

Material	Conditions	Irradiation (nvt)	Corrosion Rates (mg/cm^2-mo)
347	25 cc H_2/L	F-1.1 x 10^{19} S-5.5 x 10^{19}	0.078
347	25 cc H_2/L	F-1.8 x 10^{19} S - 9 x 10^{19}	0.105
17-4 PH		S-3.3 x 10^{19}	-0.012
Stellite-3		S-3.33 x 10^{19}	0.006

Later tests at Hanford employed samples which were irradiated, and control specimens under the same conditions which were not to obtain the following comparisons.

TABLE XXVII: ARGONNE WATER LOOP AT HANFORD
540°F; 1 x 10^{19} nvt fast; 1 x 10^{20} nvt slow

Material	In Flux (mg/cm^2-mo)	Control (mg/cm^2-mo)
347 no treatment	0.41	-0.10
347 inhibited with Pyrex	0.34	0.05
347 machined	0.30	0.09
17-4 PH	0.19	0.07
Stellite	0.03	0.33
17-4 coupled with Stellite-3	0.19	0.09
17-4 coupled with Stellite-3	-0.13	0.14
Monel	0.21	-0.86
Haynes Alloy 25	0.22	0.08
Stellite-6 with USS/W	0.01	0.16
Stellite-6 with USS/W	0.06	0.03

The results are erratic, although the tendency for the irradiated samples to corrode at a higher rate is quite apparent. An examination of the materials seems to indicate that a fair portion of the weight increases may be attributed to transport corrosion products described earlier in the report.

Other materials run at an ORNL irradiation loop for two weeks at 500°F, and nine months at 150° to 200°C in an integrated flux of 1.5×10^{20} nvt gave more satisfactory results, as listed below:

Material	Corrosion Rate (mg/cm^2-mo) Irradiated	Non-Irradiated
347	-0.014	-0.009
347	-0.017	-0.005
A-Nickel	-0.10	-0.20
A-Nickel	-0.20	-0.14

The evidence thus far indicates that irradiation does increase the susceptibility of materials to corrosion, although this effect does not appear to be very large.

13.3.8 Effects of Irradiation of Water on Gases in Solution

Water under irradiation decomposes in part into its elemental components, oxygen and hydrogen. In tests run in an autoclave at Chalk River, with a volume of 1/8 liter at 500° F at 200 psi above saturation pressure, in a neutron flux of $1.2 \times 10^{12}/cm^2/sec$ (fast) and $5 \times 10^{12}/cm^2/sec$ (thermal), an analysis of previously degassed water showed the following

Hours	H_2 cc/L	O_2 cc/L	CO_2 cc/L	Inert	Total
20.5	4.8	0.72	0.4	2.7	8.6

thus, indicating a formation of new gases. The large excess of hydrogen beyond its stoichiometric ratio with oxygen suggests that the oxygen is removed, for instance, by combining with the metals to form oxides, combining with carbonacious materials to form carbon dioxide, and combining with nitrogen to form nitrates or nitric acid.

The corrosion products in stainless steel loops have been found to contain iron as the major component. The chemical compounding or iron with oxygen is suggested to occur according to the following formulas:

1. $H_2O + 3\ Fe \longrightarrow Fe_3O_4 + 4\ H_2$

2. $O_2 + 3\ Fe \longrightarrow Fe_3O_4$

Experiments conducted by Argonne at Chalk River on in-pile and out-of-pile and pile-down experiments shows evidence that both these reactions occur. One effect of irradiation is then to supply oxygen for corrosion along the lines of Eq. 2. The decomposition of the water under steady-state conditions

and at 500° F was roughly estimated to vary as the square root of the radiation intensity. This is borne out in part by tests at Argonne with different flux densities; a greater oxygen deficiency was found under a higher intergrated neutron flux.

Irradiation of water, in addition to causing its decomposition, also affects the recombination of the oxygen and the hydrogen which is dissolved in the water. The net amount of oxygen and hydrogen released in the water reaches an equilibrium. The equilibrium quantity is a function of temperature, pressure, presence of a vapor phase, presence of impurities, etc. The tests at Chalk River further established that the presence of excess amounts of either oxygen or hydrogen suppresses the generation of the other.

In a Hanford loop at 540° F, no oxygen was discerned after steady-state conditions were reached. Oxygen was originally present but its concentration gradually decreased to an immeasurable quantity. The hydrogen concentration reached about 2 cc per liter at steady-state conditions in this loop and has gone as high as 35 cc per liter. At Oak Ridge, the hydrogen concentration has reached 10 cc per liter under steady-state conditions.

The CO_2 concentration at steady-state conditions and 540° F at Hanford reached about 6 cc per liter without demineralizer, but went higher if oxygen was introduced into the system. The quantity of nitric acid formed by irradiation of water was estimated at 0.06 to 0.09 ppm.

The effect of the irradiation of water in the package reactor may be summed up as follows:

a. Irradiation of water causes dissociation of the water and its recombination. The rate of these reactions is a function of the neutron density.

b. An excess of hydrogen in the reactor will inhibit the formation of oxygen. The net quantity of oxygen remaining in a hydrogenated system will be low but finite and will be combined with the materials in the system to form oxides.

c. There will be a partial pressure of each of the gases formed in the vapor space of the pressurizer.

13.3.9 Effects of Purity of Water on Corrosion

The tabulation of the corrosion rates does not correlate the effect of water purity upon corrosion because an insufficient number of samples included data on water purity. It has been fairly well established, however, that low amounts of total dissolved solids must be maintained in the water to keep the corrosion rates low. The effects of undissolved corrosion particles upon the heating surfaces is discussed in other sections of this appendix. It has also been established that the corrosion products themselves are not very soluble, but that the effect of certain other ions in the water is to supply an electrolyte which can increase corrosion effects.

The effect of an ion exchanger upon corrosion is illustrated in the following results reported by Argonne:

TABLE XXVIII: EFFECT OF ION EXCHANGER ON CORROSION
Water at 500° F, 2 cc O_2/L, 500 hours

Material	Without Ion Exchanger (mg/cm^2-mo)	With Ion Exchanger (mg/cm^2-mo)
304	0.17	0.04
316	0.16	0.04
410	0.16	0.34
440C	0.24	0.21

Experiments at Westinghouse also resulted in improved corrosion rates for materials run in loops with an ion exchanger, as follows:

TABLE XXIX: EFFECT OF ION EXCHANGER ON CORROSION
Water at 500° F, 0-1 cc O_2/L, 1700 hours

Sample Number	Circuit with Ion Exchanger ($mg/cm^2/mo$)	Circuit without Ion Exchanger ($mg/cm^2/mo$)
1	-0.05	-0.09
4	-0.06	-0.09
7	-0.05	-0.09
8	-0.05	-0.09
10	-0.06	-0.10

The effect of lessened corrosion is further evidenced in improved heat transfer in loops at Babcock and Wilcox. In one circuit, an ion exchanger was turned off during the 38th day of operation and the overall heat transfer was 3,300 Btu/hr-ft^2-°F. By the 39th day the coefficient was reduced to 2,850 Btu/hr-ft^2-°F and by the 45th day it was further reduced to 1,600 Btu/hr-ft^2-°F or a total decrease slightly over 50% in the overall heat transfer coefficient.

Conversely, a second loop was operated initially without an ion exchanger; an exchanger was then placed in the circuit and the overall heat transfer coefficient began to increase. During the subsequent 10 days operation the coefficient increased from 2400 to 2900 Btu/hr-ft^2-°F and then stabilized. The increase in this latter loop indicates that not only has the corrosion rate been lessened but that some of the corrosion products already on the heat transfer surface were either dissolved by the pure water or were transported in a solid condition to the ion exchanger where they were filtered out of the circuit.

A similar improvement was observed in the reactor at Chalk River (NRX) after the installation of an ion exchanger. Without an ion exchanger it was determined that the resistivity of the water was 0.02 megohm-cm and the rate of decomposition of D_2O was 80 cc D_2 and 40 cc O_2/min. After the installation of an ion exchanger, consisting of two sets of filters and a one-liter mixed-resin bed, the resistivity of the liquid increased to 2 megohm-cm and the decomposition rate was reduced to 0.4 cc D_2/min and 0.022 cc O_2/min.

The size of the resin bed in the Chalk River installation was based on the corrosion of 0.702 mg/cm^2/mo of aluminum which came to about 9 gm aluminum per month. The liter of mixed resin was based on 2/3 gm equivalent of both cations and anions; a 60 mesh screen was used to contain it.

The operation of the ion exchangers in an irradiated loop resulted in the resin carrying practically all of the radioactivity. After elution with acid the gamma activity was reduced from 300 to 5 mr/hr at one inch. The average activity of the resin beds before elution after 3 to 6 weeks use was 500 mr/hr at one inch. The pickup of metal ions that contribute heavily to long-lived activity, such as Co, Cr, Mo, and Mn, was relatively low. The anion resins were in most cases exhausted by CO_2. In general, the resins were not harmed by the radioactivity.

It was found erroneous to base the ion exchange size upon the corrosion rate since only about 5% of the calculated aluminum corrosion appeared in the ion exchanger.

The use of ion exchangers has also been found useful in reducing the long-lived gamma activity due to Cobalt-60, and activities other than N^{16} and O^{19}, in pumping and heat exchanger areas by as much as sixfold.

13.3.10 Effects of Stress on Corrosion

It might be expected that stress on a metal would decrease its corrosion resistance, particularly in the instance of welded austenitic stainless steels and other materials subject to carbide precipitation at the grain boundaries. This has not been the case for the austenitic stainless steels stressed to 10,000 psi and submerged in 600° F water containing some oxygen in solution. Furthermore, dissimilar stainless steel materials welded together, such as 304 welded to 347, showed no excessive corrosion rate after 1217 hours under the same conditions. Likewise, SS 321 tested in 600° F water and stressed at 10,000 psi for 3149 hours showed a corrosion rate of 0.084 mg/cm^2-mo. In still another instance, 304 welded to 347 and tested in a dynamic loop at 30 fps, and 10,000 psi stress for 895 hours, resulted in a corrosion rate of only 0.0028 mg/cm^2-mo. The Stellites, K-monel and others, likewise did not seem to fare any worse when stressed, than in the unstressed condition.

Later tests at Argonne showed the following effects of stress-corrosion testing, in a dynamic loop at 25 to 30 fps, 500° F deionized water, containing 1.2 cc O_2/L and stressed at 10,000 psi.

TABLE XXX: CORROSION RATES AND TENSILE PROPERTIES OF STRESSED MATERIALS

Material	Corrosion Rate (mg/cm^2-mo.)	Physical Properties Ultimate,(psi)	% Elong.(% in 2")
304L, #1	-0.011	85,500	78.8
304L, #2	+0.005	86,300	68.2
304L welded to 304L #1	+0.006	83,250	43.6
304L welded to 304L #2	+0.005	82,000	44.7
Type 310 #1	+0.004	102,800	36.9
Type 310 #2	-0.039	105,500	42.3

The corrosion rates are low and are comparable to the corrosion rates of unstressed corrosion specimens. The physical properties of the materials themselves likewise do not differ from the normal physical properties expected of these materials.

If 10,000 psi is considered a safe working stress for materials specified for the package reactor, no difficulties should arise due to excessive corrosion on this account. Some indication that much higher stresses can be used without any detrimental corrosion was obtained by tests at Battelle in which SS 347 was stressed to 30,000 and 50,000 psi for 16 days and exposed to degassed, superheated water at 1000° F; no cracks were evident, although some permanent set did occur where the yield stress was exceeded.

A working stress of 10,000 psi is a rather low figure to use on some of the alloys whose yield strength is well above 50,000 psi. Although definite evidence is lacking that a higher working stress value than 10,000 psi may be used, it it felt that a normal conservative factor of safety could be applied in the instances of very high strength materials. The stressing of a material may be likened to the sensitizing of a material discussed earlier in the report, wherein the grain boundaries became susceptable to corrosion attack. The fact that the water temperature is just not high enough to cause this corrosion should also apply to grain boundary conditions caused by stressing.

13.3.11 Effects of pH on Corrosion

In Section 13.3.9 it was indicated that the purity of the water is measured either by its specific resistivity or by the ppm of dissolved solids. A third measure of water purity is its hydrogen-ion concentration, or its pH. The latter gage of water purity is however a very rough yardstick and, consequently, for very pure water the specific resistivity is determined in preference to the pH.

It is only when large variations from the neutral pH of 7 occur that it becomes worthwhile to employ pH measurements. This is particularly true if it is necessary to determine whether a solution is acid (low pH) or alkaline (high pH). The determination of the pH of a solution will then help to establish whether excess CO_2 is present, or whether a proper amount of buffers or alkaline inhibitors have been added to the water. In these instances either the amount of total dissolved solids, or the resistivity of the solution alone, would not give a true picture of the condition of the water.

The effect of dissolved CO_2 in the water on its pH is shown in the following table:

TABLE XXXI: EFFECT OF DISSOLVED CO_2 ON pH OF SOLUTION

CO_2 ppm	pH	Resistivity ohms-cm
0.8	6.0	9×10^6
20.0	5.0	2×10^6
400.0	4.2	4.2×10^5

It has also been determined that the presence of either sodium hydroxide or lithium hydroxide in the water can raise the pH to between 9 and 12. This increase in pH will tend to reduce local pitting of the material at some sacrifice to the overall passivity. The effect of such additions is apparent in the corrosion compilation summaries and is further discussed in Section 13.3.12.

It has long been established that highly acidic water is very corrosive. Thus, in the areas of water quality determination, where its value has some meaning, the pH of a solution has been shown to have a definite qualitative correlation to the corrosion potential of the solution. In the near-neutral solutions, the approximate nature of the pH value and the small number of samples in which an accurate check of the pH was maintained made it impossible to arrive at any relationship between corrosion rates and pH values.

13.3.12 Effects of Inhibitors on Corrosion

Corrosion inhibitors are presently being successfully used in several water cooled and moderated reactors. The Hanford pile employs water in which sodium dichromate and sodium silicate are added. The swimming pool reactor at ORNL uses sodium dichromate. These additives are used to prevent corrosion to materials, such as aluminum and carbon steel, which are normally much more readily corroded than those being investigated. The corrosion tabulation includes listings of corrosion tests in which inhibitors were added; in some instances a definite inhibition trend can be detected. The most promising inhibitor is hydrogen; its effect upon corrosion rates has been discussed in Section 13.3.4. Other additives which will be discussed in this section and which have shown inhibitor tendencies are sodium hydroxide, lithium hydroxide and hydrozine hydrate.

The effects of small quantities of sodium hydroxide on the corrosion rate of various materials are illustrated in tests run at Babcock and Wilcox. In these tests, NaOH was added to the water to obtain a pH of 10.

TABLE XXXII: EFFECT OF NaOH ADDITION ON CORROSION ($mg/cm^2/mo$)

	30 fps		1 fpm	
Material	pH-10 1.7 cc O_2/L	pH-7 2.1 cc O_2/L	pH-10 1.7 cc O_2/L	pH-7 2.1 cc O_2/L
Monel	-0.15	-0.46	-0.01	-0.14
SS 304	-0.05	-0.06	0.01	0.01
440 C	-0.17	-0.09	--	--
K-monel, annealed	-0.04	-0.45	0.000	0.01
K-monel, hardened	-0.18	-0.44	0.00	-0.05
Inconel	-0.02	-0.22	0.02	0.01
316	-0.07	-0.04	0.01	0.01

The addition of lithium hydroxide to the water has effected similar corrosion inhibition. It had been shown previously that crevice corrosion caused equipment to bind, and that the addition of H_2 to the water loop minimized this crevice corrosion effect. In additional experiments, reported by Battelle, small quantities of LiOH (20 ppm) alleviated the crevice corrosion to some extent, as shown in the following table:

TABLE XXXIII: EFFECT OF LiOH ADDITION ON CREVICE CORROSION

Water at 600° F with 300 cc O_2/L

Couple	Clearance Mils	No LiOH Seizure		With LiOH (20 ppm) Seizure	
		2 Weeks	8 Weeks	2 Weeks	8 Weeks
410 vs 410	0.5	Severe	Severe	None	Severe
347 vs 347	0.5	None	None	None	None
430 vs 430	0.5	Slight	Severe	None	Severe
17-4 vs 17-4	0.5	None	None	None	None

Although mitigation of seizure has been accomplished in some instances, the alleviation is not quite as complete as when hydrogen is used. Hydrogen additions prevented seizures in all the combinations listed above. The above experiments were run with excess oxygen, however, and the use of LiOH in the water together with degassification may improve the hydroxide's inhibitor qualities. Lithium hydroxide may be added to the water by means of a LiOH regenerated ion exchanger. A summary of such a run shows low corrosion rates for the materials.

TABLE XXXIV: EFFECT OF LiOH ON CORROSION USING REGENERATED ION EXCHANGER

Temperature 500°F, pH 10-10.5

Material	Corrosion Rate (mg/cm^2-mo) 10 fps	20 fps
347 machined	+0.0 to -0.01	--
347 machined	--	-0.005 to 0.00
347 electropolished	--	-0.01
304 machined	0.005	0.005
17-4 PH machined	-0.01	-0.02
Inconel machined	--	0.04
Inconel-X machined	0.06	--
410 machined	-0.08	-0.09

The use of hydrazine hydrate has been suggested as an inhibitor and is being tested at Brookhaven. In use, hydrazine decomposes and introduces hydrogen gas into the solution.

Still other inhibitors are being investigated. These include sodium diphosphate, sodium arsenate, morpholine, and pertechnetate. Sufficient progress is being made on the use of these materials on normal carbon steel so that it may be expected that some reactor in the near future will employ a proper inhibitor to permit the use of regular carbon steel as the major structural material.

13.3.13 Effects of Galvanic Couples and Crevices on Corrosion

Any discussion of galvanic couples touches upon what is considered the basic mechanism of corrosion; many of the previously mentioned corrosion factors can probably be shown to either inhibit or promote the formation of galvanic couples. The inhibitors probably tend to form an irreversible electrode effect, promote anodic or cathodic polarization, alter the current distribution, or increase the resistance in the liquid or metallic circuits.

Crevices, of course, are locations where the galvanic couple gap has been shortened to a point where transmission of ions is relatively easily accomplished. Methods of mitigating crevice corrosion by the use of hydrogen and by the use of hydroxides have been discussed in previous sections of this report.

The effect of the crevice width itself was checked in tests at Argonne. In these tests, Stellite-3 cylinders containing inserts of mating materials with varying crevice gaps were submerged in water containing 30 cc O_2/L. Some correlation between temperature and gap is readily discernible in the results of these tests as tabulated below:

TABLE XXXV: COUPLE-CREVICE CORROSION TESTS IN WATER

Couple	Temp. °F	Crevice Width (ins)	Comments
Stellite 3 and 17-4 PH	200	0.008 one end and 0.0024 other end	No freezing
Stellite 3 and 17-4 PH	200	0.0027	No freezing
Stellite 3 with 17-4 PH	200	0.0022	No freezing
Stellite 3 with 410	200	0.0029	No freezing
Stellite 3 with 410	500	0.0027	Partial freezing
Stellite 3 with 17-4 PH	500	0.0024	Couple froze
Stellite 3 with 410	500	0.0021 one end and 0.0084 other end	No freezing
Stellite 3 with 17-4 PH	500	0.0028	Couple froze

The journal-sleeve type of seizure was tested at Battelle to determine the clearance under which no seizure would occur.

TABLE XXXVI: JOURNAL-SLEEVE CREVICE TESTS

Test Conditions	Exposure (weeks)	Sleeve Material	Journal Materials	Dia. (Mils)	Seizure (lb to free)	Max. Build-up (Mils)
500°F, H_2O w 30 cc O_2/L	2	17-4	Cr plate 17-4	1.2	50	0.5
Same as above	2	347	347	0.9	50	0.5
600°F, degassed	2	17-4	Cr plate 17-4	0.6	50	0.5
600°F, degassed with 20 ppm LiOH	2	17-4	Cr plate 17-4	2.8	none	0.5
Same as above	2	347	347	2.1	none	0.5
600°F, 60 cc O_2/L	2	17-4	Cr plate 17-4	2.1	none	0.5
600°F, 600 cc O_2/L	6	17-4	Cr plate 17-4	4.6	none	0.5

Other coupled materials, irradiated in water at Hanford at 540°F in an integrated flux of 1×10^{19} nvt (fast) and 1×10^{20} nvt (slow), showed no galvanic corrosion effect. They are:

17-4 PH	vs	Stellite-3
17-4 PH	vs	Haynes Alloy-25
17-4	vs	USS/W
Stellite-6	vs	USS/W
Haynes Alloy-25	vs	USS/W
Haynes Alloy-25	vs	Stellite-3

The position of materials in the electromotive series is of limited assistance in the selection of non-corrosive materials in a reactor loop. Most of the materials employed are alloys of various elements whose position in the electromotive series may vary with the particular portion of the loop in which they may find themselves.

ANL has experimented with externally applied potentials aimed at the prevention of the deposition of the colloidal transport corrosion products onto the fuel plates. The methods being checked, which have met with partial success, employs (a) a charge on the fuel plates the same as that of the transport products so that these materials will be repelled and (b) an opposite charge on dummy plates so that the colloidal particles will coat out on them and so be removed from the loop.

13.3.14 Effects of Surface Finish on Corrosion

The surface finish of a material can be divided into two catagories:

a. The smoothness, which may be measured in micro-inches, is normally a function of the fabricating process. Thus, materials may be ground, machined (turned on lathe, milled, shaped), electropolished, buffed, vapor blasted, as cast, as rolled, etc.

b. Where the surface is coated or impregnated the smoothness is normally not measured. This category includes electroplated surfaces (such as chrome-plate) and impregnated surfaces (such as anodized, Malcomized, Scottsinized, Parkerized, and Chromalloyed surfaces).

Smoothness of Surface. It has been generally proven that the finer the finish of the surface, the less it is subject to continued corrosion. Tests at Westinghouse, SS 347 subjected to a 985-hour exposure in 500° F water containing 82-136 cc H_2/L, a water resistivity of 3,000,000 ohm-cm and flowing at 20 fps, showed the following corrosion rates:

Material	Average Corrosion Rate (mg/cm^2-mo)
Machined (12 pieces)	0.05
Electropolished (3 pieces)	0.03

Other tests at Westinghouse under similar conditions, for 500 hours, gave the following results:

TABLE XXXVII: EFFECT OF SURFACE FINISH ON CORROSION
Water at 500° F

Material	Time (Hours)	Conditions	Corrosion Rate ($mg/cm^2/mo.$) Machined	Vapor Blasted
347 TaCb	500	500 cc H_2/L	+0.01	-0.13
347 TaCb	1000		0.00	-0.03
347 TaCb welded	500	0.2 cc O_2/L	-0.41	-0.78
347 TaCb welded	500	Degassed	-0.09	-0.33
347 TaCb welded	1000	0.2 cc O_2/L	-0.05	-0.46
347 TaCb welded	1000	2.0 cc O_2/L	0.00	+0.01
347 TaCb welded	1000	Degassed	-0.04	-0.17
347 TaCb welded	1500	Degassed	-0.04	-0.13
316	500	500 cc H_2/L	0.00	-0.02
316	500	Degassed	-0.04	-0.35
304L	500	0.2 cc O_2/L	+0.01	-0.75
304L	500	2.0 cc O_2/L	+0.04	+0.03
304L	500	500 cc H_2/L	-0.04	-0.08

Additional tests under the same conditions but at 1 fpm showed similar results.

Surfacing Effect on Corrosion. Most of the special treatment of surfaces has resulted in increased corrosion rates for the materials. This is particularly true of surfaces hardened by a form of carburization, such as Malcomizing or Scottsinizing. Another surface treatment called "Chromallizing" also decreased the materials corrosion resistance.

Some of the effect of various surface treatments, as determined at Argonne, are summarized in the table below:

TABLE XXXVIII: EFFECT OF SURFACE TREATMENT ON CORROSION

Material	Temp.	Time (hrs)	Test Conditions	Corrosion Rate (mg/cm^2-mo.)
304 Chromalloyed	500	400	30 cc O_2/L	-2.4
304 Malcomized	500	1857	30 cc O_2/L	-0.24 to 0.064
304 Malcomized	500	1450	30 cc O_2/L	0.048 to-0.41
304 Malcomized ground & polished	500	337	Degassed	0.50
440C Malcomized ground & polished	500	4475	30 cc O_2/L	-2.2
17-4 PH Malcomized ground	500	3974	30 cc O_2/L	0.79 to 0.041
USS/W Malcomized polished	250	353	Degassed	0.27
302 ground & Scottsonized	500	325	Degassed	3.30
302 ground & Scottsonized	500	325	30 cc O_2/L	-0.29
347 polished & Scottsonized	500	1476	30 cc O_2/L	-0.017 to -0.200

Chrome-plated materials generally showed good corrosion resistance except in certain high-flow oxygenated systems.

13.3.15 Effects of Acid Cleaning and Passivation on Corrosion

It is desirable to be able to acid clean the primary loop materials for the following reasons:

a. Welds should be cleaned to remove scale and oxidized surfaces which form nuclei for crevice and pitting corrosion.

b. Strongly irradiated surfaces can be readily decontaminated with an acid bath.

c. Carbon steel particles left on the surface of stainless steels by tool bits, rolls, etc., can be removed by pickling.

d. The surface of many materials undergo passivation after exposure to acid.

In the chapter on welding and heat treatment the corrosion of non-stablized (no Cb or Ti) stainless steels in water were of concern. The investigation proved that undue corrosion did not occur in SS 304 at welds. The treatment of metals with acids may be likened to an accelerated corrosion test; no indication that acid cleaning will harm any of the 300 series stainless steels has been found.

The effect of acid cleaning on SS 347 was checked at Argonne. Three groups of welded SS 347 channel were boiled in water to remove soluble alkalis and slag and then left "as is" cleaned for 1 hour in 10% HNO_3 at 170° F, and cleaned for 1 hour in 15% HNO_3 and 2% HF solution at 170° F.

The samples were then tested in oxygenated water at 500° F for 1800 hours with the following results:

Sample a. Showed dark purplish-brown film with a narrow band of loose material at weld.

Sample b. Same as sample (a), but lighter colored film.

Sample c. Was light blue to silvery in color.

These tests indicate that some corrosion inhibition was obtained by the acid cleaning of the specimens.

Tests at Westinghouse on SS 347 in water at 500° F, 100 cc H_2/L of water, 500 hours, and 20 fps showed the following results:

TABLE XXXIX: EFFECT OF ACID CLEANING ON CORROSION

Material	Corrosion Rates (mg/cm^2-mo.) Degassed	Not-degassed
347, as machined	-0.03	-0.03
347, as machined	-0.02	-0.03
Passivated 30% HNO_3	0	-0.03
Pickled 20% HNO_3, HF 5%	+0.01	+0.01
Pickled 10% H_2SO_4	0	-0.01

A comparison of the effect of molten nitrates containing up to 10% excess nitric acid on various types of 300-series stainless steels was made by Mallinkrodt. An average of 25 exposures gave the following results:

TABLE XL: CORROSION OF STAINLESS STEEL IN NITRIC ACID (10%)

Penetration (in./mo x 10^{-3})

Form	Condition	Medium	304	304 HC	347	316	317R	309 cb
Sheet	Annealed	Vapor	0.38		0.34	1.07	0.93	0.21
Sheet	Welded	Vapor	0.69		2.40	5.53	6.71	0.23
Sheet	Welded	Liquor	0.99		1.16	3.03	4.27	0.64
Sheet	Unstressed	Liquor						0.16
Sheet	Stressed	Liquor						0.15
Cast		Vapor	0.31	0.69	0.44	0.57		0.30
Cast		Liquor	0.44	1.11	0.52	1.35		0.48

The attack of ss 316 and 317 is greater than the attack of ss 304, 347, or 309 because of the molybdenum in the steel. Stainless steel 309 showed the greatest resistance to corrosion and 304 the next best. The welded 347 sheet showed pitting all over, not just at the weld line.

Many of the corrosion specimens listed in the gross tabulation were pickled in either nitric acid or nitric acid and hydrofluoric acid prior to testing. This treatment does not seem to have increased the corrosion susceptability of the materials.

13.3.16 Fuel-Element Corrosion

The effect of corrosion of the fuel elements is of particular concern because of the possible radioactivity which would result in the water. A knowledge of the probable radioactivity in water would serve a two-fold purpose:

a. It would predict the effect of a sudden failure in the fuel cladding by rupture or by blistering, and would thereby enable the recognition of such an occurrence.

b. It would indicate the amount of break-through or pitting corrosion that could be tolerated on the fuel elements under normal operation without the need for a shutdown.

The amount of transfer of UO_2 and its radioactive fission products into the primary-loop stream can best be evaluated by using the corrosion rate of uranium dioxide. The solubility of the UO_2 would not suffice since undissolved particles would probably constitute a major portion of the material in the water. The corrosion rates of UO_2 as determined at Argonne are shown in Table XLI. From this table, it can be seen that UO_2 corrodes only moderately in degassed water. From previous experience it may be expected that the corrosion rate may be even lower in a hydrogenated system. The presence of oxygen in the system appears to have an uncertain effect on the corrosion rates. The corrosion rate, which has been averaged from the Argonne figures for the conditions of the APPR, is 5 $mg/cm^2/mo$. The formation of both a vapor and water phase in the presence of exposed UO_2 as might occur in the event of a partial loss of water and some stripping of the cladding would result in a higher corrosion rate. The negative corrosion rate of most of the specimens in the table indicates that the material chips and flakes off and is lost to the stream.

TABLE XLI: CORROSION OF URANIUM DIOXIDE

Material	Test Conditions	Time (Hours)	pH Before	pH After	Resistivity (Ohm-cm) Before	Resistivity (Ohm-cm) After	Corrosion (mg/cm^2-mo)
Sp gr 10.6,fired at 1750° C	500° F degassed	330	7.1	5.8	195,000	65,000	-4.4
Repeat of above	500° F degassed	333	7.0	5.7	180,000	28,000	-2.4
Sp gr 10.6,fired at 1750° C	500° F oxygenated	330	7.0	5.5	290.000	60,000	+0.76
Repeat of 3	500° F oxygenated	333	7.0	5.4	210,000	49,000	-15.4
Sp gr 10.3, pressed, fired at 1750° C	600° F degassed	358	6.7	6.0	470,000	47,000	+0.22
Sp gr 9.3,fired at 1750° C	600° F degassed	358	5.9	5.4	320,000	15,000	-7.05
Sp gr 5.0, extruded, fired at 1700° C	600° F degassed	358	6.4	6.0	140,000	11,000	-0.67
Sp gr 10.6, pressed, fired at 1750° C	600° F oxygenated steam phase	354	6.9	---	165,000	---	0.00
Sp gr 10.6, pressed, fired at 1750° C	600° F oxygenated steam phase	400	6.7	6.8	160,000	30,000	-36.9
Sp gr 10.6, pressed, fired at 1750° C	600° F oxygenated water phase						+3.38

13.3.17 Coolant Activity Resulting from Matrix Exposure

Approximate calculations have been made to determine the amount of radioactivity which could be expected in the cooling water, should the fuel matrix be exposed. Two mechanisms have been considered: A. corrosion of the exposed matrix; B. recoil of fission fragments through the exposed surface into the water. The calculation rests on the following assumptions: 1) the power distribution is uniform; 2) the coolant is purged at the rate of 30 gal/hr; 3) the corrosion rate of the matrix is about 5 $mg/cm^2/mo$; 4) the equilibrium gamma-ray activity of fission products after a long operating period is 6.3 Mev/sec per fission/sec, or 2.0×10^{18} Mev/sec at 10 Mw operating power; 5) the fission products in equilibrium can be represented roughly by two groups, one having an initial intensity of 2.0×10^{18} Mev/sec and a half-life of 10 sec, the other having an initial intensity of 2.0×10^{16} Mev/sec and a half-life long compared to the purging "half-life" of ~45 hours; and 6) the mean range of fission fragments in the matrix is about 8×10^{-4} cm.

A. Corrosion. The activity due to corrosion reaches an equilibrium given by

$$\frac{dI}{dt} = S - \lambda I; \quad I = S/\lambda$$

where S is the rate at which activity is being added to the water and λ is the probability per unit time of removal, (by decay and purging). Using numbers given above, the result is:

$$I_A = 8 \times 10^7 \text{ Mev/sec/cm}^2$$

The activity is almost entirely from the long-lived group.

B. Recoils. Expressions for the gamma source strength of fission products, in Mev/sec at a time t after one fission, are found in Reactor Handbook Vol. 1, p. 739. The activity from recoils is found by integrating

the gamma energy/sec from t_1 to t_2. t_1 is taken to be 10 sec, the time required for the coolant to flow from the core to the heat exchanger, which is the largest volume of primary coolant outside the primary shield. t_2 is taken as the purging "half-life", 45 hours. The number of fissions/sec to be considered is αf, where α is the fraction of fission fragments that recoil into the water, and f is the total number of fissions/sec at 10 Mw. α is given by

$$\alpha = \frac{1}{V} \int_0^X \frac{w(x)dx}{4\pi}$$

where V is the matrix volume, X is the mean range of fission fragments and $w(x)$ the solid angle into which a fragment of range X can be emitted and still reach the surface.

The equilibrium activity from recoils is then

$$I_B = \alpha f \int_{t_1}^{t_2} E(t)dt = 1 \times 10^{10} \text{ Mev/sec/cm}^2$$

While these calculations are quite approximate, it is evident that the recoils contribute much more activity than does corrosion.

An estimate can now be obtained of the surface area of matrix that could be exposed without creating a radiation hazard. The criterion adopted is that the radiation dose rate from recoil fission fragments should be 5.3 mr/hr outside 3.8 ft of concrete, at a distance of about 3 meters from the center of the heat exchanger. Since the heat exchanger constitutes only one-fifth of the primary loop volume, the source strength is 2×10^9 Mev/sec/cm^2. The gamma-rays are considered to have 1 Mev energy. The dose rate per cm^2 of exposed surface is found to be 3×10^{-3} mr/hr. Therefore, 1800 cm^2 of exposed matrix surface would give rise to an additional tolerance dose outside the heat exchanger compartment.

13.3.18 Effects of Added Poisons in Water

Experiments were conducted at Argonne to determine a suitable liquid poison which might be employed in an emergency. It would be desirable for such a poison not to injure the materials it comes in contact with during the time it is in the loop. Of the many solutions investigated, boric acid was found to be the only compound stable at 600° F. The salts considered included LiCl, $LiNO_3$, $LiSO_4 \cdot H_2O$, $LiBO_2$, and $LiB_4O_7 \cdot 5H_2O$. In order to make the boric acid more soluble, lithium hydroxide is also added to the solution. The results of corrosion tests run in a boric acid-lithium hydroxide loop are shown in Table XLII.

The corrosion rates are erratic and do not follow the general pattern set by the corrosion rates of specimens in a pure water loop. The corrosion rates are sufficiently low, however, so that no permanent injury should result to any of the loop components.

TABLE XLII: EFFECT OF SUBMERSION OF MATERIALS IN BORIC ACID POISON LOOP

Demineralized water: 5 gm/L H_3BO_3, 0.8 gm/L LiOH, 500° F, 1-3 cc O_2/L, pH = 9, velocity 3.1 fps, and 620-hour operation.

Material	Corrosion Rate ($mg/cm^2/mo$)
304L	0.088
304	-0.22
309	0.16
316	0.035
USS/W	0.26
347	-1.05
17-4 PH	0.12
17-7 PH	0.42
410	0.07
440C	0.0
A nickel	0.51
L nickel	0.44
K-monel, aged	0.12
Inconel, aged	0.09
Monel	0.20
Hastalloy C	0.11
Stellite-3	3.5
Stellite-6	0.63
Vascalloy Ramet 166	-0.12

13.3.19 Evaluation of Corrosion Tabulation

It may be said that, in general, the primary objectives of the package reactor material investigation have been fulfilled insofar as the missing vital information about the materials has been supplied; and insofar as the conditions under which the reactor is to operate have been determined. The possibility of errors has prompted the use of a large number of results, where possible, so that any peculiar result may be minimized by gross averaging.

In most instances the findings are in agreement with the other materials selection lists, see Table XLIII. The most notable difference, one which involves over 80% of the material in the reactor, is the selection of SS 304 instead of SS 347. Graphitar 14, which is used as a bearing material in some of the canned-rotor pumps, did not show up very well and its use augers more frequent pump overhauls than had been anticipated for the rest of the system. It may be that a substitute bearing material, liquid bearings, or actual operational tests of the bearings in existing pumps may solve this problem.

TABLE XLIII: EVALUATION OF MATERIALS

Loops 1 and 3 at Argonne at 500° F, pH 7, with mixed-bed ion exchanger

Material	Loop 1 100 cc H_2/L 1 fpm	Loop 1 100 cc H_2/L 3 fpm	Loop 3 1-2 cc O_2/L 1 fpm	Loop 3 1-2 cc O_2/L 3 fpm
304	G	G	G	G
304L	G	G	G	G
304 Malcomized	-	-	-	G
309	G	G	G	G
309 Malcomized	-	-	-	D
310	G	G	G	G
316	G	G	G	G
318	G	G	G	G
321	G	G	G	G
347	G	G	G	G
410	-	G	D	D
430	D	G	D	-
440 C	-	G	-	-
USS/W	G	-	-	-
17-4 PH aged	G	G	D	G
17-7 PH aged	-	G	D	G
17-7 Hardened	G	-	D	-
Inconel X aged	-	G	G	P
K-monel aged	-	G	G	P
Hastalloy C	-	D	G	D
L-Nickel	-	-	-	P
Inconel	-	D	G	P
Stellite 3	G	G	G	P
Stellite 6	-	-	-	P

Where: G = good D = doubtful P = poor

It must be remembered that although the weight change is an important factor in corrosion evaluation, it can sometimes give an erroneous picture of the corrosion. Thus, a zero weight change can be caused by the formation of an oxide and the loss of some of this oxide by erosion or flaking.

One of the prime factors to be considered in any corrosion analysis is the temper of the corrosion film. If the temper is firm, then it must be assumed that a weight gain is preferable to a weight loss. A weight gain indicates the formation of a metallic compound, usually an oxide, whose composition is only partly that of the metal, possibly only 1/3. On the other hand, a weight loss indicates that at least the amount of loss is in actual parent metal. Of course a large loss or a large gain are both objectionable.

A study of the detailed corrosion rates has indicated that the corrosion rates of most materials decrease with time. This decreasing corrosion rate is attributed to either a reduction in surface open to attack or to the formation of films which shield the metal from the water. Fig. 54 illustrates this reduction in corrosion rate as found for 304 ss in hydrogenated water.

In making the averages of the corrosion rates, the type of corrosion, gain or loss, was ignored. However, in rating materials on the basis of corrosion, some allowance should be made for the fact that a positive corrosion rate is preferable to a negative one. Thus, the corrosion standard grading as suggested by Argonne should be adjusted for this factor as follows:

Grade I: Uniform, adherent corrosion or temper film; no pits and no weight decrease more than 0.25 mg/cm^2-mo nor weight gain more than 0.15 mg/cm^2-mo.

Grade II: Uniform corrosion and some loose corrosion products but no pits. No weight increase in excess of 2.5 mg/cm^2-mo nor weight loss in excess of 1.5 mg/cm^2-mo.

Grade III: Non-uniform corrosion and pitting and weight changes in excess of 2.5 mg/cm^2-mo.

It is felt that for the package reactor all the materials, where possible, should be in Grade I.

Another variation in the test results is caused by different methods of obtaining the corrosion rates for different materials. Some investigators have felt that the corrosion product must be stripped from its host in order to obtain the corrosion rate; this is generally shown as a weight loss and the above grading criteria should not be applied in instances where the corrosion rates have been established in this manner.

Table XLIV shows the relationship between corrosion specimens which have been rated "as is" and specimens which have been electrolytically stripped, under various water conditions. A close similarity in corrosion rates is evident between the 30 fps with scale and unscaled conditions, indicating that the 30 fps fluid may do its own descaling.

The many different corrosion rigs prevalent point up the need for a standard corrosion test procedure which would eliminate much of the blind hunting and which would permit duplication of results.

The use of the descaling method offers one means of obtaining fairly accurate and consistent results. The descaling method, within its accuracy, enables the investigator to determine the portion of the sample which has been lost to corrosion and it eliminates all outside influences

TABLE XLIV: EFFECT OF ELECTROLYTIC DESCALING ON CORROSION RATES AT VARIOUS GAS CONCENTRATIONS

Loop Condition	Time (Hours)	Corrosion Rate ($mg/cm^2/mo$) As Is 30 fps	As Is 1 fpm	Descaled 30 fps	Descaled 1 fpm
		-SS 304-			
0-1 cc O_2/L	500	0	0.01	-0.08	-0.24
	1000	0	0.02	-0.06	-0.08
	1000	0.03	0.06	-0.03	-0.03
	1000	0.02	0.06	-0.03	-0.05
	1500	0.01	0.04	-0.03	0.0
	1500	--	0.02	--	-0.09
1-5 cc O_2/L	500	0.03	0.09	-0.04	0.0
	500	0.03	0.02	-0.02	-0.12
	1500	0.01	--	-0.03	--
100 cc H_2/L	500	0.02	0	-0.02	0.0
	500	0.03	0	-0.01	-0.02
50 cc H_2/L	500	0.01	-0.01	0	0.0
	1000	0	-0.01	-0.01	-0.01
25 cc H_2/L	500	-0.02	+0.04	-0.04	-0.02
	500	-0.02	0	-0.04	-0.08
		-SS 304L-			
0-1 cc O_2L	500	--	0.01	--	-0.12
	500	--	0.03	--	-0.23
	1000	0	0.01	-0.02	-0.06
	1000	0.02	--	-0.03	--
	1500	0.01	0.03	-0.03	-0.07
	1500	0.01	0.02	-0.02	-0.10
1-5 cc O_2/L	500	0.01	0.02	-0.04	-0.13
	1000	--	0.03	--	0.05
25 cc H_2/L	500	0.01	0	-0.01	-0.03
	1000	-0.01	--	-0.03	--
50 cc H_2/L	500	--	0	--	0
	1000	0	0	-0.01	-0.01
	1500	0	0	-0.01	0

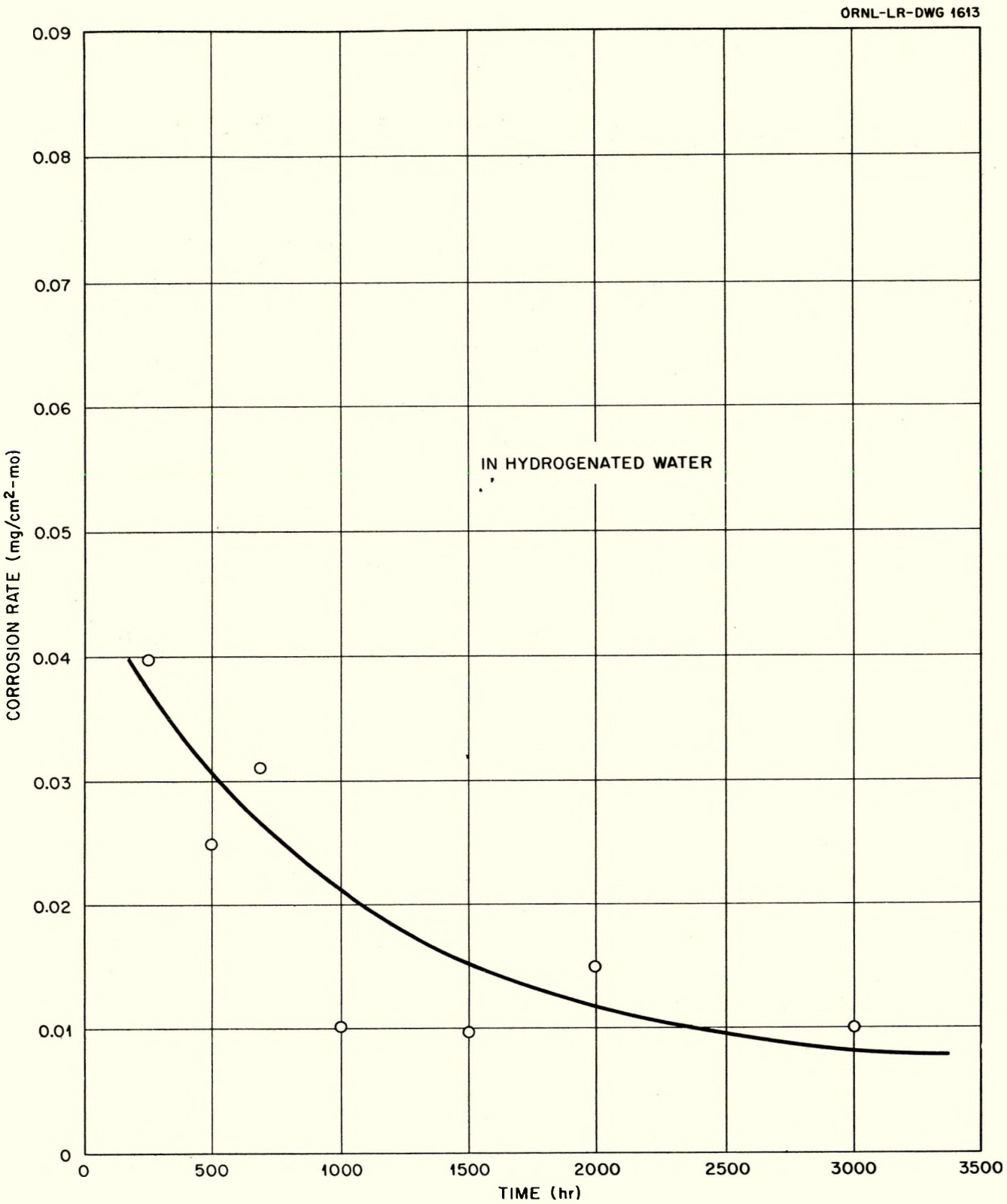

Fig. 54. Corrosion of Type 304 Stainless Steel as a Function of Time.

such as the deposition of corrosion products from a different source. In the investigations of materials which form highly resistant films, however, such as most of the austenitic stainless steels, fairly accurate results are obtainable on non-descaled samples which employ visual inspection to augment the weight change in the test procedure.

The eventual standardization of test procedures would not only assist in the selection of materials for specific applications, but it would aid materially in the overall corrosion mechanism investigation.

13.3.20 Design and Operation Recommendations

Loop Cleanliness. The methods for purifying and maintaining pure water in the primary loop have been discussed in the main body of the report. Of equal importance in obtaining and maintaining a pure water circuit is the cleanliness of the loop components. The materials undergoing fabrication and assembly often have embedded in them or on their surface iron, oil, grease, silica, chips, fibers, and other miscellaneous materials. These materials not only contaminate the water but they also provide foci for pitting and crevice corrosion. The loop components should be cleaned and the specific cleaning process should either be indicated in detail on the component drawings or it should be referred to in an appropriate specification. The suggested methods are as follows:

a. Oil, grease, paint, dirt, etc., should be removed from all surfaces by detergent or solvent washing or by vapor degreasing. The detergents should not contain borax or chlorides.

b. Welds should be wire brushed with a 300-series stainless steel wire brush or ground with an aluminum oxide grinding wheel. Weld film (or flash and splatter) should be removed until bright metal is secured. Where exceptional corrosion resistance is desired the ground surfaces should be made even and smooth.

c. The austenitic stainless steel components should be acid cleaned in a commercially available pickling solution, such as 10-15% HNO_3-2% HF, at 120°-140°F for 1 1/2 hours. This will remove the embedded iron and scale and will somewhat passivate the surface. The pickled surfaces should be thoroughly rinsed with distilled or deionized water until no acid reaction is noted with litmus paper. The cleaned surface may be dried with steam or lint-free cloth.

d. Foundry products, pumps, and valves should be degreased and acid washed, according to the cleaning procedure above, before assembly into the final unit. Castings should be pickled after final heat treatment and prior to finish machining. Surfaces to be welded should be wiped free of oil and dirt before welding. Parts fabricated by polishing or lapping should be cleaned with solvents and hot water until all traces of lapping compound

or grit have been removed. No acid cleaning should take place after polishing.

e. Piping should be received from the mill in a pickled condition. The areas adjacent to welds should be wiped free of oil and dirt prior to welding. The finished joint should be clear of all foreign metal, weld splatter, excess bead, etc. This can be accomplished by wire brushing and by grinding as previously described. The complete welded component should then be cleaned and acid washed whenever possible. It may be difficult to acid wash piping which is joined in the field, but if efficient rinsing is possible, the acid bath should be considered.

f. Fabricated vessels, tanks, and columns should be treated the same as the piping. The cleaning and acid bathing should be done after the vessel has been pressure tested. Distilled water should be used for pressure testing. The tube side of the heat exchanger should be cleaned and acid washed in the same manner.

g. Specifications in the materials must be closely followed. Most of the structural components are made of 304 ss but composition of the specific parts should be accurately ascertained. Nuts for 304 ss bolts should be 303 ss.

General Design Considerations. The design of the piping should be such that smooth flow of the water is obtained. Sharp corners and dead spaces should be avoided if possible. The purge-valve outlet should be at a low point in the system and preferably in an area of low turbulence, possibly at the bottom of the reactor. An access hole might be supplied in one of the primary loop pipes to permit the installation of filters and/or magnets for the removal of large particles which may initially be present in the system.

Equipment Exercise. Because of the possible effect of crevice corrosion it is suggested that a schedule of mechanism exercise be worked out for such devices as the control-rod drives and certain valves. Under the operating condition of 50 cc H_2/liter of water and a water purity of 2 ppm total dissolved solids, it would be sufficient to operate

the idle equipment once every three months. If the water purity, the hydrogen concentration, or both, should drop off, however, more frequent exercising is indicated. If no hydrogen should be present, the equipment should be exercised about once a week. The extent of exercise must necessarily depend on the reactor operating conditions. Valves may just be cracked several times. The control-rod drives should be run, if possible, to give a complete revolution of the seal rings.

13.4 APPENDIX D: CARRIER DESIGN CALCULATIONS

Present plans for handling the spent fuel elements of the package reactor call for a cooling off period of one year at the site, following an operating period of two and one-half years. After a year, the fuel elements will still be exceedingly active, and must be packed in lead containers to be shipped for processing and recovery of unexpended fuel. A survey of the decay rates and gamma-ray energies of the products of U-235 fission* shows that, under the conditions stated above, the following activities contribute nearly all of the gamma-ray flux at the outer surface of a shield thick enough to reduce the dosage to permissible levels.

Nuclide	Eγ, Mev	
Rhodium-106	2.90	Decay rate fixed by 1.0-y Ru 106
Praseodymium-144	2.60, 2.20	Decay rate fixed by 275-d Ce 144

As a consequence of the long operating cycle, these long-lived fission products are much nearer to their saturation activities, and therefore the activity is relatively much more intense than in other reactors in which this problem has been encountered.

For each of these products, the decay rate after two and one-half years of operation and after one year of cooling, is given by

$$A = f\, y_f\, y_\gamma\, (1-e^{-2.5/\tau})_e^{-1/\tau}$$

where τ is the mean life of the long-lived parent, expressed in years, f is the fission rate, y_f is the yield of the fission chain to which the nuclide belongs, and y_γ is the γ-ray yield per disintegration. For 6-Mw operation (and 193-Mev fission), f = 1.94×10^{17}/sec, or 4.3×10^{15}/sec per fuel element.

---

*Moteff, John, Fission Product Decay Gamma Energy Spectrum, APEX-134.

In calculating the attenuation of gamma rays in a thick shield, it is necessary to take into account the forward scattering of the gamma rays, which reduces the effective attenuation. This was done by using dose build-up factors computed by Goldstein, Wilkins, and Spencer*.

A self-shielding factor for the array of four assemblies was calculated by assuming the sources and absorbers of γ-rays to be uniformly distributed over the cross section of the array. For the package reactor fuel assemblies, this factor is 0.63.

Calculation of the dose rate at a point outside the coffin was made by assuming the activity of the element to be concentrated at its center, o.

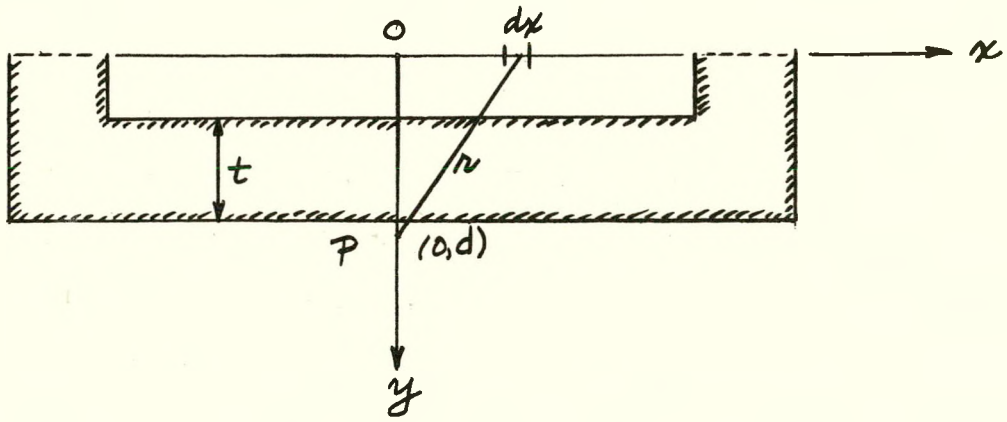

This procedure evidently overestimates the flux, since parts of the source are farther away from P, and their gamma rays must reach P through greater thicknesses of lead. When an approximate value for the thickness, t, of the shield has been found, the flux estimate can be corrected by applying the factor.

$$k = \left(\frac{e^{-\mu t}}{d^2}\right)^{-1} \frac{1}{a} \int_0^a \frac{e^{-\mu\alpha r}}{r^2}\, dx$$

$k < 1$; $\alpha = t/d$.

---

* Goldstein, H., Wilkins, J. E., Jr., and Spencer, L. V., Gamma Ray Penetrations, NDA Memo 15C-2.

Some results of the calculation are listed below:

				t = 20 cm		t = 25 cm	
Eγ	A(1-yr)	μ	ϕ / mr·hr	$B_t\ e^{-\mu t}$	D(d,t)	$B_t\ e^{-\mu t}$	D(d,t)
2.90	3.2×10^{11}	0.47	180	4.1×10^{-4}	86	5.1×10^{-5}	9
2.60	1.9×10^{12}	0.48	200	3.4×10^{-4}	527	2.8×10^{-5}	58
2.20	1.9×10^{12}	0.49	230	2.8×10^{-4}	373	2.5 x 10-5	33

A(1-yr) = γ's/sec after 1-year cooling.

μ = absorption coefficient in lead, in cm^{-1}.

ϕ/mr·hr = flux in γ's/cm^2-sec, to produce a dose rate of 1 mrep/hr*.

B_t = buildup factors cited above.

D(d,t) = dose rate for four assemblies, in mrep/hr, for d = 35 cm, before applying the correction factor, k.

By plotting these dose rates as a function of t, it is found that 22 cm of lead is required for an uncorrected dose rate of 400 mr/hr, at a mean distance of 35 cm from the source. The additional thickness required to halve the flux is 1.6 cm. For d = 35 cm, a = 28 cm, t = 22 cm, μ = 0.48, the factor k = 0.45. The actual dose rate just outside the transfer coffin should therefore be about 200 mr/hr. At 3.5 meters from the source, the dose rate would be about 4 mr/hr. (For this case, k ≅ 1).

* MTR Project Handbook, ORNL-963.

13.5 APPENDIX: REACTOR SIMULATOR TEST RESULTS

The package reactor power plant was examined* by means of the ORNL Control Computer**. This section describes the system simulated in a block diagram; the design point parameters used; the simplifying assumptions used for approximations; and gives data in the form of curves showing responses of mean fuel-plate surface temperature, mean coolant temperature, and response of reactor power to perturbations in reactivity and load demand.

Fig. 55 is a block diagram of the reactor and heat exchanger system simulator. The seven operational amplifiers shown generate electrical equivalents of the thermal quantities indicated in the blocks. Transport lags and heat capacities are approximated by first-order lags produced by linear passive networks. These approximations are conventional and are probably satisfactory when the lag is not strictly transport but involves considerable fluid mixing as in the case of the package reactor coolant. To improve the approximation requires considerable equipment and was not considered worth the investment needed for such equipment.

Operational amplifier #1, Fig. 55, with its associated network generated $\bar{\theta}_f$, the mean fuel temperature. Steady state inputs to this amplifier are 94% of reactor power and a quantity proportional to $\bar{\theta}_f - \bar{\theta}_c$, where $\bar{\theta}_c$ is the mean coolant temperature. The capacitor across the amplifier is determined by the total heat capacity of the reactor fuel. It was calculated by selecting that capacitance which will allow $\bar{\theta}_f$ to rise at design point rate to design point power when no heat is extracted.

* Mann, E. R., Green, F. P., Analog Simulation in the Package Reactor Study, ORNL CF-54-1-104, March 2, 1954.

** Stone, J. J., Mann, E. R., ORNL Reactor Controls Computer, ORNL 1632, March 1954.

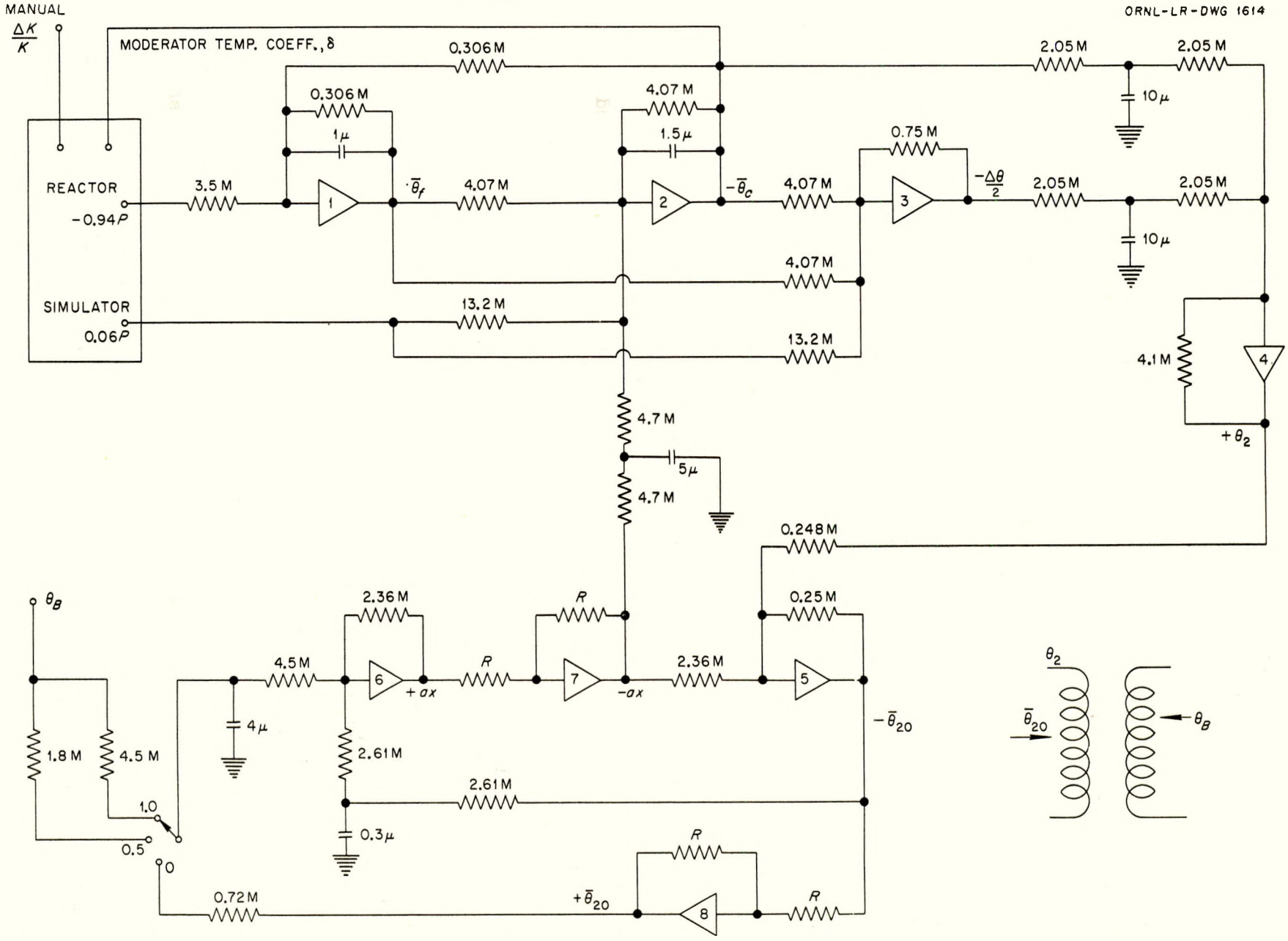

Fig. 55. Block Diagram of Reactor Simulator.

297

The heat capacity of the coolant in the reactor was taken as the heat capacity of the coolant flowing through the reactor in unit time. Since the coolant transit time for the reactor was 0.5 sec, the heat capacity of the coolant was taken as twice that of the coolant in the reactor at any instant. The capacity of the condenser across amplifier #2 was determined by using this definition of the coolant heat capacity. Actual determination of this capacitor was as follows: With the shunt resistor removed from the condenser and with a current, simulating design point power, flowing into amplifier #2, the latter becomes an integrator. The output of the integrator gives the magnitude of the rate of change in mean coolant temperature, $\dot{\bar{\theta}}_c$, at design point.

The reactor coolant outlet temperature was never determined at the reactor. It was assumed that once the coolant came out of the reactor its temperature remained constant until it entered the heat exchanger or in fact, by mixing, altered the heat exchanger input temperature. Since there is a long time lag here, approximately 10 sec, and since it is likely that the lag in fact is more nearly a first-order lag than a transport lag due to the mixing which may take place between reactor outlet and heat exchanger inlet, it was assumed that insertion of a first-order lag network between the reactor outlet and heat exchanger inlet would simulate the system well enough. So, by means of amplifier #3, one half of $\Delta\theta$, the difference between inlet and outlet temperatures, was added to $\bar{\theta}_c$, the coolant mean temperature. Both quantities $\bar{\theta}_c$ and $1/2\Delta\theta$ were lagged to give the heat exchanger inlet temperature through amplifier #4.

Now if it is assumed that $\bar{\theta}_{2_o}$, the output of amplifier #5, is the mean reactor coolant temperature in the heat exchanger and if the heat exchanger heat capacity is approximated by a linear network, then the difference

between this mean temperature and the mean temperature of the secondary fluid in the heat exchanger determines the rate at which heat is extracted. Since the secondary coolant boils and is returned to the heat exchanger as a liquid with no loss in mass, the mean temperature of the secondary liquid is a weighted mean and is slightly lower than the boiling temperature. It is assumed that the return coolant always enters the heat exchanger at the same temperature. A first order lag is shown on the steam side to allow for liquid return time.

The output of amplifier #6 gives the rate at which power is extracted from the primary coolant at the heat exchanger. Amplifier #7 merely changes the sign of this quantity. The output of amplifier #7, along with the output of amplifier #4, is coupled to the input of amplifier #5. The output of amplifier #5, $-\bar{\theta}_{2o}$, has already been defined as the mean temperature of the reactor coolant in the heat exchanger.

The quantity "ax", output of amplifier #7, is fed through a linear network delay to the input of amplifier #2 and its polarity is such that it lowers the mean reactor coolant temperature.

The switching input to amplifier #6 determines the power-load demand (total reactor power) and simulates changing the mean temperature of the secondary coolant, i.e., changing the secondary coolant's boiling point. Raising the boiling point lowers the power demand, and vice versa.

Amplifier #8 merely inverts the polarity of $-\bar{\theta}_{2o}$. When the input to amplifier #6 is made equal to $K(\bar{\theta}_{2o} - \bar{\theta}_{2o})$, where K is any constant, the reactor will shut itself down from whatever power it may have been operating, provided the temperature coefficient is negative. This means, of course, that the secondary coolant of the heat exchanger is not absorbing

the heat, which would be true were the temperature of the primary and secondary identical. Amplifier #8 makes this operating condition simple, although it is doubtful that it would be so simple in the actual power plant.

The equations of the electrical networks shown in the block diagram, Fig. 1, can be obtained by application of Kirchoff's law for current at the inputs to the operational amplifiers. They are as follows:

$$(1)\quad -\frac{0.94P}{3.5 \times 10^6} + \frac{\bar{\theta}_f - \bar{\theta}_c}{0.306 \times 10^6} + 10^{-6}\frac{d\bar{\theta}_f}{dt} = 0$$

$$(2)\quad +\frac{0.06P}{13.2 \times 10^6} - \frac{ax(t+2)}{9.4 \times 10^6} + \frac{\bar{\theta}_f - \bar{\theta}_c}{4.07 \times 10^6} - 1.5 \times 10^{-6}\frac{d\bar{\theta}_c}{dt} = 0$$

$$(3)\quad \frac{0.06P}{13.2 \times 10^6} + \frac{\bar{\theta}_f - \bar{\theta}_c}{4.07 \times 10^6} - 1/2\,\frac{\Delta\theta}{0.75 \times 10^6} = 0$$

$$(4)\quad \frac{-\bar{\theta}_c\left(t - \frac{\tau_1+\tau_2}{2}\right)}{4.1 \times 10^6} - 1/2\,\frac{\Delta\theta\left(t - \frac{\tau_1+\tau_2}{2}\right)}{4.1 \times 10^6} + \frac{\theta_2}{4.1 \times 10^6} = 0$$

$$(5)\quad P_o(t-3) - \frac{\bar{\theta}_{2o}(t-4)}{5.2 \times 10^6} + \frac{ax}{2.36 \times 10^6} = 0$$

$$(6)\quad \frac{-ax}{2.36 \times 10^6} + \frac{\theta_2}{0.248 \times 10^6} - \frac{\bar{\theta}_{2o}}{0.25 \times 10^6} = 0$$

(7) and (8) Inverters only.

The equations of the pile simulator are conventional equations for a stationary fuel reactor with negative moderator temperature coefficient of reactivity*.

A further assumption made for this analysis was that power density in the fuel elements was uniform throughout the lattice.

---

* Stone, J. J., Mann, E. R., ORNL Reactor Controls Computer, ORNL 1632, March 1954.

Design point data used in the simulation are:

P_o, design point power = 10 Mw = 9482 Btu/sec

P_f, power developed in fuel = 0.94 P_o

P_m, power developed in moderator = 0.06 P_o

C_f, fuel heat capacity = 66.53 Btu/°F

$\bar{\theta}_f$, mean fuel temperature = 483 °F

$\bar{\theta}_c$, mean coolant temperature = 442° F = $\bar{\theta}_{2o}$

$\Delta\theta$, coolant temperature gradient across reactor = 16°F

z_θ, = $\bar{\theta}_f - \bar{\theta}_c$ = 41°F

ϕ_o, heat exchanger secondary mean temp. = 355.4°F

Moderator (coolant) flow = 4000 gpm = 556.5 lb/sec

C_c, specific coolant heat capacity = 0.873 Btu/lb- °F

W_o, average exchanger secondary flow rate = 7.915 lb/sec

C_s, specific steam heat capacity = 1.025 Btu/lb - °F

p , mean steam pressure = 200 psia

τ_1, reactor coolant pass time = 0.5 sec

τ_2, external loop time = 21.2 sec

τ_3, heat exchanger primary pass time = 1.4 sec

Time scale: 1:1

Temperature scale: 10°F/volt

Power scale: 0.2 Mw/volt

δ, temperature coefficient = -10^{-4}/°F

$z_\phi = \bar{\theta}_{2o} - \phi_o$ = 86.6 °F

Transient conditions induced by step reactivity changes and step load (total power) changes are shown, Fig. 56 - 67. The parameters recorded are power, mean fuel temperature, and mean coolant temperature in the reactor.

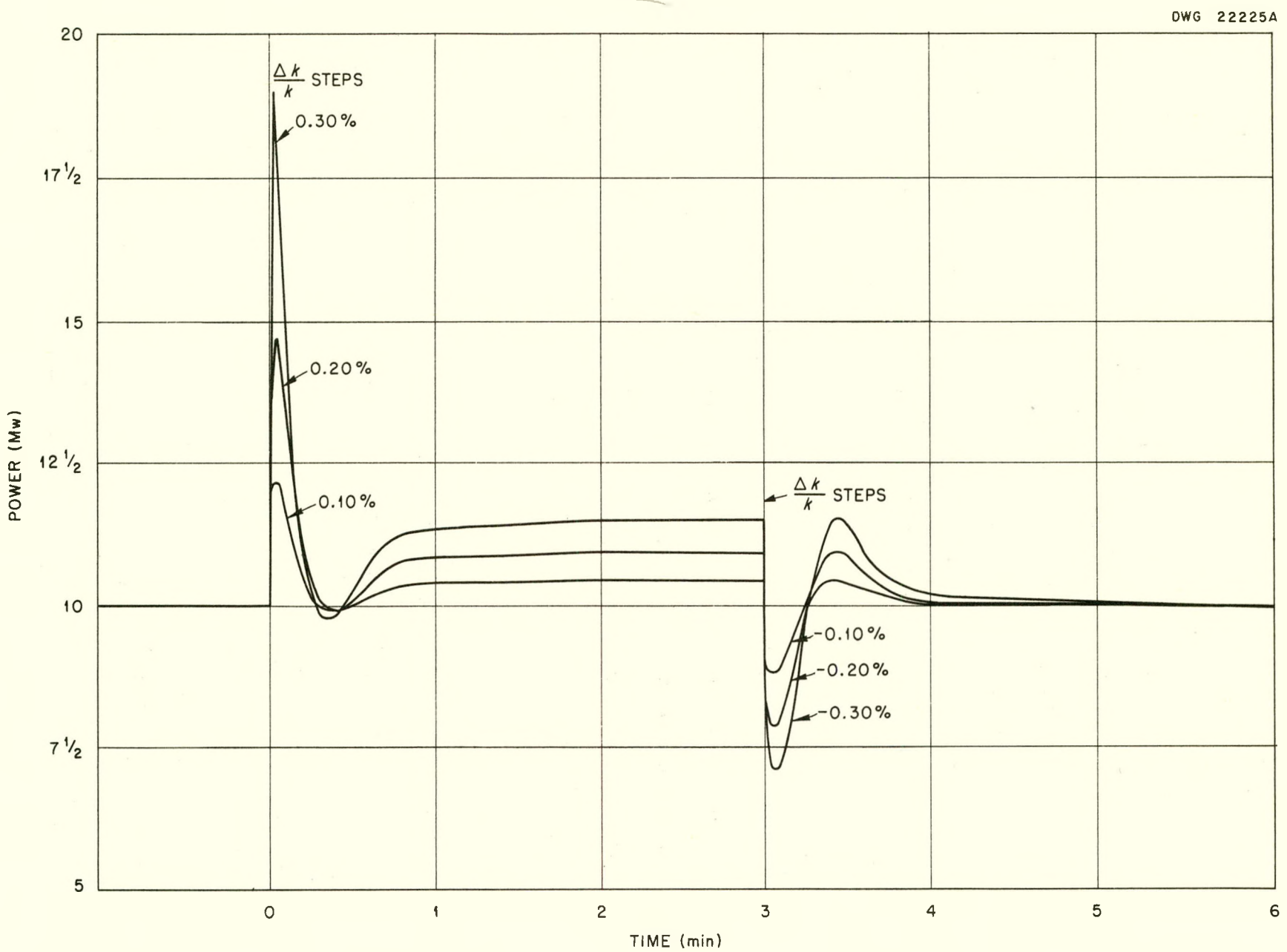

Fig. 56. Simulator Test No 1.

302

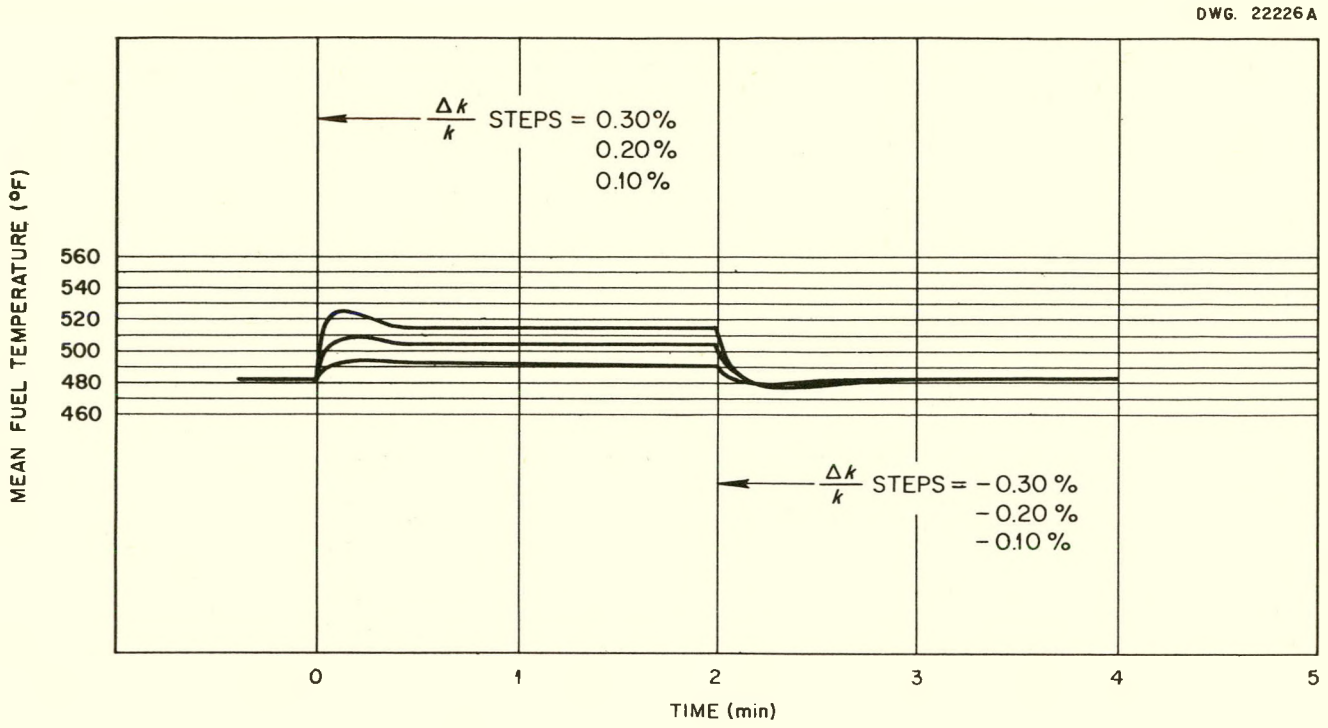

Fig. 57. Simulator Test No. 2.

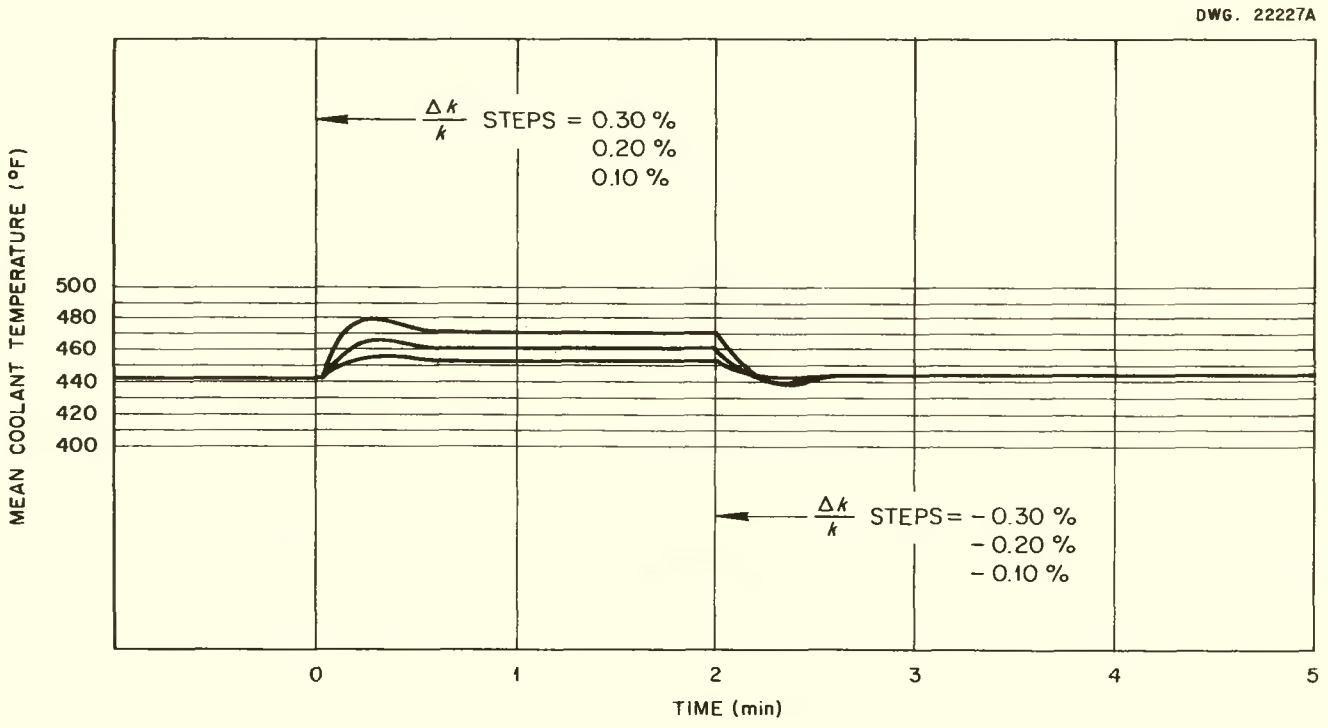

Fig. 58. Simulator Test No. 3.

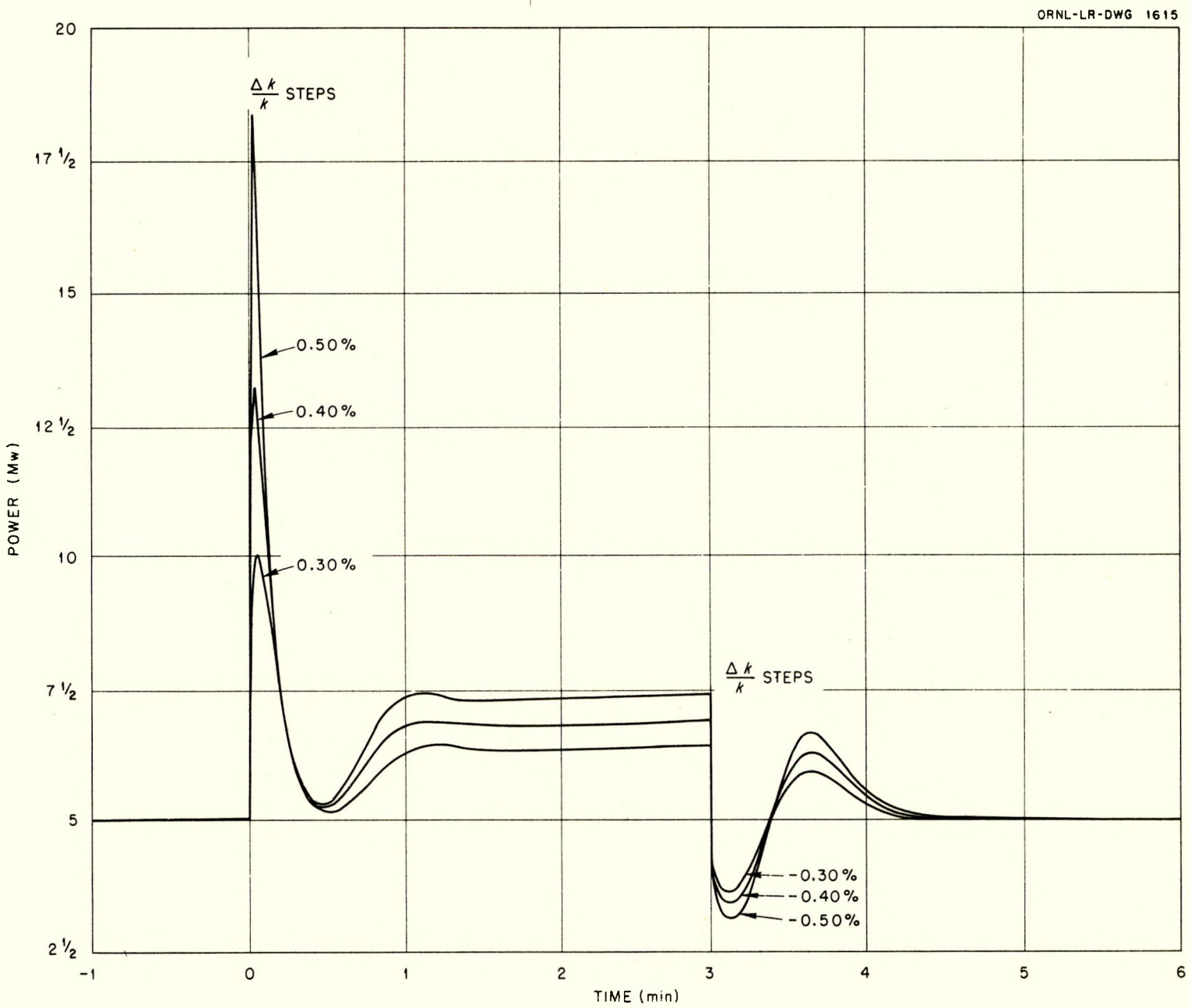

Fig. 59. Simulator Test No 4.

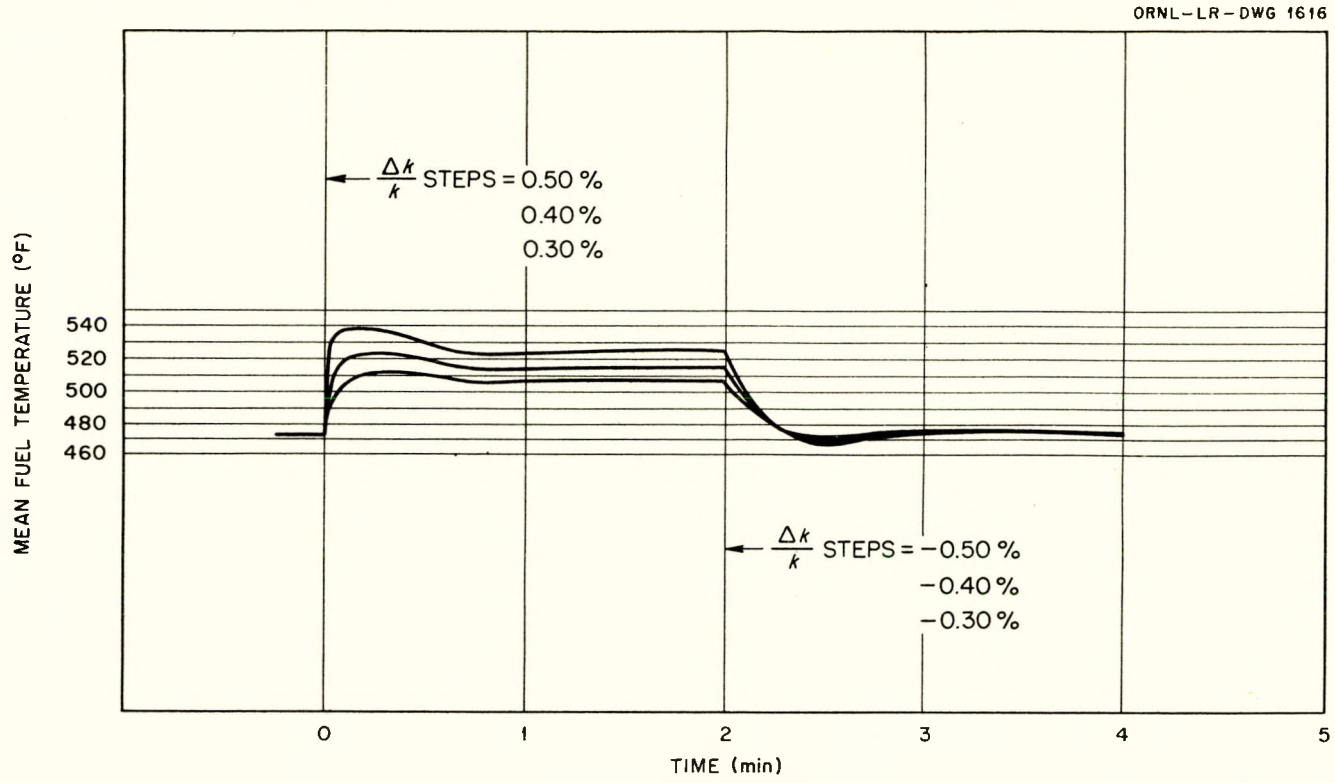

Fig. 60. Simulator Test No. 5.

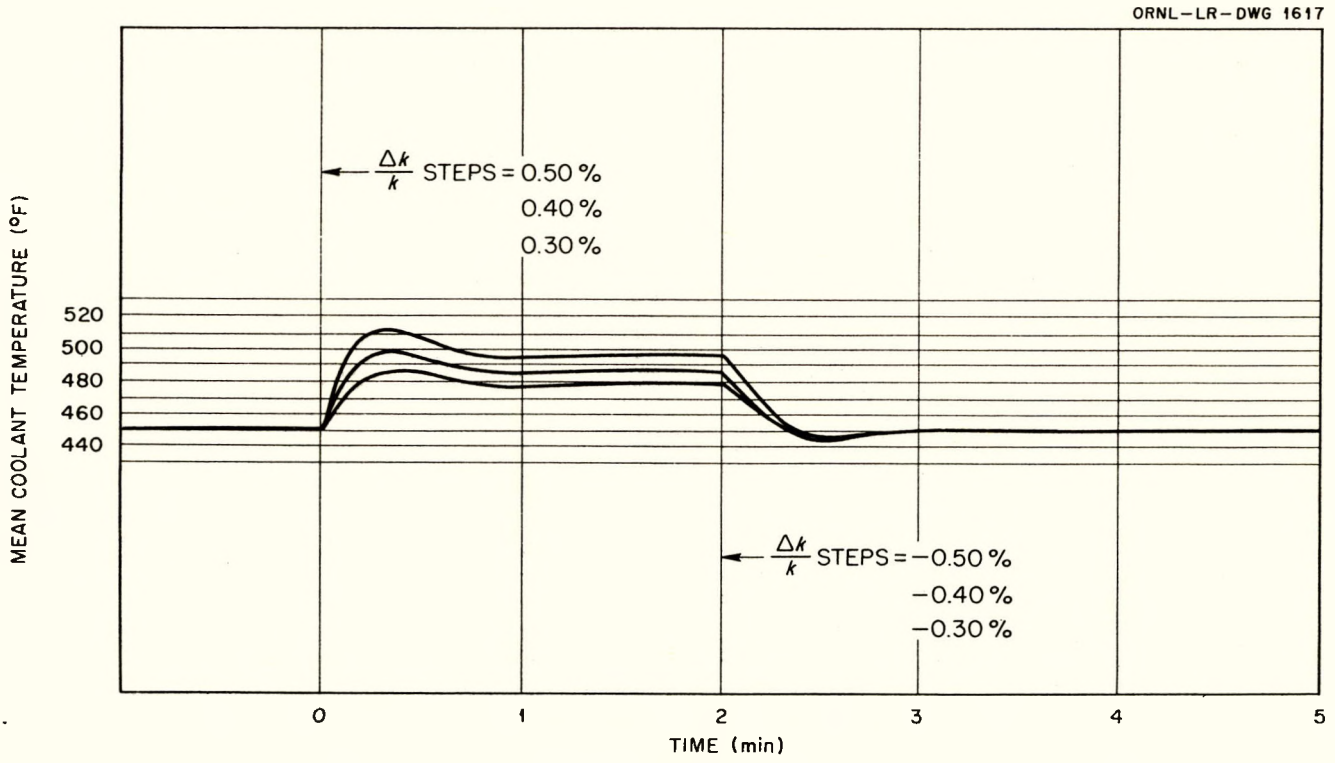

Fig. 61. Simulator Test No. 6.

DWG 22228A

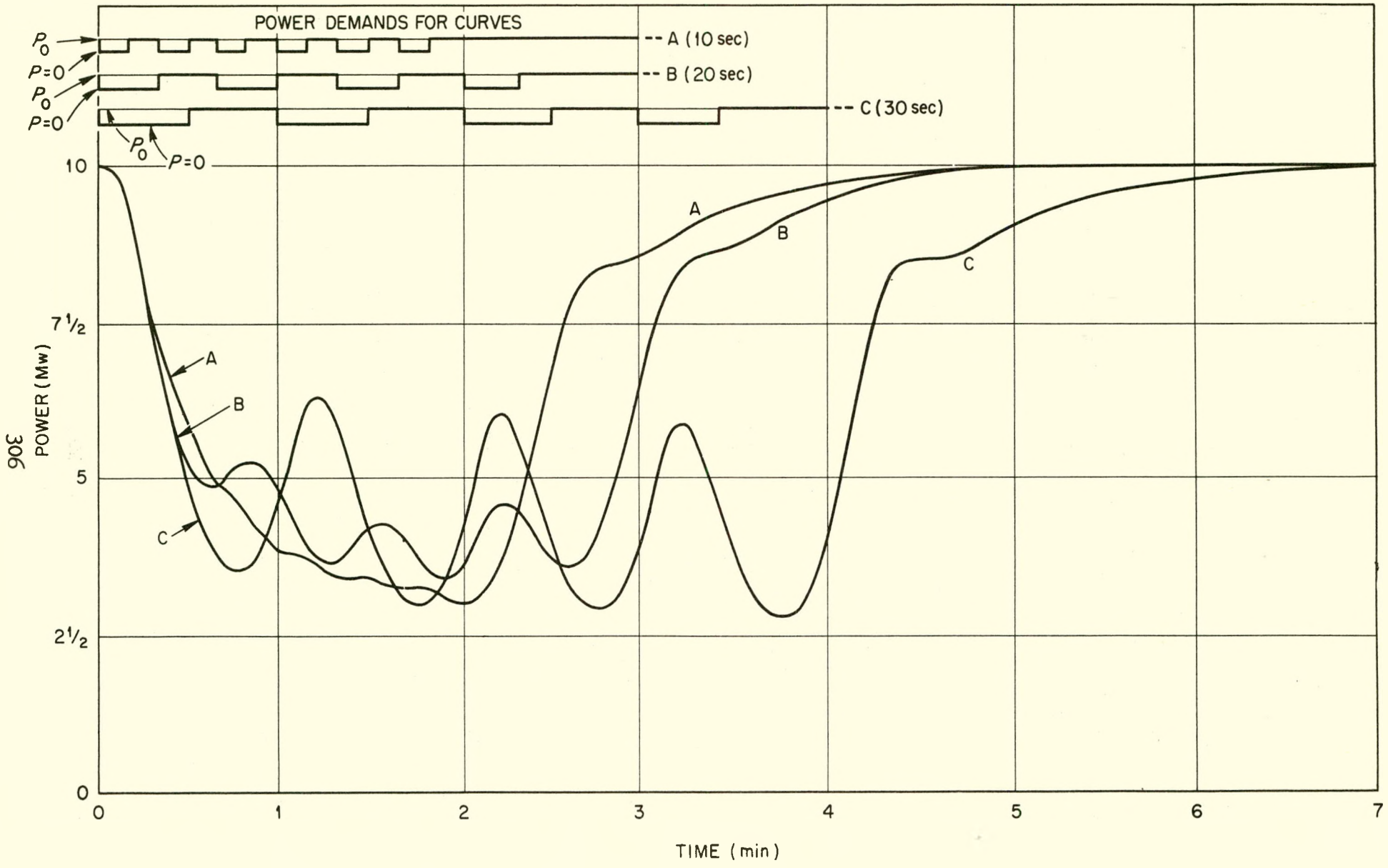

Fig. 62. Simulator Test No. 7.

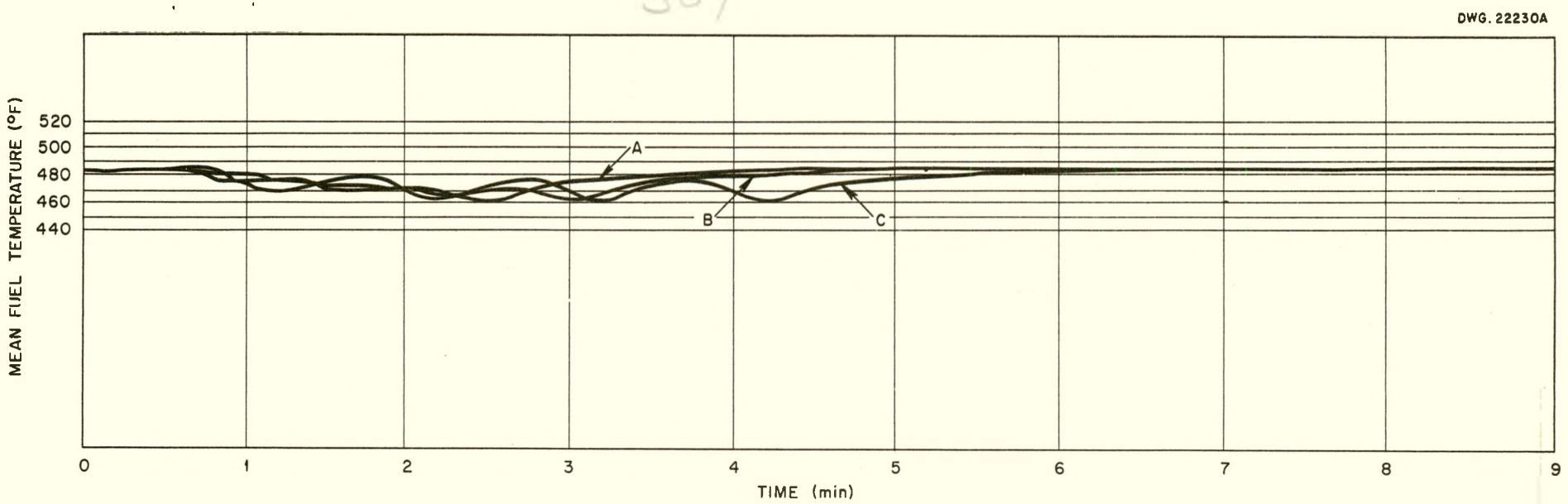

Fig. 63. Simulator Test No. 8.

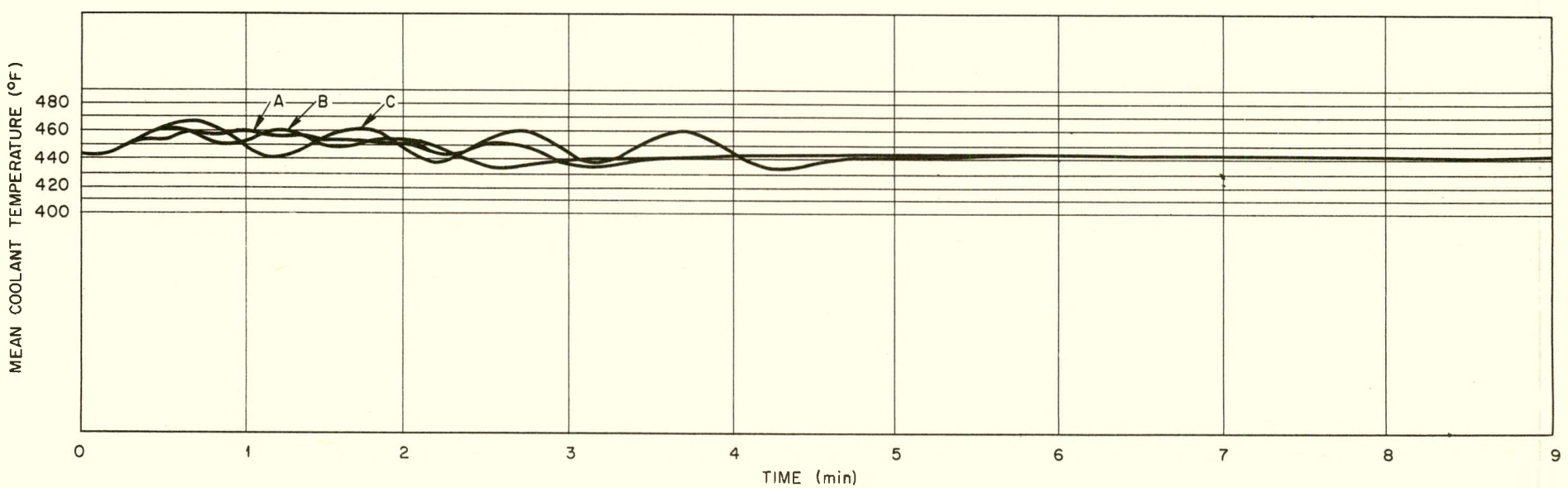

Fig. 64. Simulator Test No. 9.

307

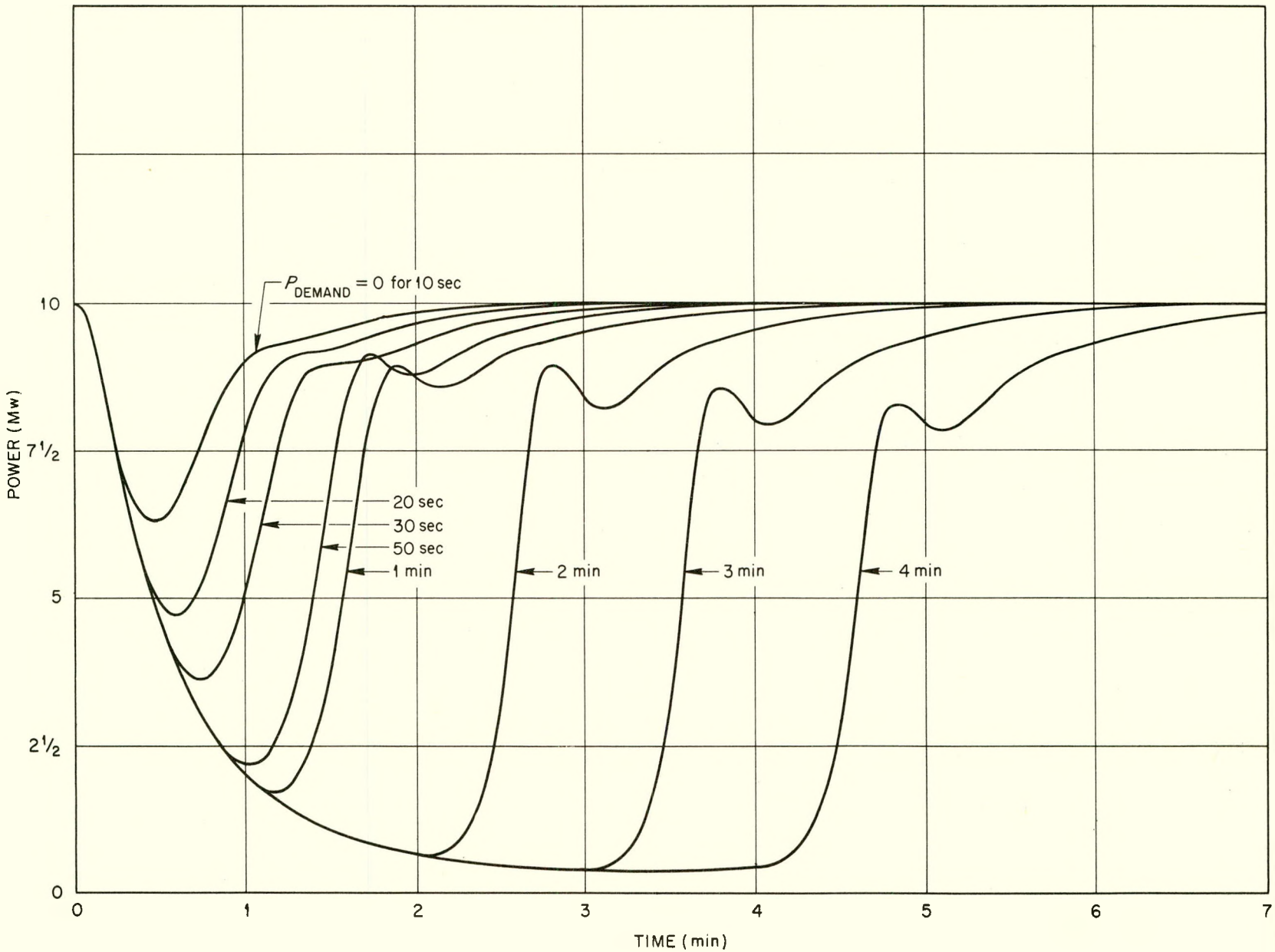

Fig. 65. Simulator Test No. 10.

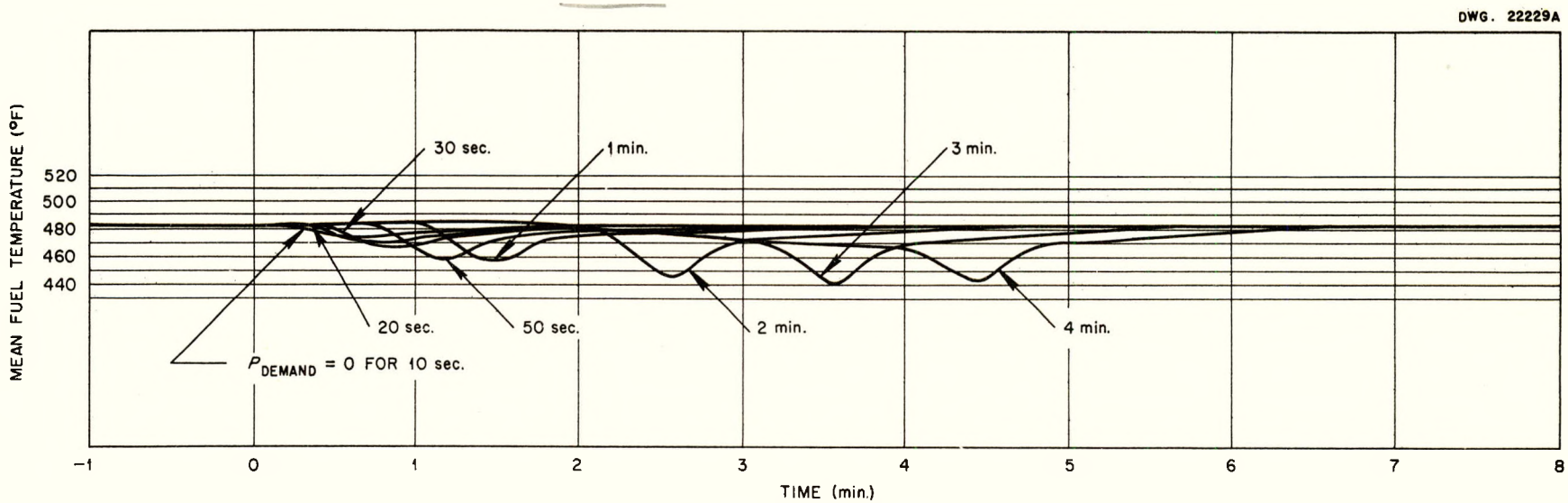

Fig. 66. Simulator Test No. 11.

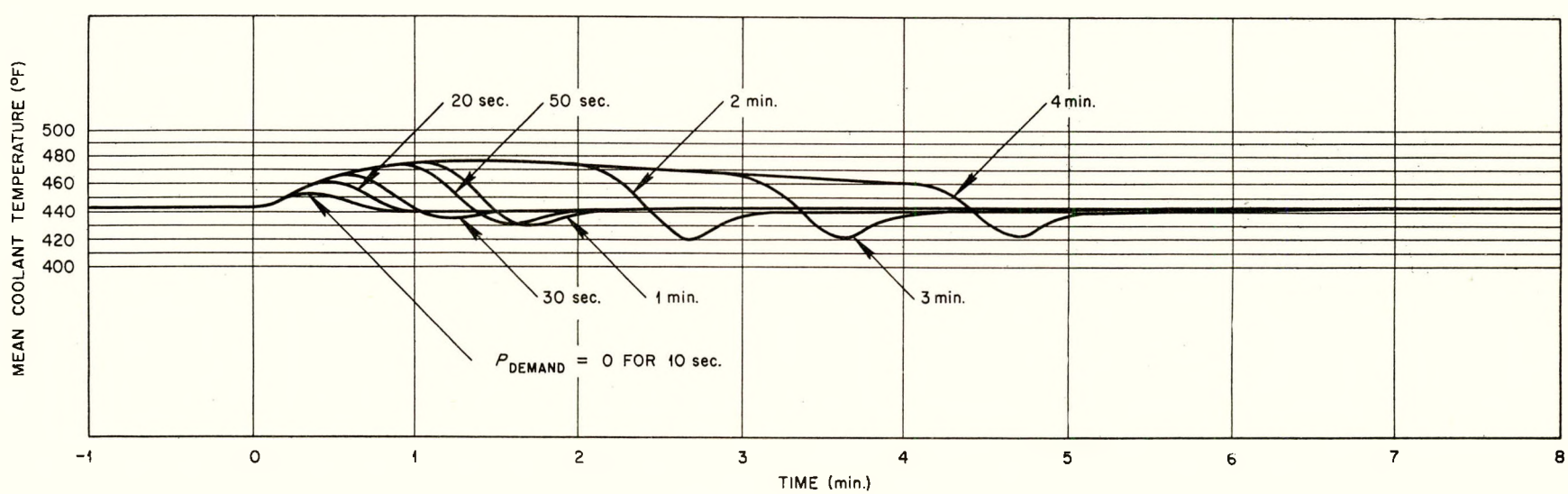

Fig. 67. Simulator Test No. 12.

The sequence of transients shown in Fig. 56 - 61 consists of two sets of alternatively positive and negative reactivity steps, one for the reactor at full design point power, and the other at 1/2 power. The fuel temperature can be seen to "drive" the coolant temperature during the positive-k transient and the fuel temperature, after its initial steep drop, can be seen to "ride down" on the coolant temperature during the netative-k transient. The maximum fuel temperature during such transients cannot exceed 590° F, or local (nucleate) boiling will occur. The corresponding fuel-plate surface temperature would be 567° F.

Periods were observed for these tests and none of less than 7 seconds occurred. Other tests, using several moderator temperature coefficients of reactivity, indicated that no coefficient less than -2×10^{-5} was permissible.

Since the negative moderator temperature coefficient of reactivity stabilizes the reactor power for a positive step of $\Delta k/k$, it should be noted that it does so by raising the mean coolant temperature. As this power plant was simulated, this increase in mean reactor coolant temperature actually gives an increase in power output since the mean temperature of the secondary coolant remains constant. In the actual power plant this added power would be rejected by the load on the secondary if one wished to continue at constant load through the $\Delta k/k$ transient. It was not considered worth-while to devise such a rejection simulator.

Fig. 62 - 67 are the records of power, mean fuel temperature, and mean coolant temperature for two types of load-demand transients. The first group, Fig. 62 - 64, consists of oscillatory load demands of three different time intervals, applied to show the damping characteristics of a circulating moderator (loop time = 21.7 seconds). The second group,

Fig. 65 - 67, consists of eight transient, zero load time intervals, applied to illustrate the stability and self regulation of this system to maximum demand excursions without movement of the control rods.

APPENDIX 13.6: CONTROL-ROD DRIVE MECHANISM TESTS

The operating characteristics of the control-rod drive mechanism, control-rod latch, rod bearings, and shock absorbers, were determined in a "dry-run" test by the American Machine and Foundry Company. These preliminary tests were not run under the operating conditions of 450° F and 1200 psia water, but in air at normal room temperature. Tests are presently being conducted under the pressurized hot-water conditions.

The equipment which was used in this preliminary testing and will be used in those to follow consists of all component parts of the control rod and drive mechanism as described in sections 3.1.2 and 3.3 of this report. This includes a full-size shock absorber, a mock-up fuel element, and rod segments. The motor-package unit consists of the motor, magnetic clutch, gear box, seal assembly, and indication system. For the purpose of these tests, the components were assembled in a "jury-rig" or "bread-board" layout, as may be seen in Fig. 68. In the final design, these parts would be assembled much more compactly.

13.6.1 Test Procedure and Discussion:

A. Preliminary checkup - after the mechanism was completely assembled the rod was run through the full 22-in. stroke, down and return 10 times. The pinion rotated at 4 rpm and the rod velocity was 2 ft/min. During this initial operation the following were checked and adjusted.

   1. Limit switch settings.

   2. Rack backup-roller clearance. After adjustment this clearance was 0.005 in.

   3. Position indication system.

   4. Motor torque indication system. During this phase of the test, the motor torque was approximately 8 oz.-in.

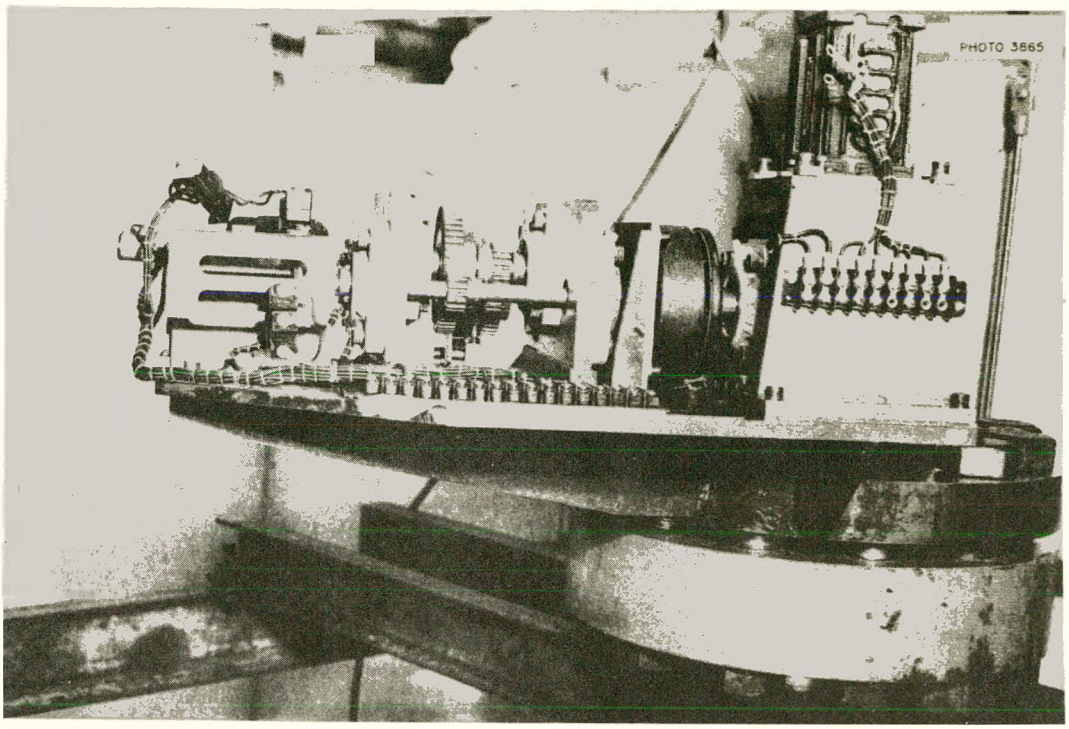

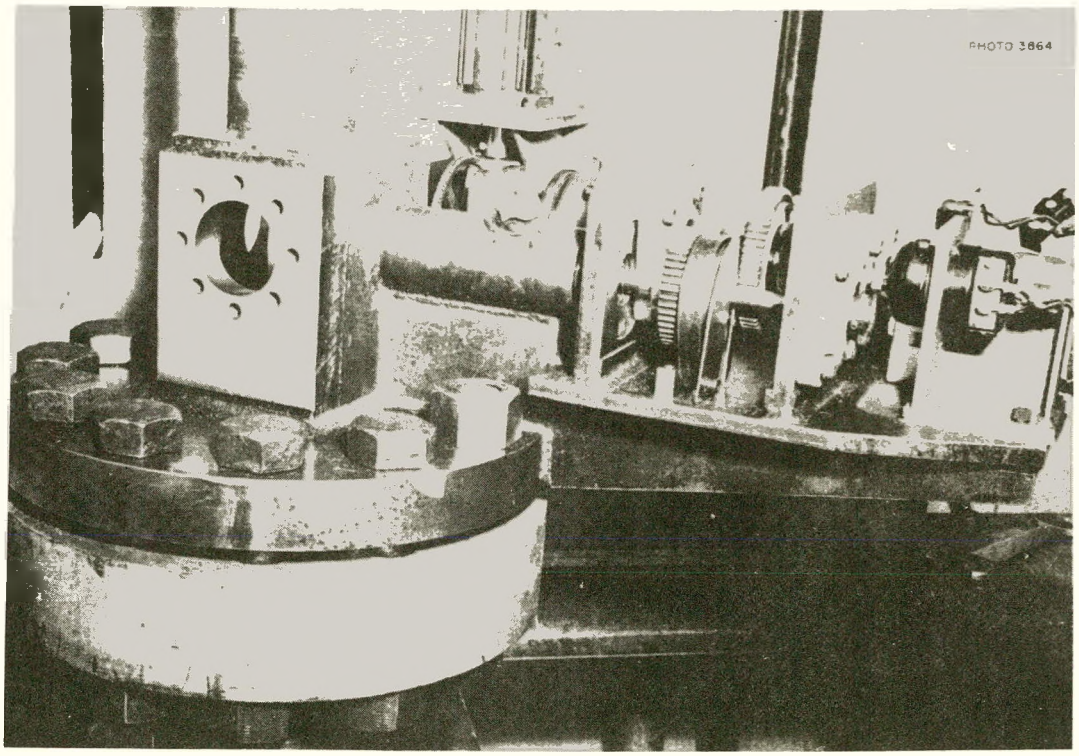

Fig. 68. Control-Rod Drive Mechanisms, Test Model.

B. Dry Scram Test - The shock absorber position of the guide tube was immersed in water before starting. The rod was scrammed 20 times from the top position and 10 times from the mid position. Scram velocities and scram times were recorded on a Brush recorder.

1. Fig. 69a shows the velocity-time curve of a full scram with a maximum spring load of 30 in.-pounds. The portion of the curve from A to B shows the increase in velocity due to the acceleration of rod fall. The acceleration during this scram was 8 ft/sec^2. The curve section B-C shows the velocity of the rod during the snubbing by the shock absorber. The portion from C to D shows the "bounce" of rod. The deceleration due to the shock absorber during this scram was 19.1 ft/sec^2. The straight line portion from A^1 to A shows the time from scram actuation to clutch release. The time shown on this curve was 50 milliseconds.

2. Fig. 69b shows the velocity-time curve of a full scram without the scram spring. The clutch release time, A^1 to A, was 160 milliseconds. The acceleration of the rod drop was 4.34 ft/sec^2. With a lower maximum velocity, the shock absorber performed more successfully. The deceleration was 11.7 ft/sec^2. This acceleration was sufficient to cause some bounce as can be seen from the C-to-D portion of the curve.

3. Fig. 69c shows a velocity-time recording of a scram from the mid position with a 20 in.-pound scram spring load. The scram acceleration was 10 ft/sec^2. The clutch release time was 280 milliseconds. Since the rod was dropped from the mid-position, the maximum velocity was 5 ft/sec. The shock absorber performance was satisfactory under these conditions. The deceleration was 10 ft/sec^2. As can be seen from the C-D portion of the curve, little or no bounce was detected.

4. As mentioned previously in this report, the clutch friction is the greatest single factor in retarding scram acceleration. Fig. 69d shows a velocity time curve of a scram test which was run in the following manner:

   a. With the rod resting on the bottom and the latch engaged to the rod, the scram button was actuated. This released the holding voltage from the clutch field.

   b. The clutch armature was manually pushed away from the rotor. There was at least a 1/8-in. air gap between the rotor and armature.

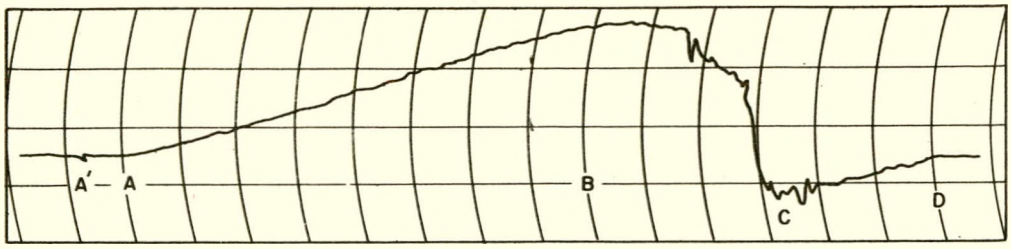

FIG. 69a

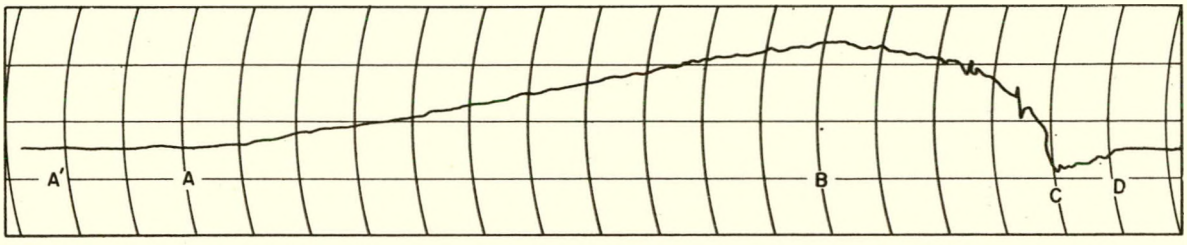

FIG. 69b

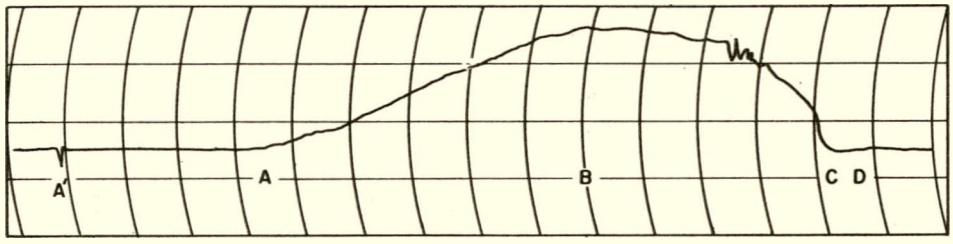

FIG. 69c

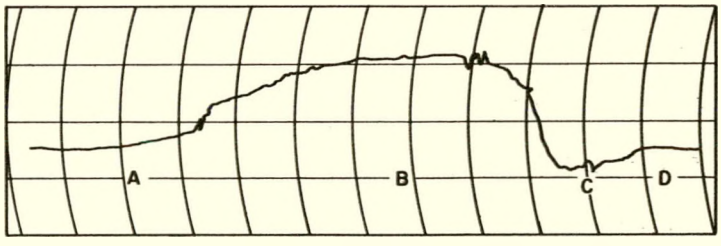

FIG. 69d

Fig. 69. Motion of Control Rod During Scram.

c. The rod was raised manually to the mid position. It should be kept in mind that the rod, latch, rack, pinion, and gear train remained in engagement during this test.

d. The rod was released and the scram velocity recorded. The acceleration of scram on this test was 17 ft/sec^2. This increase in acceleration indicated the necessity for a clutch design incorporating a spring-release armature. The deceleration was again too high, (19 ft/sec^2) and rod bounce was again detected.

C. Rod-Release Test - The rod-release tests were run to determine whether the latch would release the rod automatically when the reactor cover was removed. When the rack was driven to a lower over-travel position, the jaws of the latch would open and the rod and latch would be disengaged. It was impractical to raise the latch from the rod but it was a simple matter to lower the rod from the latch. The procedure was as follows:

1. With the latch jaws in the open position the rod was raised approximately 1/4 in. from the shock absorber bottom. The rod was held in this position.

2. The flange bolts which connect the lower portion of the shock absorber to the guide tube were removed and this portion of the shock absorber was lowered 6 in.

3. The rod was allowed to drop from the latch jaws.

4. The above procedure was performed 20 times. Fifteen tests were performed under normal conditions and five were performed under conditions of misalignment up to 10° between the latch and the rod. During each test the rod dropped freely from the latch.

13.6.2 Conclusions These conclusions are based on preliminary test results. The tests were not run under the operating conditions of 450° F and 1200 psi water; they were run in air at normal room temperatures. A later report will give the results of the pressurized hot-water test.

A. The shock absorber as originally designed and built operated somewhat less than satisfactorily. The rod came to a complete stop 0.3 seconds after maximum velocity was attained. The rod deceleration was 14.8 ft/sec^2. This deceleration gave some rod bounce as can be seen from the curves. With some development of the shock absorber taper and orifice it is expected that the bounce can be eliminated.

B. The design of the control rod bearings was altered to render the bearings self-aligning. This was accomplished without an addition in the amount of stainless steel to the original design. The bearings operated satisfactorily during both normal cycling and during scramming cycling.

C. The control-rod latch operated as specified during cycling and scram. With the latch in the open position, the rod was easily lowered from the latch regardless of any misalignment between the two units. The center rod of the latch was removed since it did not aid in latch operation and could possibly cause a column load to be imposed on the rack.

D. The alignment of the rack backup roller was found to be critical. During scram the rack tends to cock and only close clearance between the rack and backup roller will prevent this. Since the rack is made of stainless steel and the backup roller of Stellite-3, a slight galling of the stainless steel rack occurred during the high speed scram tests. The portion of the rack which contacts the roller was re-ground and hard chrome plated. Data on the performance of the redesigned rack will be given in a future test report.

E. The acceleration during scram ranged from 6 to 20 ft/sec^2. This acceleration is not satisfactory. Friction of the clutch after voltage release is the greatest single factor in retarding the scram speed. The clutch electrical-release time ranged from 30 to 75 milliseconds. This time is satisfactory.

F. The driving motor as originally specified is too large and the resultant inertia causes rod coast. The coast in the down direction ranged from 3/8" to 3/4". A short development program was undertaken in an effort to achieve the fineness of control desired. The 100-watt Diehl motor was replaced with other motors of varying sizes. It was found that a 7 1/2-watt Diehl motor adequately lifted the rod and gave no perceptable coast. By actuating the down and off buttons in rapid succession it was possible to control the rod motion within 0.020 in. as specified.

13.6.3 Recommendations

A. It is believed that with the following three revisions a satisfactory scram can be attained.

1. The clutch should be mounted on the intermediate shaft adjacent to the seal shaft.

2. The clutch armature should be spring released.

3. The scram spring should be increased from 30 in.-pounds maximum torque to 75 in.-pounds maximum torque.

B. Although the desired fineness of control of the rod was achieved, it is felt that more development is necessary. The 7-1/2-watt motor does not have a sufficient factor of safety for a long-term operation. A larger motor augmented by a DC-braking system would seem to be a sounder solution to the problem.

C. The following provisions should be included in the final design:

1. The center rod should be removed from the latch

2. The back and sides of the rack which contact the backup roller should be hard chrome plated.

3. The control rod bearing should be redesigned.

D. The shock absorber design should be refined to eliminate the rod bounce following full scram.

13.6.4 Future Test Program Testing of the control rod and drive mechanism under operating conditions of temperature and pressure has already been initiated by the American Machine and Foundry Company. Fig. 70 shows the heating and pressure equipment already constructed for these tests. In addition to determining the characteristics of operation under these conditions, these tests will also determine the seal leakage, rack and gear wear, and durability of the mechanism. A report giving the results of these tests should be available in the near future.

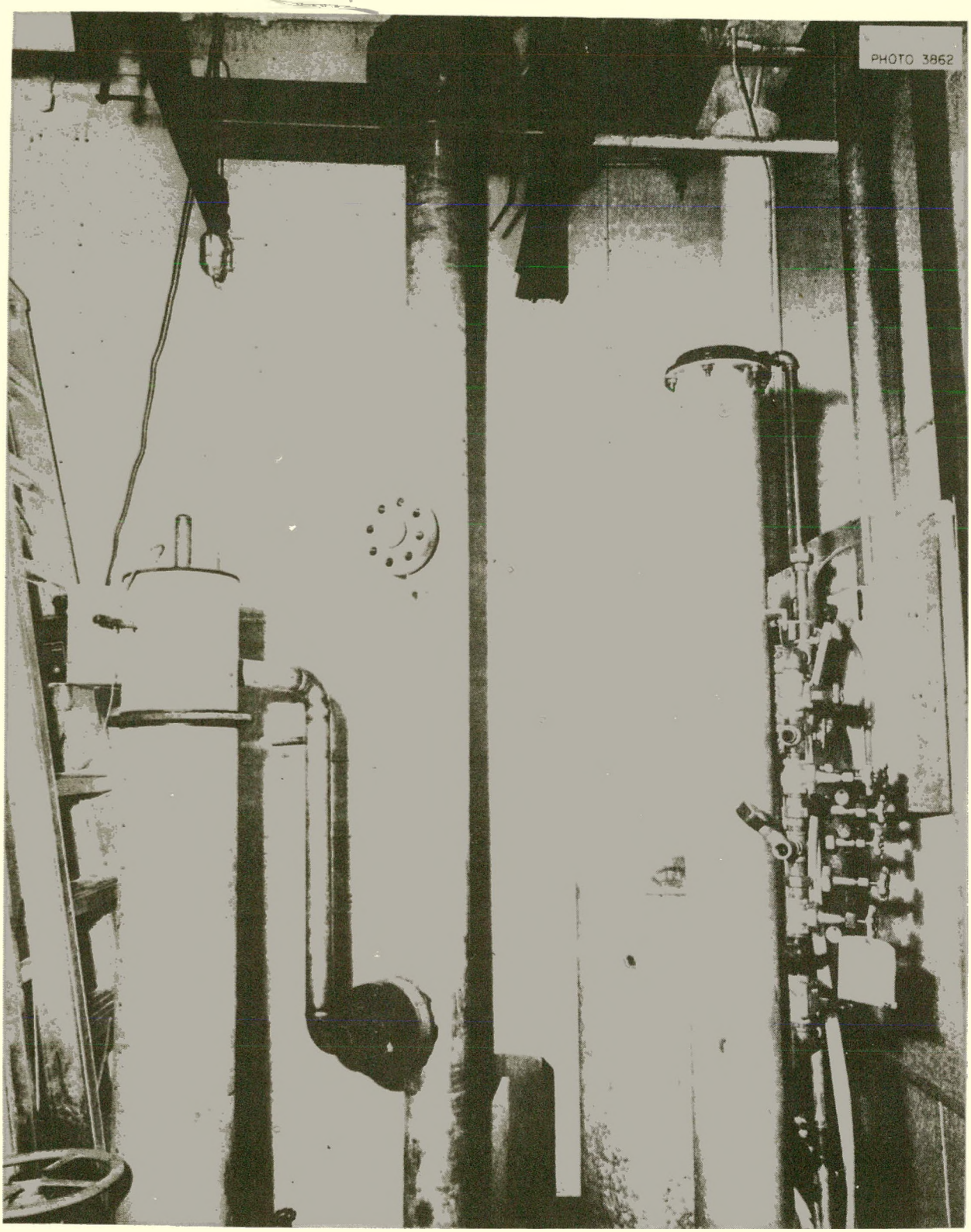

Fig. 70. Equipment for Control-Rod Tests.

320

13.8 APPENDIX E: LIST OF DRAWINGS

Dwg. No.	Title
TD-E-2426	Flow Diagram
TD-E-2418a	L-Sec thru Reactor Core and Vessel
TD-E-2417	X-Sec thru Core
TD-E-2390a	Fuel Assembly
TD-E-2425	Control-Rod Assembly
TD-E-2415	Grid Support Structure
TD-C-2433	Control-Rod Bearing, upper
TD-C-2434	Control-Rod Bearing, lower
TD-E-2411a	Pressure Vessel
TD-D-2457	Control-Rod Drive Arrangement
TD-D-2458	Control-Rod Drive Unit
TD-D-2450	Pressurizer
TD-E-2444	Steam Generator
AMF 77854-1	Control-Rod Drive Mechanism - General Assembly
AMF 77854-2	Control-Rod Drive Mechanisms - Sections
AMF 77854-3	Pressure Vessel and Control-Rod Drive Mechanism
TD-E-2423	Building Layout

321

13.9 APPENDIX F: SUPPLEMENTAL REACTOR AND SHIELDING CALCULATIONS

1.0 INTRODUCTION

Since the completion of the main body of this report, enough additional information has been obtained to warrant its presentation in this appendix. The program of calculations with the Univac and Oracle computers has yielded results which generally confirm and extend the results of the modified two-group calculations report in Chapter 5, page 122. In addition, the calculations of primary and secondary shielding requirements have been reviewed and revised somewhat, Chapter 6, page 147.

322

2.0 NUCLEAR CALCULATIONS

2.1 Methods Employed

Fuel and burnable poison requirements for the APPR were investigated by three methods. Results of the modified 2-group diffusion theory calculations were reported in Chapter 5, page 122. Calculations were also made by means of a 30-group, 9-region diffusion theory method, coded for the Univac; and by a 3-group, 3-region diffusion theory method, coded for the Oracle. The Univac program uses a technique, known as the Goertzel-Selengut method, in which moderating materials heavier than hydrogen are treated by a continuous slowing-down model, while for hydrogen, the correct slowing-down kernel is employed. The program has been applied to several spherical aqueous homogeneous critical assemblies, with excellent results. Because the program is applicable to spherical reactors only, an extensive investigation was made by the ORNL Reactor Calculations Group to determine, for a wide range of fuel concentrations, the radius of a spherical reactor which is critical at the same concentrations of materials as a given critical cylindrical reactor. Results of this investigation were used in the package reactor calculations.

A shortcoming of the Univac method is that it does not take into account the energy loss of neutrons by inelastic scattering. This process is rather important in the package reactor, since the core contains about 200 kg of stainless steel. Inelastic scattering was considered in the modified 2-group and 3-group calculations, and the magnitudes of its effects on reactivity and on critical mass were estimated. It is,

323

therefore, possible to apply inelastic scattering corrections to the results of the Univac calculations.

The three-group Oracle code requires, as input data, group constants for each of the three groups in each region of the reactor. The methods used to calculate the constants are described in ORNL-1613, in connection with the modified two-group method.

2.2 Criticality Calculations

Values of several important quantities, obtained by the three methods described above, are presented in Table I.

TABLE I: COMPARISON OF THREE CALCULATIONS

Quantity	Univac	Oracle	Modified 2-Group
Critical mass, for cold, clean reactor	8.03 kg	7.40 kg	7.26 kg
Critical mass for hot reactor, end-of-cycle (fission products for 15 Mw-yr), and peak xenon	10.60 kg	10.35 kg	10.16 kg
Initial loading, U^{235}	18.10 kg	17.85 kg	17.7 kg
Mass of B^{10} required for criticality; hot reactor, beginning of cycle, peak xenon	38.18 g	34.9 g	32.4 g
Multiplication factor, k, of cold reactor, beginning of cycle, no xenon	1.0625	1.0888	1.096

It should be pointed out that these results are not all completely independent, since essentially the same input data were used in both the 3-group Oracle calculation and the modified 2-group calculations.

While the results given in Table I are not in serious disagreement, there are discrepancies of a few percent which can perhaps be related qualitatively to limitations in one or another of the methods. To facilitate the comparison, Table II gives the effective multiplication factors of a few cases, as calculated by each method.

TABLE II: MULTIPLICATION FACTORS CALCULATED BY THE THREE METHODS

Reactor Condition	M (U^{235})	M (B^{10})	Multiplication Factors		
			Univac*	Oracle	Modified 2-Group
Cold, clean, critical	8.03 kg	0	1.000	1.030	1.044
Hot, end-of-cycle	10.60 kg	0	1.000	1.001	1.015
Hot, beginning-of-cycle, peak xenon	18.10 kg	38.18 g	1.000	0.985	0.971
Cold, beginning-of-cycle, no xenon	18.10 kg	38.18 g	1.0625	1.078	1.067

*Corrected for inelastic scattering

The modified 2-group method gives a multiplication factor which is: (1) about 4% higher than the Univac calculation for the cold, clean, critical case, (2) about the same as Univac for the hot, poisoned case, and (3) about 3% lower for the hot, fully loaded case. It is believed that the discrepancy in the first case is chiefly due to neglect, in the modified 2-group method, of resonance neutron absorptions in water and steel, which would over-estimate the fraction of resonance neutrons absorbed in fuel. This is not an inherent defect of the method but only of the way in which it was applied. The corrected Univac calculation is believed to be the best estimate of the cold, clean, critical mass. In the hot, end-of-cycle case, the over-estimate in the resonance multiplication factor is offset by the discrepancy in reactivity change of the

reactor between room temperature and operating temperature. In the hot, beginning-of-cycle case, resonance absorptions in boron were taken into account in the modified 2-group method, thus the error in resonance multiplication factor is much smaller. The discrepancy in k_{eff} is, then, primarily a consequence of the small reactivity change from room temperature to operating temperature in the 30-group method.

Allowing 3 percent for the effect of xenon, the reactivity change between 68° F and 450° F is about 3 percent by the Univac method, and about 6 percent by the other methods. The reasons for this difference are not apparent; but, it throws doubt on the calculation of the temperature coefficient of reactivity. The temperature coefficient was calculated, by the Univac method, by varying the temperature of the beginning- and end-of-cycle cases 10° C from operating temperature. The value found in each case was $dk/dt = -2.2 \times 10^{-4}/°F$; this may be regarded as a lower limit in magnitude.

2.3 Flux Distributions

The neutron flux distributions obtained in the Oracle 3-group calculations are shown in Figs. 1 and 2. A comparison of thermal fluxes obtained by Oracle and Univac methods is given in Fig. 3.

2.4 Derivatives of k_{eff} with Respect to Various 3-Group Constants

In order to make small corrections to the calculations reported here and to estimate the accuracy to which the group constants should be known, the 3-group, 3-region Oracle code was used to determine the derivatives of k_{eff} with respect to various group constants. The k_{eff} was computed at the design point and at a point corresponding to a ±10% change of each group

326

ORNL-LR-Dwg. 3610

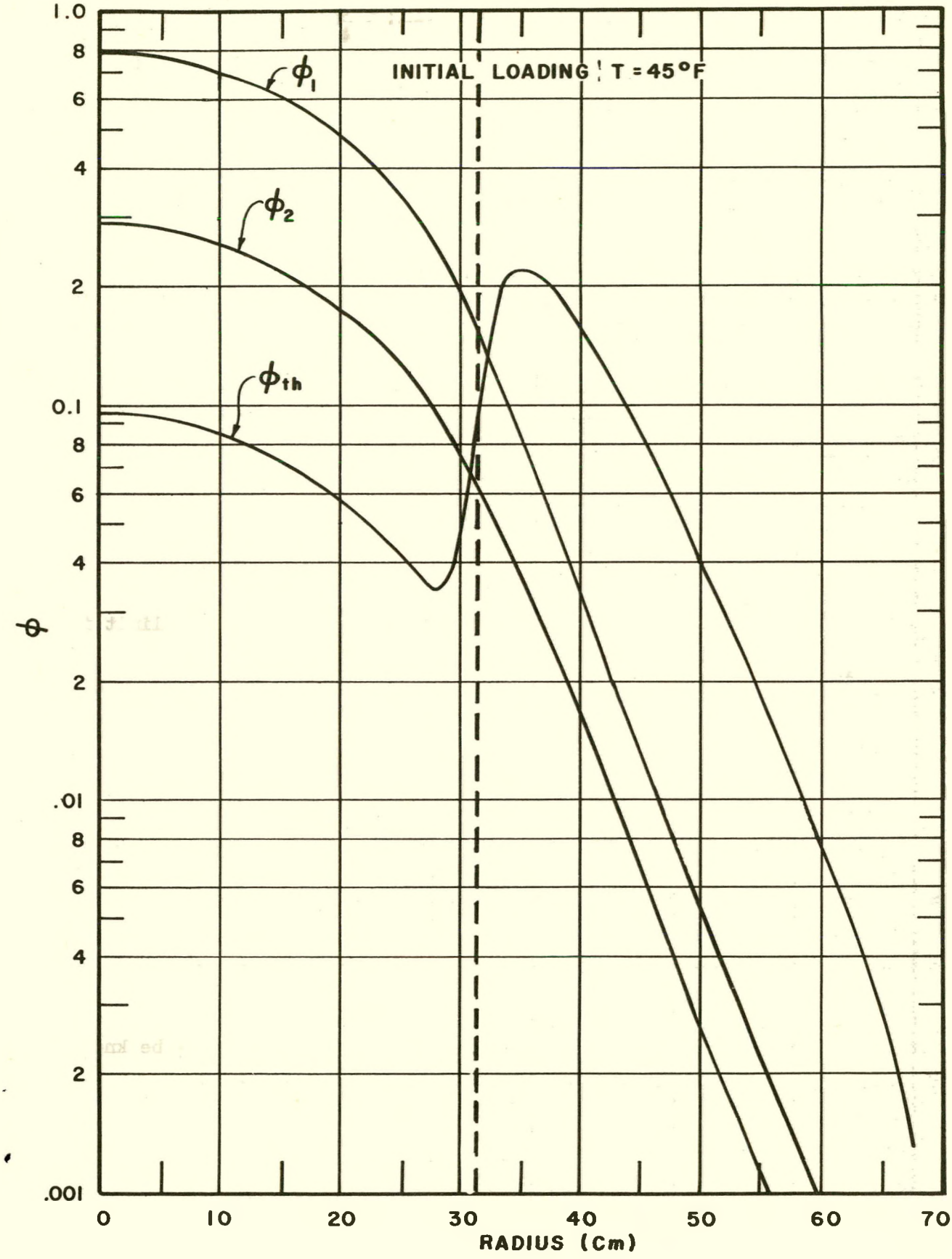

FIG. 1 FLUX DISTRIBUTION (ORACLE 3-GROUP)

ORNL-LR-Dwg. 3611

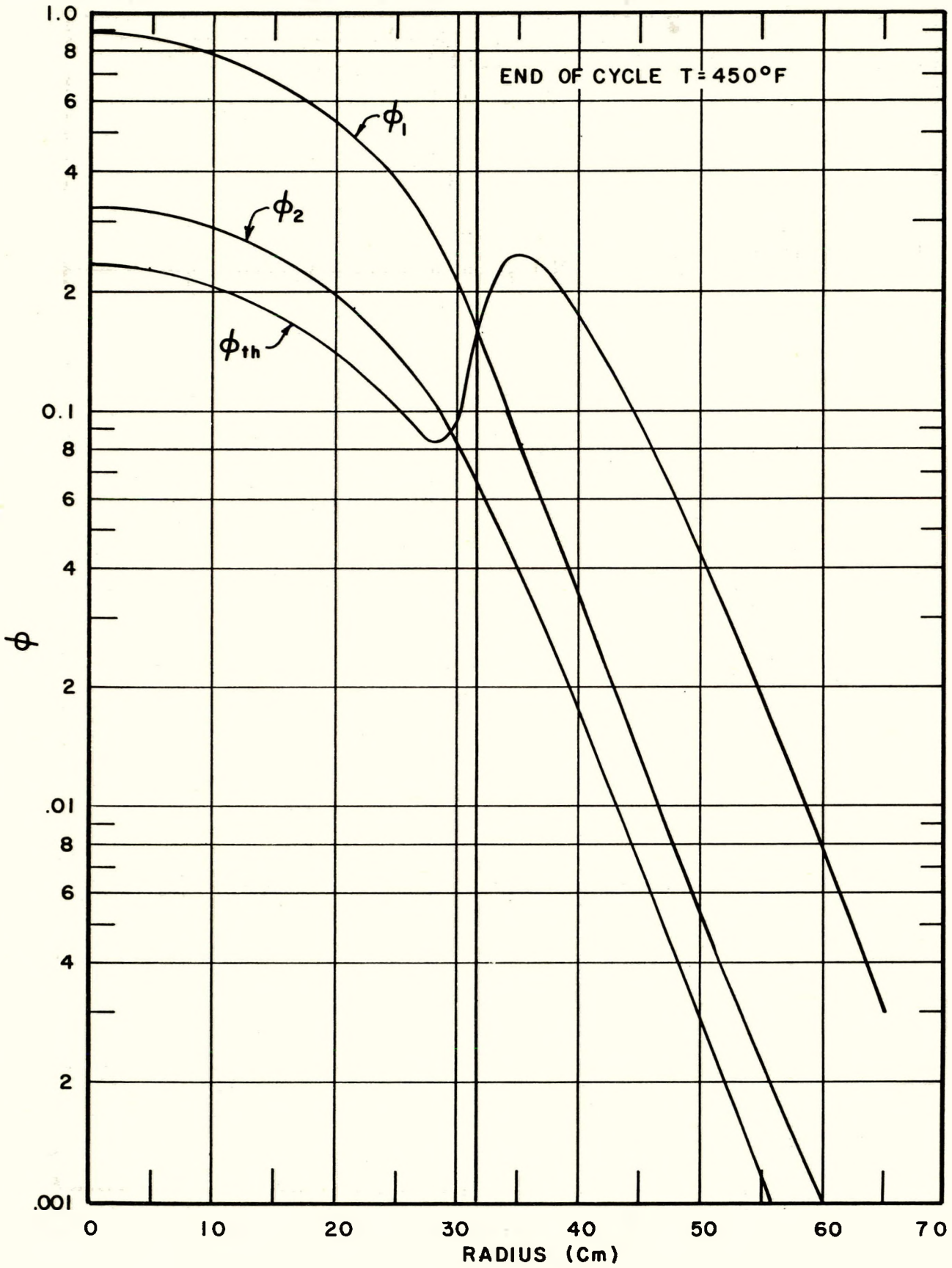

FIG. 2 FLUX DISTRIBUTION (ORACLE 3-GROUP)

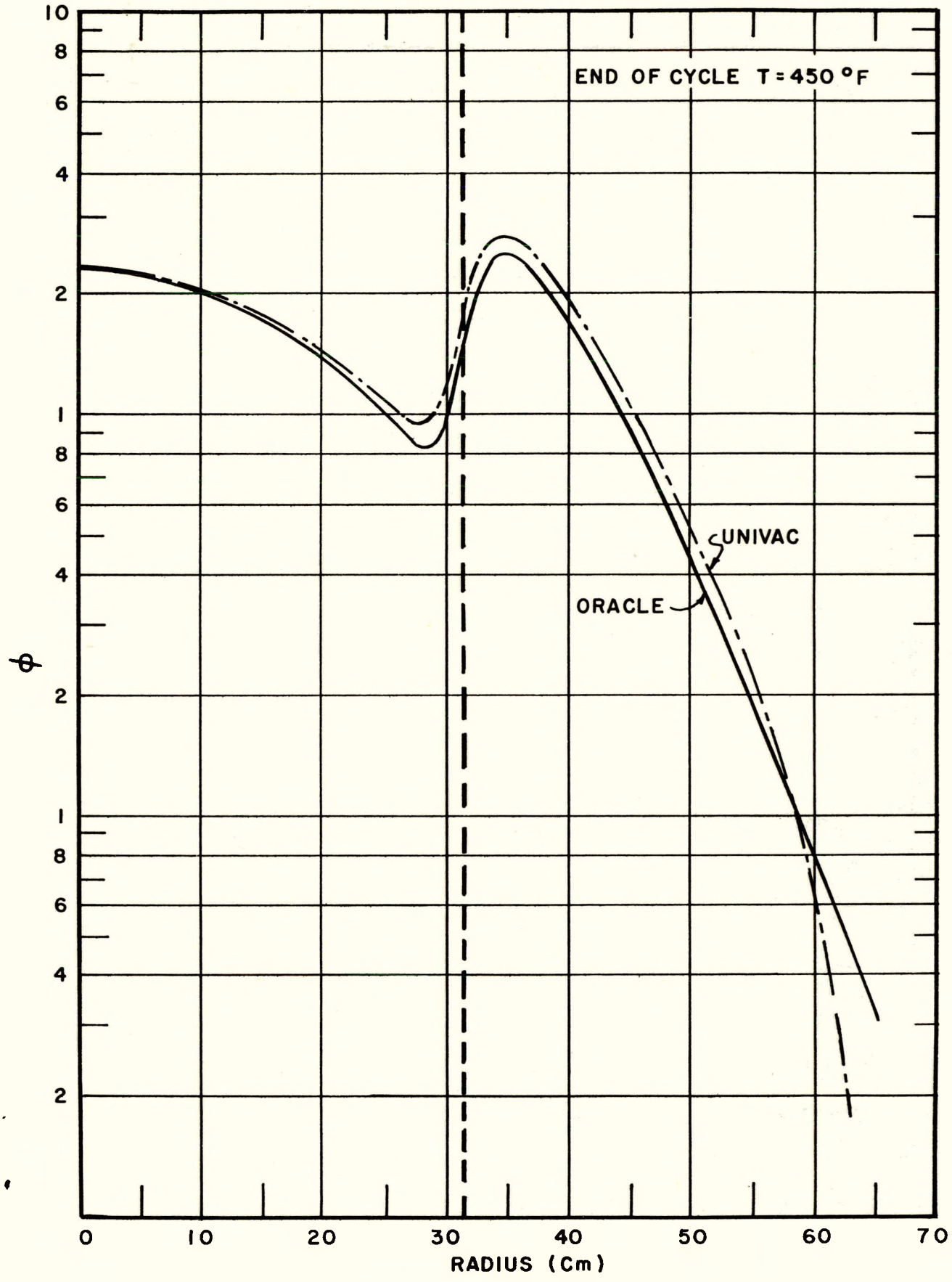

FIG. 3 THERMAL FLUX DISTRIBUTION

329

constant, varied one at a time. The design point is 10.35 kg of U^{235}, no boron, fission products for 15 Mw-yr, temperature 450° F, at which point $k_{eff} = 1.00257$. It is assumed that $k_{eff} = F(\tau_{1c}, \tau_{2c}, D_{1c}, D_{2c}, \tau_{1r}, \tau_{2r}, D_{1r}, D_{2r}, M^{235})$, where τ is the age, and D is the diffusion coefficient. The first subscript indicates the group and the second indicates the region (core or reflector). Table III gives the value of the coefficient

$$P = \left(\frac{\partial k}{\partial x}\frac{x}{k}\right)$$

where x represents one of the variables above.

Table III: DERIVATIVES OF k_{eff}

x	$\frac{\partial k}{\partial x}\frac{x}{k}$	Value of x at Design Point
τ_{1c}	-0.207	43.1 cm^2
τ_{1r}	+0.0106	40.6 cm^2
D_{1c}	+0.0687	1.71 cm
D_{1r}	-0.0689	2.40 cm
M^{235}	+0.353	10.35 kg
τ_{2c}	-0.0397	5.77 cm^2
τ_{2r}	+0.00748	4.98 cm^2
D_{2c}	+0.0135	0.60 cm
D_{2r}	-0.0135	0.647 cm

The dependence of k_{eff} on fuel and poison content at 450° F and at 68° F is shown in Fig. 4. Although these curves were computed for a 31.5-cm-radius sphere, the mass of U^{235} indicated by the abscissa is the correct value for the cylinder of 139.5 liters volume.

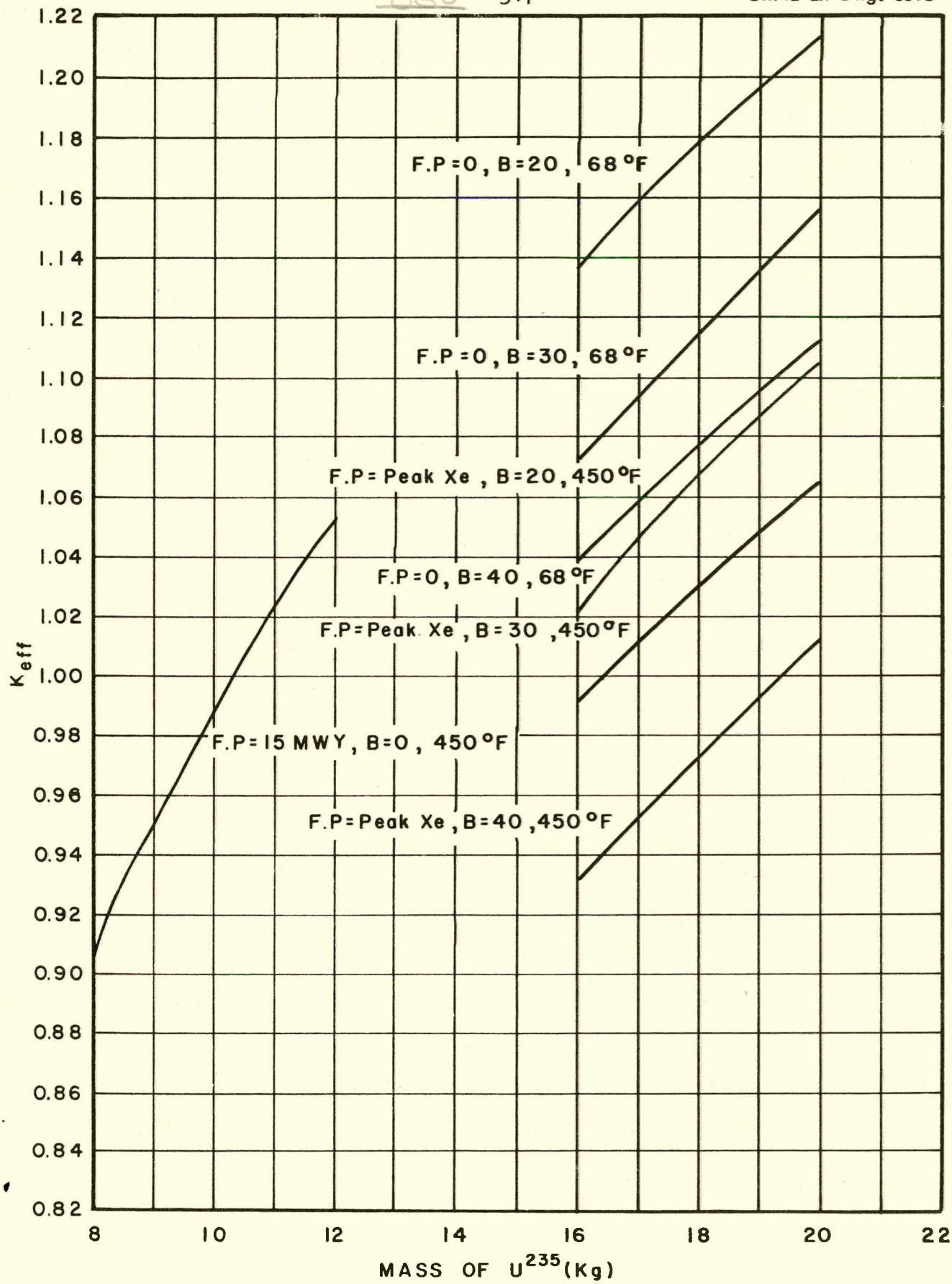

FIG. 4 K_{eff} vs MASS OF U^{235} (ORACLE 3-GROUP CODE)

331

2.5 Control Rod Effectiveness

The worth of a central control rod was determined by using the 3-region, 3-group code on the Oracle. The model used for this calculation consisted of four concentric cylindrical regions: a central water region, a thin shell of boron, the fuel region, and the water reflector. The thin shell of boron is treated by transport theory and the remaining regions are treated by diffusion theory. Concentrations appropriate to the reactor at 7.5 Mw-yr and 68° F were used. Table IV contains the results of this calculation. In order to compare with the method in ORNL-1613, par. 5.4, the worth for a case where the boron shell is completely transparent to second-group neutrons and the worth for a shell completely black to second-group neutrons were computed. In both cases the shell was assumed transparent to fast-group neutrons and black to thermal-group neutrons.

It is felt that the value $\Delta\rho = 0.0674$ for a 4.4-cm rod, semi-transparent to resonance neutrons, is the best available value for the worth of the central rod. Since the maximum reactivity expected is $\rho = 0.138$, even the smallest value indicates that the system of rods described in ORNL-1613 should be adequate to shut down the reactor at the peak reactivity.

The 3-group flux distributions in the reactor with a central control rod are shown in Fig. 5. The importance of the moderator in the rod interior is revealed both by the slope of the fast-group flux at the rod boundary, and by the large accumulation of thermal neutrons inside the rod. These neutrons will, indeed, contribute more to heating and depletion of the control rod than will thermal neutrons from the fuel region of the core.

6

TABLE IV: COMPARISION OF CALCULATIONS OF CONTROL ROD EFFECTIVENESS

Method	Rod Radius (cm)	Transparency to 2d-group neutrons	k	Δk	Δρ*
Oracle	No rod	--	1.1570	--	--
Oracle	4.0	Semi-transparent	1.0825	-0.0745	-0.0595
Oracle	4.4	Semi-transparent	1.0733	-0.0837	-0.0674
Oracle	4.8	Semi-transparent	1.0643	-0.0927	-0.0753
Oracle	4.8	Black	1.0547	-0.1023	-0.0838
Oracle	4.8	Transparent	1.0761	-0.0809	-0.0650
ORNL-1613	4.4	Transparent	--	-0.059	-0.0557
Nordheim-Scallettar	4.4	Transparent	--	-0.109	-0.098
Estimate from Oracle, above	4.4	Transparent		-0.0719	-0.0571
Estimate from Oracle, above	4.4	Black		-0.0933	-0.0759

* $\Delta\rho = \frac{k - k_o}{k\, k_o}$ where $k_o = 1.1570$, except for ORNL-1613 and N-S results; for these $k_o = 1 + (\Delta k)$, and $k \leq 1$.

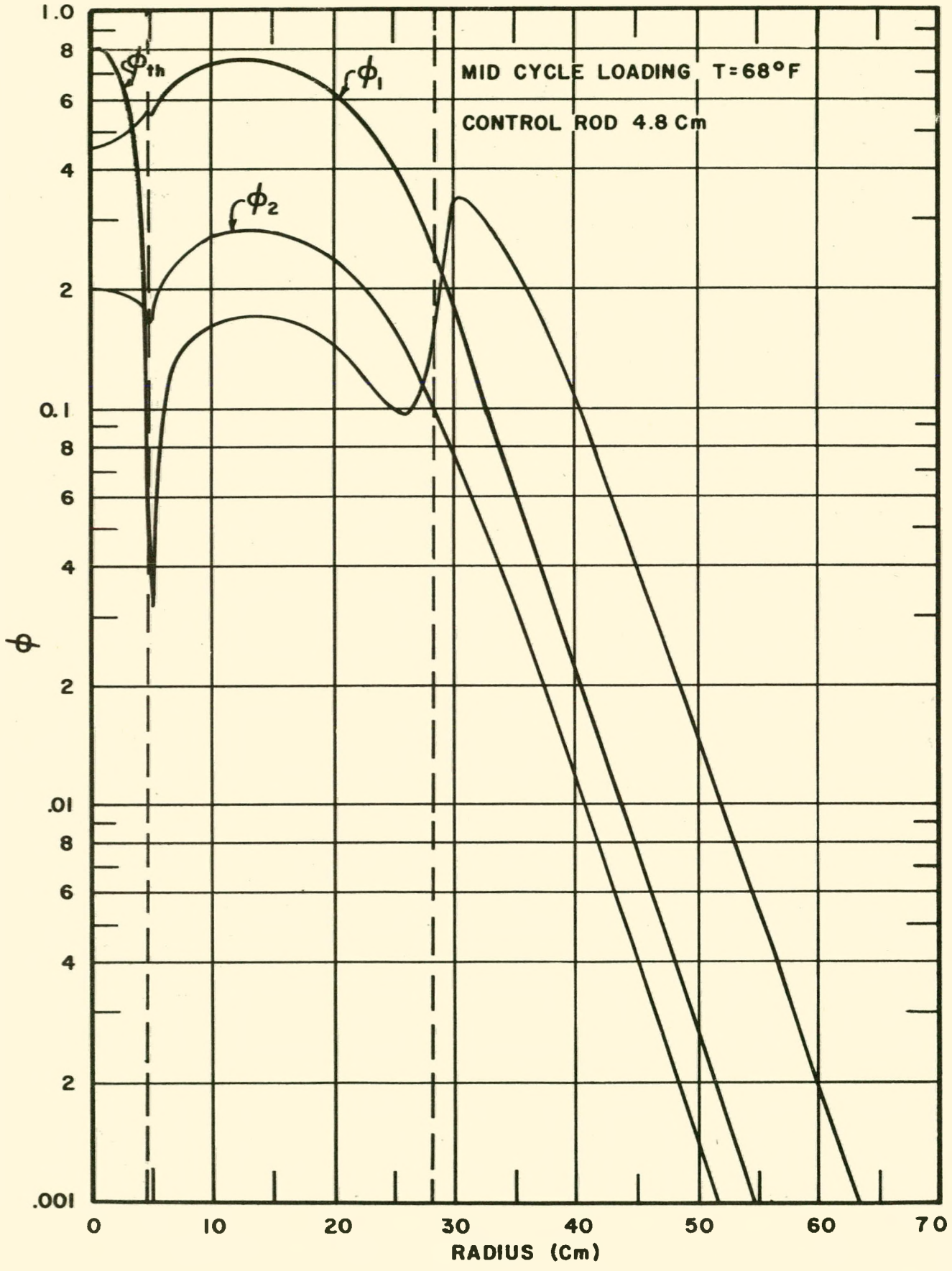

FIG. 5 FLUX DISTRIBUTION (ORACLE 3-GROUP)

The method of control rod calculations for one rod described in ORNL-1613 has now been extended to a system of several rods, including a central rod and a ring of eccentric rods. For the package power reactor the worths of several configurations of rods are shown in Table V; the earlier results quoted in ORNL-1613 are also reproduced here for comparison.

It will be remembered that the peak reactivity excursion expected at room temperature and without xenon is $\Delta\rho = (0.16)/(1.16) = 0.14$. Although this estimate of the worth of all rods is somewhat lower than that given in ORNL-1613, it still appears that the rods are adequate to shut down the reactor at any time.

2.6 Additional Results from Univac

The multigroup calculations provide much information that may be useful in evaluating the applicability of simpler methods.

Calculation of the fast-group diffusion coefficient in 2-group theory involves the assumption that the space dependence and energy dependence of the slowing-down neutron flux are separable (cf. ORNL-1613, p. 127). The validity of this assumption may be seen in Fig. 6, which gives normalized spatial distributions of several energy groups of neutrons.

The flux distributions (not normalized) for several energy groups in the reflector are given in Fig. 7. These may be used to compute the relaxation lengths of fast neutrons in the reflector. The downward curvature of the fluxes beyond about 55 cm is a result of the condition that the fluxes vanish at the outer boundary, at 63 cm. The straight middle portion should be used for computing relaxation lengths.

335

TABLE V: CONTROL ROD EFFECTS

Configuration	Δk(1)	$\Delta\rho$(2)	Σ(3)	$\frac{\Delta\rho}{\Sigma}$	$\Delta\rho$ ORNL-1613
1 eccentric rod	0.026	0.025			
1 central rod	0.058	0.055			0.056
2 eccentric rods, opposite	0.068	0.064	0.050	1.28	
2 rods, central and eccentric	0.099	0.090	0.080	1.13	
3 eccentric rods(4)	0.118	0.106	0.075	1.41	
2 eccentric rods opposite plus central rod	0.147	0.128	0.105	1.22	
4 eccentric rods	0.171	0.146	0.100	1.46	
3 eccentric(4) rods plus central rod	0.188	0.158	0.130	1.22	
4 eccentric rods plus central rod	0.241	0.194	0.155	1.25	0.210

(1) $\Delta k \equiv \frac{k}{k_o} - 1$

where k_o is the infinite multiplication factor of the critical reactor with no control rod; k is the infinite multiplication factor of the reactor with no control rod, but with the concentration of fuel that is critical with the given configuration of rods.

(2) $\Delta\rho = \frac{\Delta k}{1 + \Delta k} = \frac{k_{eff} - 1}{k_{eff}}$

(3) Σ is defined as the sum of the worths of the rods in the given configuration taken individually, i.e., without interference effects.

(4) Because of the formulation of the theory, these three rods are located at the vertices of of an equilateral triangle, rather than as in the design reactor.

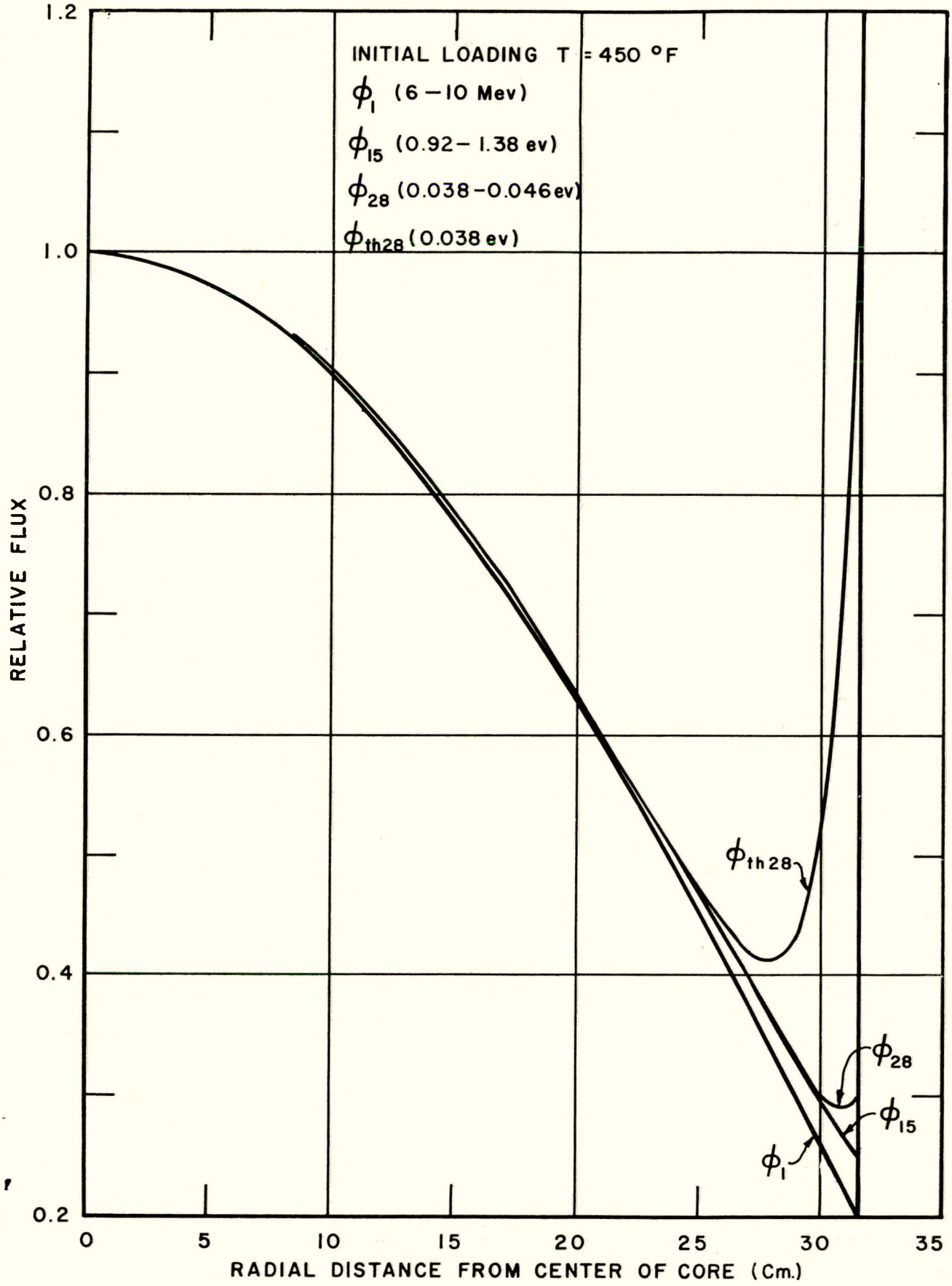

FIG. 6 FLUX DISTRIBUTIONS (UNIVAC 30-GROUP)

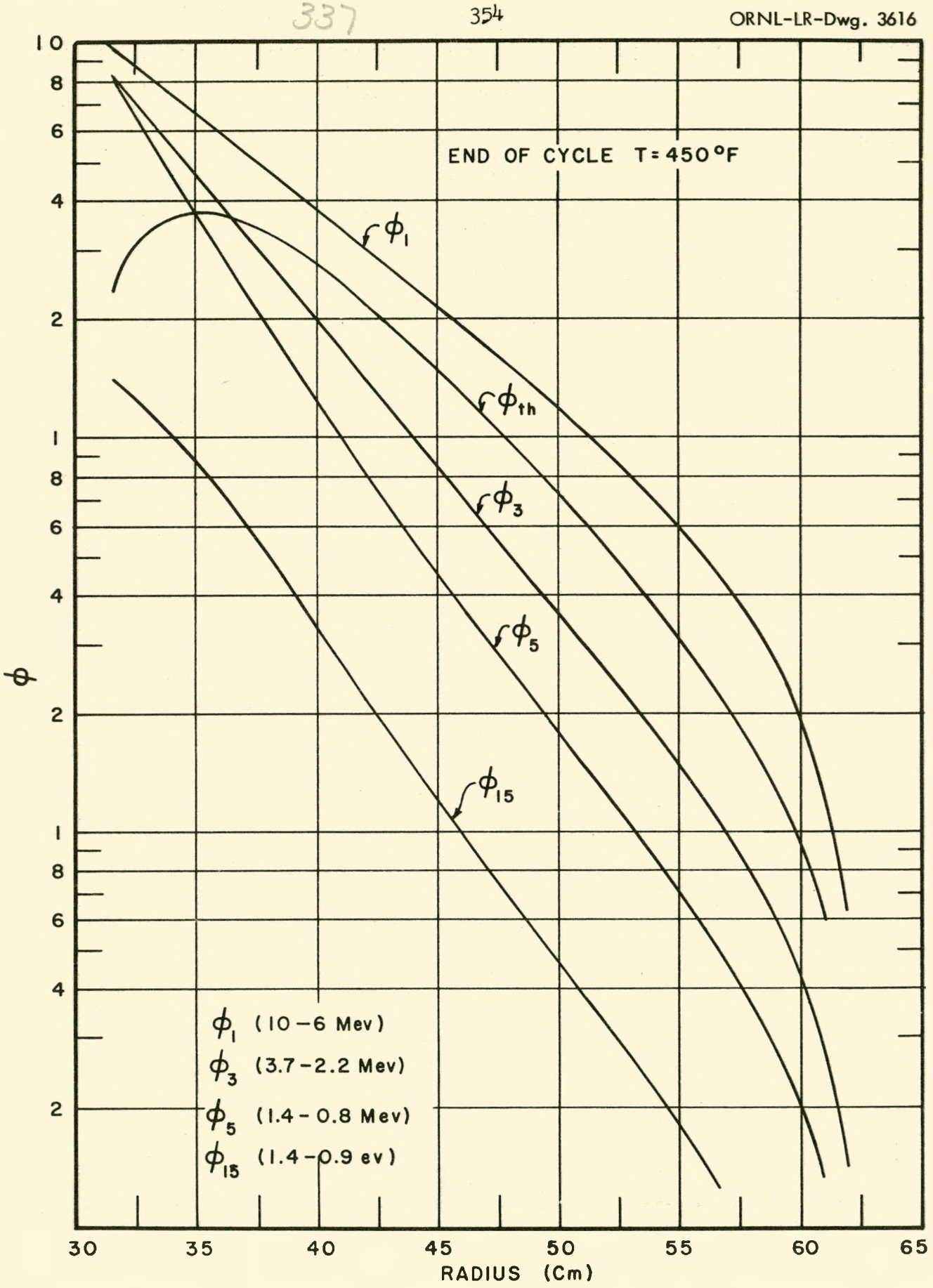

FIG. 7 FLUX DISTRIBUTION (UNIVAC 30-GROUP)

An important question in heat transfer considerations is the extent to which the power (fissioning) distribution follows the thermal flux distribution. Figs. 8 and 9 give these distributions at the beginning and at the end of the operating cycle; uniform fuel and poison distributions are assumed. While there are relatively fewer resonance fissions near the core-reflector boundary than at the center, the thermal flux distribution appears to be a reasonably good representation of the power distribution.

It is also of interest to know the distribution of fission-producing neutron absorptions as a function of neutron energy. The lethargy distributions of fission, at the beginning and at the end of the operating cycle, are shown in Fig. 10. It should be noted that fissions produced by thermal-group neutrons are not plotted. The upper histogram thus, represents only 32 percent of the fissions and the lower histogram only 21 percent of the fissions.

2.7 Non-Uniform Burnup of Uranium and Boron

The 30-group, 9-region Univac code was used to determine very approximately the distribution of fuel and boron in the reactor after various times of operation. The following procedure was used: (1) At first, the fuel and boron were loaded uniformly (so that the concentrations in all eight inner regions were the same, the ninth region was the water reflector); (2) the flux and k_{eff} were computed; and (3) the concentration for the next run was determined from the formula

$$N^{235}_{\ell\, j} = N^{235}_{\ell-1,j}\left[1 - \Delta \int_0^{th} \bar{\phi}_{\ell-1,j}(u)\, \sigma_a^{235}(U)\,du\right]$$

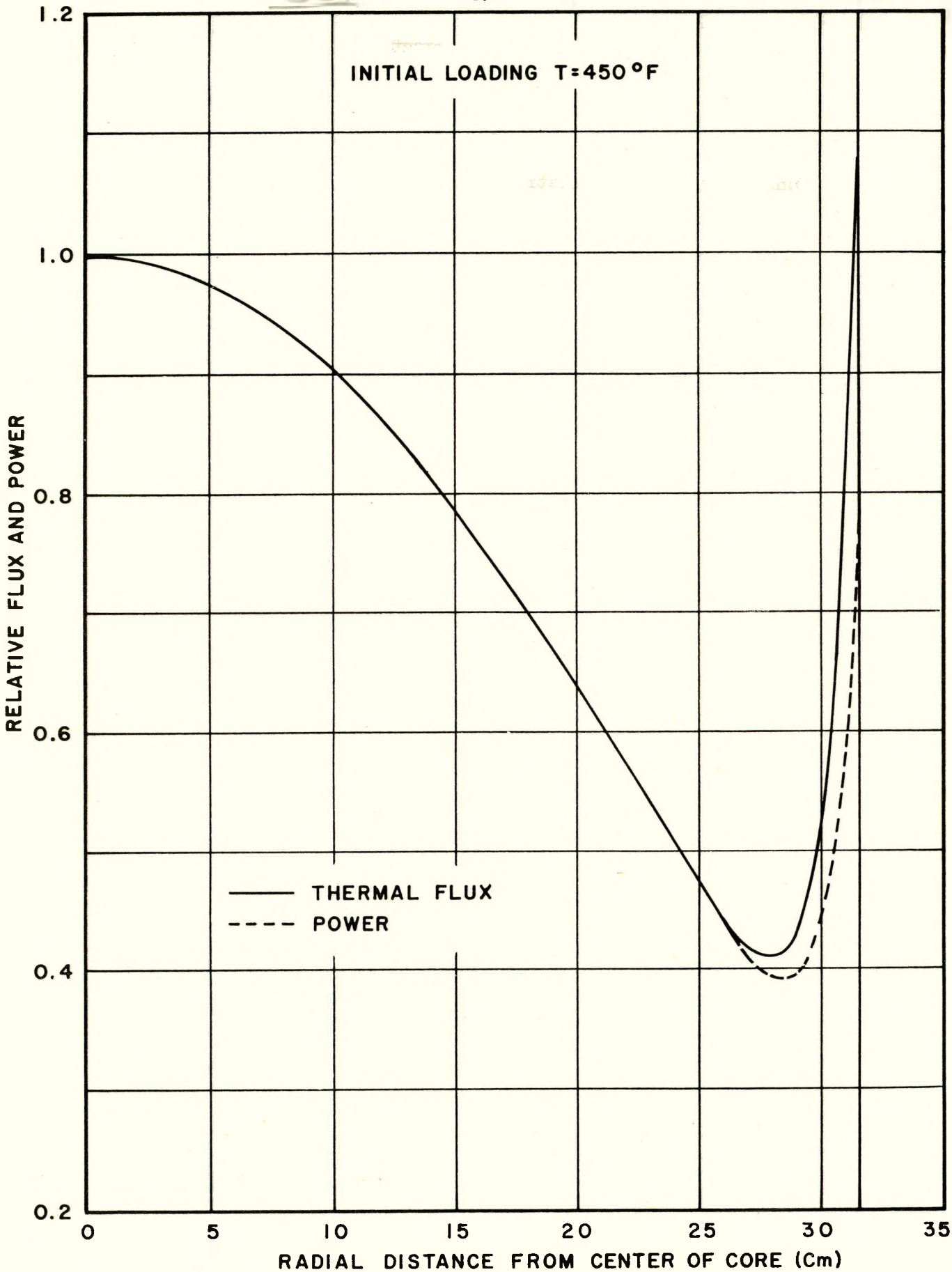

FIG. 8 THERMAL FLUX AND POWER DISTRIBUTION (UNIVAC 30-GROUP)

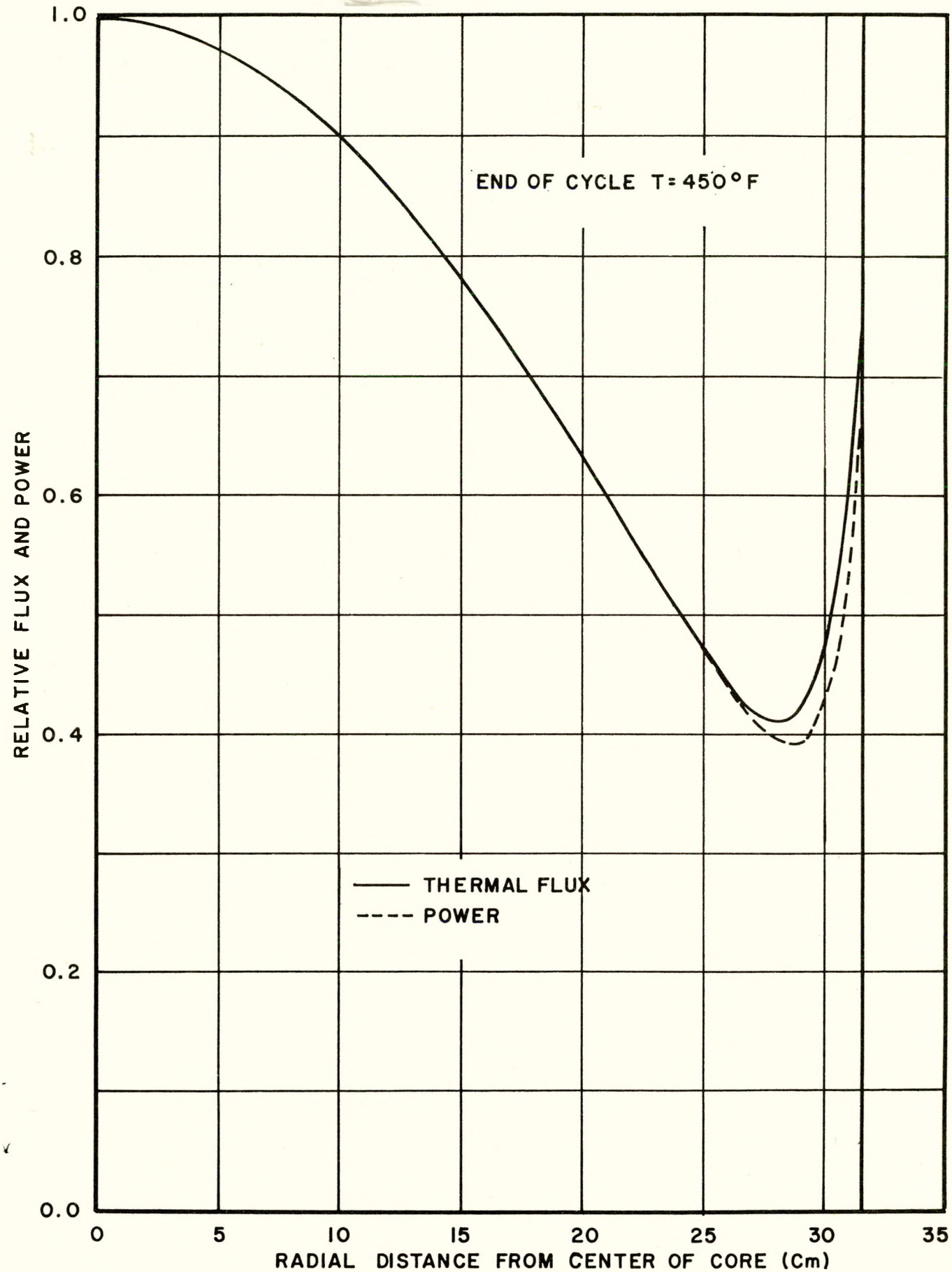

FIG. 9 THERMAL FLUX AND POWER DISTRIBUTION (UNIVAC 30—GROUP)

ORNL-LR-Dwg. 3619

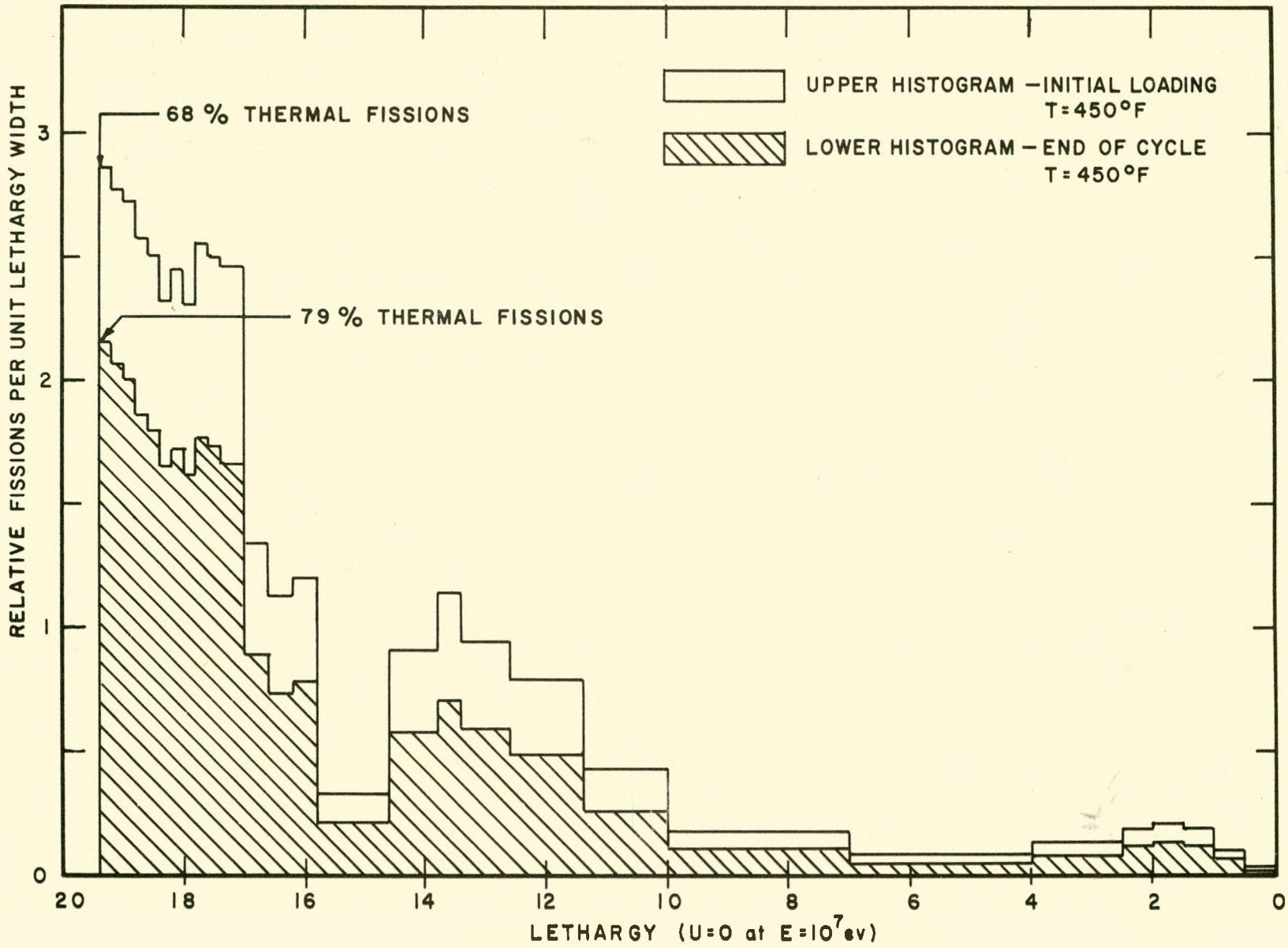

FIG. 10 FISSION DISTRIBUTION (UNIVAC 30-GP)

342

and a similar formula for boron, where ℓ indicates the run, j the region, $\bar{\varphi}$ the value at the midpoint of the region, and Δ a constant proportional to the time of operation between computations.

The results of this computation should be used with care in predicting the actual behavior of a reactor. The model for this computation differs from the actual reactor in the following important ways:

1. The effect of control rods on the flux distribution was neglected.
2. The reactor was assumed to be spherical.
3. The buildup and burnout of fission products was neglected.

Because of the large departure from uniform loading shown in Fig. 11, the previous calculations of critical mass at the end of the operating cycle, which were made by assuming uniform distribution of all constituents of the core, probably underestimate the true critical mass. Thus, the design reactor may be expected to operate a somewhat shorter time before refueling is necessary than the results of ORNL-1613 indicate.

The distribution of U^{235} and B^{10} at various times during the operating cycle are shown in Figs. 11 and 12. The numbers on each curve is the fraction of design life (15 Mw-yr) elapsed when that distribution prevails. The left-hand scale indicates the fraction of original density remaining.

The k_{eff} is shown in Fig. 13 as a function of time at 6-Mw power for the non-uniform burnup problem. This curve has a higher maximum than is expected in the real reactor because of the neglect of fission-product poisoning buildup.

The power density distribution is shown in Fig. 14 for three points during the operating cycle. Initially this distribution becomes more

343

ORNL-LR-Dwg. 3620

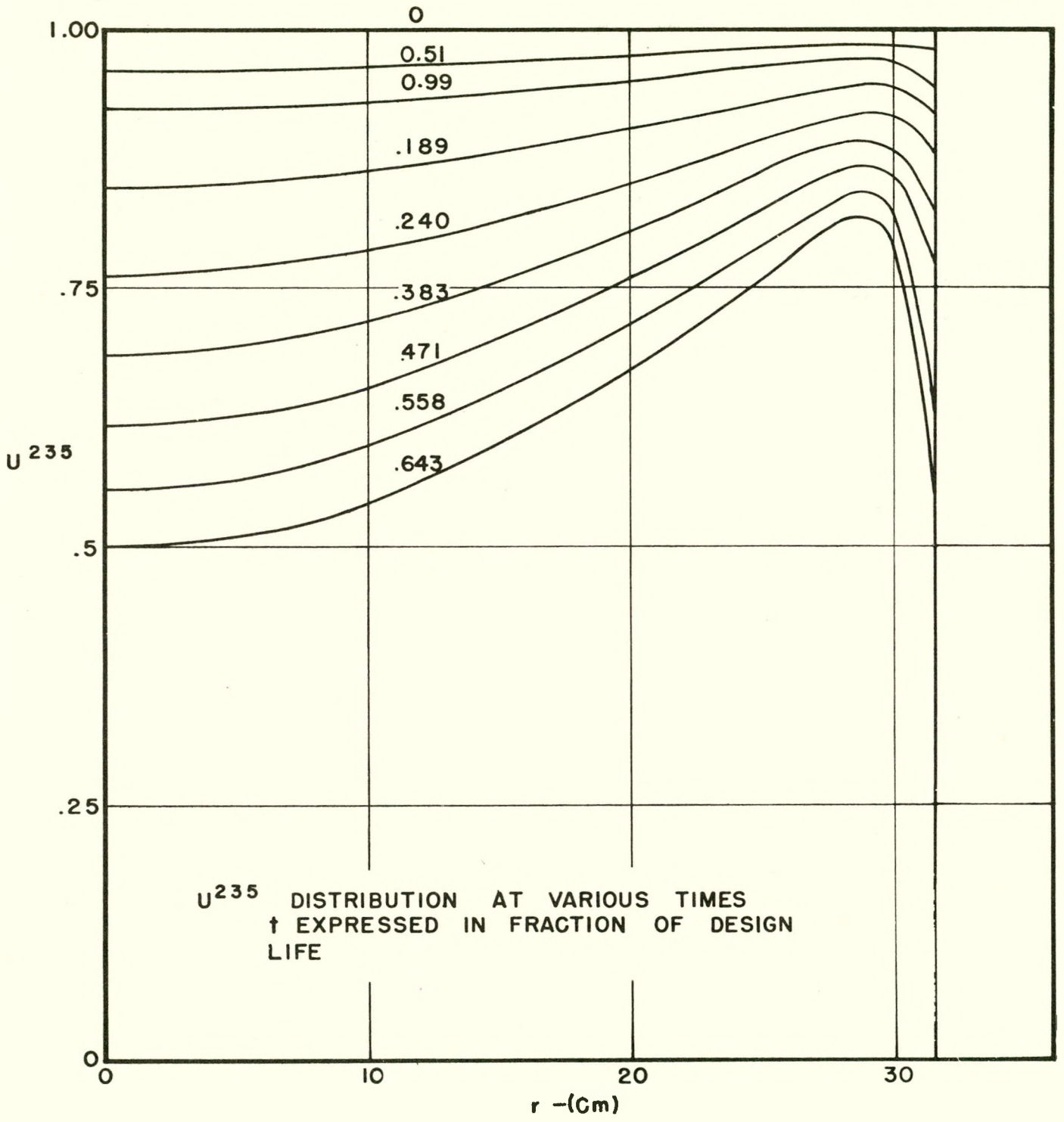

FIG. 11 NON-UNIFORM BURN-UP (UNIVAC 30-GROUP)

344

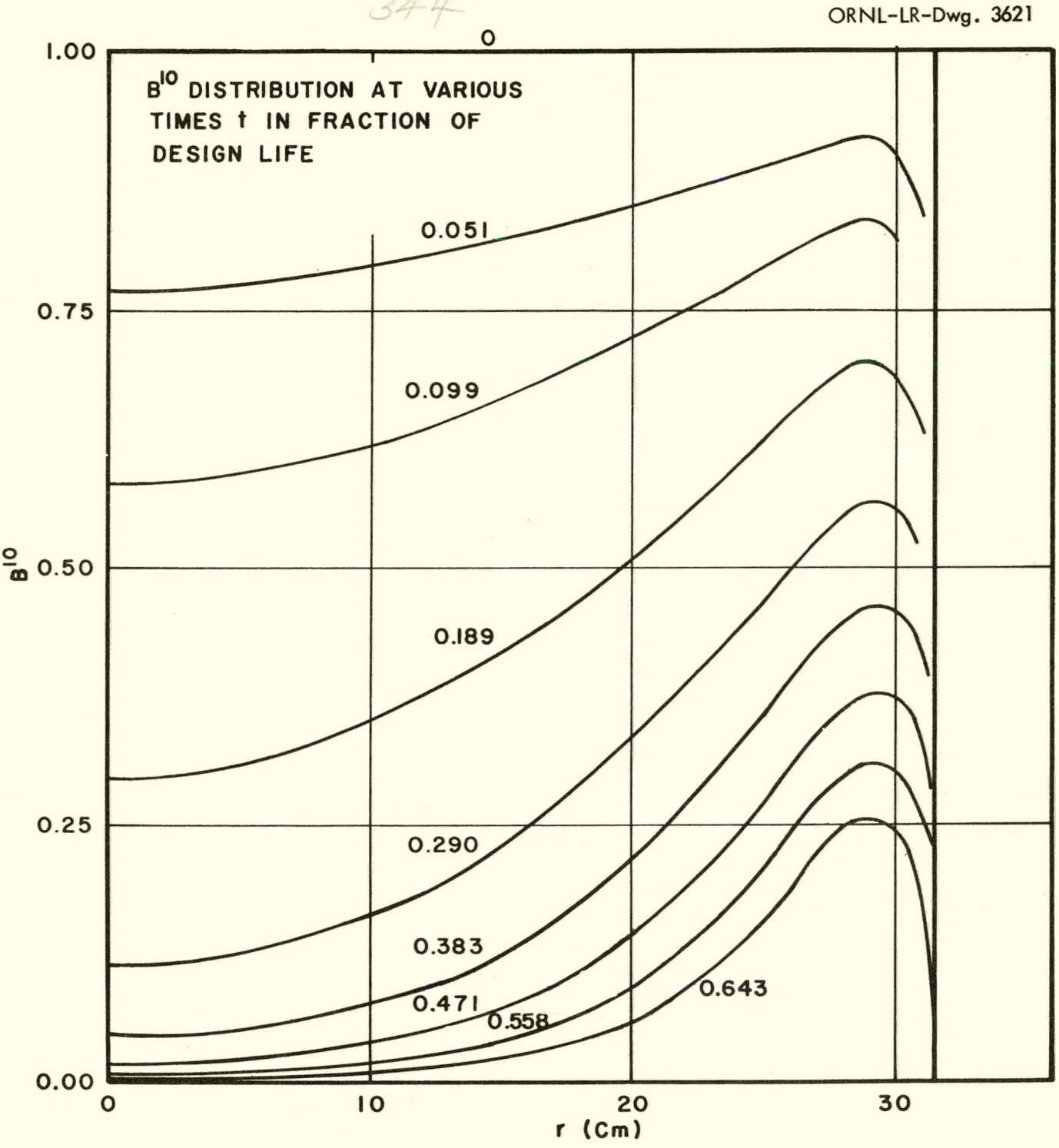

FIG. 12 NON-UNIFORM BURN UP (UNIVAC 30-GROUP)

ORNL-LR-Dwg. 3622

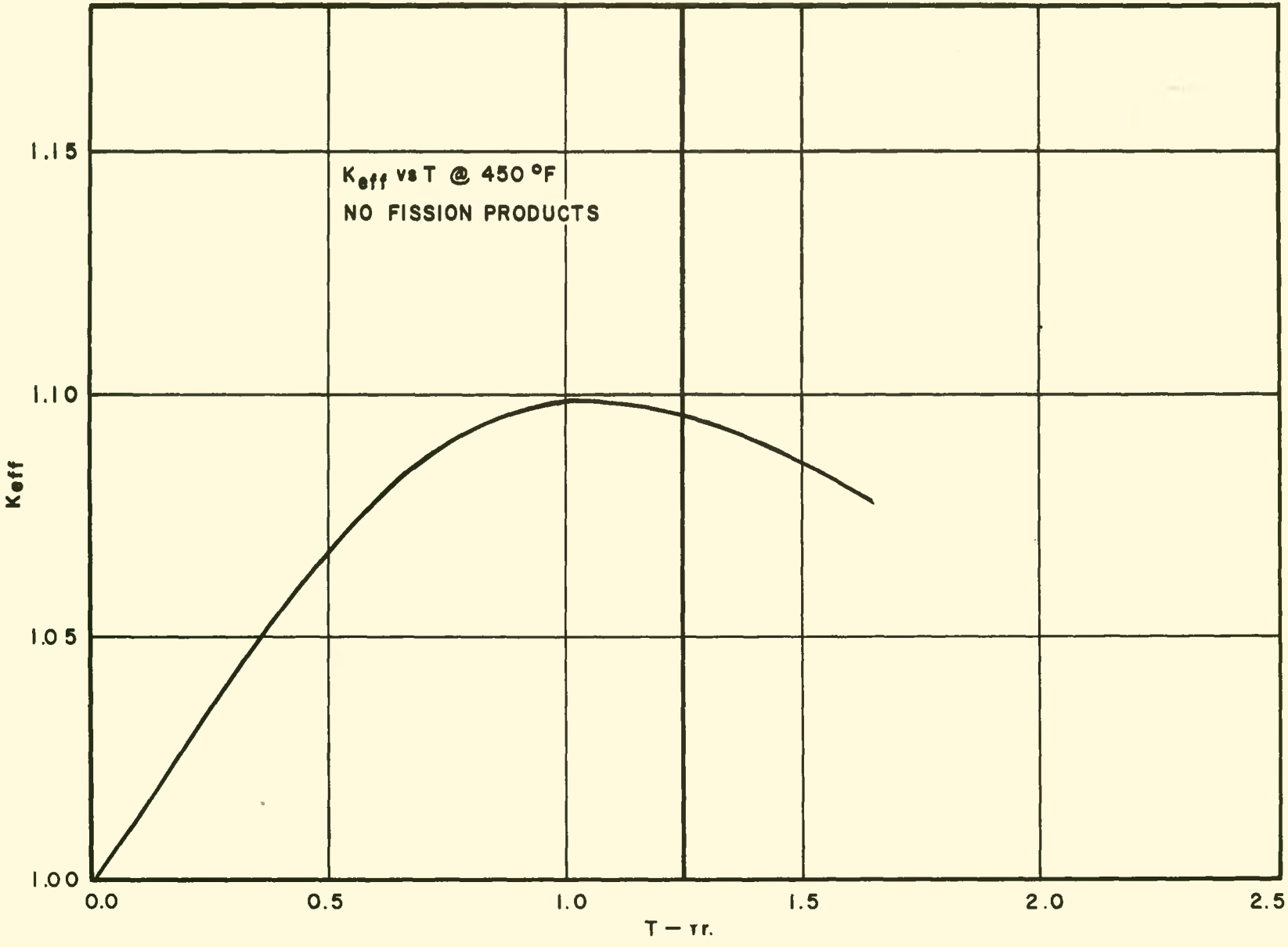

FIG. 13 NON-UNIFORM BURN UP (UNIVAC 30-GROUP)

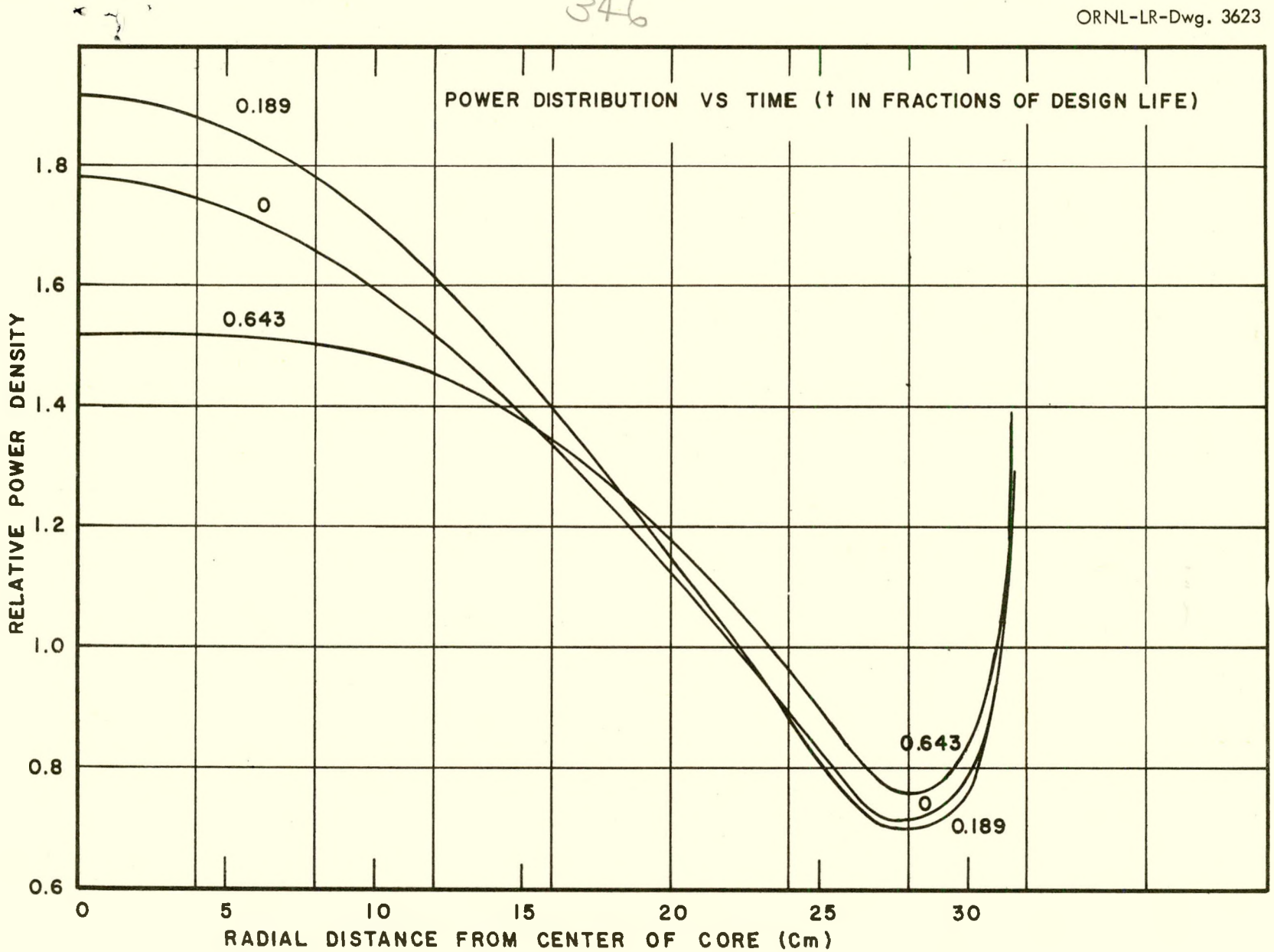

FIG. 14 NON-UNIFORM BURN UP (UNIVAC 30-GP)

peaked at the center because of the rapid burnout of B^{10}; then, the distribution becomes progressively flatter as the U^{235} burns out in the central high flux region. All three curves in Fig. 14 are normalized to the same total power.

3.0 SHIELDING CALCULATIONS

348

The calculations for the biological shield around the package reactor were reviewed. The new calculations differ from those reported in Chapter 6, page 147 in the following respects:

(1) The absorption coefficient, in ordinary concrete, of 7-Mev gamma rays (the controlling radiation in determining the biological dose rate outside the shield) was re-evaluated. The value now being used is 0.059 cm^{-1}, instead of 0.073 cm^{-1}. The larger value was based on barytes concrete, with a density correction; the present value is based on aluminum, for which excellent experimental results are available and which, because its atomic number is close to the effective atomic number of concrete, should have approximately the same mass absorption coefficient.

(2) In the earlier calculations, dose buildup factors in concrete were approximated by the number of relaxation lengths, μr. The present calculations employ a linear approximation, $a + b \mu r$, of the buildup factors for aluminum reported in NDA Memo 15C-2*.

(3) The earlier calculations were based on a heavier fuel loading for the reactor than that presently contemplated. The reduction in fuel inventory results in a greater number of high energy capture gamma rays in stainless steel.

(4) Revision of the estimated number of gamma rays resulting from neutron capture in the thermal shield and pressure vessel has a minor effect on the dose rate.

The result of these several changes is to increase the calculated shielding thickness by approximately one foot, mostly because of the

* Goldstein, Wilkins, and Spencer, Gamma Ray Penetrations, NDA Memo 15C-2.

349

lower absorption coefficient for 7-Mev gamma rays. The required thickness of concrete around the reactor compartment, at 10 Mw, is now calculated to be:

for 10 times the tolerance dose rate	8.1 ft
for tolerance	9.3 ft
for 1/10 tolerance	10.6 ft

The required thickness of the concrete plug over the reactor access well is:

for 10 times tolerance	6.7 ft
for tolerance	7.9 ft
for 1/10 tolerance	9.2 ft

Figs. 43 and 44 in ORNL-1613, which give dose rates as a function of radial and axial shield thickness, must be revised in accordance with the new dose rates tabulated above.

The dose rate at the top of the reactor well, after shutdown and with the concrete plug removed, was recalculated, by taking into account individual fission-product activities, whereas the earlier calculations employed the Way-Wigner formula and assumed 1-Mev gamma rays. The revised dose rates are considerably higher than those given in ORNL-1613. They were calculated for different depths of water over the pressure vessel, with and without the pressure vessel lid in place, see Fig. 15. In computing these curves, fission products whose half-lives are greater than ten minutes and whose gamma-ray energies are 1 Mev or greater were considered.

If, according to the tentative unloading schedule, there is 2 ft of water over the pressure vessel, a man removing the nuts holding the vessel lid would experience an exposure rate of 400 mr/hr one hour after shutdown, or 100 mr/hr one day after shutdown.

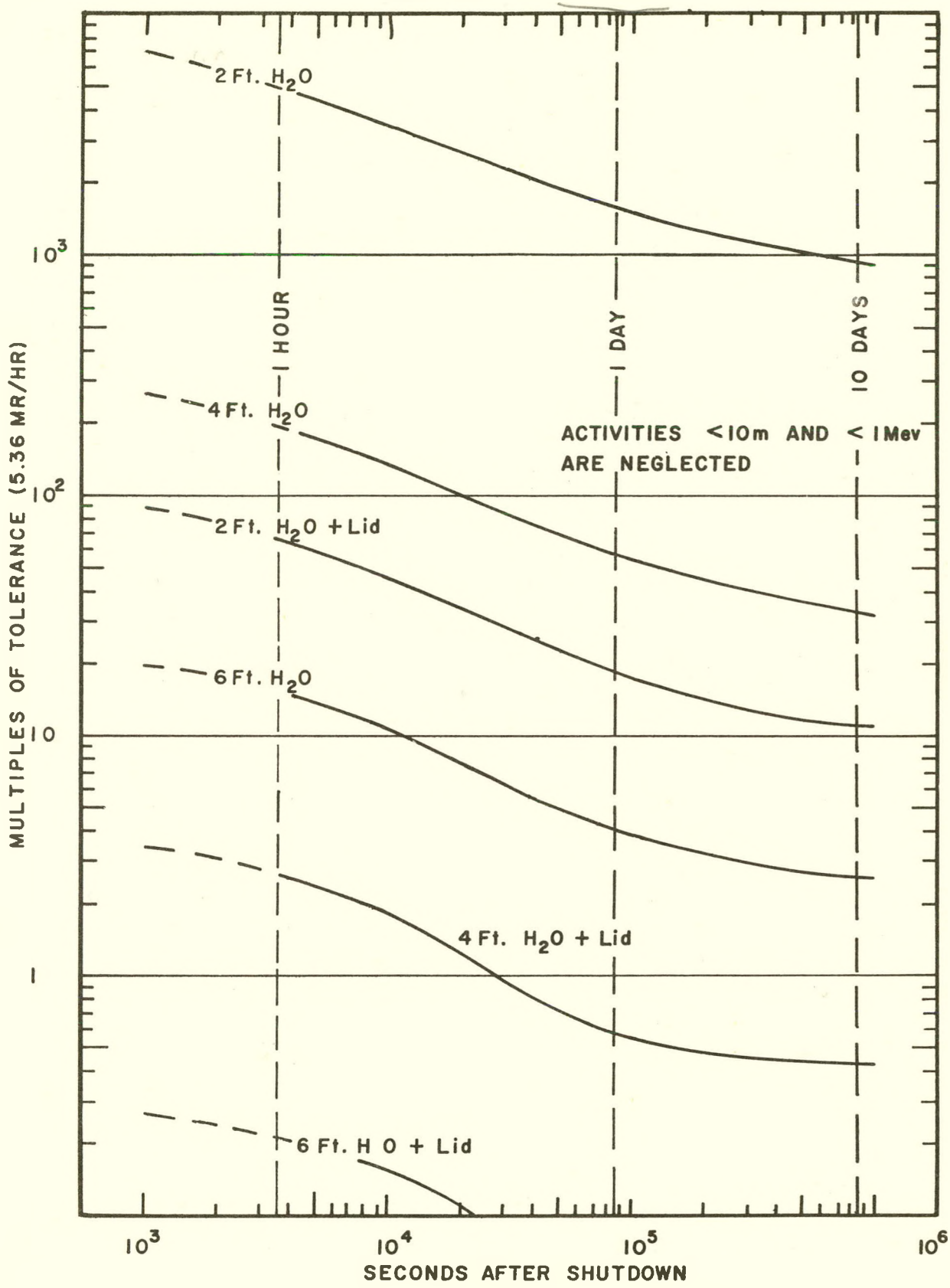

FIG. 15 DOSAGE RATES AT TOP OF REACTOR WELL AT SHUTDOWN AFTER 2.5 YEARS CONTINUOUS OPERATION AT SIX MEGAWATTS

351

ACKNOWLEDGMENTS

The authors are much indebted to Nancy Given of the ORNL Mathematics Panel, who coded the 30-group diffusion theory calculations and carried them out on the Univac. Thanks are due also to William Kinney of the ANP Division, who assisted in the preparation of the 3-group Oracle program; to William Pearce of Bendix Aviation Corporation, who performed the shielding calculations; and especially to Raymond L. Murray of North Carolina State College, who developed the multiple control rod theory and performed the calculations described herein.

352

5.0 APPENDIX: ERRATA FOR THE ORNL-1613 REPORT

Several errors and misprints have been noticed in ORNL-1613; the most important are listed below:

Page 8 — Primary coolant pump power is "35 hp", not "25 hp".

Page 27 — Shield thicknesses and dimensions are to be modified in accordance with the calculations described in Sec. 3 of this supplement.

Page 75 — In line 15, solution of the differential equation should read:

$$t = t_f + \frac{S}{2k} (10^{-4} - x^2), \text{ not } (x^2 + 10^{-4}).$$

Page 101 — In the table, units of resistivity are "megohm-cm", not "meg-cm".

Page 110 — Line 1: "(lethargy u = 19.23)" not "= 10.23".

In Eq. (1) the resonance escape probability was omitted; the equations should read:

$$D_1 \nabla^2 \varphi_1 - \Sigma_1 \varphi_1 + (1 - p)\, k_2 \Sigma_2 \varphi_2 + k_3 \Sigma_3 \varphi_3 = 0$$

$$D_2 \nabla^2 \varphi_2 - \Sigma_2 \varphi_2 + \Sigma_1 \varphi_1 = 0$$

$$D_3 \nabla^2 \varphi_3 - \Sigma_3 \varphi_3 + p \Sigma_2 \varphi_2 = 0$$

Page 129 — Line 5 should read "----$L(H_2O)$ =2.70 cm at 68° F, and L = 4.28 cm at 450° F".

Page 131 — Line 21: "radiative capture" not "radioactive".

Pages 144,146 — (Sec. 5.6): Negative signs were omitted in temperature coefficients. Also the magnitude, $-2.34 \times 10^{-4}/°F$, was incorrectly reported as $3.35 \times 10^{-4}/°F$. See the new values given in Sec. 2 of this Supplement.

Page 147 — Shield thicknesses and dimensions are to be modified in accordance with Sec. 3 of this Supplement.

Page 148 — Line 13: "A 56-hour working week", not "50".

Page 156 — Data given in the table are superceded by Sec. 3 of this Supplement.

353

Page 157 Delete line 3 "10 Mw activity ... 387 mr/hr".

Page 165 Last line, add "at full load".

Page 207 Line 25: "60% average load", not "70%".

Page 248 Table, units in the last two columns are also cc/L.